UNIVERSITY OF BIRMINGHAM

Experimental study on diesel spray with single and multiple injection under room temperature and low temperature

BY

ZIMAN WANG

A thesis submitted to the

College of Engineering and Physical Sciences of

The University of Birmingham for the degree of

DOCTOR OF PHILOSOPHY

School of Mechanical Engineering

College of Engineering and Physical Sciences

The University of Birmingham

August, 2015

UNIVERSITY OF
BIRMINGHAM

University of Birmingham Research Archive

e-theses repository

This unpublished thesis/dissertation is copyright of the author and/or third parties. The intellectual property rights of the author or third parties in respect of this work are as defined by The Copyright Designs and Patents Act 1988 or as modified by any successor legislation.

Any use made of information contained in this thesis/dissertation must be in accordance with that legislation and must be properly acknowledged. Further distribution or reproduction in any format is prohibited without the permission of the copyright holder.

Abstract

Multiple-injection strategy can effectively downsize the diesel spray penetration and boost the atomization, achieving robust flammable mixture. This injection strategy causes higher IMEP and lower emissions. It also considerably stabilizes the engine performance and reduces misfire for cold start and cold idle operation. Multiple-injection however shows complex characteristics because of the interaction between split injections in term of mass flow rate (MFR), spray and combustion characteristics. Significant variation of fuel properties under cold condition further complicates the characteristics of multiple-injection.

To systematically study this injection strategy, the MFR characteristics were first studied by applying a purpose-built long tube measuring instrument based on Bosch method. Both single and split injection strategies were employed. The instantaneous MFR and total fuel mass delivered in each split were quantitatively studied to assess the importance of the duration of each split. Furthermore, the interaction degree among splits was quantitatively linked to dwell interval and injection duration distribution of each split. The influences of low temperature on the injection characteristics and interaction between splits were also studied. It was found that the injection characteristics of split injection were quite different from those of single injection and the influence of fuel temperature was profound.

A long distance microscope and an ultrahigh speed CCD camera were then employed to study the primary breakup of diesel spray by photography technique with the help of

backlighting. The primary breakup at the injector opening and closing stages was investigated at injection to atmospheric conditions. With the combination of MFR measurement and ultrahigh speed imaging, the regime for the formation of mushroom shaped spray head was analyzed and the dispersion quality in the near field was quantified. The breakup regimes study was also successfully carried out. By employing an in-house built cooling system, the influence of fuel temperature was also investigated. It was found that flow regimes in nozzle hole dominate the primary breakup. Dwell interval, injection pressure, injection duration of the first injection, the number of injections and fuel temperature determined the interaction between split injections and the resultant breakup.

The following study is the investigation of macroscopic characteristics (penetration, cone angle and spray area) with high speed imaging technique. A high pressure vessel was used to study the effects of back pressure and the interaction between split injections. The impact of cold fuel temperature on macroscopic characteristics was investigated and various correlations were employed to probe the profound influence of fuel temperature. It can be concluded that back pressure and fuel temperature dramatically affect the macroscopic characteristics of spray when split injection strategy was employed. Generally, higher back pressure boosted the interaction between split injections and low temperature lead to smaller spray area and lower penetration due to less injected fuel and poorer dispersion.

The velocities and sizes of droplets were finally studied with Phase Doppler Particle Analyzer (PDPA) technique under atmospheric ambient condition. The effects of injection strategy and fuel temperature were investigated. It was found that split injection strategy

caused larger droplets. Poor dispersion under low fuel temperature also resulted in obviously larger droplets.

List of Abbreviations

ASOI	After start of injection
BDC	Bottom dead centre
BEOI	Before end of injection
CAI	Controlled Auto ignition
CCD	Charge-coupled device
CFD	Computational fluid dynamics
CVC	Constant Volume Chamber
D_{10}	Mean diameter (μm)
D_{32}	Sauter mean diameter (μm)
DPF	Diesel particulate filters
fps	Frame per second
HC	Hydrocarbon
HCCI	Homogeneous charge compression ignition
HRR	Heat release rate
IMEP	Indicated mean effective pressure
LIF	Laser induced fluorescence
LSD	Laser Sheet Dropsizing
LT	Low temperature
MFR	Mass flow rate
NAC	Nitrogen dioxides absorber catalyst
SCR	Selective catalytic reduction
SMD	Sauter mean diameter (μm)
ULSD	Ultra-low sulphur diesel
RT	Room temperature
PDPA	Phase Doppler Particle Analyser
PIV	Particle imaging velocimetry
TWC	Three Way Catalyst

List of Notations

ξ	Flow coefficient of the injector.	
λ	Light wavelength	nm
λ_{ratio}	fuel mass/spray area ratio	mg/mm^2
ϕ	Phase difference	^{o}
θ	Cone angle	^{o}
β	Detector phase factor	
δ	Boundary layer thickness	μm
σ_l	Liquid surface tension.	$pa \cdot s$
a	Sound speed	m/s

List of Symbols

AF	Injector conicity	
C_d	Discharge coefficient	
C_{LIF}	Calibrating coefficient for inelastic signal.	
C_{Mie}	Calibrating coefficient for elastic signal	
D	Drop size	μm
d_c	Sac diameter	mm
d_i	Diameter of i level drops	μm
d_{in}	Hole inlet diameter	mm
d_0	Hole outlet diameter	mm
f	Frequency of light intensity variation	Hz
Δf	Frequency difference	Hz
F	Flow area	cm^2
κ	Air/ fuel density ratio	
K	Cavitation number	
K_B	Liquid bulk modulus	
K_c	Nozzle convergence factor	
l	Feature length	mm
L	Hole length	mm
L_b	Length of the continuous jet	mm
I_c	Interaction coefficient	
LL_{max}	Maximum liquid length	mm
$\dot{m}_{act}$	Actual mass flow rate	g/s
$\dot{m}_{th}$	Theoretical mass flow rate	g/s
n_{hole}	Number of orifices	
N_i	Number of the i level drops	
Oh	Ohnesorge number	
ρ_q	Gas density	kg/m^3

ρ_l	Liquid density	kg/m^3
Δp	Pressure difference	pa
P_b	Back pressure	pa
p_v	Vapor pressure	pa
Q	Liquid volume flow rate	m^3/s
Re	Reynolds number	
S_{Mie}	Mie signal	
S_{LIF}	LIF signal	
t_b	Time for primary breakup	s
t_{edge}	Time for spray penetrating out of view field.	s
u	Flow speed	m/s
u_d	Drop velocity	m/s
u_{inj}	Jet speed	m/s
V_{act}	Actual flow velocity	m/s
V_{av}	Average velocity	m/s
v_l	Liquid kinematic viscosity	cSt
We	Weber number	
Z	Stability of droplets	

Acknowledgements

I greatly appreciate my lead supervisor Professor Miroslaw Lech Wyszynski for his guidance and help during my study. I thank my second supervisor Professor Hongming Xu for his very helpful advice and access to optical diagnostics equipment. I would like to thank the Head of School, Professor Duc Truong Pham, who helped me to apply the "Li Si Guang Scholarship" for my PhD. I am grateful to Dr. Athanasios Tsolakis who gave me a lot of valuable suggestions.

I acknowledge the financial support from the "China scholarship Council" and "The University of Birmingham" which funded me through a joint scholarship - Li Si Guang Scholarship. The "China scholarship Council" paid my living cost while "The University of Birmingham" waived my tuition fees. This generous financial support enabled me to focus on my study.

Thanks also go to the my colleagues and friends, Dr Haichun Ding, Dr He Ma, Dr Jose Martin Herreros Arellano, Dr Changzhao Jiang, Dr Fan Zhang, Dr Hamid Mahmoudi, Dr Shahrouz Norouzi, Dr Jakub Piaszyk and Daliang Jing for their technical help and support.

Finally, special appreciation from the bottom of my heart should go to my parents, brothers, sisters and my wife for their unconditional support and help.

Table of Contents

List of Figures

List of Tables

List of Publications

Papers published in Journals

1. Wang, Ziman; Ding, Haichun; Wyszynski, Miroslaw L; Tian, Jianyi; Xu, Hongming. Experimental study on diesel fuel injection characteristics under cold start conditions with single and split injection strategies. Fuel Processing Technology. March 2015 131:213-222.

2. Wang, Ziman; Wyszynski, Miroslaw L; Xu, Hongming; Abdullah, Nik Rosli; Piaszyk, Jakub. Fuel injection and combustion study by the combination of mass flow rate and heat release rate with single and multiple injection strategies. Fuel Processing Technology. 132 (2015) 118-132.

3. Wang, Ziman; Wyszynski, Miroslaw L, Xu, Hongming. Experimental study on blending diesel fuel with dimethyl carbonate with aid of ultrasonic emulsification process. Archivum combustionis. Vol. 34 (2014) - No 1.

Papers submitted to journals

1. Haichun Ding, Ziman Wang, Xiao Ma, Hongming Xu, Miroslaw L Wyszynski. Ultra-high Speed Imaging Study of the Diesel Spray Close to the Injector Tip at the Initial Opening Stage - Part 1 (Single Injection), Applied Energy, 19th March, 2015.

2. Ziman Wang, Haichun Ding, Xiao Ma, Hongming Xu, Miroslaw L Wyszynski. Ultra-high Speed Imaging Study of the Diesel Spray Close to the Injector Tip at the Initial Opening Stage - Part 2 (Split Injection), 20th, March, 2015.

Chapter 1 Introduction

1.1 Background

Internal combustion engine has gone through a blooming stage for the past century. Its development has exerted profound influence on people's lives and is of paramount importance for the development of economy. However, the two severe problems, namely, global warming and fuel shortage, pose a detrimental threat on its advantages. In the past, maximizing the efficiency and minimizing the fuel consumption were focused. By contrast, recently the aims are to decrease the fuel consumption and emissions due to the increasingly stringent laws enforced or to be enforced [1].

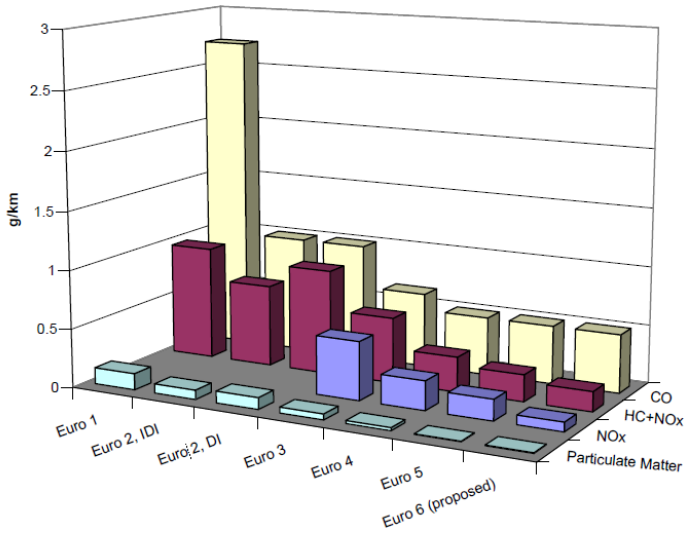

Figure 1-1 European emissions regulations for passenger cars [1]

According to European Union, the emission standard becomes increasingly stringent, as shown in Figure 1-1. The enforcement of Euro 5 or Euro 6 impels the manufacturers and researchers to further the development of internal combustion engines. Much energy and time are invested into the better understanding of fuel spray and combustion to get a finer

eco-friendly energy management, driven by the aforementioned increasing depletion of fuels and environmental contamination [2].

1.2 Methods to improve engine performance

The increasing fuel demands can be eased, partly by utilizing alternative fuels and partly by improving the efficiency of engine through the usage of more advanced fuel injection system. However, the emission problem can be, to an astonishing degree, combated by the better air/fuel mixture preparation and the adoption of effective emission after treatment devices, for instance, Diesel particulate filters (DPF), Three Way Catalyst (TWC), Nitrogen dioxids absorber catalyst (NAC) as well as the selective catalytic reduction (SCR). The employment of novel combustion modes, for instance, Homogeneous Charge Compression Ignition (HCCI), Controlled Auto Ignition (CAI), can also relive the emission problem [3].

Air movement is a process that regulates the mixture preparation, combustion, heat rejection and thermal efficiency. The air moving status when sucked into the cylinder and piston reciprocation regulate the two features of air movement, namely, turbulence and bulk air movement. When the piston moves towards the Bottom dead center (BDC), fierce air rotating movement is created at the intake valve. Owing to the piston reciprocation and the interaction among air, piston and cylinder wall, these vortex and eddies lose their stability and disintegrate into turbulence, boosting the mixing process [4]. A host of methodologies have been adopted to rule the airflow in the chamber. One effective way is to control the

shape and layout of the intake port [5]. Another favorable method is the formation of squish generated by the cylinder head and upper surface of the piston crown [5].

1.3 Fuel spray

Fuel injection is another dominant factor that impacts the mixture preparation. The mixture quality is regulated by many factors, for instance, injection timing, piston and chamber morphology, injection strategies and injection conditions. The emissions can be considerably relieved by better formation of mixture if the spray parameters are carefully selected [2].

The fuel mass flow rate (MFR) and injection features are of great importance for the combustion characteristics and emissions [6, 7]. This is because the MFR governs the hear release rate (HRR). Lower initial MFR led to lower HRR, prolonged ignition delay and lower maximum HRR, leading to the reduction of NO_x. Higher initial MFR contributed to earlier appearance of peak temperature. By contrast, higher MFR is favorable for main injection as it boosts the mixture formation and soot consumption. It suggests that the "boot-like" fuel MFR shape could improve the trade-off between engine performance and emissions [8, 9].

Dolenc et al. [10] studied the influence of injection profile on the combustion process and proposed a model for the shape of the MFR, as shown in Figure 1-2. The regulation of the noise and emission can be achieved through the regulation of the injection shape.

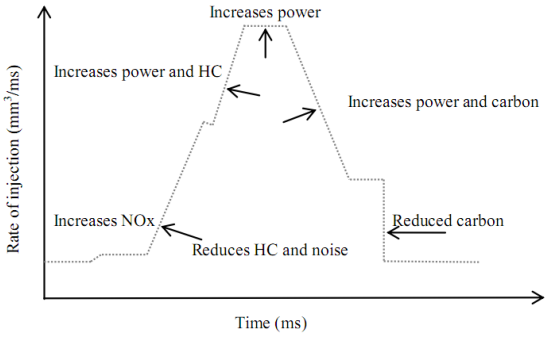

Figure 1-2 Implication of injection profile on the combustion [10, 11]

The profile of the MFR is thought to be complex if good engine performance is to be obtained due to the variation of conditions in the engine. In addition, the rise of injection pressure for one thing drives up the parasitic cost and energy loss and for another deteriorates of the NOx emission. To address these problems, the integration of high injection pressure and cutting edge injection strategy can lower both the NOx and soot level [11]. Modified injection system and metering system which are capable of different injection strategies, including split injection strategy, were born [12]. Split-injection strategy is an effective way to downsize the penetration and boost the atomization, achieving robust flammable mixture [13]. Multiple-injection is a good way to realize the desired MFR shape. This injection strategy causes higher IMEP and lower emission [14, 15]. The shorter injection duration for each split injection can effectively avoid the impingement and lower HC can be achieved. In addition, the interval between split injections allows the fuel to mix with air sufficiently and better mixture can be obtained [16-18].

Figure 1-3 presents a model for the concept of the split injection [19]. Three parameters are involved, namely, the injection duration for each split T_i, the injection dwell τ_i and fuel

mass for each split M_i. The total fuel mass is $M_t = \sum M_i$ and total injection duration is $T = \sum T_i + \sum \tau_i$. If τ_i=0, the injection pattern is actually the single injection. If τ_i is considerably larger than T_i, there is few chances that the splits can interact with each other and the injection model become similar to the single injection. If $M_1 \ll \sum_{i=2}^{n} M_i$the pilot injection strategy is likely to achieve and if $\sum_{i=1}^{n-1} M_i \gg M_n$, the post injection strategy is likely to be achievable. For split injection strategy, the time interval and injected mass ratio between two splits are two additional factors that need to be considered.

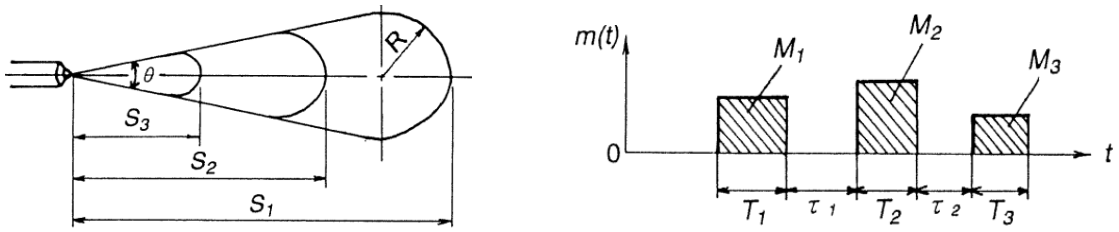

(a) (b)

Figure 1-3 Model of split injection strategy [19]

According to Zhao [20], a small amount of pilot fuel can greatly lower the noise as the pilot injection can shorten the premixing process. Consequently, the amount of fuel mixture for premixed combustion is smaller and the pressure rise rate is lower. The slow increase of injection rate can lead to lower NOx, whereas in the process of combustion the fuel should be injected as soon as possible to prohibit the generation of soot. A post injection boosts the combustion of soot generated during the diffused combustion (Figure 1-4).

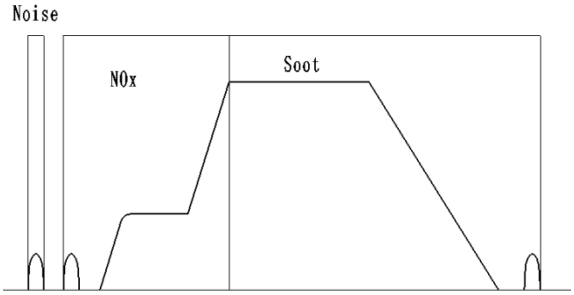

Figure 1-4 An ideal model of MFR [20]

Multiple-injection (closely-coupled) on the other hand shows complex injection characteristics because of the interaction between split injections in term of MFR, spray characteristics and combustion characteristics. Dwell interval is an important parameter that governs spray behavior and combustion performance. The needle movement when split injection strategy is used is different to that when single injection strategy is employed [21, 22]. The MFRs and spray characteristics for consecutive split injections are therefore to be different. The difference of macroscopic characteristics is intensified by the ambient conditions.

Shorter dwell leads to stronger spray-combustion interaction [23]. The flame interacting surface between the first split injection and the second split injection increases with shortened dwell. The combustion of the first injection influences that of the second one by changing the temperature and compositions [23]. Therefore, shorter dwell results in higher temperature in the middle of the second spray due to raised temperature by the closely coupled first injection. On the other hand, short dwell leads to insufficient oxygen, contributing to insufficient combustion for the second injection. With overlong dwell, the

hot gas produced by the combustion of the first split injection cools down, showing little combustion interaction [23].

1.4 Engine operation under cold condition

Under cold condition, the fuel properties are thought to be significantly affected. The spray characteristics (both macroscopic and microscopic characteristics) and dispersion are expected to vary considerably. Generally, poorer dispersion under low temperature (LT) than that under room temperature (RT) can result in longer ignition delay and higher possibility of misfire. The engine performance tends to be poor due to high variation of combustion characteristics. This increases the fuel consumption because of lower combustion efficiency. In addition, the emissions are inevitably high because of incomplete combustion [1].

Multiple injection strategy can considerably stabilize the engine performances and reduce misfire for cold idle operation [1, 24]. Better fuel mass distribution and fuel mixture when split injection strategy is employed shorten the ignition delay. Higher flexibility of the innovative injection strategy can therefore control the combustion characteristics effectively. The emissions can be considerably improved as a result of the better combustion.

1.5 Aim and Approaches

The aim of this study is to study the novelties of closely coupled split injection strategy and to investigate the influence of low temperature (fuel temperature) on the spray

characteristics when split injection strategy is employed in order to provide useful information for engine design, fuel injection system design and control strategy design. This study can also provide helpful information for engine control strategy. The specific objectives are:

(1) To build a real-time fuel MFR instrument based on Bosch method.

(2) To study the injection characteristics of both single and split injection strategies as well as the influence of fuel temperature on the injection characteristics.

(3) To develop the technique and instrument for the investigation of primary breakup.

(4) To develop the cooling system for the fuel injection system.

(5) To study the regimes of the primary breakup, primary breakup characteristics of both single and split injection strategies and the influence of fuel temperature on the primary breakup characteristics.

(6) To investigate the macroscopic characteristics of spray with single and split injection strategies and the influence of fuel temperature on the macroscopic characteristics.

(7) To investigate the microscopic characteristics of spray with single and split injection strategies and the influence of fuel temperature on the microscopic characteristics.

1.6 Thesis outline

This thesis consists of 8 chapters which are briefly described below:

The first chapter gives a very brief review of motivation and the aims of the study. The following chapter is about reviews on the injection and spray characteristics. The frequently employed techniques are also introduced. Chapter 3 describes the experimental setup employed in this study, including the long tube measuring instrument, long distance microscope, high pressure vessel, cooling system and PDPA rig. This is followed by the results and findings about the injection characteristics with single and split injection strategies and the influence of fuel temperature in Chapter 4. Chapter 5 then illustrates the regimes of primary breakup, characteristics of primary breakup with single and split injection strategies and how these characteristics are varied by the variation of fuel temperature. The macroscopic characteristics (penetration, spray area and cone angle) and microscopic characteristics (droplet size and droplet velocity) are presented in the next two chapters in sequence. Again, the impact of fuel temperature on these characteristics is presented and discussed separately. The last chapter, Chapter 8, presents the conclusions and proposes the future work.

Chapter 2 **Literature review**

Spray is the process of providing an accurate demanded amount of fuel to an internal combustion engine. The spray is generated when the liquid is injected into gaseous condition from an injector. The injected liquid begins to interact with air instantly and the interaction leads to the decomposition and detachment from the periphery of the jet. After the fuel dispersion, flammable mixture is expected to be generated through vaporization. The evolution processes, namely the breakup, atomization and evaporation, are of great importance for the mixture preparation [20].

2.1 Spray structure

Parameters to quantify the spray are spray shape (temporal and spacial morphology development), macroscopic features (plume angle, penetration, breakup and atomization) and microscopic features (droplet diameter, velocity and momentum flux).

One model of spray structure proposed by Hiroyasu et al. [25] is shown in Figure 2-1 (a), including the key parameters. In this model, two parts, namely primary breakup and secondary breakup are shown. In the vicinity of the nozzle tip, the liquid fuel was densely and uniformly distributed. Below this dense part, the fuel starts to disintegrate, and waves appear on the periphery. Liquid stripes are also observed, and the pitches between these stripes rise further downstream of the plume. With the evolution of the plume, the ambient air and plume interacts and the resistant air compresses the clusters to be compact. The

spray also transfers its momentum to the air and enhances the air entrainment, which leads to further disintegration of the plume [11, 26].

(a) [25] (b) [27]

Figure 2-1 Models for spray structure

Zhu [27] studied the plume structure with LIF technique and put forward a modified model (Figure 2-1 (b)). According to the model, the plume can be divided into three sections:

a) Entrainment section, namely the intact part, where the spray surface is smooth and the air entrains into the side periphery due to the induced air pressure difference;

b) Recirculation section, the spray front capturing region in which the momentum exchanges intensively and air entrainment develops strongly thanks to the relatively high droplets velocity and gas movement;

c) Capturing section, the lateral recirculating region at the downstream of the nozzle where the momentum of the droplets passes to the gas and decreases progressively, leading to the radial and axial movement of both air and fuel particles.

2.2 Breakup regimes

The turbulence in the jet turns up just after the fuel leaves the outlet of the nozzle. The periphery decomposes into small particles due to the air drag force. As a matter of fact, the liquid is internally and externally undergone various forces, which leads to the generation of droplets with various diameters [28].

According to the dominant implication of various factors, the regimes of the breakup were categorized into three types by Arcoumanis [29], that is, breakup caused by the external air forces, breakup caused by turbulence and breakup caused by internal cavitation. For the first mechanism, the air drag force and the fuel-gas interaction is pivotal. For the second one, the magnitude of the jet radial velocity caused by the turbulence in the nozzle is high and the inertial force overtakes the restoring force. For the last one, the growth and decomposition of the air foams are responsible [30].

In the whole breakup process, many forces are involved simultaneously, leading to the deformation and disintegration of the spray. The important forces are surface tension force, viscous force and inertial force. These forces can be quantified through dimensionless numbers to identify the breakup regimes.

Weber number (*We*): referring to the ratio between inertial force of particles and the surface tension force. The higher fuel pressure and denser ambient air lead to stronger air dynamic force, thus higher *We*.

$$We = \frac{Inertial\ force}{Surface\ tension\ force} = \frac{D\rho_l u_d^2}{\sigma_l}$$ Equation 2-1

Where D is drop size, $\rho_l$is liquid density, $u_d$is drop velocity and $\sigma_l$is the liquid surface tension.

Small *We* means relatively low inertial force but relatively high surface tension force, which is detrimental for the plume break-up.

Reynolds number (Re): denoting the inertial force / viscous force ratio. This number is used to denote the turbulent flowing characteristics.

$$\mathrm{Re} = \frac{Inertial\ \ force}{Viscous\ \ force} = \frac{\rho_l l u_d}{\mu_l} = \frac{u_d l}{\nu_l}$$ Equation 2-2

Where *l* is the feature length, $\rho_l$is the liquid density and $\nu_l$is the liquid kinematic viscosity.

The rise of the Re leads to the rise of the values of macroscopic parameters. This changing trend is obvious when the temperature raises because the viscosity, which greatly affects the Re, is sensitive to the temperature.

Ohnesorge number (*Oh*): expressed as the viscous force / surface tension force ratio.

$$Oh = \frac{Vis\cos ity}{Tension} = \frac{\sqrt{We}}{\mathrm{Re}}$$ Equation 2-3

Air density -fuel density ratio κ : denoting the air drag force.

$$\kappa = \frac{\rho_g}{\rho_f}$$

Equation 2-4

Applying these dimensionless numbers as criteria to distinguish the state of the spray, Zeng [31] analyzed the behavior of the spray. It was revealed that under non-evaporative condition, *We* and gas-fuel density ratio could exert more obvious effects on the macroscopic features than *Re*. The implication of droplet inertia as well as the gas drag force outbalanced that of viscosity and surface tension. Under different injection conditions, many macroscopic characteristics are the same if *Rd*, *We* and the gas/fuel density ratio are the same. The root reason for these similarities was that the forces, which can be quantified by *Rd*, *We* and the gas/fuel density ratio, determine the break-up regime. In addition, the macroscopic characteristics were the outcome of the competition of the aforementioned forces [31].

Under a wide range of conditions, the jet decomposition regime changes as the aforementioned numbers vary. Reitz [32] classified the regimes into four categories (Figure 2-2). The examples of these breakup regimes are shown in Figure 2-3.

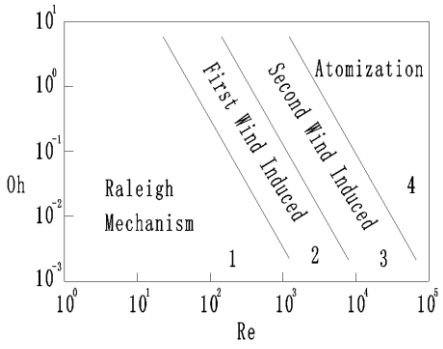

Figure 2-2 Break-up mechanisms [32]

(1) Rayleigh jet break-up

This principle works when injection velocity is low, namely $We_{Liq} > 8$ and $We_{Gas} < 0.4$. Due to the low injection pressure, the aerodynamic force is weak and its influence is negligible. The disintegration of the jet is triggered by the waves induced by the surface tension and disturbance. The breakup can be partly attributed to the asymmetric oscillations produced by the viscous forces [33].

(2) First wind-induced break-up

As the jet velocity rises, the implication of the air drag force comes into effect, with $13 > We_g > 0.4$. The drag force and the force generated by the pressure difference enhance the oscillations and the magnitudes of the waves are amplified. The disintegration tendency of jet correspondingly increases.

(3) Second wind-induced break-up

If $40.3 > We_g > 13$, the radially enhanced effects of the air continue to be boosted and the opposing effects by the surface intension rise but with a smaller degree. The droplet is much smaller than the jet diameter and the decomposition ensues in the vicinity of the nozzle.

(4) Atomization

Under this operating condition, the jet velocity is extremely high, with $We_g > 40.3$. The liquid atomizes completely just after injecting out of the nozzle because of the high velocity difference between the fuel and ambient air.

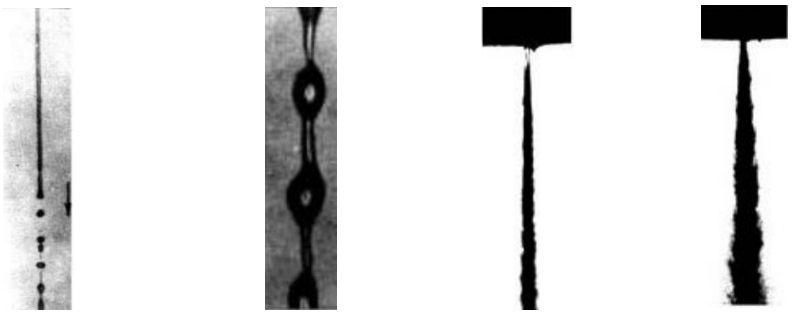

(a) (b) (c) (d)

Figure 2-3 Morphology of spray under various breakup regimes [32]

2.3 Macroscopic characteristics of spray

2.3.1 **Breakup length**

The length of the continuous liquid part is termed as the breakup length L_b displayed in Figure 2-1. When injection pressure is low, the unbroken part is long thanks to the poor atomization. Under high injection pressure, the unbroken part is short as the jet atomizes drastically. However, as shown in Figure 2-4, the intact length does not change linearly with the droplet velocity because the breakup regimes are different.

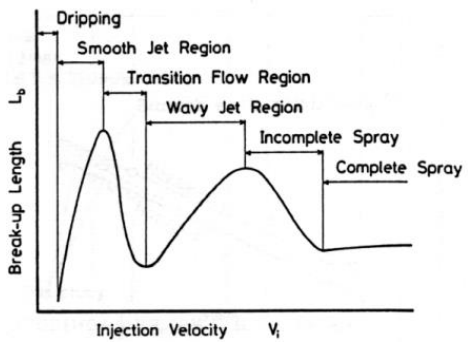

Figure 2-4 Breakup length vs injection velocity [25]

It can be found that when the jet velocity rose, the breakup length rose quickly and peaked around 60m/s. As jet velocity further increased, the length decreased gradually and then increased before leveling off [25].

Basing on a number of tests, Hiroyasu [34] put forward a mathematical expression of the breakup length displayed as:

$$L_b = 7d_0\left(\frac{p_g}{\rho_l u_{inj}^2}\right)^{0.05}\left(\frac{d_{in}(1+0.4)}{2d_0}\right)\left(\frac{L}{d_o}\right)^{0.13}\left(\frac{\rho_f}{\rho_g}\right)^{0.5} \quad \text{Equation 2-5}$$

Where L_b is the length of the continuous jet, d_0 is the hole outlet diameter, p_g is the back pressure, u_{inj} is the jet speed, d_{in} is the hole inlet diameter and L is the hole length.

Salters and Yule [35] found that this length was approximately 100 times of the hole size under the condition similar to the real working ones. Gülder [36] reported that the plume can highly atomize within 20 nozzle diameters distance. Bruneaux [37] claimed that the full atomization can be achieved within 1 to 2 mm. Lee reported that the primary disintegration fall in the range of 10 to 40 mm below the nozzle [38, 39].

Shimizu [40] measured the decomposing length with electric method and his results showed that higher fuel pressure and smaller nozzle caused shorter breakup length, shown in Figure 2-5. It was also revealed that the breakup length was sensitive to the nozzle structure, for instance, hole diameter, hole length and shape of the hole inlet [40].

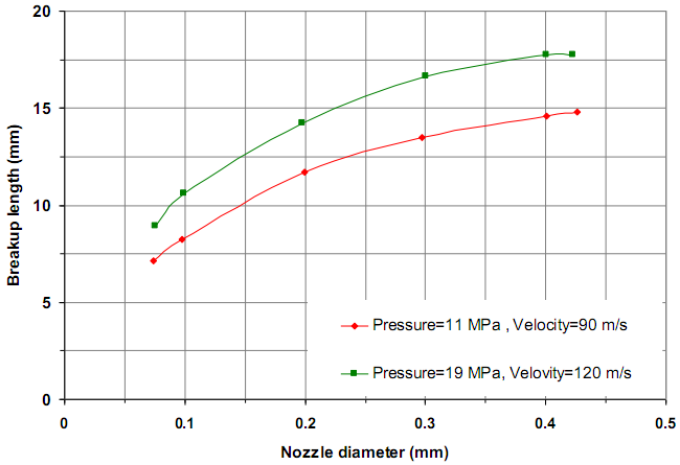

Figure 2-5 Effect of nozzle diameter on breakup length [40]

2.3.2 **Penetration length**

Penetration length refers to the distance between the nozzle tip and the farthest point the fuel reaches before it evaporates completely. The penetration is one of most important factors that impact the utilization of the air in the chamber, fuel combustion efficiency and the tendency of the soot formation and impingement [11].

Wakuri [41] proposed a refined correlation based on the one proposed by Binder [42], and the new one showed good agreement with the experiment results.

$$L(t) = \sqrt{\frac{1}{\tan(\theta/2)} t d_0 \sqrt{\frac{2\xi \Delta p_m}{\rho_g}}}$$

Equation 2-6

Where ξ is the flow coefficient of the injector.

With help of photography technique, Hiroyasu & Arai [25] investigated the spray development. They reported that the penetration length went up linearly at the beginning

and then the rising rate reduced when a time point was reached, but still linearly. The developing trend is shown in Figure 2-6.

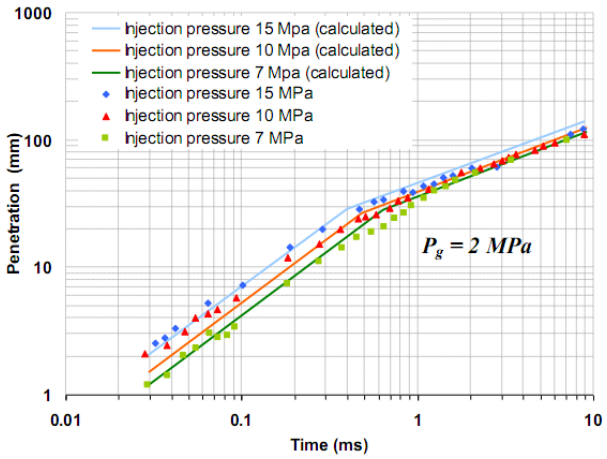

Figure 2-6 Penetration evolution vs time [25]

Basing on the results, a series of empirical equations were proposed. A time turning point t_b where an obvious variation of penetration rate is observed is expressed as:

$$t_b = 28.65 \frac{d_0 \rho_l}{\sqrt{\rho_g \Delta p}} \quad \text{Equation 2-7}$$

If $0 < t < t_b$, the penetration is expressed as:

$$L = 0.39 \sqrt{2\Delta p / \rho_l}\ t \quad \text{Equation 2-8}$$

If $t > t_b$, the penetration is expressed as:

$$L = 2.95 \sqrt[4]{\Delta p / \rho_g} \cdot \sqrt{d_0 t} \quad \text{Equation 2-9}$$

Where Δp is the pressure difference.

Actually, the transition of the two lines is not abrupt but smooth as the penetration develops continuously. To address this problem, Yule [43] put forward a refined penetration equation which showed great agreement with the experimental results, as shown:

$$L = 3.8\left(\Delta p / \rho_g\right)^{0.25}\sqrt{td_0}\ \tan(h\left(t / t_b\right)^{3/5}) \qquad \text{Equation 2-10}$$

Wei Zeng [31] probed the plume features by changing the injection conditions but keeping the aforementioned four dimensionless numbers constant according to the requirements. Many correlations were put forward, shown in Table 2-1.

Table 2-1 Correlations of spray penetration and cone angle [31]

Penetration and cone angle correlation	specification
$S = 0.076(\rho_g / \rho_l)^{-0.268} \cdot We^{0.318} \cdot \mathrm{Re}^{0.152}$	$\mathrm{Re} < 12500$
$S = 0.33\,(\rho_g / \rho_l)^{-0.268} \cdot We^{0.318}$	$\mathrm{Re} \geq 12500$
$\theta = 0.12(\rho_g / \rho_l)^{0.287} \cdot We^{0.46} \cdot \mathrm{Re}^{0.1}$	$\mathrm{Re} < 12500,\ \rho_a / \rho_l \geq 0.002$
$\theta = 0.0273\,(\rho_g / \rho_l)^{0.287} \cdot We^{0.46}$	$\mathrm{Re} \geq 12500,\ \rho_a / \rho_l \geq 0.002$
$\theta = 0.002(\rho_g / \rho_l)^{-0.38} \cdot We^{0.46} \cdot \mathrm{Re}^{0.1}$	$\mathrm{Re} < 12500,\ \rho_a / \rho_l < 0.002$
$\theta = 0.0046\,(\rho_g / \rho_l)^{-0.38} \cdot We^{0.46}$	$\mathrm{Re} \geq 12500,\ \rho_a / \rho_l < 0.002$

2.3.3 **Cone angle**

Generally, cone angle is generated by two radials which start from the nozzle tip and pass through the periphery of the spray at a certain distance from the originating point. Figure 2-1 shows the cone angle defined by Hiroyasu [25]. It can be employed to denote the radial

propagation and dispersion quality of spray. Cone angle generally shows a drastic increase after the very appearance of the plume, then almost keeps constant [44, 45].

Various correlations have been proposed basing on the experimental and simulating results. Arai et al. [46] proposed an equation of plume angle:

$$\theta = 0.05\sqrt{\frac{d_0}{\nu_g \rho_g} \cdot \sqrt{\rho_g \Delta p}}$$

Equation 2-11

Although the effects of various factors are expected to be considered, Wakuri et al. [41] believed that the ratio of liquid density and gas density was the only factor that affected the angle, as shown in Equation 2-12.

$$\theta = 2\arctan\left[0.427\left(\frac{\rho_g}{\rho_f}\right)^{0.35}\right]$$

Equation 2-12

Hiroyasu [25] studied how the plume angle changes with fuel viscosity and pressure. It was reported that with the increase of the jet speed, the plume angle initially increased, reached a peak, dropped slowly and then kept constant. The changing rate and the peak were dependent on the fuel viscosity. Higher viscosity slowed down the rise rate and lowered the peak value, shown in Figure 2-7.

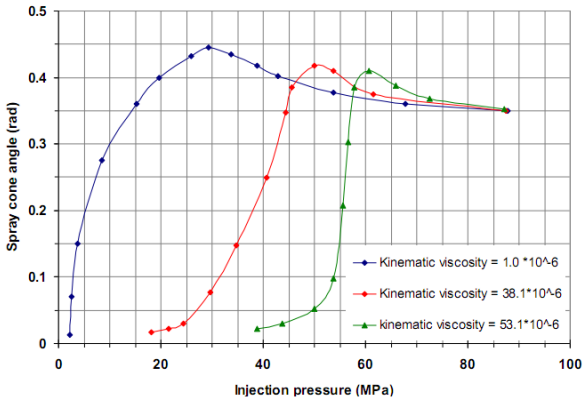

Figure 2-7 Implication of viscosity and fuel pressure on the plume angle [25]

Basing on these findings, a correlation was proposed:

$$\theta = 83.5\left(\frac{L}{d_o}\right)^{-0.22}\left(\frac{d_o}{d_c}\right)^{0.15}\left(\frac{\rho_g}{\rho_f}\right)^{0.26}$$

Equation 2-13

Where L is the length of injector hole and d_c is the sac diameter.

In Kourosh's [11] study, the plume angle was metered at half of the penetration length. It was reported that, with the gas density of 47 kg m^{-3}, the stable dispersion angle was around 20° (Figure 2-8). By contrast, under the same injection condition, Crua [47] reported about 11° plume angle. Kourosh [11] argued that this difference was due to luminosity difference.

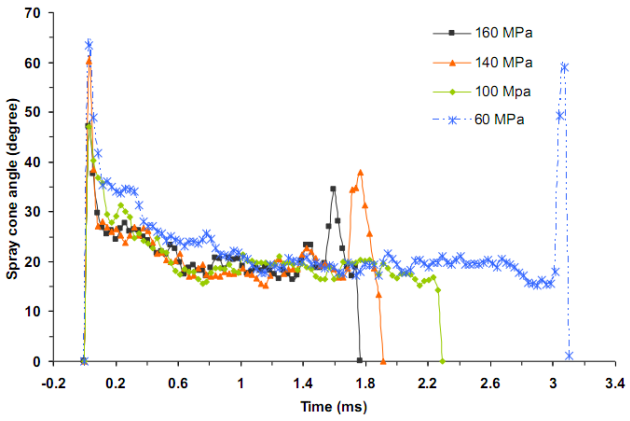

Figure 2-8 Cone angle under various injection pressure [11]

2.4 Microscopic characteristics

After the atomization, there are three typical processes engaging in the vaporization: first, the fuel particles decelerate gradually thanks to the aerodynamic friction and drag force; then the fuel transfers from liquid phase into gas phase; after this, the fuel mass transfers to further places. During these periods, particle features are temporal and spacial variables which show strong functions of both time and injection parameters. When the injection pressure is low, the sizes of the ligaments maybe bigger than the hole diameter due to the fuel surface tension being higher than the air drag force. When injection pressure rises, the droplets will be smaller and are more ready to evaporate. To quantify and characterize the microscopic features, the mean parameters should be expressed properly.

2.4.1 Droplet diameter

The droplet diameter is a reliable symbol to denote atomizing quality. Since droplets cover various diameters and the size distribution is spatially and temporally stochastic, the diameter shown in Equation 2-14 is proper to denote the atomizing quality [48].

$$d_{ab} = \left(\frac{\sum_{i=0}^{N} N_i d_i^a}{\sum_{i=0}^{N} N_i d_i^b} \right)^{\frac{1}{a-b}}$$

Equation 2-14

Where d_i is the diameter of i level drops, N_i is the number of i level drops, a and b are integers which vary according to the measurement requirements.

The Sauter method, SMD (D_{32}) has been proven to denote the atomization quality effectively [48]. This parameter varies significantly temporally and spatially [32]. Sauter mean diameter is shown as

$$D_{SM} = \left(\int D_d^3 dn\right) \Big/ \left(\int D_d^2 dn\right) \quad \text{Equation 2-15}$$

Jin-soo Kim [23] reported that owing to the secondary break-up, the SMD decreases gradually before 15mm from the nozzle, however an apparent increase is observed further downstream of the plume because of the coalescence. Kadota [49] found that, radially, SMD is lower at the periphery and higher at the axis. In addition, axially, SMD is discovered to be high near the nozzle. SMD then drops gradually along the axis before showing a rise again which can be ascribed to the aforementioned collision and coalescence.

2.4.2 **Droplet velocity**

Phase Doppler Particle Analyser (PDPA) technique is frequently employed to study the particle velocity. For the gasoline spray obtained by PDPA, two parts, “head” and “tail”, are generally observed [50, 51]. The division standard for the two parts is the time point where the axial speed shows a sharp reduction (Figure 2-9). The time from the beginning of energization to the capture of the droplets includes the injector picking-up time and the traveling time to the metering point. The velocity fluctuation is ascribed to the collision and overtaking of the particles.

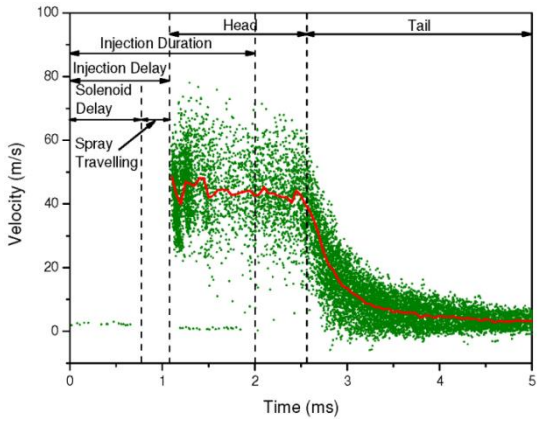

Figure 2-9 Gasoline droplet velocity [50]

For the tail part, droplets with negative speed and eddies are found and this can be contributed to the ambient air motion induced by the pressure difference between the plume periphery and the jet core. However, for diesel spray, the 'head' may not be detected due to the high droplet density.

Along the axis, the droplets further downstream of the nozzle present higher velocities. The velocity generally goes up until it almost keeps constant farther away from the nozzle. Mitroglou [45] Levy [52] also observed the same trend. However, Koo and Martin [26] reported that, from 10 to 120mm away from the nozzle, the droplet velocity showed a downward trend.

Lacoste [51] reported the droplets are decelerated considerably by the raised back pressure. If the fuel is injected with low fuel pressure and high back pressure, the velocity gap between the head and the tail is small. Mitroglou [45] reported that ambient pressure substantially boosted the atomization and when the back pressure went up to 12bar, the

droplets velocity decreased by four-fold, while the injection pressure had little effect on the droplet size.

2.5 Affecting factors

The main factors that regulate the spray are injector structure (inner structure and hole geometry), injection conditions (injection pressure and duration, fuel temperature, injection strategy), fuel properties (density, viscosity, surface tension and volatility) as well as ambient condition (gas temperature, gas density, gas pressure an air movement induced by air intake) [20].

2.5.1 Injector geometry

The quality of atomization is sensitive to injector technology, including injector type and injector geometry [20]. Two types of injectors, piezo and solenoid injectors, are available for diesel engine. The piezo-driven injector tends to be widely used due to its quicker response. The shorter injection delay and quicker opening of piezo injector allow the fuel to mix with the air more quickly, thus finer mixture and better engine performance. The quicker response is also beneficial to the control of fuel mass delivery and MFR profile [53].

Cavitation and the plume evolution are tightly related to geometry. In a whole, in terms of nozzle geometry, 3 types of nozzles can be classified, namely, the mini sac, micro sac and valve covered orifice (VCO), shown in Figure 2-10.

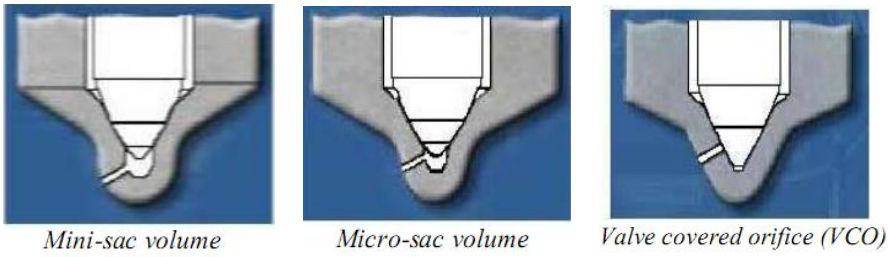

(a) (b) (c)

Figure 2-10 Injector types [11]

The nozzles with sac can lead to the rise of HC thanks to the fuel left in the sac after the injection, as a result the sac should be minimized. Farrar et al. [54] evaluated the effectiveness of the sac by varying the volume. The results showed that SMD can be lowered by circa 3 to 4μm with the drop of the sac volume.

However, the ones without sac show inferior spray quality since the holes are located just under the seat of the needle and this arrangement deteriorates the throttling effect [20]. In addition, VCO is susceptible to eccentricity, which leads to the needle oscillation. For multiple-hole injectors, as the pressure is not distributed evenly round the needle during the opening process, the mass flow variation between holes and cycles occurs [11]. The VCO can be easily adopted to deliver a certain amount of fuel and control the injection time as there is no need to fulfill the sac. It also should be noted that the mechanisms of the cavitation in VOC and sac nozzles are different. The conventional cavitation occurs in the VOC nozzle whereas the cavitation featured by vortex appears in the sac category [29, 30, 55, 56]

Lacoste [51] probed the impact of the hole size, and the droplet velocity and SMD were studied. The hole diameters were set to be 0.1 and 0.2 mm. Low (60 MPa) and high (160

Mpa) injection pressures were employed and the measurement was taken at 40mm downstream of the nozzle. The results showed that smaller hole can accelerate droplets and lower the drop size more obviously. The cavitation was boosted by the reduction of the hole size, consequently, the turbulence was enhanced and velocity was driven up. It is advisable to improve the atomization quality by raising the injection pressure and dropping the hole size simultaneously [27].

The convergence of nozzle hole can exert profound influence on the spray characteristics [51]. The convergence factor K_c is defined as:

$$K_c = \frac{d_{in} - d_0}{10} (\mu m) \qquad \text{Equation 2-16}$$

It is well acknowledged that higher K_c contributes to higher penetrating rate. Cavitation can be effectively alleviated or eliminated by increasing *Kc* factor. By utilizing the CFD simulation, Caprotti [57] found that the injector with convergent holes presents higher discharge coefficient as the cavitation is suppressed.

Schugger [58] performed an experimental study to reveal how the hole geometry impacted the spray features. In his study, two injectors featured with different hole structures were employed. For the first one, the hole size and included angle were 0.15mm and 162° respectively. The other one was convergent with the entrance size of 0.151mm, and outlet size of 0.137mm. The hole entrance for the second nozzle had hydro-eroded edge. The results suggested that the nozzle structure played a pivotal role in the spray and a convergent injector with round inlet hole caused longer penetration and smaller plume angle.

2.5.2 **Injection pressure**

The influence of injection pressure on spray is extraordinary. High inertia results in high velocity, good dispersion and small droplets. Kourosh [11] focused on the mixture formation using optical diagnostic technique under a variety of injection pressures ranging from 20Mpa to 100Mpa. It was shown that similar quantity of fuel injection was achieved with much shorter duration under high injection pressure. For the high injection pressure cases, the fuel concentration was rather high at the beginning but the propagation was much faster due to the finer atomization. Furthermore, the rise of injection and back pressures contributed to the reduction of breakup time and length.

Jingyu [27] reported that the raised injection pressure enabled the air entrainment from the lateral to fully develop and the momentum to transfer intensively. The whole rate of gas mass flow showed a strong positive function with the rise of injection pressure, that is, the raised liquid momentum enabled the droplets to fiercely interact with the air through the lateral and front periphery.

2.5.3 **Ambient pressure and density**

The change of the ambient pressure and density can considerably affect the macroscopic characteristics. Larger plume angle and lower spray length result from the rise of the ambient density [25, 27, 31, 59]. With the air density changing from 14 to 49 kg/m^3 and fuel pressure ranging from 60 to 160 MPa, Kennaird [60] studied the changing trend of the spray

length by using a injector with 0.2mm hole diameter. Their results (shown in Figure 2-11) showed that the rise of ambient density obviously caused lower penetration due to higher air resistance.

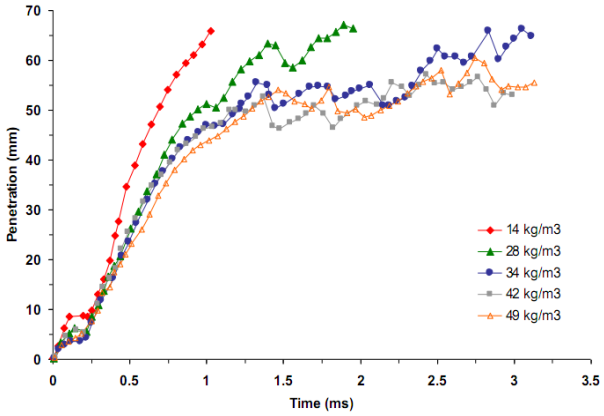

Figure 2-11 Spray evolution under various air density [60]

In Kourosh's study [11], the plume length presented a linear increase, especially under low injection pressure and back pressure. When the air density decreased from 47 to 20 kg/m^3, the dispersion angle reduced from 20°to 16° shown in Figure 2-12.

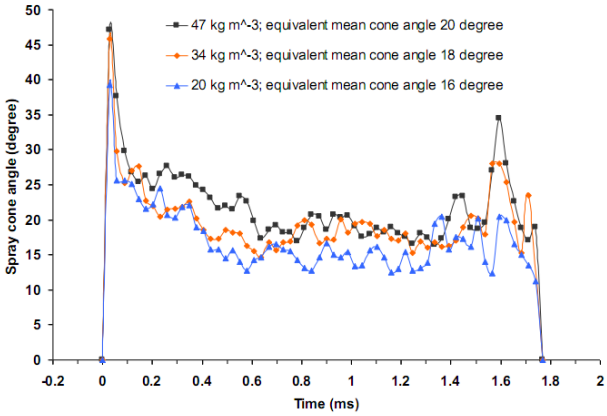

Figure 2-12 Plume angle development with various air density [11]

2.5.4 **Ambient temperature**

The ambient temperature mainly impacts the evaporation rate thus the microscopic and macroscopic features. Hiroyasu & Arai [25] reported that hot ambient air can reinforce the fuel evaporation at the outer edge and considerably suppress the development of the plume angle. Siebers [61] investigated the characteristics of diesel spray with ambient temperature varying from 700 to 1300 K and fuel temperature ranging between 375 and 400K. It was shown that raising both temperatures leads to a considerable reduction of penetration length. Aleiferis [62] also reported similar results.

Kourosh [11] compared the penetration length of plume under hot and cold ambient air condition and reported that elevated ambient air temperature can substantially decrease the plume length (Figure 2-13). The boosted evaporation at the front is responsible for this reduction. Owing to the dense jet at the beginning of the injection, the plume penetration rate showed little dependence on the ambient temperature but was more susceptible to the gas density. However, as the plume progresses, the drop concentration decreased and the heat and momentum transfers were boosted at the front periphery. Consequently, the clusters at the leading edge detached more quickly, leading to much lower plume length although the lower gas density elevated the penetration rate. What's more, when the temperature was increased from 273 to 667K, and the injection and gas pressure kept constant, being 160 and 6Mpa respectively, the cone angle dropped from 20 to 18°.

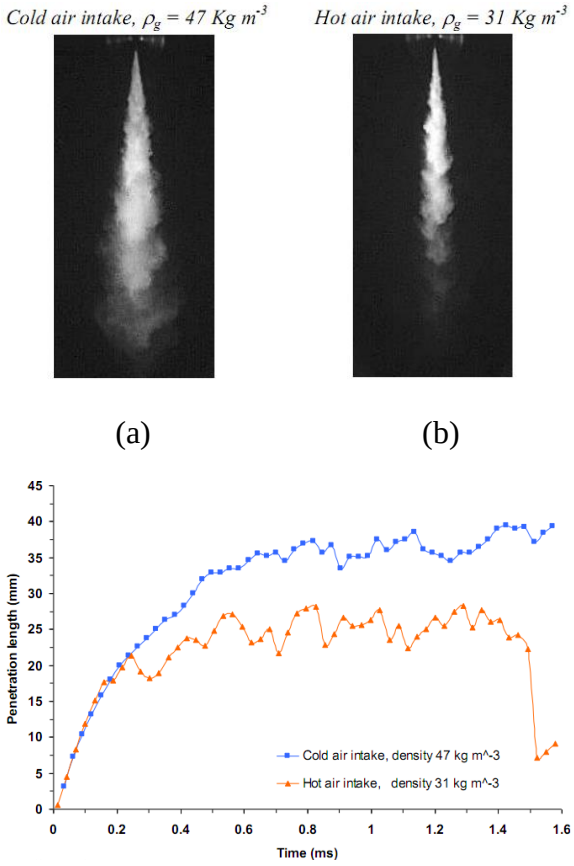

Figure 2-13 Influence of ambient temperature (160/ 6 Mpa) [11]

Lacoste [51] reported that raised air temperature lead to smaller droplets at the periphery. The particles at the core center on the other hand were nearly immune to the variation of temperature due to the high density. Tabata [63] also reported that the enhanced evaporation under high ambient temperature caused smaller SMD.

2.5.5 **Fuel temperature**

The dominant effect of raised fuel temperature is the appearance of the cavitation which boosts the plume break-up [31]. Cavitation and turbulence coupling with atomizing physics exert profound influence on the spray performance [64]. Cavitation is beneficial to break-up,

liquid atomization, droplets breaking-up and air-entrainment, but under extreme condition, can lead to hydraulic flip which can deteriorate the atomisation [65].

One of the well accepted expression of cavitation number *K* is:

$$K = \frac{p_{inj} - p_v}{p_{inj} - p_b} \qquad \text{Equation 2-17}$$

Where p_v is vapor pressure.

Aleiferis [62] experimentally studied to what extent can the fuel temperature, fuel properties and fuel pressure impact the cavitation with gasoline and its blends with ethanol. The injectors were refined to be a real-sized optical one with hole diameter of 0.2 and 0.5mm, with the length/diameter ratio of 5. The temperature was set to 20, 50 and 90℃. It was revealed that cavitation turned up in the liquid when the ambient pressure was lower than vapour pressure. The air resolved in the liquid was released, and foams and bubbles were observed (Figure 2-14). When *We* number was higher than 3500-3900 and Re was higher than 17000-19000, the transition to cavitating flow would ensue. In all cases, the spray was not symmetric, that is the side cone angle with cavitation was wider than the counterpart. The result also demonstrated that the cavitation which originated at the upstream of the flow generally propagated to the downstream of the nozzle hole with the rise of the fuel temperature.

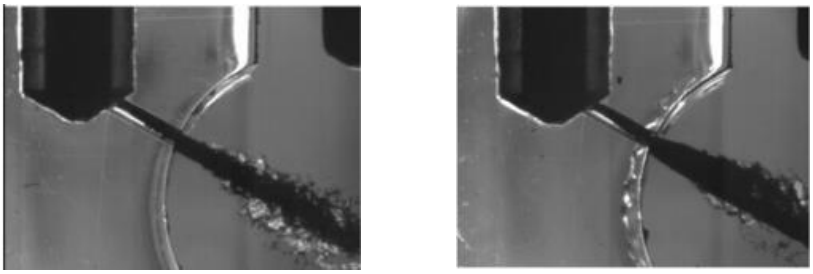

(a) (b)

Figure 2-14 Cavitation under (a) low (20℃) and (b) high (90℃) temperature [62]

High temperature condition enhance the fuel disintegration further as the rise of temperature can significantly alter the fuel physical properties ,for example, the vaporization pressure, viscosity as well as surface tension, accelerating the formation of bubbles. In this case, the foams and bubbles do not collapse but explode.

2.5.6 **Fuel properties**

Viscosity exerts significant influence on the mixture formation as both the MFR and particle size distribution are highly determined by the viscosity. High viscosity stabilizes the plume and prohibits the disintegration because more energy is required to counter the effects of the viscous force [44]. The reduction of fuel viscosity results in larger surface area for each unit mass, meaning better dispersion. The resultant better dispersion leads to lower penetration but larger plume angle [40, 66, 67].

Grimaldi et al. [68] reported that high viscosity and surface tension of the bio-diesels severely inhibit the atomization. Xiangang [59] investigated the macroscopic characteristics of diesel and bio-diesel (palm and cooking oil) with the injection pressure as high as 300 MPa.

Narrower angle was found for the bio-diesel. Under low back pressure condition, the spray length of bio-diesel was initially comparable to its counterparts before 0.3ms and then exceeded considerably. By contrast, little gap was shown under high ambient pressure, as shown in Figure 2-15.

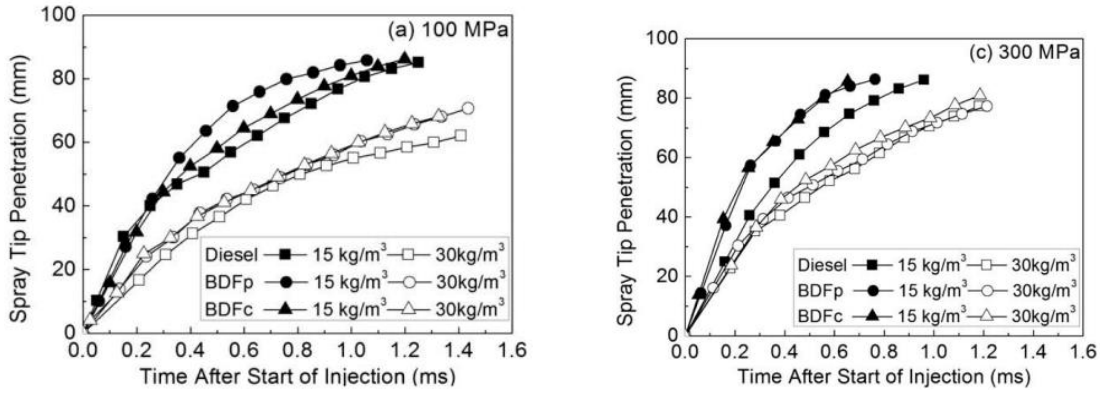

(a) (b)

Figure 2-15 Penetration comparison between diesel and bio-diesel [59]

Surface tension is another imperative factor for atomization since it denotes how much energy should be depleted to allow the bubbles to increase [62]. The increase of fuel surface area is greatly decided by the surface tension. Volatility is tightly involved with the spray evolution and mixing progresses. Highly volatile composition vaporizes with higher rate and this results in lower SMD, leading to shorter plume length. By contrast, for low volatile fuel, the drops size is larger and the plume length is longer, which presents the risk of wall impingement.

2.6 Investigating techniques

The optical methods are widely employed to study the spray because they are non-intrusive. The optical methods can be further classified into two types, photography and non-photographic methodologies. Generally, photography technique is adopted to investigate the macroscopic characteristics, for instance, the spray length, plume angle, fuel distribution and vortex. By contrast, the non-photography methodologies are applied to study the microscopic characteristics [11].

2.6.1 Direct Imaging

Direct Imaging is the most commonly employed diagnostic method. It is a technique that employs the CCD camera or the CMOS camera to take photos with a certain time interval to capture the evolution of the plumes or droplets. Aim to distinguish the spray and back ground, the illumination is employed by adopting the flashlight of laser. The layout of experimental system is shown in Figure 2-16. A photo is usually taken in advance. This initially taken photo is used as the back ground and should be subtracted during the image process to acquire better images through software.

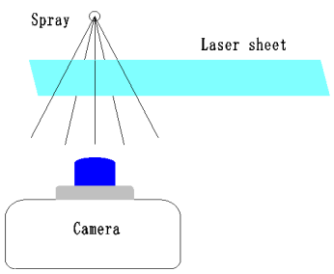

Figure 2-16 Schematic of direction imaging (adapted from [48])

2.6.2 **Schlieren technique**

Schlieren is used to capture the concentration of fuel by detecting the variation of refractive index caused by the variation of density. This technique enables the detection of both liquid phase and gaseous phase. The setup is shown in Figure 2-17. The parallel light beam is generated by a lens, L1, from light source S. After passing through the measuring field, the beam is then converged by the second lens, L2, and can be visualized by the screen. Some light of beam is deflected when the density of fluid in the test section changes. The deflected light shows a different trajectory to that of unaffected light. A key knife edge is placed at the focus of the second lens to block part of the unaffected light. The concentration of the interested fluid is shaped on the screen [69].

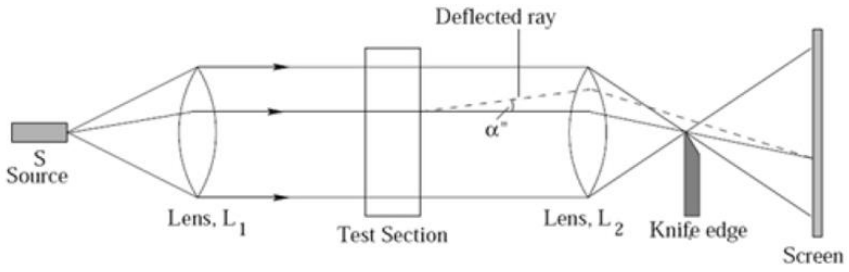

Figure 2-17 Set up of Schlieren technique [69]

2.6.3 **Laser Induced Fluorescence (LIF)**

LIF can be adopted to visualize the fuel no mater it is in vapor or liquid state [70]. LIF refers to the theory that the molecules are excited from ground state to a higher state when illuminated by a homogeneous light. The fluorescence signal can be obtained when the molecules return to their initial state. This process (step 1 and 2) is shown in Figure 2-18.

According to Seitzman [71], for the first step, if the molecules are illuminated by the light and the energy carried in the light goes well with the electronic transition in the molecules, the electrons are excited to a upper energy orbital as some light is absorbed. For stage 2, the energy is released and the fluorescence signal can be detected.

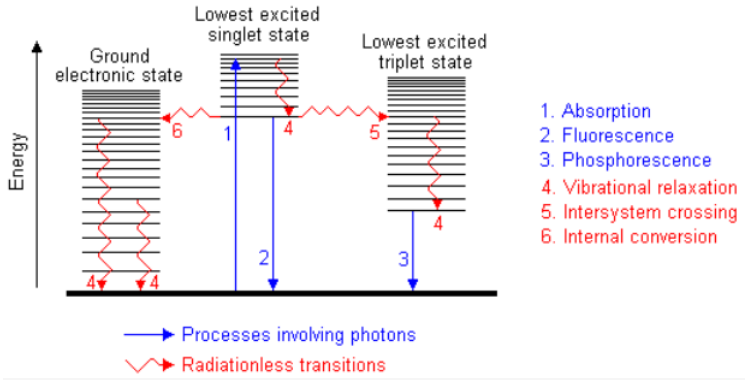

Figure 2-18 Energy state variation of molecular electron [72]

Two types of methods are involved for the signal capture. One is to get fluorescence from a deliberately added tracer and the other is to get fluorescence from the interested composition. For instance, fluorescence from OH can be used to calculate the front flame [73]. In CI engine, many tracers, for instance, acetaldehyde [74], 2-Butanone [75], can be used to visualize the spray.

LIF however has an inborn shortcoming, namely the high propensity of fluorescence quenching due to the oxygen [20]. This drawback is highly sensitive to many factors such as concentration and temperature, and some special measures should be taken during the testing process to alleviate the baneful influences [47, 60]. To minimize these downsides, the tracer should be carefully selected [76].

2.6.4 **Particle Imaging Velocimetry (PIV)**

Direct Imaging cannot be only used to capture macroscopic features but also detect the particle velocities. For this technique, some seeds or particles are added into the air in advance. To meter the particle speed, two consecutive illuminating pulses are produced and two corresponding photos for the droplets could be taken. Consequently, the locations of the droplets are mapped and captured, allowing the calculation of the velocities via dividing the distance between the locations by the time interval [48]. This methodology allows the time-averaged and space-averaged measurement.

2.6.5 **Laser Sheet Dropsizing (LSD)**

This technique is the combination of LIF and Mie scattering optical technique, which can be applied to map the SMD distribution [77]. LIF relates to non-elastic light scattering and Mie scattering relates to light elastic scattering. For LSD, some light is absorbed to stimulate the atoms, leading to the generation of fluorescent signal, and the rest is scatted elastically. That is to say, there are two categories of light, red-shifted and non-red-shifted. A filtering system is utilized to distinguish the two types of light. The elastic signal density relating to the particle surface area can be expressed as:

$$S_{Mie} = C_{Mie} d_i^2$$ Equation 2-18

The inelastic signal density relating to the particle volume can be expressed as:

$$S_{LIF} = C_{LIF} d_i^3$$

Equation 2-19

Where C_{Mie} and C_{LIF} are calibrating coefficients for elastic signal and inelastic signal respectively.

By integrating the two signals, the LSD signal, namely, the SMD, can be expressed as:

$$SMD = D_{32} = \frac{S_{LIF}}{S_{Mie}} = \frac{C_{LIF} \sum_i d_i^3}{C_{Mie} \sum_i d_i^2}$$

Equation 2-20

Sauter mean diameter is the ratio of the mean volume and mean total area. This parameter can be utilized to estimate the evaporating rate, so smaller SMD means finer breakup and atomization. The shortcoming to this methodology is the need of calibration as the dribble size should be known in the calibrating process. The PDPA technique is generally employed as it can precisely measure the drop size.

2.6.6 **Phase Doppler Particle Analyzer (PDPA)**

PDPA system could be utilized to meter the size and velocity of liquid droplets [27]. The PDPA diagnostic methodology is the combination of laser Doppler anemometer (LDA) and drop sizing technique. The layout of this technique is shown in Figure 2-19.

The laser emitted from the light source is divided into several beams with identical intensity and then converges at a certain distance by a lens to form a measuring volume. The

spatially distributed interfering fringes or stripes are correspondingly generated when the beams interfere at the measuring volume.

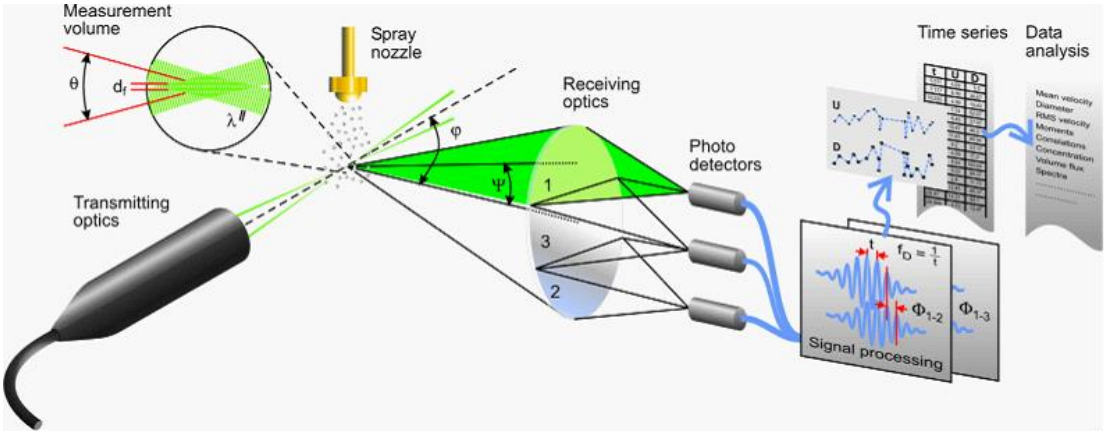

Figure 2-19 Schematic of PDPA [78]

The measurement of the drop speed and diameter can be achieved when the droplets flow through the stripes. The traverse of the drops leads to the light scattering, leading to a fluctuation at the measuring volume in terms of the light intensity. This fluctuation can be detected by the detectors which are amounted with a certain angle with the axis. The signal can be transferred into electric signal and the change rate is strongly related to the particle velocity. The frequency f of the variation of the light intensity in the measuring volume can be calculated via the Equation 2-21 [78].

$$f = \frac{2u_d \sin(\theta/2)}{\lambda} \qquad \text{Equation 2-21}$$

Where λ is light wavelength.

As the frequency can be detected, the particle velocity can be easily obtained when the rest parameters are known.

However, some problems need to be addressed before accurate measurement can be realized. From Equation 2-21 and the schematic of PDPA (Figure 2-19), same results can be derived no matter the particle traverses in the forwarding direction or inversely. Therefore, some measures should be taken to discriminate the two directions. Generally, the Bragg cells need to be applied to shift the frequency of laser beam, and frequency difference Δf is obtained. In this case, if the particle travels downward, the detected frequency is $f + \Delta f$, while if the particle travels upward, detected frequency is $f - \Delta f$.

To measure the particle size, two detectors are to be employed to capture the spatially scattered light by the round particle, presented in Figure 2-20.

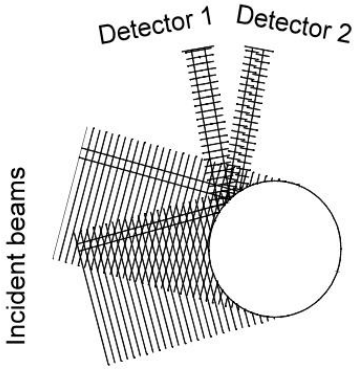

Figure 2-20 Light interference by the particle [78]

Although the two detectors receive the scattered light with the same amplitude and frequency, a phase difference which relates to the circular position exists between the two signals, as presented in Equation 2-22 and Figure 2-21. The equation shows a linear

relationship between the particle diameter D and phase difference $\emptyset$. Consequently, if the phase difference is obtained, the droplet diameter can be calculated.

$$\phi_{12} = \phi_2 - \phi_1 = 2\pi f \cdot \Delta t = \frac{\pi}{\lambda} D \times (\beta_2 - \beta_1)$$

Equation 2-22

Where $\Delta t$is time difference for the two detectors to receive the light due to position difference, β_1 and β_2 are the detector phase factors.

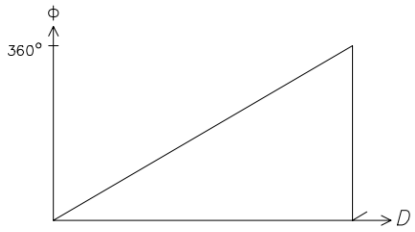

Figure 2-21 Relationship of phase difference and diameter [78]

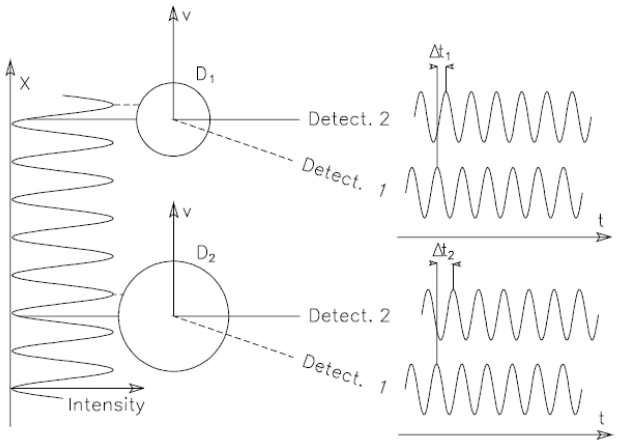

Figure 2-22 Phase difference between two detectors at different angles for particle with different sizes [78]

Equation 2-21 shows that bigger particles lead to larger phase differences. However, when the diameter of the particle rise to a certain point, the phase difference can be over 2π and false signal appears. To solve this problem, a third detector is adopted to get another

phase difference, eliminating this ambiguity. This additional detector can expand the measuring range with less accuracy, while the original two detectors enable accurate measurement but low measuring range.

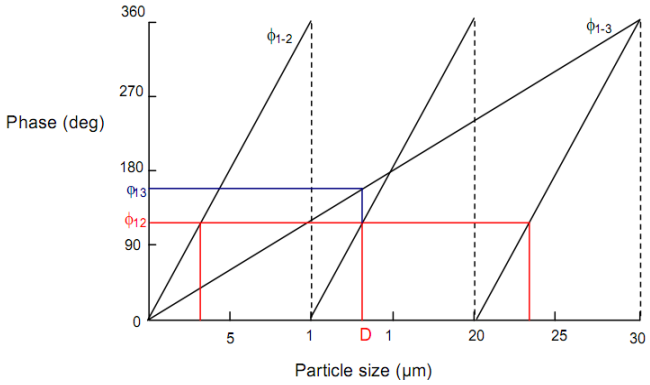

Figure 2-23 Phase difference calibrating curve [78].

In Figure 2-23, the phase difference between detectors 1 and 2 is $\emptyset_{12}$ and that of detectors 1 and 3 is $\emptyset_{13}$, the actual phase difference therefore can be gained by combining $\emptyset_{12}$ and $\emptyset_{13}$.

Another problem needing to be solved is that the type of light received by detector needs to be identified as there are several scattering mechanisms when the incident light illuminating a spherical droplet, namely the reflection , first order refraction and second order refraction, as shown in Figure 2-24.

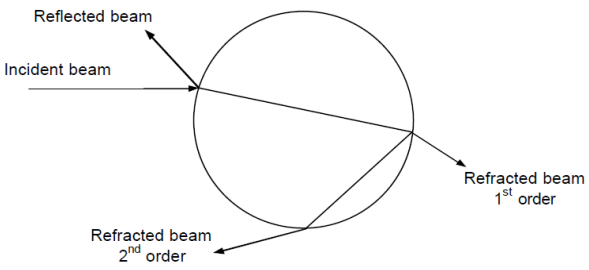

Figure 2-24 Light scattering mechanisms [78]

Both of the reflected and refracted light can be captured to determine the particle size. To distinguish the two kinds of light, the establishment of the system needs to guarantee that one type of the light is dominant. The light intensities for various lights are different for different directions and positions, as presented in Figure 2-25.

Generally, the dominant light at 30º to 80º is the refracted one, by contrast, between 80º and 110º the dominant light is the reflected. PDA measurement generally is based on the detection of the first refracted light, thus the detectors are oriented at 70º where strong desired signal can be got.

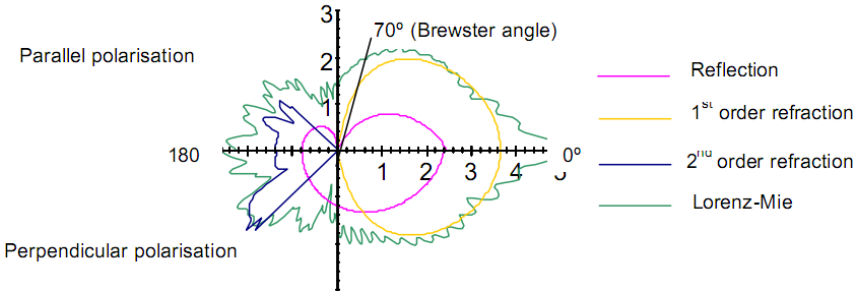

Figure 2-25 Light intensity at various angle [78]

Chapter 3 **Experiment apparatus**

This chapter mainly focuses on the introduction of experimental setups involved. The methods of data processing are also discussed.

3.1 Mass flow rate measurement instrument

It is of overriding importance to accurately measure the rate of fuel injection and manage the working characteristics of the engine, minimizing the fuel consumption. Several methods are available for the measurement of MFR. The principles are briefly introduced, including the principle of Bosch method employed in this study.

3.1.1 **Milan Marcic's method**

Milan Marcic proposed two methods to measure the MFR. The theory of the first method (also called electrical charge method) is based on the detection of the electrical charge produced by the electrode when being collided by fuel with high velocity (Figure 3-1) [79].

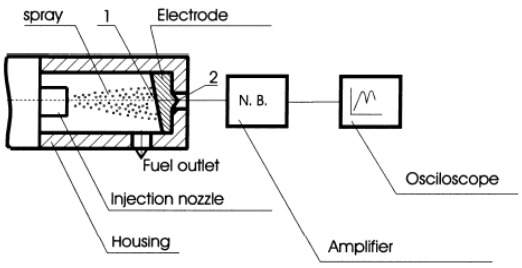

Figure 3-1 Diagram of the electrical charge method [79].

When the fuel droplets with high speed hit the lean surface of the electrode, a large proportion of the kinetic energy is automatically transformed into heat due to dispersion,

heating the electrode. Consequently, the electric signal is produced, partly, owing to the temperature difference between side 1 and side 2 caused by the heating and partly thanks to the loss of free electrons caused by the rub [79]. However, as the electric charge is composed by two parts, complicated algorithm to deal with the signal is required and super surface finish of the electrode is demanded to guarantee the reliability and stability of the signal.

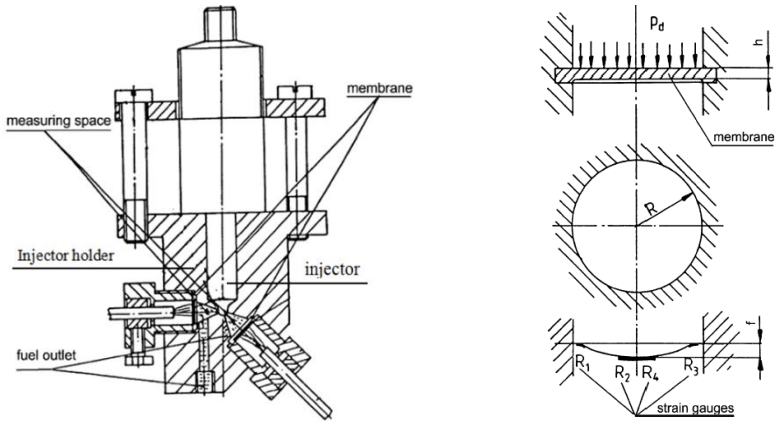

(a) (b)

Figure 3-2 The structure of the deformation measuring instrument [80]

The principle of the second Milan Marcic method (also called deformational measuring method) is shown in Figure 3-2 [80]. Four strain gauges were attached on the membrane, establishing a Wheatstone bridge. The membrane deformation occurs when the fuel is injected into the measuring space, establishing a high pressure. The deformation of the membrane can be expressed by the resistance variation of the strain gauges, which can be translated into electric signal. As a result, the accurate mathematical relationship between the pressure at the outlet of injector and the output of the Wheatstone bridge can be

determined, thereby measuring the MFR. However, the drawback is the complexity and it can only be used for injectors without too many holes (three or four) [80].

3.1.2 **Zeuch method**

The principle of this well-known method, constant volume method, is shown in Figure 3-3. This method works on the fact that the pressure of the constant chamber with volume V increases from p to (p+dp) when more fuel with volume of dv is injected in. The relationship between dp and dv reflects the compressibility of the liquid, known as bulk modulus. The MFR can be obtained through the varying trend of pressure, shown as [81]:

$$\frac{dm}{dt} = \rho_l \times \frac{V}{K_B} \times \frac{dp}{dt} \qquad \text{Equation 3-1}$$

Where: m is fuel mass, V is volume of the chamber, K_B is the bulk modulus of the liquid.

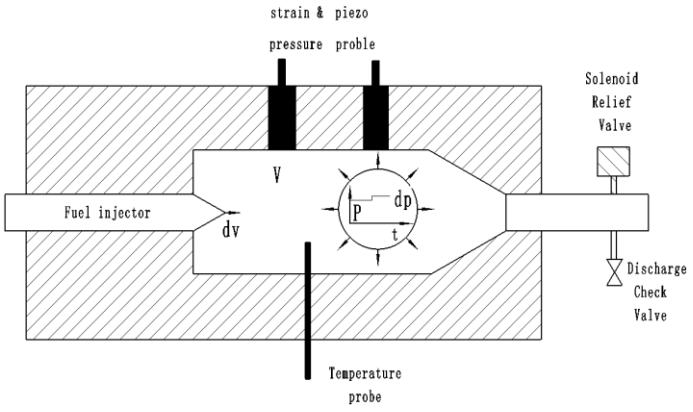

Figure 3-3 Schematic of Zeuch method [82]

3.1.3 **Bosch method**

1) Principle of Bosch method

Bosch method [83] was employed in the present study due to its simplicity and high accuracy. The fundamental principle of this method lies in the fact that the MFR can be calculated when the fuel with a certain speed passes through a known area. The governing formula is

$$Q = F \times u \qquad \text{Equation 3-2}$$

Where Q is fuel quantity (L/s), F is the flow area (dm^2) and u is spray speed (dm/s).

Pressure can be obtained through the relationship with velocity [84] shown as:

$$p = a\rho_l u \qquad \text{Equation 3-3}$$

Where a is sound speed in the tested fuel.

For a measuring chamber with fixed cross-section area, when tested fuel flowing through, the increment of pressure dp is attributed to the fuel spray velocity increment du. This relationship can be given as: $dp = a\rho_l du$

Combining the aforementioned two equations, one can get the flow rate:

$$\frac{dQ}{dt} = \frac{F}{a\rho_l} p \qquad \text{Equation 3-4}$$

By integrating the this equation over the injecting duration, the quantity of the injected fuel can be expressed as [83]:

$$Q = \int_{start\,of\,injection}^{end\,of\,injection} \frac{dQ}{dt}.dt = \frac{F}{a\rho_l} \int_{start\,of\,injection}^{end\,of\,injection} pdt$$

Equation 3-5

2) Schematic of the long tube instrument

According to Equation 3-5, it can be found that the fuel flow is a function of pressure varying with time and can be calculated as long as the pressure is known because other variables (cross area, sound speed and fuel density) could be obtained. Basing on the aforementioned principle, a long tube measuring system was built with an improved method of measuring the pressure pulses using external strain-gauges. Strain gauges were used to detect the real time fuel pressure at the outlet of the injector and the signals were recorded by an ultrahigh speed data acquisition card (500k Samples/sec). These data were then conditioned and processed with an in-house built code.

The schematic of the improved instrument is shown Figure 3-4. The lock (1) is employed to fix the injector (3) on the injector holder (4). One end of measuring tube (6) is connected to the injector holder (4) and the other end is connected to the relief valve (8). Two strain-gauges (5) located at the tip of the injector (3) are employed to gain the pressure waves. The instrument is protected from damaging by a relief valve (8) in the case of being over pressurized. The back pressure (P_b) in the measuring pipe (6) can be regulated by the needle valve (11). A pressure gauge (10) is used to measure P_b. The fuel temperature can be monitored through a thermocouple (K type) installed on the thermocouple holder (12). The volume and weight of the injected fuel can be measured through the cylinder (13) and the

weighing scale (14) respectively. A leaned injector holder base (3) and tube holder (7) are used to make sure that no air bubbles are trapped in the tube.

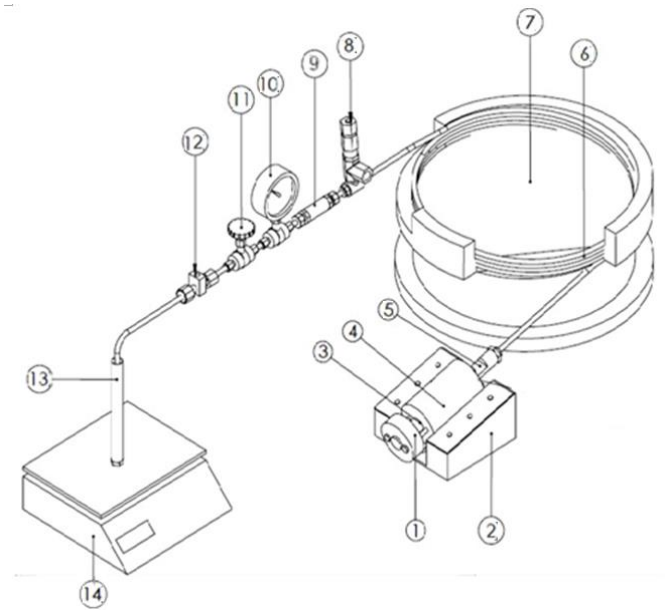

1-Lock；2-Injector holder base; 3-Injector; 4-Injector holder; 5-Strain gauges; 6-Measuring tube; 7-Tube holder; 8-Relief valve; 9-Filter; 10-Pressure gauge; 11-Needle valve; 12-Thermocouple holder; 13-Cylinder; 14-Weighing scale;

Figure 3-4 Isometric view of the MFR measurement instrument (adapted from [84])

High measuring accuracy for mass flow rate measurement (over 94% when injection pressure is higher than 35 MPa and lower than 130 MPa) and repeatability can be obtained with this instrument after careful calibration. It should be noted that the accuracy is related to the injection pressure. If the injection pressure is too low (30 MPa in this study), the resultant low signal/noise ratio of the data acquisition system leads to inaccuracy. During the process of calibration, 5 times of injections (200 injections for each time, meaning 1000 injections in total) were carried out. For each group, the accumulated fuel mass obtained by

integrating the MFR was used to compare with the actual injected fuel mass (obtained by measuring with a weighing scale). The results showed high accuracy for fuel mass injected with the error of less than 6%. Comparison of fuel mass gained from integration among the 5 groups presented the highest variation of 5.8%. After the calibration, 200 injections tests were carried out for each case studied.

When aim to study the influence of fuel temperature on the injection and spray characteristics, the injector and its accessories (1-5 parts) were kept refrigerated in a freezer. With this freezer, the fuel temperature can be kept at -18 degC. When the required fuel temperature was higher than room temperature (25 degC) to study the effect of fuel temperature on the injection characteristics, the injector and its accessories were kept in a trough. The trough is filled with warm water and the temperature can be varied from room temperature to 50 degC or even higher.

3) Injector

Two injectors were employed in this study. One is a solenoid driven single-hole injector with sharp inlet. The diameter of the cylindrical hole is 0.18 mm and length-diameter ratio L/D is 4.4. The other one is an 8-hole piezoelectric injector with the degree conicity $AF = \frac{Inlet\ area}{Outlet\ area} = (d_i^2 - d_0^2)/d_i^2$ of 19%. The outlet diameter of the holes is 0.118 mm. For the study of injection strategy, the 8-hole piezoelectric injector was used due to its quicker response and higher MFR (stronger signal/ noise ratio). The single-hole solenoid driven injector is used for MFR measurement with single injection strategy. This single-hole

injector was also employed for all photography tests so that the hole-to-hole variation for multiple-hole injector can be eliminated.

4) The data acquisition system

Data acquisition and processing system (including the circuit, amplifier and the codes for data acquisition and processing) was developed by the author, shown in Figure 3-5. The pressure signal is transferred into strain and then into voltage. The weak voltage signal obtained from the circuit is amplified by the amplifier, acquired by the NI data acquisition card and then stored in a computer. With the components and printed circuit board bought form RS components, the author built and calibrated the amplifier, shown in Figure 3-6.

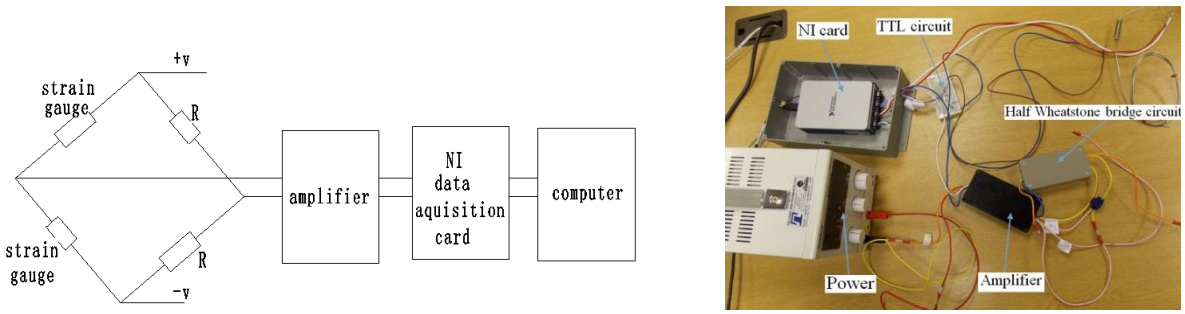

(a) (b)

Figure 3-5 Data acquisition system

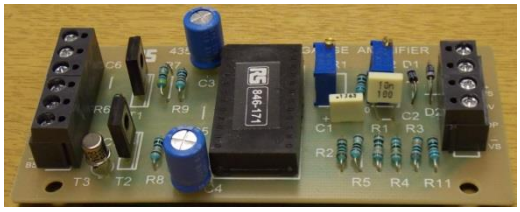

Figure 3-6 Amplifier

The data acquisition card is a NI card 9222 with the sample rate as high as 500k Hz and gain error ranging from -0.02 % to +0.02 %. The data acquisition and processing programs were written with Labview script. The panel of the code can present the pressure signal, TTL, MFR and injected fuel mass, as shown in Figure 3-7.

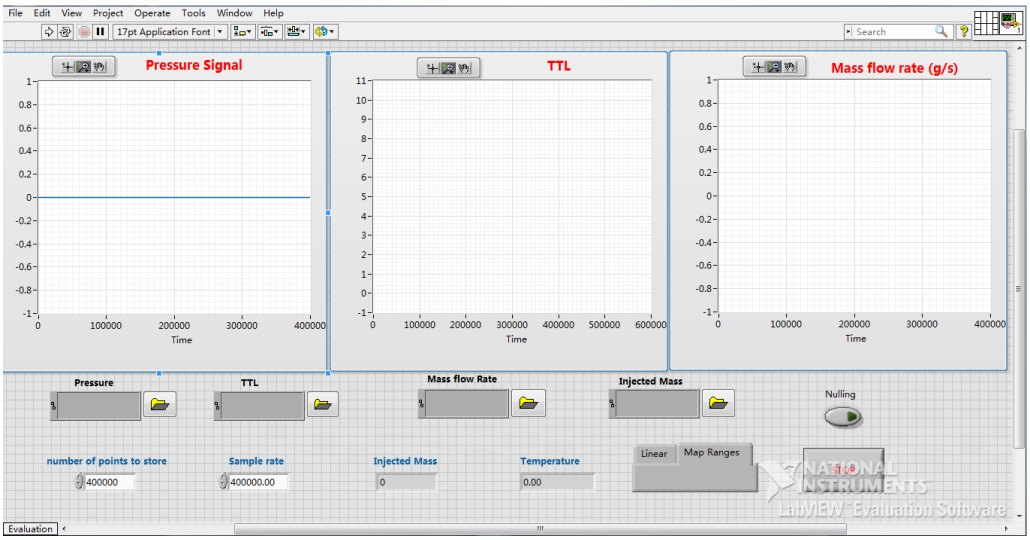

Figure 3-7 Panel of data acquisition

3.2 Setup for ultra-high speed photography

Ultra-high speed photography technique was employed to study the primary breakup characteristics.

3.2.1 The cooling system

The primary breakup tests with ultra-high speed photography technique were carried out under room temperature (RT, 25 degC) and low temperature (LT, -2 degC) for fuel temperature. However, ambient temperature was kept at RT and ambient pressure was atmospheric for both test conditions. As mentioned before, the study on the effects of low

fuel temperature is very useful for the engine performance under cold start condition or cold idle. It is interesting to investigate how the spray behavior changes with the variation of fuel temperature and what the special spray characteristics are when split-injection is employed.

The temperature of the pressurized fuel from the high pressure pump varies significantly during the test. The success of the tests for LT is therefore to keep the fuel temperature low and stable. A special in-house built cooling system, the blue part shown in Figure 3-8, was employed to stabilize the fuel temperature. A pre-cooling barrel which was filled with ice and water was used to precool the pressurized fuel from the common rail. Since it was difficult to cool the warm pressurized fuel directly, the injection rate was set to very low (1 Hz) so that the water/ice mixture can cool the pipe and then the fuel effectively. The pre-cooling barrel was wrapped with adiabatic material to minimize the heat transfer between the ice-water mixture and the ambient. The high heat capacity of water and ice enables the system to precool the warm pressurized fuel effectively up to 5 hours. A thermocouple was installed in the pre-cooling barrel to monitor the temperature of ice-water mixture. The temperature of the mixture varied between 0 and 1 degC during the tests.

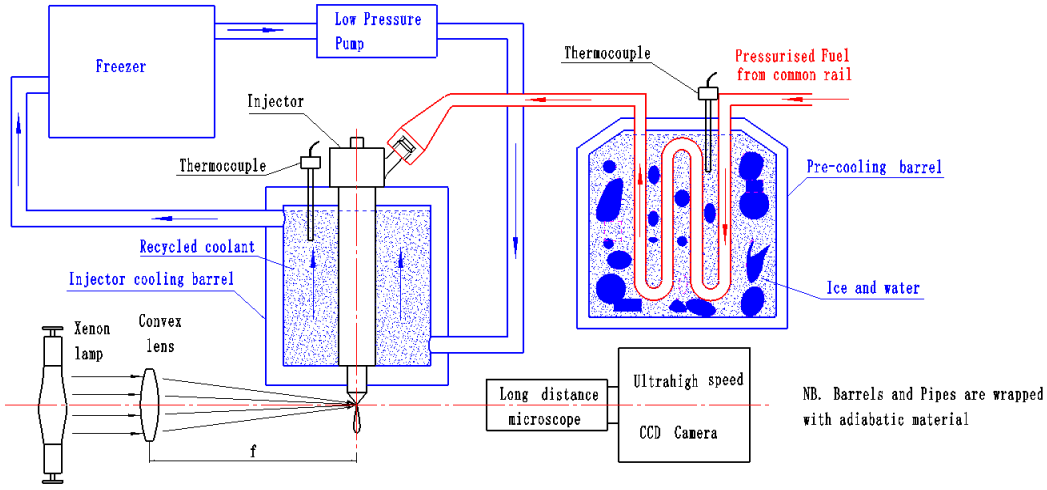

Figure 3-8 Layout of the experimental setup

To further effectively cool the pressurized fuel, the injector was cooled through a recycle cooling system. The recycle cooling system consists of an injector cooling barrel, a freezer and a low pressure pump. The injector was plugged into the cooling barrel and only the tip of injector was exposed in the air. The freezer can keep the temperature stable as low as -18 degC. The flow rate of the coolant was regulated by the low pressure pump controlled by a control module. Another thermocouple was employed to monitor the temperature of the coolant in the injector cooling barrel. The lowest stable temperature of the coolant in the injector barrel was -2 degC due to heat transfer between the coolant and the ambient environment. The temperature of the coolant in the injector cooling barrel generally varied between -3 and -1 degC. All the parts (pipes, barrels and low pressure pump) were wrapped with adiabatic material to minimize the heat transfer between the cooling system and the ambient environment. During the test, if any of the temperatures for the ice-water mixture in the pre-cooling barrel and the coolant in the injector cooling barrel varied beyond their corresponding ranges, the test was stopped to allow the coolant to be refrigerated. Generally,

due to the superb cooling effect of the cooling system, the tests could be being carried out for up to 1 hour continuously and high testing condition consistency was successfully achieved.

3.2.2 **Optical arrangement**

It should be noted that the optical setup (Figure 3-8) was developed by a former PhD student (Dr Haichun Ding) with the help of the author of the present thesis. A highly resolved Questar QM 100 Long Distance Microscope (Figure 3-9 (a)) was employed to visualize the spray morphology development. The specifications are shown in Table 3-1. The working distance of 17 cm which enables the CCD camera to focus on the view field of 2.3 mm downstream of injector was employed in the present study. It should be noted that this microscope is very sensitive in terms of focusing and great care was taken during the process of focusing.

Table 3-1 Specifications of the long distance microscope

Working distance	Resolution	Magnification	Format
15-35 (cm)	1.1 microns at 15 cm	To 34 times at image plane	Diffraction limited field 12 mm

The ultrahigh speed camera involved is a Shimadzu HPV2 CCD digital camera (Figure 3-9 (b)) with maximum frame speed of 1,000,000 fps. The constant resolution is 312×260 $pixel^2$. The advantage of this CCD camera is its ultra-high frame speed, however, only 102 images can be stored due to the limited memory. Because of the employed ultrahigh frame speed for primary breakup test, 1 million fps (meaning 1 μs interval between two consecutive images), a xenon lamp with power rate of 500 Watt was used as light source. It was found

that direct back lighting could not provide sufficient light for illumination. A convex lens was therefore employed to focus the light to sufficiently illuminate the spray.

(a) (b)

Figure 3-9 (a) QM 100 Long Distance Microscope and (b) ultra-high speed camera

3.3 Setup for high speed imaging

The high speed photography tests were carried out under both RT and LT. Under RT, a high pressure vessel with which the back pressure can be varied was employed, shown in Figure 3-10. This vessel was built by a former PhD student (Dr. YanFei Li). The pressure limit of the vessel is 11MPa which allows the combustion test in the chamber. The three side windows allow the application of back-lighting, PDPA and Schlieren [85]. The height of the chamber is 100 mm and the inner diameter is 86 mm. More details about the vessel can be found in [85].

In present study, the single hole injector was vertically installed. The xenon lamp was positioned at the side window to illuminate the spray. The aforementioned CCD camera

with a 105 mm Nikon lens (aperture was set to maximum, 2.8) was located at another side window, forming a 110° angle with the side window for the xenon lamp.

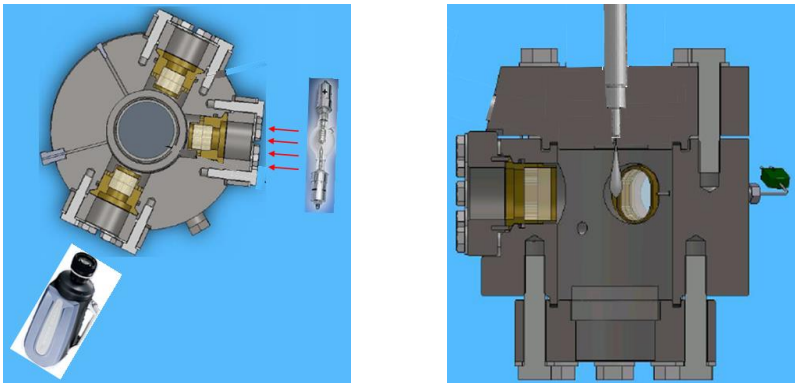

Figure 3-10 Set up for the high speed imaging(adapted from [85])

For LT tests, the former cooling system shown in Figure 3-8 was used. The xenon lamp and CCD camera were positioned the same to the setup under room temperature, namely, same angle and distances. For this setup, the injector was installed in the cooling barrel (as shown in Figure 3-8) and it is therefore impossible to vary the back pressure due to physical interference. The back pressure was consequently set to atmospheric condition. For high speed imaging, to capture the whole process of the spray development, the frame speed of the camera was set to 63k Hz (resolution of 312×260 pixel^2) for single injection and 2-split injection strategies due to the limited memory of the camera. The corresponding time interval between two images is 16 μs. By contrast, for 3-split injection strategy, with this frame speed, it is impossible to capture the whole process of the spray development due to the limitation of memory. This problem was solved by taking the images for injections twice with a certain time difference, as presented in Figure 3-11. This method inevitably leads to some inaccuracy due to injection-injection variation. However, since the separated split

injections are distinguishable and this inaccuracy does not affect the analysis of spray characteristics.

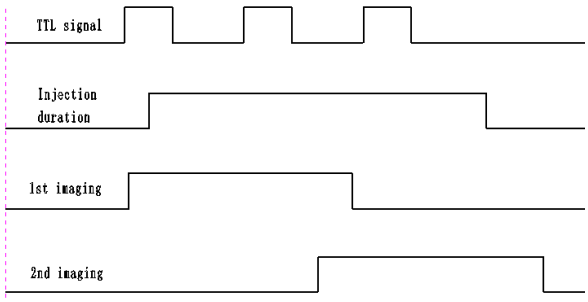

Figure 3-11 The synchronization of the imaging for 3-split injection

3.4 PDPA setup

The microscopic characteristics were investigated by employing PDPA under atmospheric condition because of the difficulty of the application of high pressure vessel. It can be seen from the schematic of the rig (Figure 3-12) that one PC was used to control the PDPA signal processor and the other PC was separately used to control the injection parameters. An air blower and a filter were employed to suck the air out so that the lab was free of contamination and health risks. The main parameters of the PDPA setup are shown in Table 3-2. More details about the setup of the PDPA can be found in [85].

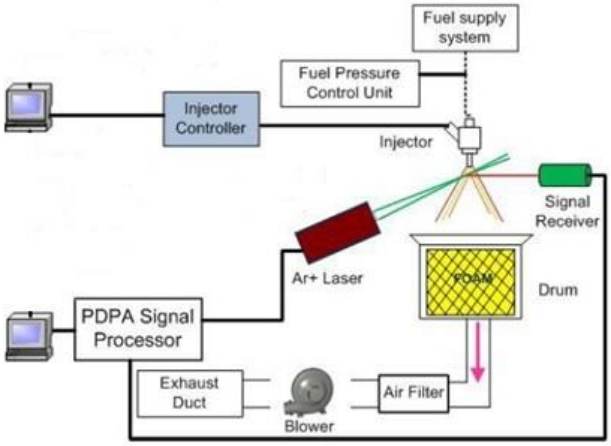

Figure 3-12 PDPA setup (Adapted from [85])

Table 3-2 Main parameters of PDPA setup [85]

Wavelength	Scattering mode	Scattering angle	Beam diameter	Optic focus
514.5/488 nm	Refractive	70 deg	2.2	310 mm

3.5 Test fuel

In this study, winter grade pump-grade diesel (WD) which shows good flowing ability at low temperature was utilized. WD is less viscous than ultra-low sulphur diesel (summer grade) (ULSD), especially under low temperature (2.06 cSt for WD and 2.87 cSt for ULSD @ 40 degC [85]). WD also has lower density than ULSD (806 kg/m^3 for WD and 827 kg/m^3 for ULSD @ 15 degC). The density has slight effects on the injection characteristics except on the MFR and on the effective velocity. The variation of density (around 3% when fuel temperature decreases from 25 degC to -2 degC) under low temperature is much smaller than that of viscosity [24, 86]. The variation of density is therefore ignored in this study.

The significant variation of fuel properties with temperature is of great importance for spray characteristics. Two important properties, namely viscosity and surface tension, were quantified under various temperatures, shown in Figure 3-13. According to the measured values of the two properties, it can be seen that viscosity varies exponentially while the surface tension varies linearly. An exponential function and a linear function are therefore proposed to fit the measured values respectively, shown in Equation 3-6 and Equation 3-7 [24].

$$\nu = A*e^{K_\nu *T+B} + \nu_0 \qquad \text{Equation 3-6}$$

$$\sigma = K_\sigma *T + \sigma_0 \qquad \text{Equation 3-7}$$

Where K_σ, σ_0 , A, K_ν, B and ν_0 are coefficients.

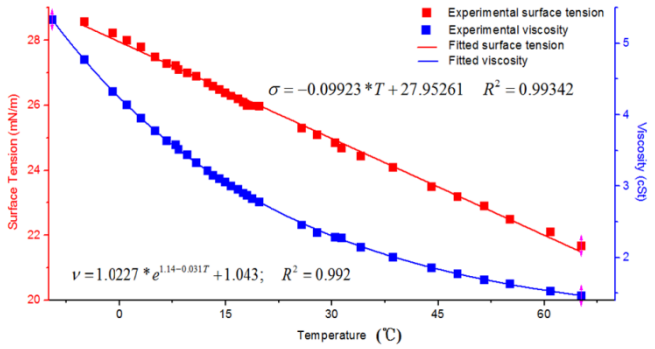

Figure 3-13 The variation of fuel properties with temperature

The values of these coefficients are presented in Figure 3-13. It clearly shows that high accuracy is obtained with R^2=0.992 for viscosity fitting and R^2=0.993 for surface tension fitting.

3.6 Data processing

The data of MFR were processed with the codes written by the author with Labview script and these codes were embedded in the data acquisition system. The images were processed with Matlab codes written by a former research fellow (Dr Xiao Ma). It should be pointed out there are some differences for spray characteristics between primary breakup and high speed imaging though the methods of image processing are similar.

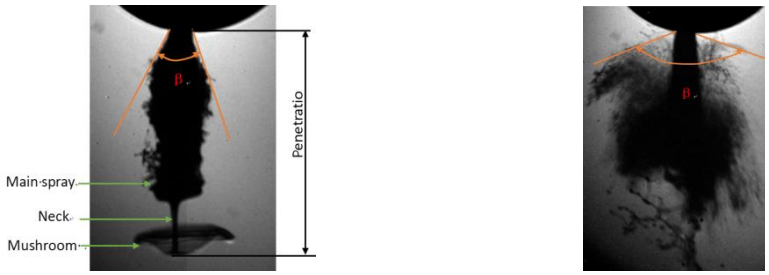

a b

Figure 3-14 The defination of penetration (a) and cone angle (single injection (a) (60 MPa) and split injection (b) (the third split injection under 90 MPa with 0.2 ms dwell))

(1) Image processing for primary breakup; the fuel spray area, cone angle and penetration are employed to characterize primary breakup. The cone angle is formed by two tangent lines originating from the injector tip and passing through the maximum radial positions of the two sides of the spray, as shown in Figure 3-14. It should be noted that for split injection, the cone angle may be very large due to collision and this is different from the traditional macroscopic cone angle, as shown in Figure3-14 (b). The penetration length is the distance between the injector tip and the farthest point of the spray (Figure 3-14 (a)). For some cases with split injection (Figure 3-14 (b), the third split injection under 90 MPa with 0.2 ms dwell), it is

impossible to identify the boundary between split injections and the penetration is not calculated.

(2) Image processing for high speed imaging; for single injection strategy, it is easy to process the images and high accuracy can be obtained. Attention should be paid to the image processing of split injection strategy. When the injection pressure and back pressure are high and the dwell interval is short, the interaction between two split injections is strong, making the distinction of boundary between split injections difficult.

Figure 3-15 Example of the image processing (Pinj = 60 MPa, Pb = 2.0 MPa, dwell = 0.2 ms)

In this study, to abstract the information for the second injection, two different thresholds for image processing were employed to identify the boundaries of closely coupled split injections. This means that if the boundary detection of the first split injection is accurate, the detection of the second injection is not accurate. That is to say the values of the macroscopic characteristics (penetration, spray area) of the second split injection are smaller than those of the first injection because the remaining undispersed fuel of the first split injection should not be detected, as shown in Figure 3-15. In this study, the side-lighting can lead to unevenly distributed illumination, causing the failure of the detection of the periphery

of the illuminated side. However, since side-lighting was employed for all tests and this failure is ignored in this study.

The injection condition is important for the interaction intensity between consecutive split injections. When the interaction is stronger, the detection failure of the second split injection occurs, as shown in Figure 3-16. It is shown that the inaccuracy increases with the interaction intensity . The cases with too strong interaction (under high injection pressure and back pressure) were not considered due to the high inaccuracy.

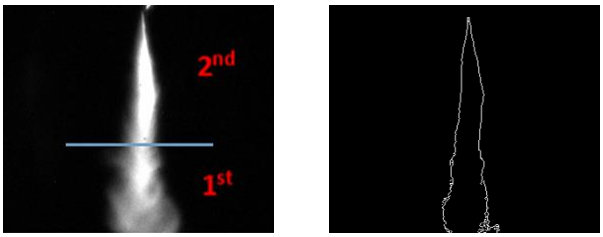

Figure 3-16 Influence of interaction on the identification of spray boundary

(P_{inj} = 60 MPa, P_b = 3.5 MPa, dwell = 0.2 ms)

The choice of the thresholds (0.12 and 0.2 in present study) is paramount for the accuracy of the spray boundary identification. If the difference between the two thresholds is large, the detection of the first or the second split injection is distorted although the two consecutive split injections can be clearly separated. By contrast, if the difference between the two thresholds is small, it is difficult to distinguish the two closely coupled injections. In this study the thresholds were obtained when two closely coupled injections can be separated and the inaccuracy is smaller than 8% (the actual penetration length and area can be obtained by counting the pixels).

Chapter 4 **Injection characterization under room temperature and cold condition**

The objective of this chapter is to investigate the injection characteristics with single and closely coupled multiple injection strategies under room temperature (25 degC) and low temperature (-18 degC). The effects of cold condition were also studied under both room temperature and low temperature with various injection pressures and back pressures. All tests were carried out with long tube MFR measuring instrument.

4.1 Introduction

Laminar flow, turbulent flow and cavitating flow are the main flow patterns in nozzle hole [87-90]. Turbulence and the transition from laminar to turbulent flow are the main flow regimes for convergent nozzles. Cavitation can be considerably relieved for convergent injectors, and the hole convergence allows fuel and nozzle wall to interact strongly [87, 91]. For laminar flow, the reduction of effective discharging area results in low discharge coefficient (C_d), while turbulence leads to high C_d.

Recent studies of light duty diesel engine show the trend that lower compression ratio with boosted air intake eases the emission control. However, the engine cold start becomes a problem because the variation of temperature contributes to the change of ignition delay thus changes of in-cylinder pressure [1, 92]. Consequently, the injection characteristics under low temperature (LT) require to be deeply studied. Influences of viscosity are more apparent

under low temperature because of its significant variation with temperature. Low temperature generally contributes to lower Re thereby to lower velocity coefficient and lower C_d [93, 94]. The reduction of temperature also leads to the decrease of MFR by increasing the chances of laminar flow [95-97].

Multiple-injection which shows complex injection characteristics can effectively improve engine performance by stabilizing the engine combustion and reducing misfire for cold idle operation [1, 16, 17]. Carlucci [24] reported that split injection can effectively control the ignition, giving high flexibility to control the emissions. The author pointed out that split injection can effectively boost the cold start and cold idle performance because of better fuel mass distribution and fuel mixture.

Some studies on injection characteristics with split injection strategy are accessible. For instance, Mohammad and Álvaro [21, 22] studied the influences of fuel quantity distribution between split injections and dwell on MFR. This study seems to show great similarity to the present study. However, the measurement of the MFR in that study was carried out by employing a Constant Volume Chamber (CVC). By contrast, in present study, the Bosch method was used. The principles of the two methods are different, and the measuring accuracy is different. Kourosh [11] reported that split injections present less injected fuel mass than the single injection case with equal energizing duration.

The aforementioned studies have given details on the basic injection features under room temperature. However, it is still unclear how the flowing regime changes under cold start

condition when injection parameters vary. Apart from that, the split injection strategy has not been sufficiently studied. The injection characteristics with split injections are significantly different from single injection because the needle reciprocates several times in a short time [19]. The splits interact with each other to different degree with a wide range of injection dwells and injection durations, and the MFR interaction is thought to significantly affect the injection characteristics. Besides, the impact of fuel temperature on the interaction between splits also requires a deep study.

4.2 Theoretical background for injection characteristics

Discharge coefficient is a useful parameter used to study the flow characteristics in a nozzle hole. It denotes the effective fuel flow of the nozzle. It can be calculated by the ratio of actual and theoretical fuel MFR, shown as:

$$C_d = \dot{m}_{act} / \dot{m}_{th} \qquad \text{Equation 4-1}$$

Where $\dot{m}_{act}$ is the actual MFR measured through the long tube measuring instrument and $\dot{m}_{th}$ is the theoretical MFR calculated through Bernoulli's equation expressed as:

$$\dot{m}_{th} = n_{hole} * (\pi d_o^{\,2} / 4) * \sqrt{2\rho_l \Delta p} \qquad \text{Equation 4-2}$$

Where Δp is the pressure difference between injection pressure and back pressure.

Re is another important parameter that denotes the significance of injection pressure difference for the flow characteristics. The injection pressure difference results in different outlet velocities. The adapted *Re* from Equation 2-2 is shown in Equation 4-3:

$$\mathrm{Re} = V_{act} * d_o / \nu \qquad \text{Equation 4-3}$$

Where V_{act} is the actual flow velocity at the injector outlet which can be calculated using the following Equation:

$$V_{act} = \frac{\dot{m}_{act}}{n_{hole}(\pi d^2/4)\rho_l} \qquad \text{Equation 4-4}$$

More detailed information about the explanation of these equations can be found in [91, 94, 98].

4.3 Test conditions and procedures

The 8-hole piezo-driven convergent injector was employed to study the MFR characteristics in this chapter. The tests are divided into two sets. The first set of tests was carried out under room temperature with single and split injection strategies to outline the novelty of the split injection strategy. The test conditions and procedures are:

(1) Aim to provide a reference for multiple injections, the single injection tests were carried out under RT. The injection pressure ranged from 60 to 120 MPa and injection duration varied between 0.3 and 1.5 ms. P_b was set to 3 MPa for all single injection tests.

(2) Split injections were then performed to reveal the interaction between splits with varied injection durations and dwell intervals. The testing matrix for each case will be shown in the result part separately. The injection pressure was set to 100 MPa and Pb was set to 3 MPa for all cases.

The second part of the tests was to study the effects of low fuel temperature. The injector and its fixing accessories were kept in the freezer. During the testing process under LT condition, the injection rate was set to 1 injection per second, allowing the fuel to be refrigerated sufficiently. For this part of tests, the test conditions and procedures are:

(1) Single injection with long energizing duration of 1.5 ms (achieving quasi-steady flow) was used under both RT and LT. Injection pressure varied from 35 to 120 MPa and back pressure ranged between 0.1 and 5.5 MPa under both RT and LT.

(2) Split injection strategy was employed under both RT and LT. Low injection pressures (35 and 60 MPa) and low back pressure (0.1 MPa) were used.

4.4 Injection characteristics under room temperature

4.4.1 Single injection

4.4.1.1 MFR shape under various injection pressures

The MFR shape under 120 MPa is presented in Figure 4-1 and several stages are shown. The injection delay stage A includes injector electric delay and mechanical delay. The

needle rising stage B largely depends on effective injection pressure difference and viscosity. For a specific injector, because the fuel flow regimes are different when the effective injection pressure difference varies, the motions of the needle are expected to be different. Stage B is consequently affected by the variation of flow regimes and needle motion. Under the same injection condition, the flow regimes also vary for different injectors. For instance, sharp inlet orifice injectors and cylindrical orifice injectors tend to develop cavitation easily [94, 99]. In addition, the variation of flow regime (especially under turbulent and cavitating condition) may cause the oscillation and stagnation of the needle, leading to different spray patterns under the same injection condition [51]. It was reported that the increase of the number of the holes can relive the oscillation and stagnation because the needle motion is more balanced [51]. It can be expected that stage B also largely depends on injector technology.

Stage C is the duration when the TTL signal given to the piezo-injector and the measured MFR signal overlap. In some studies [44, 100], an obvious MFR dip was observed at the very beginning of this stage due to the bounce-back of the needle. However, this was not found in this study. The next stage D is the period when the TTL signal disappears while the injector may still remain fully open. For solenoid injector, this characteristic is attributed to the injector electro-magnetic lag [11]. However, the injector employed in this paper is a piezo injector and the characteristics of the piezo material may be responsible [101]. The last stage is the closing stage E. Some researchers reported that a small amount of fuel is injected after the closing due to the needle bounce back [11]. By contrast, this was not found in the study. In [11, 44, 100], the employed injector was a gasoline injector while the one

employed in present study is a diesel injector. This means that the injection characteristics highly depend on injector technology. It is worth noting that the duration of the closing stage is considerably long and the MFR is very low at the end of closing. It can be expected that the low MFR contributes to low spray velocity, poor spray breakup and large droplets. The longer closing stage means more injected fuel with low velocity and poorer fuel-gas mixture. The resultant poor mixture tends to lead to high soot level in emission.

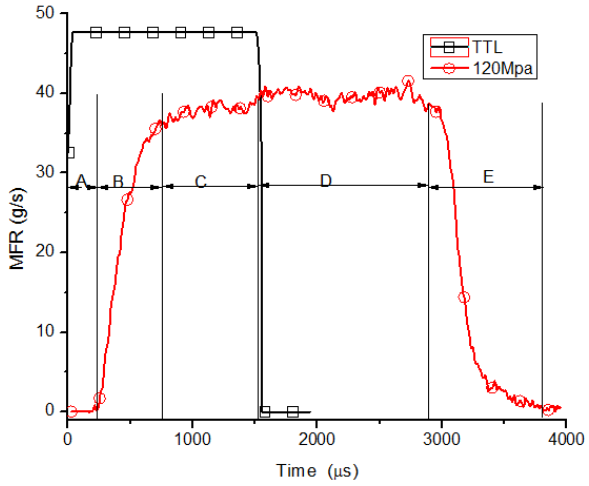

Figure 4-1 MFRs for 1.5 ms injection duration under 120 MPa

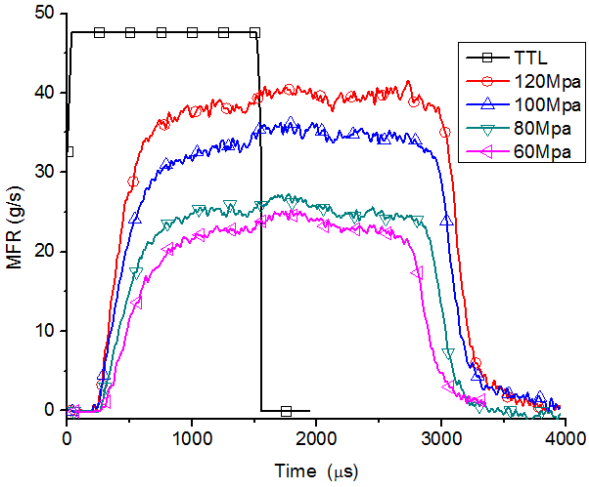

Figure 4-2 Shape of the MFR under various injection pressures

The MFR for 1.5 ms injection duration with the injection pressure varying from 60 MPa to 120 MPa is shown in Fig 4-2. The four cases show good agreement in terms of varying trend. It is interesting to find that the slope of the ascending phase (stage B) with higher injection pressure is steeper than the ones with lower injection pressure. It is reasonable to say that the raised injection pressure can open the injector much quicker and shorten the injection delay [11, 102]. More details about the injection delay can be found in Figure 4-13 shown in the next section.

More importantly, the injection duration is much longer than the duration of the corresponding TTL. This phenomenon is more obvious with the rise of the injection pressure, so it is likely that higher injection pressure could postpone the closing of the injector. The rise of injection pressure leads to the increase of fuel density and viscosity [24], thus the increase of friction for the needle if it is not energized. The raised friction inevitably leads to the retardation of the injection closing [85, 87].

4.4.1.2 MFR with various injection durations

It is widely accepted that the injected fuel mass does not necessarily increase linearly with the increase of injection duration. To further study this feature, the MFR characteristics with various injection durations are analyzed. The MFRs for different injection duration cases under 60 MPa and 120 MPa injection pressures are shown in Figure 4-3. It can be seen that short injection duration causes incomplete injector opening thus lower maximum MFR. Under high injection pressure (120 MPa), approximate 0.45 ms injection duration is

sufficient to fully open the injector, while under low injection pressure (60 MPa), approximate 0.6 ms energization duration is required to fully open the injector. This again supports that high injection pressure leads to quicker injector open and shorter injection delay (especially the mechanical injection delay).

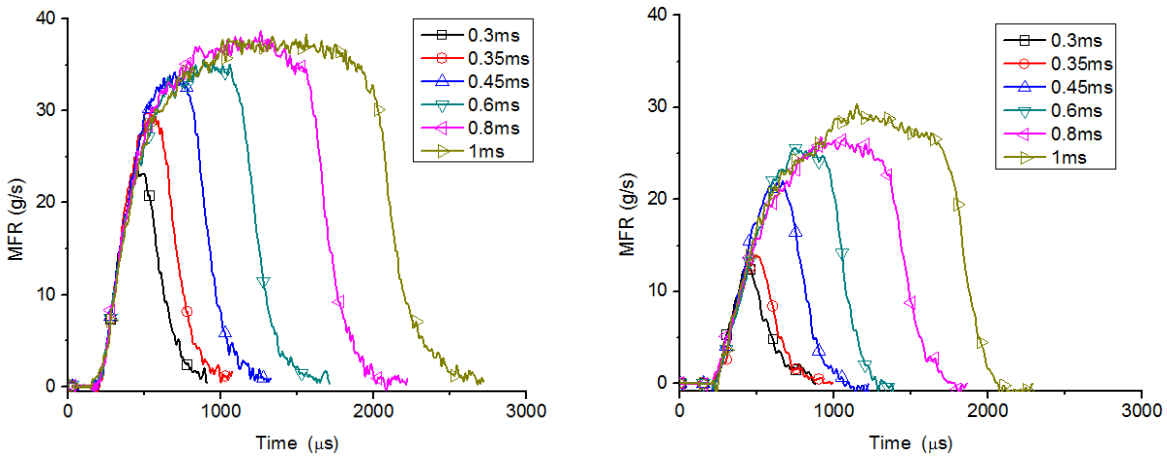

(a) (b)

Figure 4-3 MFR for different injection durations under (a)120 MPa and (b) 60 MPa

The injection delays are the same for all injection cases under same injection pressure, suggesting that the injection duration has little influence on the injection delay. For the 0.3 ms and 0.35 ms injection duration cases under low pressure, the peak MFRs show slight difference, however for 0.45 ms case, peak MFR jumps to a much higher value. It is quite possible that the movement of the injector needle is greatly accelerated after the injection duration reaches 0.35 ms. By contrast, this "jump" is not found for the cases with injection pressure of 120 MPa. This phenomenon needs to be further studied.

4.4.2 **Two-split injection**

For multiple injection strategy, the time interval and injection duration ratio among split injections are two additional factors that need to be considered. The interaction between injection events is expected to be complex [11, 86]. It is important to investigate the injection features to provide fundamental injection knowledge for spray and combustion study.

4.4.2.1 Split injection with fixed split injection durations

For the fixed injection duration, the injection dwell can exert profound influence on MFR features. The dwell greatly determines the extent of the interaction between splits. In this part, various tests with fixed injection duration, 0.45 ~ 0.45 ms but with variable dwell between the end of first and the beginning of the second injection, were performed. The test matrix is shown in Table 4-1.

Table 4-1 Test matrix for split injection with fixed split duration

Injection duration (ms)	0.45 ~ 0.45
Injection dwell τ (ms)	0.2 ~ 0.8

(1) MFR shape

As presented in Figure 4-4, the MFR of splits shows strong interaction when the dwell is less than 0.6 ms, presenting continuous MFR shapes. The continuous MFR can be attributed to the assumption that the needle has not closed the injector when the energization of the

second split injection starts [21]. When the dwell varies from 0.6 to 0.8 ms, although the MFR shapes separate, the interaction still obviously exists between the two split injections because the second split injections show different peak MFRs compared with the first ones. It is interesting to find that after the splits become independent, the first splits are approximately the same with slight variation, whereas the second ones vary significantly. Generally, the peak MFR of the second splits reduces before recovering to values as high as those for the first ones as the dwell time increases to 0.8 ms.

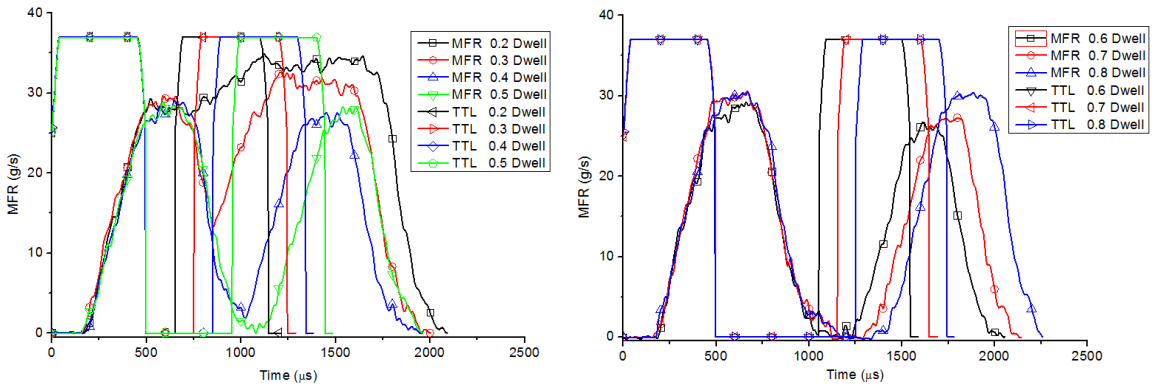

(a) (b)

Figure 4-4 MFR for 0.45 ~ 0.45 ms injection duration with different dwells

The reduced MFR may be attributed to the shortened actual injection duration although the TTL signal is the same as single injection [11]. It should also be noted that the fluctuation of the fuel pressure can lead to the variation of the injection characteristics [11]. It can be expected that for the cases where interaction exists and the second split injections show lower MFR than the first ones, the needle is moving to close the injector when the energization of the second split injection starts. This means that the actual moving direction of the needle is opposite to the desired moving direction driven by the energising signal.

Consequently, the needle moves in its initial closing direction for some time continuingly before changing its moving direction. This argument can be supported by the facts shown in Figure 4-4 (a). For the cases with 0.3, 0.4 and 0.5 ms dwell, the energisation of the second split injection (TTL signal) starts when the MFR of the first split injection is decreasing. However, the appearance of the lowest points of the continuous MFR curves retards, meaning the retardation of the reversion of the needle moving direction. Besides, direction reversion may lead to oscillation and stagnation of the needle, causing shorter effective injection duration or / and the change of flow regimes in the injector. The shortened effective injection duration is likely to cause lower peak MFR and less injected fuel. The change of flow regimes may in return enhance the oscillation and stagnation of the needle, for instance, the turbulent flow and the breakup of the bubbles in cavitating flow exert unbalanced radial forces on the needle. According to Lacoste [51], the oscillation and stagnation causes less injected fuel although the needle continuingly rises. In addition, the variation of the effective injection pressure is another possible reason for the lower peak MFR of the second split injection.

(2) MFR comparison between single injection and splits

The single injection with 0.45 ms duration is utilized to compare with the splits, shown in Figure 4-5. The comparison is only carried out for the injection cases where the splits are separated. The first splits are almost comparable to the single one, however, the second ones are apparently lower than the single one except the case with 0.8 ms interval where the

interaction is weak or may disappear. This mean that, as mentioned before, the actual effective injection duration of the second one is shorter. The dwell determines the degree of interaction between split injections.

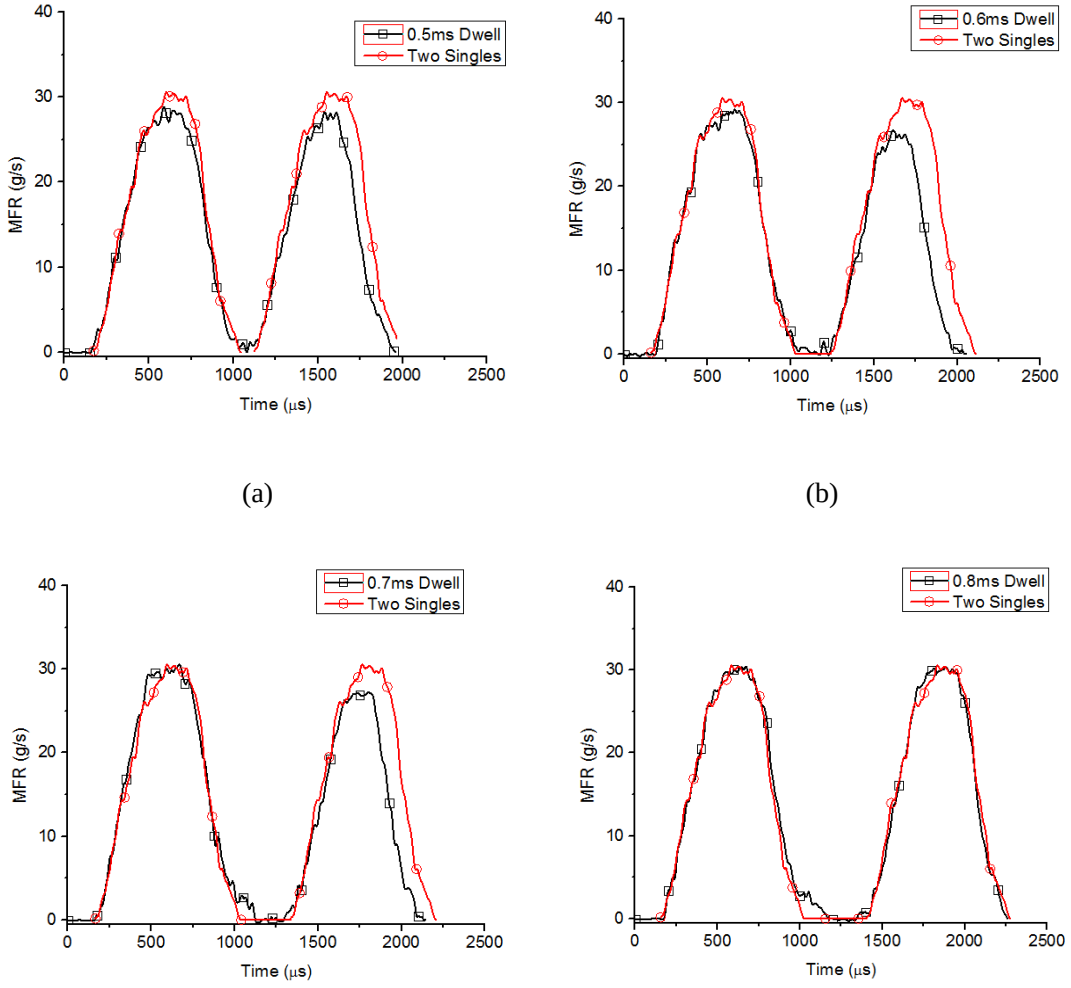

Figure 4-5 MFR comparison between single injection and 0.45 ~ 0.45 ms split injections

(3) Fuel mass comparison between single injection and split injections

The quantitative comparison between single and multiple injection strategies for the total fuel mass is shown in Figure 4-6 (a). In this study, the fuel mass with single injection

strategy is employed as the baseline. When the interval is short, the total fuel mass with multiple injection is much higher than that of the single injection, at 0.2 ms interval point, the fuel mass being 55% higher. This is because the injector is still open for the first split when the energising signal of the second split arrives [21]. This means that the fuel is still continuously flowing during the dwell, resulting in the increase of effective injection duration. As the dwell increases, the fuel mass drops gradually to the lowest point, at 0.6 ms interval with 16% less fuel, after which the fuel mass resumes progressively and approximates to that of single injection. This shows that the interaction can be either positive or negative for the fuel mass, depending on dwell interval.

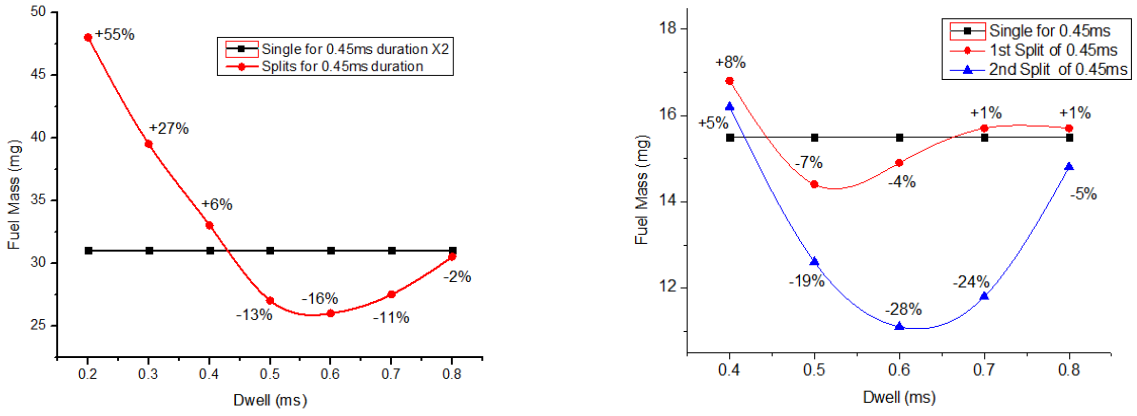

a b

Figure 4-6 Mass comparison between single and split-injection (a) and that between single and splits (b)

Fuel mass comparison between single and splits is showed in Figure 4-6 (b). In this study, the fuel mass of each split injection event is given only when the clear boundary between split injections exists, namely the split injection events being separated. The curves for each split are almost similar to the total mass curve in terms of the changing trend. Both

drop from points where the fuel mass is slightly higher than the single injection to the lowest points before a rise appears. 28% less fuel is injected for the second splits at 0.6 ms interval point. The first split, however presents around 7% less fuel at the lowest point at 0.5 ms interval point. Furthermore, the first split shows higher MFR therefore more fuel mass than the second, suggesting that the second split is more vulnerable to the interaction.

4.4.2.2 Two-Split injection with various split injection duration distributions

For split injection strategy, the injection duration of each split is also interesting as the combustion characteristics can be considerably different for various injection duration ratios between consecutive splits [22]. In this part, three groups of tests were performed with total 0.9 ms energizing duration by changing the injection duration for each split, shown in Table 4-2.

Table 4-2 Test matrix for multiple injections with various split durations and fixed total injection duration

Injection duration (ms)	0.3~0.6			0.45~0.45			0.6~0.3
Injection interval (ms)	0.2	0.3	0.4	0.5	0.6	0.7	0.8

(1) MFR shape

The corresponding MFRs with 0.3~0.6 ms and 0.6~0.3 ms injection strategies are shown in Figure 4-7 and Figure 4-8 respectively. The duration of the first split injection is thought to greatly influence the interaction between split injections. This test arrangement allows the

study on the effects of the long and short duration of the first injection on the injection characteristics and the interaction between split injections.

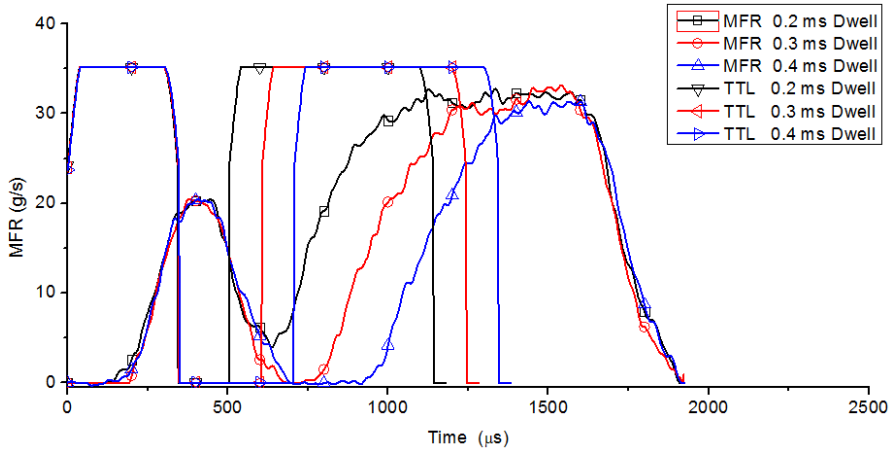

(a)

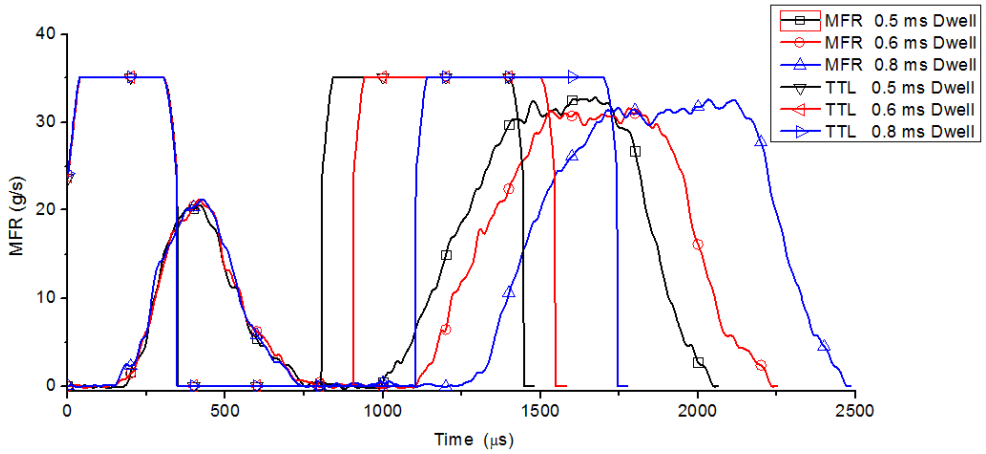

(b)

Figure 4-7 MFR of the 0.3~0.6 ms injection duration with (a) short dwell and (b) long dwell

For 0.3~0.6 ms test group, only the MFR shape of the case with 0.2 ms interval is integral and the rest are independent. On the other hand, the 0.6~0.3 ms group shows another picture. The two splits cannot be isolated until the dwell reaches 0.7 ms. Another difference is that, after the interaction between splits becomes relatively weaker, the second

splits of the 0.3~0.6 ms group are characterized with similar peak MFRs but different actual fuel injection durations. By contrast, the second splits of the 0.6~0.3 ms groups are featured with progressively reduced peak MFR with the increase of the dwell. By comparing the two groups, it can be concluded that the energizing duration of the first split determines the degree of interaction with the second one [21]. The aforementioned shorter effective injection duration for the second split injection tends to be the main reason for both 0.3~0.6 and 0.6~0.3 ms cases. The reversion of the needle moving direction, needle oscillation and needle stagnation "consume" some injection duration of the second split injection. For the 0.3~0.6 ms group, the injection duration of the second split injection (0.6ms) is sufficiently long to open the injection fully, with less injector fully opening duration, shown in Figure 4-7 (a). For the 0.6~0.3 ms group, the injection duration of the second split injection (0.3s ms) is not sufficiently long to fully open the injector, with gradually reduced peak MFR, shown in Figure 4-8 (b).

Combining Figures 4-4, 4-7 and 4-8, it is interesting to find that the injection characteristics with different injection duration distributions between splits vary significantly, meaning that the interaction between two injections not only depends on the dwell time but also on the previous injection. It is shown that longer injection duration for the first split tends to cause more continuous MFR curves. That is to say, a big injection + a second injection has higher possibility to become a single injection than if a small injection is followed by a second one. The assumed reason for several injections to merge in a single one is the needle lift, the longer the injection the higher the lift and more possibility to merge

with a second injection. In addition, longer previous injection duration tends to adversely affect the second split injection, namely, lower peak MFR for the second split, when the interaction becomes relatively weak. It can be found that, for the split injection strategy, when splits are separable, the split with the longest injection duration shows the strongest immunity to the interaction between splits.

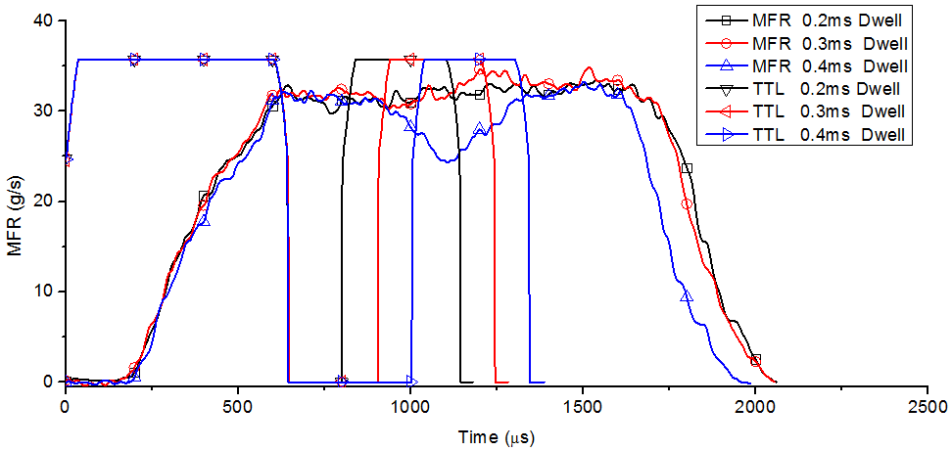

(a)

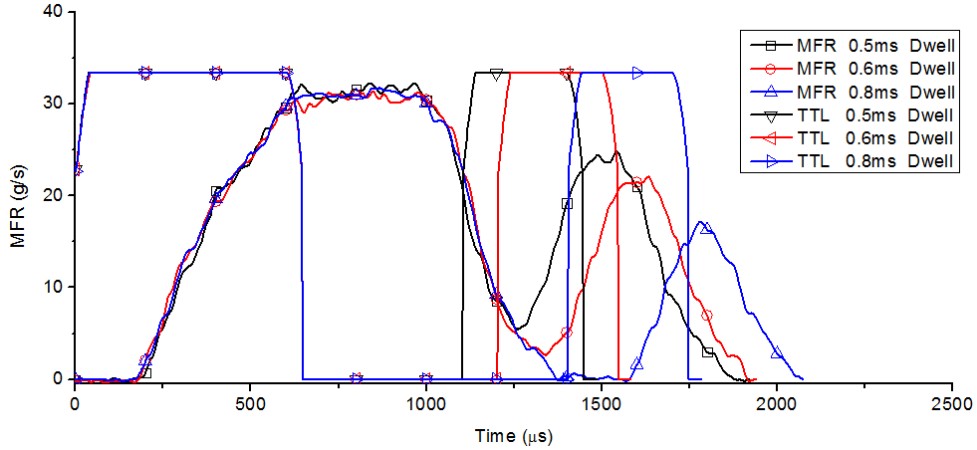

(b)

Figure 4-8 MFR of the 0.6~0.3 ms injection duration with (a) short dwell and (b) long dwell

(2) Fuel mass comparison between single injection and splits

The fuel masses for the three groups of tests and the single ones are presented in Figure 4-9. The varying trends of fuel mass effectively reflect the degree of interaction between splits, namely, the effects of dwell and the duration of the first split injection, discussed in the former subsection. It is seen that the longer injection duration for the first split, the more fuel is injected when the interval is short. In this study, with 0.2 ms interval, the 0.6~0.3 ms case allows 61% more fuel to be injected when compared with single one, followed by the 0.45~0.45 ms case, with 53% more fuel to be injected, while the 0.3~0.6 ms case allows only 20% more fuel to be injected. The three curves demonstrate the same developing trend, that is, as the interval increases, the fuel mass drops quickly all the way below the baseline and to the lowest points varying according to the duration of the first split, then increases gradually. This phenomenon was also observed in [21].

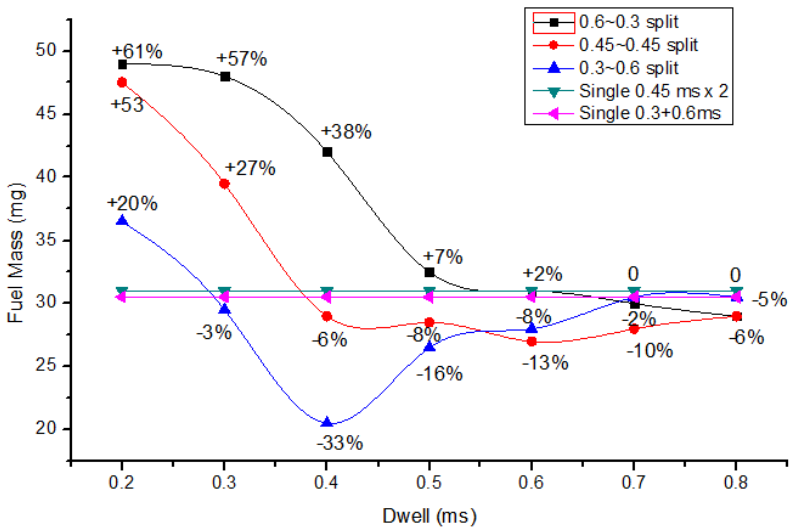

Figure 4-9 Fuel mass comparison between single and split-injection: 0.3~0.6 ms, 0.45~0.45 ms, 0.6~0.3 ms

4.4.3 **Three-split injection**

Three-split injection strategy may present different characteristics when compared with two-split ones since the third split can enhance the interaction of the first two splits, and to what an extent can this enhancement be is still unknown. In addition, the interaction between the first two splits also affects the features of the third split. Four groups of tests were carried out and the matrix is shown in Table 4-3. The total injection duration was set to1.2 ms.

Table 4-3 Test matrix for three-split injection

Injection duration (ms)	0.3~0.3~0.6		0.3~0.6~0.3		0.4~0.4~0.4	0.6~0.3~0.3	
dwell (ms)	0.2	0.3	0.4	0.5	0.6	0.7	0.8

(1) MFR shape

The MFR for the 0.4~0.4~0.4 ms group are shown in Figures 4-10. The rest are not presented to achieve concision. When dwell interval is shorter than 0.4 ms, the MFR curves are continuous, meaning single injection. The splits are segregated when the dwell is higher than 0.4 ms and all the first split injections show similar peak MFRs. When the interval is set to 0.4 and 0.5 ms, the peaks of the three splits decrease gradually. It can be found that the increase of the number of the injections leads to much lower MFR for the last injection. It is likely that the splits present decreasing resistance to the interaction with the increase of energizing sequence. This means that the last injection tends to be affected more severely.

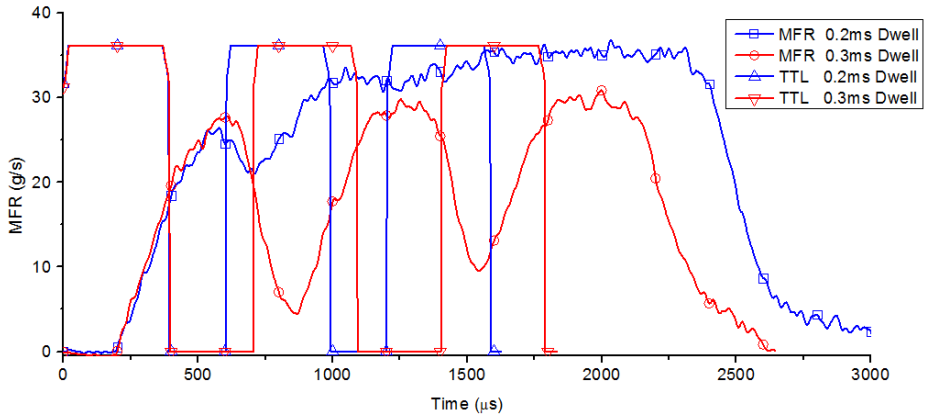

(a)

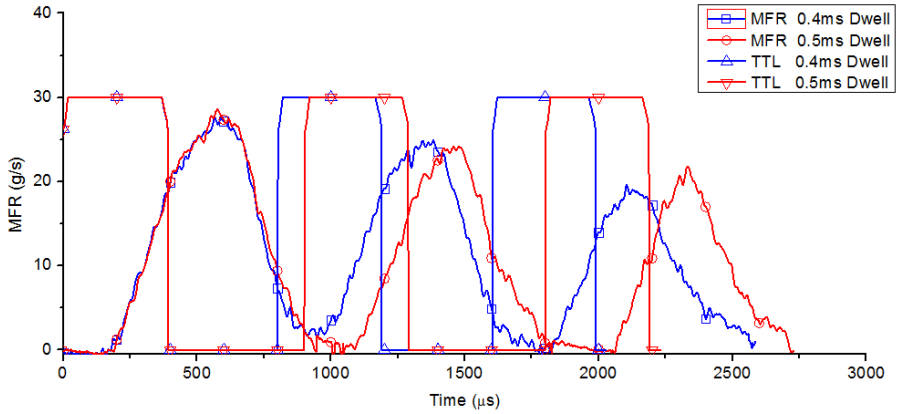

(b)

Figure 4-10 MFR of 0.4~0.4~0.4 ms split injection with (a) short dwell and (b) medium dwell

(2) Fuel mass comparison between single injection and splits

The total fuel mass comparison between single injection and multiple injections is shown in Figure 4-11. When the injector is energized intensively, the longer the first split duration, the more fuel is injected, which is consistent with the results of the two-split injections. The case with highest fuel mass, 114% more than the baseline, is the one when the duration is 0.6~0.3~0.3 ms and the dwell interval is 0.3 ms. The second highest one is the 0.4~0.4~0.4 ms case, being 106% higher at 0.2 ms dwell, while the highest point for 0.3~0.3~0.6 case is

the one with 0.2 ms dwell, being only 36% higher. As the interval increases, the interaction between split injections weakens and the total fuel mass drops below the baseline before it approximates the single injection again. By comparing Figure 4-9 and Figure 4-11, it shows that the increase of the number of the split injections results in much stronger interaction between split injections and much higher variation of MFR and injected fuel mass.

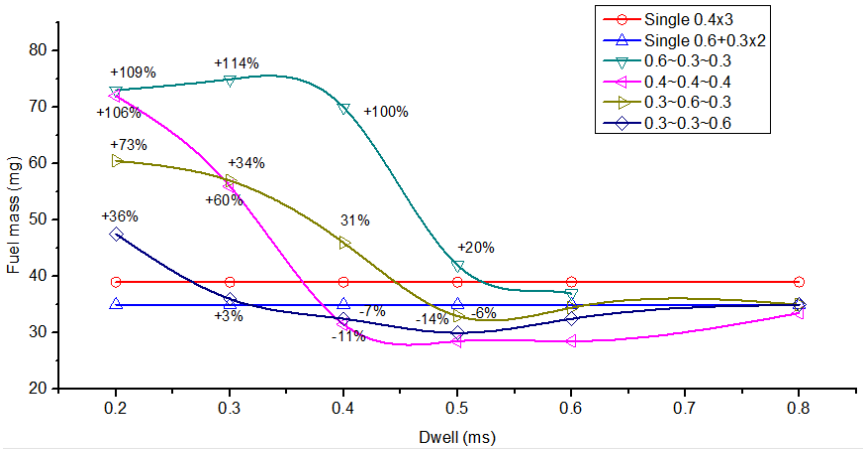

Figure 4-11 Fuel mass comparison between single injections and various split injections

4.5 Injection characteristics under cold start condition

4.5.1 Single injection

(1) MFR shapes

The MFR shapes for cases with injection pressure of 35 and 100 MPa and back pressure of 0.1 MPa under RT and LT are shown in Figure 4-12. With high injection pressure, the MFR for the quasi-steady stage under RT is observably higher than the one under LT condition. With low injection pressure, this MFR difference is more noticeable. This suggests that LT condition can lower the MFR, especially under low injection pressure.

Low temperature contributes to high viscosity which raises the friction between fuel and injector hole wall, leading to more energy loss and lower effective flow area [94]. This can clearly decrease the MFR. On the other hand, the rise of fuel density due to the temperature reduction results in the rise of MFR. From this aspect, higher MFR for low temperature cases is expected. The actual results suggest that the influence of temperature on fuel viscosity is more significant than that on fuel density. This shows good agreement with other studies [95-97].

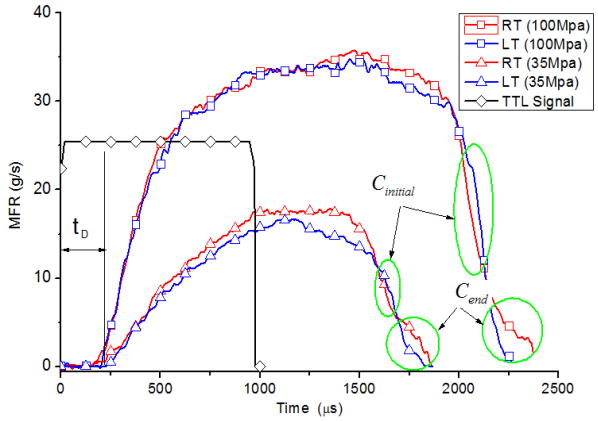

Figure 4-12 MFR shapes for both LT and RT with injection pressure being 35 and 100 MPa

It is interesting to find the distinctions during the injector closing. The injection closing can be divided into two phases, the initial closing phase ($C_{initial}$) and end closing phase (C_{end}). It can be seen that MFRs for LT cases are higher than those of RT cases during $C_{initial}$, whereas the RT cases present higher MFRs during C_{end} than the cases with LT, shown in Figure 4-12. The impact of viscosity is quite possibly responsible. When the energizing signal disappears, the needle begins to close the injector. Higher viscosity and higher fuel density for LT cases lead to higher friction, decelerating the closing movement of the needle. This needle movement deceleration contributes to the injector closing retardation, thus higher

MFR for LT cases. Near the end of the injection period, the flow rate at LT becomes much smaller than that at RT. It could be reasoned that after the needle moves to a certain point, the fuel flow becomes throttled, and the higher friction because of higher viscosity can curb the fuel flow. This causes low MFRs for LT cases at the end of the injection period.

For the whole transient injector closing stage, it should be noted that many flow regimes, for instance, cavitating flow, turbulent flow, laminar flow and the transiting flow from turbulent to laminar flow, may involve. When the needle moves to close the injector, the effective injection pressure drops drastically and the flow regime varies quickly, especially under high injection pressure condition. The quick variation of flow regime may cause the oscillation or (and) stagnation of the needle (causing needle radial vibration), leading to complex fuel flow characteristics and unpredictable MFR [51]. The increase of fuel viscosity (increase of friction) due to low temperature may be able to damp the needle radial oscillation or (and) stagnation. This radial damping effect may lead to quicker injector closing and lower MFR for the C_{end}. It should be noted that higher viscosity causes slow injector closing. However, more studies on the needle oscillation measurement should be carried out to verify this assumption based on literature and experimental results.

(2) Injection delay

The injection delays t_D (marked in Figure 4-12, denoting the time difference between the start of energization and the start of injection) are shown in Figure 4-13. LT condition leads to longer injection delay which is magnified by low injection pressure. It can be argued that high fluid friction force because of cold condition decelerates the movement of the needle

when injector energized, leading to the retardation of injection. The higher energy loss due to higher friction also contributes to lower fuel acceleration across the injector hole. Besides, the raised fuel density under LT also results in lower fuel injection velocity [88, 90, 103], and more time is required for the injected fuel to move to the signal detecting point. The increase of injection pressure can considerably lower the injection delay and narrow the injection delay difference between RT and LT cases. The elevated pressure difference across the injector results in a larger hydraulic force on the injected fuel which is the root reason for the variation. In many studies, it was pointed out that the hydraulic force is the dominant factor affecting the injection characteristics [87, 98]. This can also be observed through the initial varying trend of the MFR curves in Figure 4-12. Under low injection pressure, the viscosity dominates the movement of needle whilst under high injection pressure conditions, the pressure difference force becomes the dominant one.

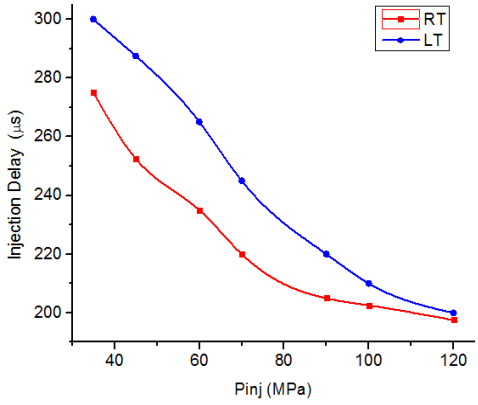

Figure 4-13 Injection delay

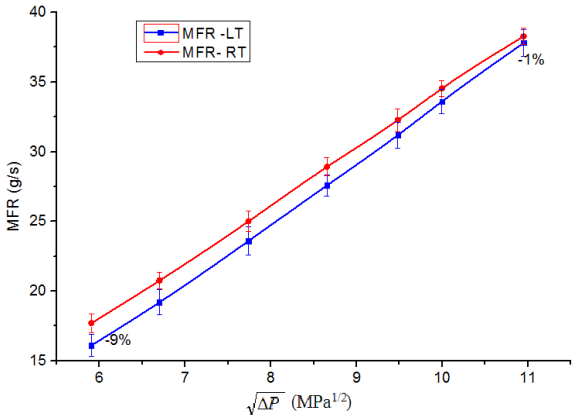

Figure 4-14 MFR vs $\sqrt{\Delta P}$ with p_b of 1 MPa

(3) Mass flow rate

As shown in Figure 4-14, MFR almost linearly increases with the square root of injection pressure difference (with back pressure of 1MPa), suggesting that the MFRs are not obviously

impacted by cavitation under high injection pressure. This is because a convergent injector can alleviate or even eliminate the inception of cavitation [86]. However, this does not mean that cavitation does not occur as the AF (19%) for the employed injector is low. Besides, it can be found that the MFRs are lower for low temperature cases. The mass deviations (fuel masses under RT are used as baselines) are all negative even when the injection pressure is high. However, the deviation is bridged by the rise of injection pressure.

To study the influences of back pressure under RT and LT, the MFRs with high (100 MPa) and low (35 MPa) injection pressures were also investigated, shown in Figure 4-15. The variation of pressure difference was achieved by varying the back pressure with constant injection pressure. Many interesting characteristics can be observed. Under low injection pressure condition, the MFR first increases linearly and then decreases slightly (RT case) or nearly levels off (LT case) with the rise of pressure difference. The MFR difference between RT and LT cases narrows from -10% to -1.5% as the pressure difference increases (Figure 4-15 (a)). By contrast, under high injection pressure, the MFR for RT shows a linear reduction while the MFR for LT decreases linearly after keeping almost constant as injection pressure difference goes up. Furthermore, the MFR differences are much smaller than the ones with low injection pressure, ranging from -1.2% to -0.8% as opposed to those varying from -10% to -1.5% under LT (Fig 4-15 (a)), for high injection pressure (Fig 4-15 (b)).

The assumed cavitation phenomenon is probably responsible for this changing trend. The drop of back pressure means the increase of effective injection pressure and higher possibility of the inception of cavitation. Under cavitating injection condition, the

appearance of cavities or (and) flow detachment from the nozzle hole wall leads (lead) to the reduction of effective flow area, thereby reduction of MFR [99]. With low injection pressure, the cavitation does not initiate until the back pressure drops to a certain point, around 0.5 MPa. This means that when back pressure is higher than 0.5 MPa, the possibility of cavitating flow is very low. However, with high injection pressure, the effect of the supposed cavitation is still observable even the back pressure is as high as 5.5MPa. The increase of back pressure from 0.1 to 5.5 MPa means reduction of injection pressure difference and reduction of cavitating intensity, thereby increase of effective flow area and increase of MFR. It is interesting to find that for the cases with LT, the assumed inception of cavitation is alleviated to a certain degree compared with the cases with RT. The raised fuel viscosity tends to be responsible and will be further discussed below. The effects of cavitation on the variation of MFR can be further explained through the effects of cavitation on discharge coefficient (C_d) in the following section.

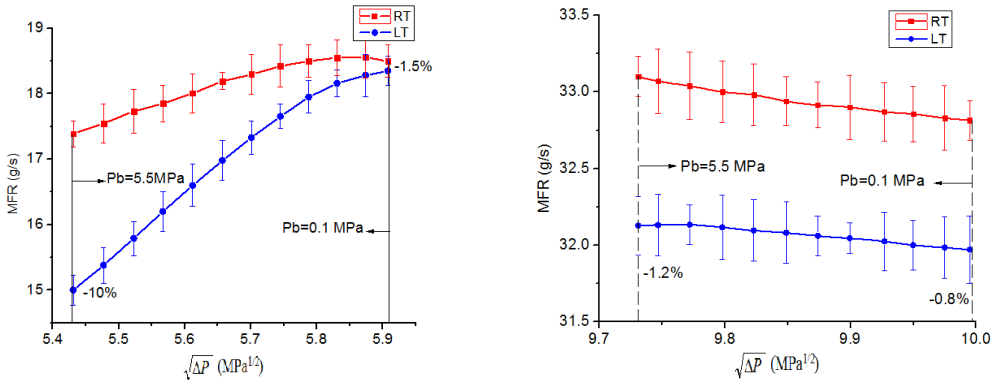

a b

Figure 4-15 MFR vs $\sqrt{\Delta p}$ with P_{inj} of (a) 35 MPa and (b) 100 MPa

(4) Discharge coefficient and flow regime transition

The variation of C_d with *Re* is a good indicator for the flow regime as *Re* expresses the ratio of dynamic forces over viscous forces. The variation of C_d versus *Re* is presented in Figure 4-16. Clearly, C_d increases monotonously with decelerating trend and reaches an asymptotic maximum value as Re rises. This characteristic has been fully studied by many researchers and the flow regime transition from laminar flow to turbulent flow is likely to be the main reason [91, 104]. It is worth noting that higher viscosity because of low temperature lowers the C_d as the effect of friction is increasing. C_d at low injection pressure is more vulnerable to the variation of temperature than at high injection pressure [86, 98].

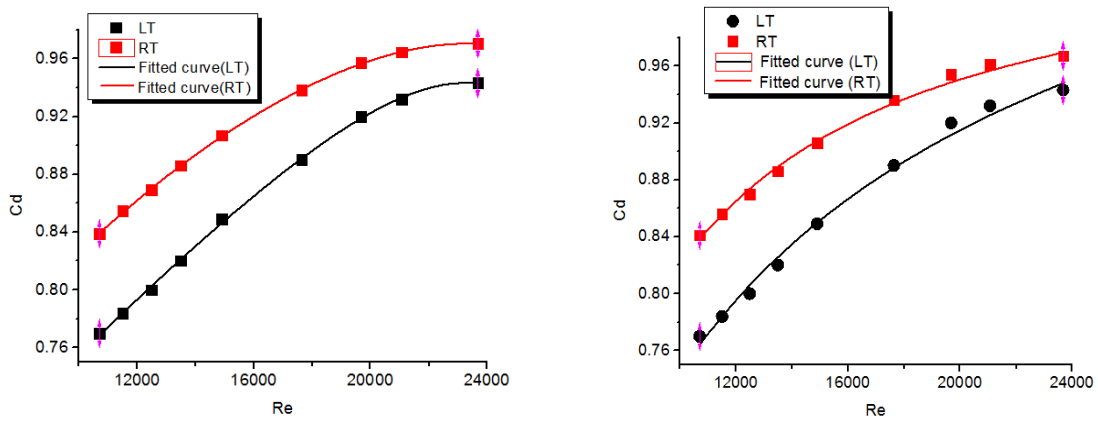

Figure 4-16 C_d vs Re fitted by (a) Payri's equation and (b) Salvador's equation with p_b of 3 MPa

Two modified correlations for C_d and *Re* are used to weigh the impacts of other factors on the development of C_d. The first one based on the correlation proposed by Payri [105] (shown in Eq 4-5) mainly takes Re and viscosity into consideration, whilst for the other one based on the correlation proposed by Salvador [106] (shown in Eq 4-6), the injector geometric structure and Re are seen as the main factors that influence C_d . The corresponding parameters are adapted with the ones used in this study. The fitting

coefficients for the two correlations are listed in Table 4-4 and Table 4-5.

$$C_d = C_{d'} + K_1 * \nu^a * \mathrm{Re}^b - \frac{K_2 * \nu^c}{\mathrm{Re}^d} \qquad \text{Equation 4-5}$$

$$C_d = C_{d'} + K_1 * AF^a * d_0{}^b - \frac{K_2 * AF^c * d_0{}^d}{\mathrm{Re}^e} \qquad \text{Equation 4-6}$$

Table 4-4 Values of coefficients for Payri's correlation

	$C_{d'}$	K_1	a	b	K_2	c	d	R^2
RT	0.39	-2.76×10^{-37}	32.68	4.81	-18.57	-7.56	-0.42	0.997
LT	0.49	-4.80×10^{-43}	12.88	8.10	-2.31	-8.93	-0.74	0.999

Table 4-5 Values of coefficients for Salvador's correlation

	$C_{d'}$	K_1	a	b	K_2	c	d	e	R^2
RT	0.99	1.04	0.85	0.94	37.38	-4.02	-0.98	1.15	0.94
LT	1.05	1.589	0.31	0.73	7.42	-2.07	-0.21	0.52	0.93

It can be seen that the correlation based on Payri's [87] fits the experimental data very well for both LT and RT regimes with high accuracy (R^2=0.997 for LT case and R^2=0.999 for RT case). This correlation suggests the influences of viscosity and Re are significant for C_d. By contrast, the fittings with the correlation based on Salvador's [106] are less accurate, especially for the LT case (R^2=0.926 for LT case and R^2=0.935 for RT case). This correlation stresses the importance of the injector hole geometric structure and Re for C_d. By comparing the accuracies of the two correlations, it is found that the impact of viscosity

outbalances that of the hole structure parameters on the values of C_d and on the flow regime.

Although convergent hole geometry injectors can alleviate the inception of cavitation, the aforementioned varying trend of MFR versus the square root of injection pressure difference (Figure 4-15) demonstrates the occurrence of the assumed cavitation. This can be further studied through the variation of the corresponding C_d. The C_d development versus the square root of cavitation number $\sqrt{K}$ can effectively represent the chances of cavitation (shown in Figure 4-17) [105]. When the fuel pressure is low, the C_d values for both the RT and LT regimes increase to a turning point (point A marked in the graph) as the cavitation number increases. The turning point refers to a so called "choking point" where the MFR does not necessarily increase with the increase of injection pressure difference because of the inception of cavitation [105]. This means that the flow is cavitating before the turning point for both LT and RT conditions. The cavitation vapour zones across the hole lead to the reduction of effective orifice area [107], therefore to lower C_d. The increase of the cavitation number due to the increase of back pressure gradually curbs the inception of cavitation, consequently leading to the rise of the values of C_d. It is noteworthy that the cavitation number corresponding to the turning point for the LT condition is smaller than that for RT, suggesting that the chances of cavitation under cold condition are lower.

After the turning point is reached, the values of C_d for the RT case nearly level off and then show a slight decrease. This is because the assumed cavitation disappears gradually because of lower injection pressure differences. The disappearance of cavitation suggests that the flow regime changes from cavitating to a turbulent one. Under this regime, the

effective flow area is almost the total area and the velocity profile at the orifice outlet is quite uniform. The slight reduction of C_d shows that the transition from turbulent to laminar flow begins at this stage. The increase of $\sqrt{K}$ results in lower Re and lower turbulence. The transport of radial momentum flux because of the turbulence weakens, therefore the velocity profile at the orifice outlet becomes non-uniform [87]. The uneven velocity distribution can also cause the reduction of effective flow area, contributing to the drop of C_d.

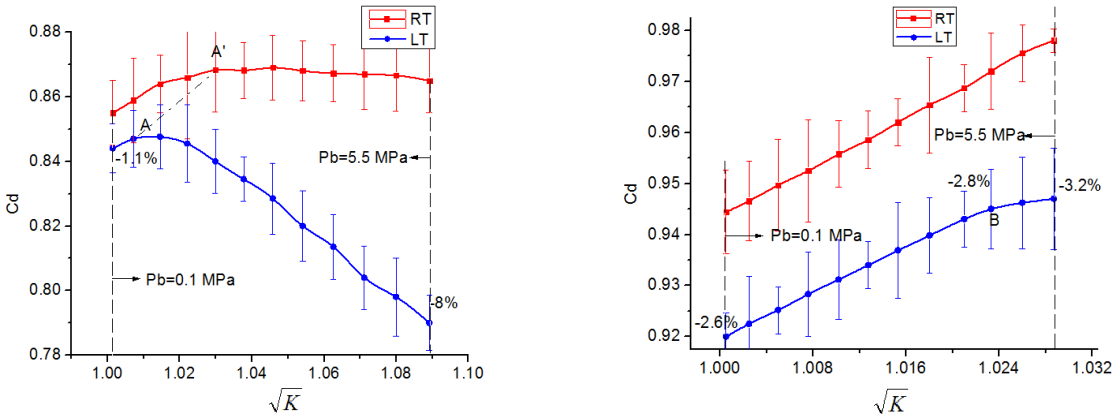

a b

Figure 4-17 C_d vs $\sqrt{K}$ with P_{inj} being (a) 35 MPa and (b) 100 MPa.

However, after the turning point, the case with LT shows a different picture. The rise of back pressure causes a slight reduction of C_d before an obvious decrease. Under LT condition, the cavitation can be effectively inhibited by the increase of viscosity and the effects of viscosity on the injection characteristics become significant. The flow regime changes quickly from turbulent to laminar flow. The flow regime variation can be explained in Figure 4-18. In this graph, f denotes friction force, τ denotes shearing force profile, $u(r)$ denotes velocity distribution across the hole section and δ denotes the laminar

flow boundary layer thickness. If δ is zero, the flow is totally turbulent and $u(r)$ is evenly distributed. If $\delta = D/2$, the flow is completely laminar and if $0 < \delta < D/2$, the flow is in the transition state.

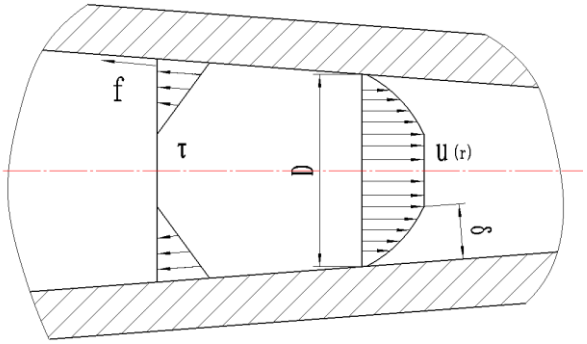

Figure 4-18 Velocity profile under laminar flow

With laminar flow, the friction across the hole wall severely curbs the velocity development and the velocity distribution depends on the non-uniform layer thickness δ. This thickness can be expressed as [108]:

$$\delta \propto \sqrt{\frac{\nu \cdot x}{V_{av}}} \qquad \text{Equation 4-7}$$

Where x is the duct length and V_{av} is the average velocity (total volume flow rate/area).

As shown in the Equation 4-7, the rise of viscosity and decrease of effective velocity contributes to higher layer thickness, increasing the chances for laminar flow. According to the viscosity/temperature correlation shown in Figure 3-13, viscosity variation can be expressed as:

$$\nu \propto \frac{1}{e^{0.031 T}} \qquad \text{Equation 4-8}$$

The effective velocity can be expressed as:

$$V_{act} \propto \sqrt{\Delta p}$$ Equation 4-9

By combining the correlations and replacing the duct length x with the hole length L, the following general correlation is obtained:

$$\delta \propto \sqrt{\frac{L}{e^{0.031*T} \cdot \sqrt{\Delta p}}}$$ Equation 4-10

This correlation can effectively explain how the main factors influence the flow regime in the injector hole. The decrease of temperature and injection pressure difference causes larger layer thickness, leading to a more uneven velocity profile. Therefore, the decrease of fuel temperature accelerates the increase of laminar layer thickness when reducing the injection pressure difference, thus accelerating the flow regime transition. Although this correlation shows that it is possible for layer thickness δ to reach D/2, the flow in the injector may not be completely laminar. As mentioned before, the injector used in this study is a convergent one. The reducing cross section area at the outlet accelerates the fuel, allowing the development of turbulent flow. Therefore, the flow is in the transition state between laminar and turbulent flow after C_d begins to exhibit the reducing trend shown in Figure 4-17 (a).

The impacts of temperature and injection pressure difference on the transition of flow regime can be further explained by the injection characteristics with high injection pressure, as shown in Figure 4-17 (b). The C_d for RT case shows a linear increase as the $\sqrt{K}$ rises, and no turning point is observed. High injection pressure contributes to strong cavitation and high back-pressure is required to prevent the occurrence of cavitation. In this study, the

5.5 MPa back-pressure resulting in cavitation number K of 1.0582 is insufficient to prevent the cavitation. The LT case presents a slight difference, showing the turning point (point B marked in Figure 4-17 (b)). This once again supports the argument that LT can effectively curb the onset of cavitation as the cavitation number $K = \frac{p_{inj} - p_v}{p_{inj} - p_b}$ increases (for constant injection pressure and vapor pressure this means an increasing back-pressure). According to the study of [105], in cavitating conditions the increase of $\sqrt{K}$ causes a linear rise of C_d, while in non-cavitating conditions, the linear rise does not appear. The rise of viscosity due to LT changes the flow from a cavitating one to a turbulent one. It can be expected that under high injection pressure (100 MPa), all cases for RT are cavitating, and most cases for LT (when cavitation number K is lower than 1.024, shown in Figure 4-17 (b)) are cavitating. This can explain the varying trend of MFRs under RT and LT when high injection pressure is employed, shown in Figure 4-15 (b).

4.5.2 **Two-split injection**

In this part, two injection pressures, 35 and 60 MPa were employed with back pressure of 0.1 MPa. Only simple split injection cases were studied to reveal the effects of fuel temperature. The injection duration for each split injection was set to 0.45 ms while the dwell varied from 0.2 to 0.8 ms. Only 2-split cases were tried under these injection conditions.

(1) MFR shapes

The MFRs with 2-split injection under 35 MPa injection pressure condition are shown in

Figure 4-19. The cases with 0.2 ms dwell show some interaction between the first and the second splits under both temperature conditions. The LT case shows lower MFR and shorter injection duration than the RT case. As the energization duration is not sufficiently long for the injector to open fully, higher viscosity due to lower temperature causes assumed lower needle lift thus to smaller opening area when the energization ends for LT cases. Assumed lower needle lift causes shorter injection duration, therefore smaller opening area contributes to lower MFR. When the dwell between two splits increases to 0.3 ms, the second split still shows higher MFR than the first one for the RT case. It appears that the interaction between the two splits still observably exists although the MFR shapes of the two splits are separated. By contrast, the LT case shows almost same MFR peaks for its two splits and the interaction appears to be weaker or even disappears. The aforementioned lower needle lift due to higher viscosity under LT is expected to cause weaker interaction between split injections because the injector opening of the second split injection is not as advanced as that for RT case. This means that the MFR shapes for split injections become more independent and more non-continuous. This also suggests that as dwell increases, more identical MFR shapes similar to single injection for each split injection can be expected. The combined effects of raised dwell and higher fuel viscosity under LT can lead to similar MFR peaks for each split injection. Besides, much lower MFR peaks for LT compared with those for RT are clearly seen. Under low injection pressure with short injection duration, the injection is persistently in the transition state. The flow tends to be laminar flow or transition between turbulent flow and laminar flow. According to Equation 4-7, the low temperature leads to higher

chances of laminar flow and more loss of effective flow area, leading to obviously lower MFR.

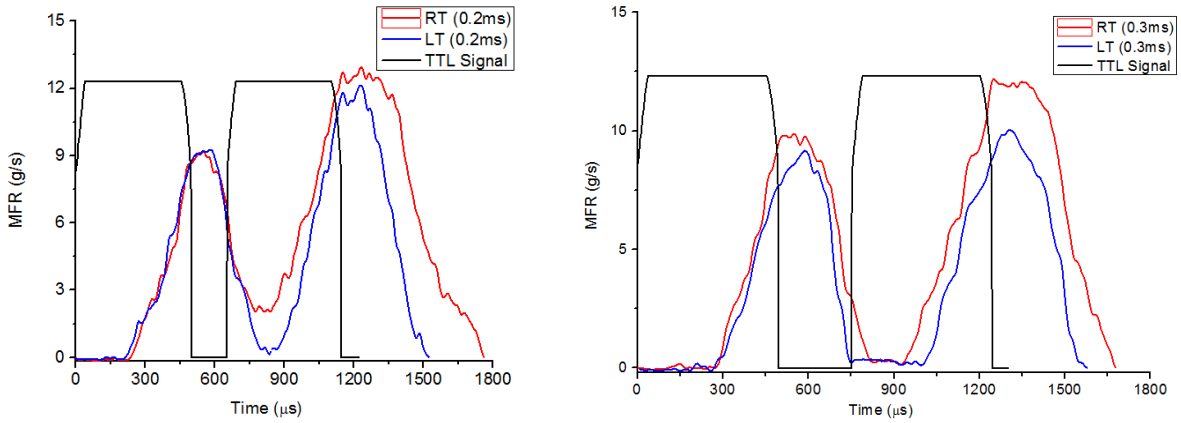

a b

Figure 4-19 MFR shapes for 2-split injection with (a) 0.2 ms and (b) 0.3 ms dwell (p_{inj} of 35 MPa)

The MFRs with 60 MPa injection pressure are shown in Figure 4-20. All cases show the same trends as mentioned above but with much stronger interaction between splits, presenting higher degree of continuation between splits and longer injection duration than the energizing duration. In all cases, the LT condition persistently results in lower MFR and interaction degree than the RT ones. This suggests that LT tends to effectively weaken the interaction between splits by influencing the opening and closing of the injector. The aforementioned effect of viscosity can explain these effects. It can be concluded that low temperature can effectively weaken the interaction between splits by changing the flow regimes more quickly.

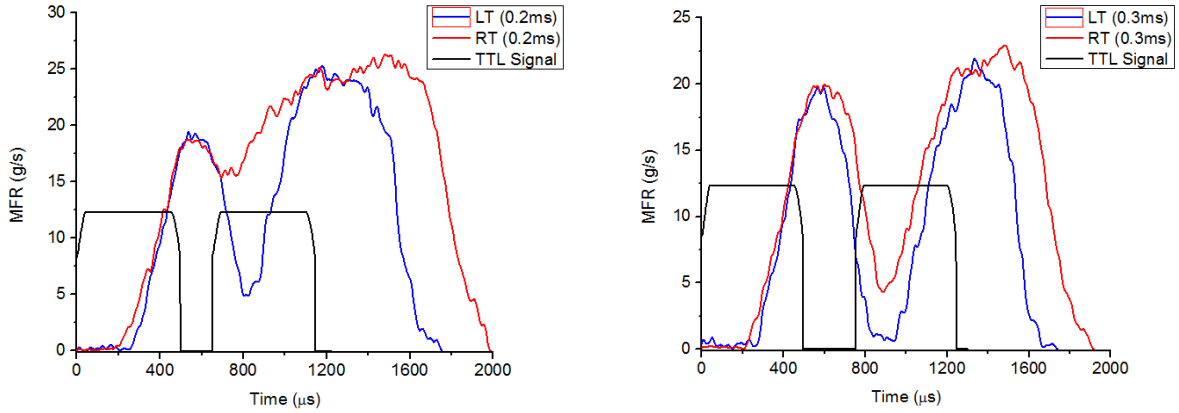

a b

Figure 4-20 MFR shapes for 2-split injection with (a) 0.2 ms and (b) 0.3 ms dwell (p_{inj} of 60 MPa)

(2) Interaction analysis

These results show that dwell interval, the number of split injections and the energizing duration of the first split injection exert profound influence on the degree of interaction. The degree of interaction directly affects the MFR thus injected fuel mass. This significantly influences the combustion and engine performance. It is therefore of great importance to analyze the interaction under various injection conditions. To quantify interaction degree, the interaction coefficient (I_c) is introduced, defined as:

$$I_c = I_{c1} \cdot I_{c2} \cdot \ldots \cdot I_{ci} \cdot \ldots \cdot I_{cn}; \quad i = 1,2,3,\ldots n-1; \qquad \text{Equation 4-11}$$

$$I_{ci} = t_i / \tau_i; \quad i = 1,2,3,\ldots n-1; \qquad \text{Equation 4-12}$$

Where n is the number of splits per injection, I_{ci} is the interaction coefficient for the i_{th} split, t_i is the injection duration of i_{th} split and τ_i is the i_{th} dwell interval duration.

The former MFR shape graphs for split injection suggest that for various values of the ratio I_c, the moment of start of injection for each split is different, leading to different peak

values of MFRs and different MFR shapes. The injection delays for each split under both RT and LT cases with 60 MPa injection pressure are very useful to study the injection features, as shown in Figure 4-21. As the value of I_c increases, the injection delays for the first split in different cases keep almost constant with LT case presenting longer delays, whereas the delays for the second split increase and peak at a certain point before showing a dramatic decrease. Specifically, when I_c is low, the interaction is weak and splits become non-continuous, consequently, the injection delay is mainly affected by the temperature (thus fuel viscosity). With the increase of I_c (long injection duration with short dwell interval), the delays for the second split increase drastically, leading to the severe retardation of injector opening and less injected fuel mass.

The further increase of I_c leads to a dramatic reduction of injection delay, and strong interaction ensues. For the RT case this process of change of I_c, with steeper changing rate, appears to result in stronger effect on the injection delay. This means that the MFR shapes for RT are more continuous. The LT case with lower decreasing rate of the delay tends to be less vulnerable to the variation of I_c.

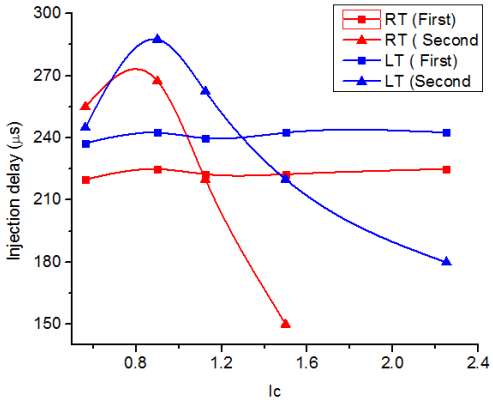

Figure 4-21 Injection delays for 2-split injection with p_{inj} of 60MPa

This injection delay increase can be assumed to be attributed to the accelerating closing movement of the needle when the second energizing signal starts. This assumption is explained below. Generally, when the energization for the first split disappears, the injector begins to close. The needle accelerates to close due to the returning force enforced by the piezo material, with initial velocity being zero (when the needle arrives the highest point, its velocity is zero). After the needle begins to move, it is controlled by both the returning force and the fluid friction force exerted by fuel. Consequently, the needle should accelerate and then decelerate. If the second energizing signal starts during the needle closing phase, the needle cannot lift right away and should move towards the hole outlet for a certain distance continuingly before changing its moving direction. This leads to the increase of injection delay for the second injection. If the second energizing signal begins at some time point when the needle (under the control of all forces) can just fully close the injector and its velocity decreases to zero, the longest injection delay for the second splits occurs. The increase of injection delay inevitably shortens the actual injection duration and leads to the reduction of fuel mass [11].

Basing on this assumption, the reduced injection delay varying trend for LT compared RT can be explained through the dominance of the physical mechanisms involved, namely, the energizing signal, fuel viscous force and needle inertia. The damping effect due to the increase of viscosity under LT can effectively weaken the interaction. This means that the needle motion is less affected by its inertia when the energization of the second split injection starts because of lower needle moving velocity. In this case, the motion regularity of the

needle is mainly governed by the energizing signal, fuel viscous force and needle inertia simultaneously. However, under room temperature, the effects of energizing signal and needle inertial tend to be more important compared with the impacts of viscosity.

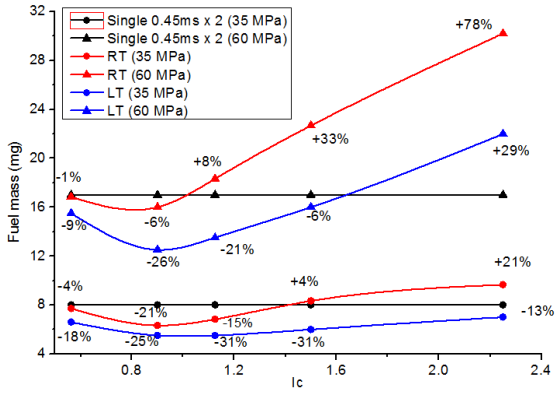

Figure 4-22 Injected fuel mass vs interaction number for 2-split injection

The corresponding fuel masses per injection for 2-split injection are presented in Figure 4-22. The varying trends of mass variation per injection are opposite to the corresponding injection delays for the second split injection in each case, as shown in Figure 4-21. This is to be expected as the retardation of injector opening on the second split leads to shorter injection duration and less fuel mass injected. The advance of injector opening on the second split injection (caused by shorter dwell between the split injections) contributes to longer injection duration and more fuel mass for the second split. For the cases with high (60 MPa) injection pressure, the LT case shows the lowest total fuel mass injected for the total TTL duration (26% less than the double TTL single injection duration baseline, showing negative interaction) at the point corresponding to its highest second split injection delay as shown in Figure 4-21. However, the RT case presents the highest total fuel mass injected (78% more than the baseline for single injection, showing positive interaction) at the point

corresponding to the shortest dwell and the lowest second split injection delay. With lower injection pressure (35 MPa), the LT case presents higher relative variation (-31%) of the total fuel mass at the lowest point compared with the variation of the total fuel mass with 60 MPa injection pressure. However, the total fuel mass injected at RT shows lower relative variation (+21%) at its final point (for highest I_c i.e. shortest dwell) compared with its counterpart for 60 MPa injection pressure.

4.6 Conclusion and summary

The injection characteristics of multiple injection strategy were successfully studied by applying the long tube measuring instrument for real-time fuel MFR measurement. The instantaneous MFR and total fuel mass delivered in each split were quantitatively studied. Furthermore, the interaction degree among splits was quantitatively linked to the dwell interval and the injection duration distribution of each split. The influences of low temperature on the injection characteristics and interaction were also studied. The following conclusions can be drawn.

(1) The injection duration is longer than the injector energizing duration. Raised injection pressure shortens the injection delay and increases the MFR. The injection duration of the first split, dwell and the number of split injections dominate the interaction.

(2) Low fuel temperature leads to lower MFR, longer injection delay, shorter injection duration and less injected fuel mass, especially under low injection pressure. The raised viscosity under low temperature retards the injector closing by decelerating the needle

movement with higher friction. The discharge coefficient (C_d) correlations show that the influences of fuel viscosity on C_d tend to be more significant than those of geometric structure of injector hole under low temperature.

(3) The inception of cavitation can be effectively curbed by low fuel temperature. Low fuel temperature accelerates the transition of flow regime from cavitating to turbulent and then to laminar flow when the injection pressure difference decreases. The combination of low temperature and low injection pressure difference tends to increase the chances for laminar flow, thereby decreasing the C_d.

(4) The injection delay is increased under cold condition, causing shorter injection duration and less fuel mass. The interaction degree between split injection events is also considerably weakened by low fuel temperature, contributing to much less continuous MFR shapes for split injection compared with the ones under room temperature.

Chapter 5 **Primary breakup close to the injector tip**

5.1 Introduction

Diesel spray theoretically involves a wide range of factors and mechanisms, for instance, nozzle structure, flow regimes (laminar, turbulent and cavitating flow), primary and secondary breakup and gas-liquid interaction [109, 110]. The liquid fuel generally begins its breakup at the outlet of the injector tip and the primary breakup determines the spray initiation and evolution, for instance the spray morphology and macroscopic characteristics [48, 111]. The spray morphology dominates momentum transfer between liquid and gas, thus the fuel distribution and mixture preparation [48, 58]. Understanding of spray primary breakup can significantly enhance the understanding of spray atomization and mixture formation as spray characteristics of the initial stage are to be passed to later breakup stages [55, 112, 113].

The studies of primary breakup mechanism through the observation of the spray morphology show that the radial expansion of liquid jet and the air drag force are important factors for the mushroom-shaped jet formation [114, 115]. The residue of the injection is also partly responsible for the formation of mushroom shaped spray jet [8, 113, 115]. It was observed that the residue penetrates obviously faster than the fresh fuel initially. This phenomenon was observed during the transient injector opening stage rather than quasi-steady stage [112]. During the other transient stage, namely the end of injection, lower effective injection pressure leads to lower initial penetrating velocity than that of quasi-steady state [112, 113, 115]. Lower injection pressure slows down the breakup of the droplets, leading

to much larger ligaments.

For the quasi-stationary phase, the primary breakup highly depends on the flow regimes in the injector. Akira Sou et al. [116] reported that the strong turbulence and cavitation considerably affect the initial breakup of the spray jet. Desantes et al.[53] investigated the impact of cavitation on the primary breakup by injecting fuel into a liquid of the same type, allowing the visualization of air bubbles induced by cavitation. The results showed that higher pressure drop led to stronger cavitation and more air bubbles, resulting in great increase of the microscopic cone angle.

The initial disintegration of spray is significantly affected by the nozzle geometry [29, 117-120]. For nozzles with sharp inlet edge, stronger turbulence and cavitation significantly boost the primary breakup. This is because the redirection of fuel at the hole inlet is more obvious for sharp inlet edge injector than for that with round edge [58].

Primary breakup also shows high sensitivity to fuel properties [121]. Generally, reduced surface tension enhances the breakup of the ligaments [113]. During the initial injection stage, smaller effective flow area for more viscous fuel results in higher boundary laminar layer and larger ligaments because of the stabilizing effect of the fuel properties. Particles therefore present more spherical shape than the same sized drops of its counterparts with low viscosity as high viscosity and surface tension enhance the retention of the spherical shape [113]. In [112], the spray primary breakup was investigated with temperature varying from 440 to 1200 K with back pressure (Pb) ranging between 5 and 79 bar. The results showed that high injection pressure and temperature diminish the influences fuel surface

tension.

The aforementioned studies revealed some important mechanisms for initial breakup. However, the relationship between the flow regime in the injector hole and the mushroom-shaped spray jet has not been deeply studied although the development of the mushroom head has been fully described [114, 115]. The fuel dispersion quality in the near field has not been quantified either. The primary breakup characteristics when using split injection strategy are still unknown. The impact of the interaction between split injection events on the primary breakup requires deep study.

In addition, engine cold start requires the studies on the unknown primary breakup characteristics under low temperature which are expected to be significantly affected by the variation of fuel properties [103, 112]. The transition of breakup regimes during the transient spray stages (injector opening and closing stages) under low temperature (LT) are still unknown. Besides, how the variation of temperature changes the primary breakup features when split injection strategy is employed still requires deep study.

5.2 Test conditions

The single-hole solenoid injector was employed in this section. The long tube MFR measuring instrument was first used to study the influences of temperature on MFR by employing single injection. The long distance microscope together with the ultrahigh speed CCD camera was then employed to investigate the primary breakup of spray by using both single and split injection strategies. The investigated area is 2.3 mm long downstream of the

injector tip.

Two groups of tests were performed in this chapter. The first group of tests was to study the formation regime of the mushroom and distinct characteristics of split injection strategy. The tests were carried out under room temperature (25 degC) with atmospheric back pressure. The injection pressure ranged between 45 and 120 MPa. 2-split and 3-split injections were employed. Under all injection pressures, the injection durations for 2-split injections were both equal to 0.5 ms and for 3-split injections three equal durations 0.5 ms were used. Dwell varied from 0.2 to 0.8 ms. To study the impact of the distribution of the duration of energization periods on the spray characteristics, an additional set of tests was carried out under 90 MPa injection pressure. For this set of tests, the injection duration is 0.6 ms injection followed by τ ms dwell time and then 0.4 ms second injection, with τ varying from 0.3 to 0.8 ms. The injection durations for different strategies are shown in Table 5-1.

Table 5-1 Test matrix for primary breakup under RT

	Single	2-split		3-split
Injection duration (ms)	1	0.5 + 0.5	0.6 + 0.4	0.5 + 0.5 + 0.5
Dwell (ms)	----	0.2, 0.3, 0.5, 0.8	0.3, 0.5, 0.8	0.2, 0.3, 0.5, 0.8

The second group of tests is to investigate the effects of fuel temperature. MFR of single injection (1ms energizing duration) under various temperatures (-18 to 48 degC) was first measured with the long tube measuring instrument. The spray development was then captured by the ultra-high speed camera. The injection pressure was set to 60 MPa (low injection pressure) and 90 MPa (high injection pressure). The injection durations are shown

in Table 5-1 with blue color.

5.3 Characteristics of primary breakup under room temperature

5.3.1 Characteristics of single injection under room temperature

(1) Studied spray stage

The spray characteristics of the quasi-steady stage have been studied by many researchers, consequently the quasi-steady stage is not the focus of this study. According to the MFR curves in Figure 5-1, it can be seen that the start and end of the injection are interesting. Low MFR means low spray velocity and low chances of breakup. It can be expected that poor fuel dispersion occurs for the two stages, leading to large droplets and poor combustion. This study therefore mainly focused on the two stages.

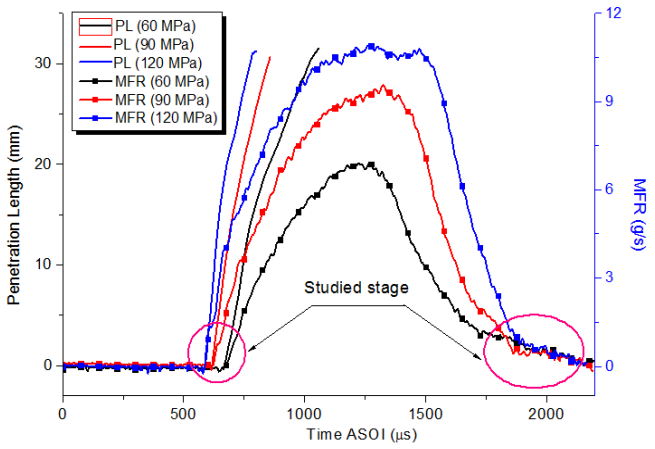

Figure 5-1 MFR and penetration length vs time

(2) Morphology development under various injection pressures

As presented in Figure 5-2, with 45 MPa injection pressure, the mushroom-shaped tip appears and shows little sign of breakup in the view field. (The shape of the mushroom spray

head is illustrated in Figure 3-14 (a)) The shape of the mushroom remains almost unchanged although the ambient air affects its movement, suggesting that the initial inertia of the mushroom is insufficiently high to overcome the fuel surface tension. Between the mushroom-shaped head and the side-waved main spray, a “neck” (stem of liquid jet) with an increasing length forms during the spray development. The increased length of the “neck” suggests that the tip has higher velocity than the main spray. It takes 23 μs for the mushroom to move through the whole view field and the velocity increment due to gravity is 0.23 m/s which is very small and can be ignored when compared with the calculated initial velocity of the jet, 24 m/s. This suggests that the effect of gravity is unimportant for the faster movement of the spray mushroom, but some other stronger force accelerates the mushroom of the jet. Besides, the main spray develops from a smooth liquid column to a side-waved one. Some large ligaments (Figure 5-2) appear at the periphery after the waves form at the sides of the spray, meaning that the inertial force of the jet increases and the influence of the ambient gas becomes stronger. It is interesting to find that the spray shows poor dispersion as even at 50μs after start of injection (ASOI), an obvious compact liquid column at the very outlet of the injector tip is still observable.

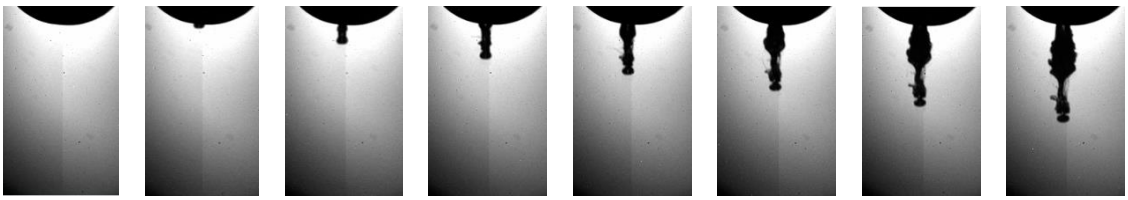

1μs 2μs 4μs 6μs 8μs 10μs 12μs 14μs

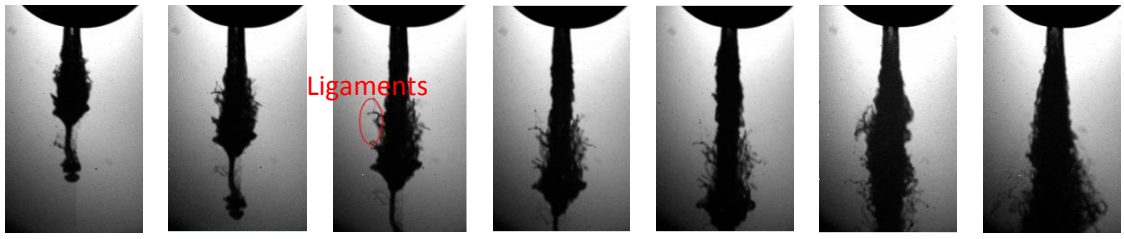

Figure 5-2 Spray morphology development of single injection under 45 MPa

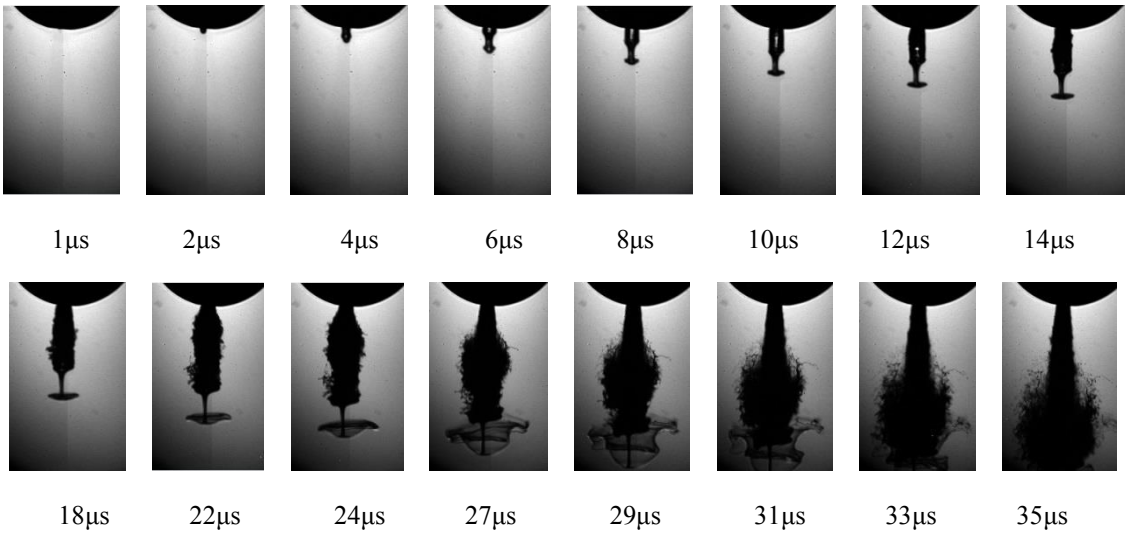

Figure 5-3 Spray morphology development of single injection under 60 MPa

The spray morphology under 60 MPa presents a similar picture, as shown in Figure 5-3. The intact liquid column, mushroom head and the increasing "neck" are also discovered. The high initial velocity (45m/s) when considering the acceleration due to gravity once again suggests that an additional force accelerates the mushroom head. However, some distinctions are also clearly observed. The mushroom-shaped head breaks up quickly, and is caught up (27μs) and overtaken by the incoming main spray. In addition, the main spray also breaks up quickly with the intact liquid column (before 12μs ASOI) becoming quite chaotic (after 14μs ASOI). The disappearance of the intact liquid column, which becomes wavy after 14μs, occurs before the breakup of the mushroom. This suggests stronger effects

of air drag force than those for the case of 45 MPa injection pressure. The spray shows larger cone angle probably because smaller sized ligaments form at the jet periphery due to higher air drag force.

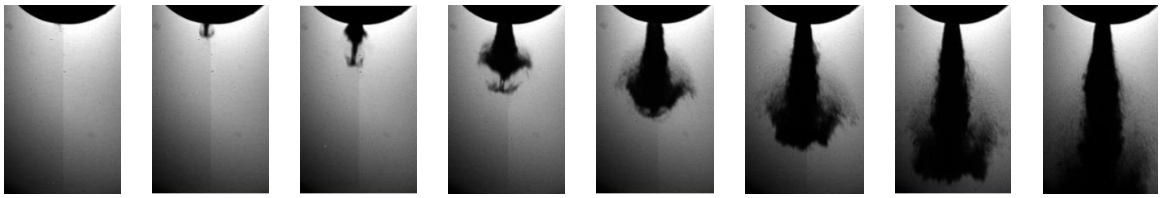

Figure 5-4 Spray morphology development of single injection under 120 MPa

Compared with low pressure cases (45 and 60 MPa), the high pressure case (120 MPa) is quite different, although the mushroom and the increased "neck" are still clearly seen in Figure 5-4. The intact liquid column does not appear at all but the fuel clusters at the periphery and spray front are clearly observed on its appearance, suggesting that the spray is dispersed at the very outlet of the injector. High injection pressure leads to strong cavitation and high turbulence which contribute to a highly dispersed spray. The cavitation and turbulence are of great importance for the primary breakup as they result in instant breakup of the jet at the very nozzle outlet [36, 122]. The high degree of fuel dispersion can greatly boost the air entrainment, denoting the momentum transfer between ambient gas and dispersed fuel cluster.

(3) The formation of the mushroom-shaped spray head

According to the development of spray morphology shown in Figures 5-2 and 5-3, the mushroom-shaped head appears just at the very outlet of the injector where the ambient air

exerts only slight effects. This means that the mushroom-shaped head (the spheroid part) may form at the very exit or have already formed in the injector. The penetrating movement of the spray leads to the enlargement of the mushroom-shape. There are, therefore, two phases for the mushroom development, namely formation and growth.

The formation of the mushroom was studied in several studies. According to Hiroshi et al. [114], the radial expansion of the fuel was the main reason for the formation. Unfortunately, in their study, the test was carried out at low frame speed (50,000 frames /sec) with the timing shift of the camera trigger for various injection events. This method leads to the loss of some very important information at the very start of the injection as the spray characteristics for each injection obviously vary. More importantly, the mushroom shape appears on the immediate appearance of the spray and this shows that fuel flow in the injector hole exerts profound influence on the mushroom formation. Therefore, the radial expansion of the spray at the initiation seems to be more suitable to explain the developing stage not the forming stage.

According to the results in the present study, the fuel flow regime in the injector hole can be assumed to be the root reason for its formation. At the initial stage of injector opening, the fuel flows relatively slowly and the flow can be assumed as laminar which causes large velocity difference between the fuel at the hole center and that at the hole wall. The laminar flow regime adapted from Figure 4-18 for single hole injector is shown in Figure 5-5.

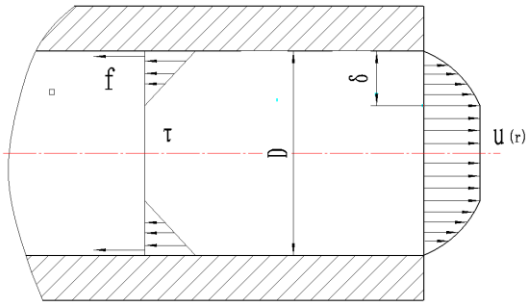

Figure 5-5 Laminar flow regime

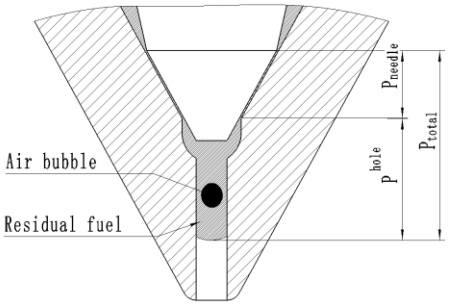

Figure 5-6 Initial injector opening

Basing on Equations 4-9 and 4-10, the following can be obtained

$$\delta \propto \sqrt{\frac{\nu \cdot L}{\sqrt{\Delta p}}} \qquad \text{Equation 5-1}$$

It can be expected that, at the injection initiation, the injection pressure difference across the injector hole p_{hole} is quite low, as shown in Figure 5-6. Therefore, the laminar flow boundary layer thickness is quite high, meaning that the fuel flow is likely to be laminar. In addition, the residual fuel of the former injection is also likely to boost the laminar flow as its initial velocity is zero. The resultant velocity $u(r)$ profile is not flat, leading to obvious velocity differences between the hole center and the periphery. When the fuel flows out, the mushroom shape might have already formed. During the initial injector opening stage, the effective injection pressure is difficult to obtain, thus the quantified boundary layer thickness.

In this case, Equation 4-7 tends to be an easier way to calculate the boundary layer thickness. A coefficient K_δ is added and the length of the nozzle hole is employed, shown as:

$$\delta = K_\delta \sqrt{\frac{\nu \cdot L}{u}} \qquad \text{Equation 5-2}$$

K_δ depends on various factors, for instance the finish of the nozzle hole surface and properties of the liquid [108]. In Amin's [123] study, the flowing fluid was hydrogen and K_δ was taken as 2.87. It can be expected that the value of the coefficient for winter diesel employed in present study is larger than 2.87 as winter diesel is more viscous than hydrogen. Due to the difficulty of measuring the accurate coefficient for the injector employed in present study, 2.87 is used although some inaccuracy is invited. The calculated boundary layer thickness and the percentage for the nozzle size under various injection pressures at the initial injection stage are calculated and presented in Table 5-2. The results suggest that the possibility of the existence of the laminar flow during the initial spray stage is quite high. The boundary layer thickness and the percentage for the nozzle size at the quasi-steady stage are also calculated, shown in Table 5-2. In this case, the laminar flow tends to be eliminated.

This assumption that the flow regime leads to the formation of the mushroom head can be further validated by the dimensionless Re ($\mathrm{Re} = V_{act} * d_0 / \nu$) which denotes the fuel flow regime at the first sight of the spray.

V_{act} can be calculated by the measured initial penetration length and time interval (1μs) for capturing the images. The calculated *Re* values under various injection pressures are

shown in Table 5-2.

Table 5-2 Initial spray velocity and the dimensionless numbers under various injection pressures

p_{inj} (MPa)	45	60	90	120
$u_{initial}$ (m/s)	24	45	77.5	120
$\delta_{initial}$ (mm)	0.02462	0.01798	0.01370	0.01101
$2\delta / D_{initial}$ (%)	27.357	19.980	15.226	12.233
δ_{quasi} (mm)	1.473×10^{-3}	1.370×10^{-3}	1.2383×10^{-3}	1.1524×10^{-3}
$2\delta / D_{quasi}$ (%)	1.636	1.523	1.376	1.280
$Re_{initial}$	1800	3000	5813	9000
$We_{initial}$	2915	8098	30400	72883

According to the values of *Re*, the flow under 45 MPa (*Re*=1800) is likely to be laminar. While the flow under 60 (*Re*=3000) and 90 MPa (*Re*=5813) is in the transition state, the flow under 120 MPa (*Re* =9000) injection pressure is totally turbulent. The predicted flow regime agrees very well with the chances of the mushroom appearance and the required breakup time under various injection pressures.

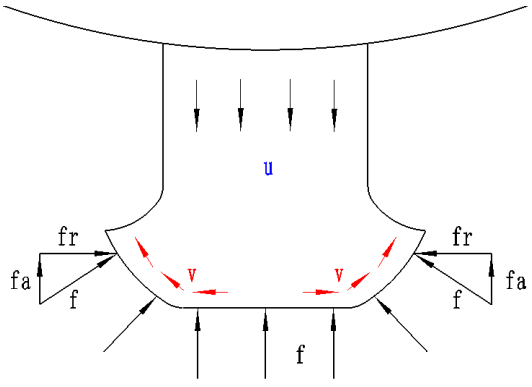

Figure 5-7 Forces exerted on the spray mushroom at the initial stage (adapted from [114])

After the formation phase, the development of the mushroom shaped tip can be attributed to the air drag force. The expected air forces exerted on the spray are shown in Figure 5-7. In this graph, f is the air resistance force, f_r is the radial component of f, f_a is the axial component of f, v is the fuel velocity at the periphery and u is the jet velocity in the center. Due to the front air resistance, the front liquid fuel shows radial propagation. Although the side air resistance force (f_r) prevents the radial propagation of the liquid fuel, the liquid still propagates radially due to lower radial fuel flow velocity thus lower side resistance force. The axial force f_a simultaneously forces the fuel to move backward. The liquid fuel therefore flows along the periphery, as shown by the red arrows, leading to the enlargement of the mushroom.

The *We* number shown in Equation 2-1 can be calculated to assess the possibility of breakup. Before the breakup of the mushroom, the diameter of the mushroom can be approximately taken as the injector hole diameter. The calculated initial *We* values are shown in Table 5-2. It is clearly shown that values of *We* under low injection pressure (45 MPa) are much lower than those under higher injection pressure (120 MPa), meaning that the mushroom under low injection pressure condition can survive much longer due to the lower possibility of breakup and lower rate of growth.

(4) The formation of the neck

The formation of the neck is interesting as it can reflect the force that is exerted on the liquid mushroom. According to the aforementioned analysis of the increase of the neck, the gravity is unlikely to be the root reason. Its formation, which may be attributed to the air

bubble that is sucked into the injector hole, was studied by Badock et al. [107]. In their study, a transparent nozzle was employed, enabling the visualization of the fuel flow. It was observed that some air was sucked into the hole when the needle lifts, as shown in Figure 5-6. If the air moves into the residual fuel of the former injection, the neck tends to appear. The air bubble and the residual fuel are compressed and accelerated by the pressure wave. The air bubble after being pushed out expands, collapses and further accelerates the residual fuel that is in its front, namely, the mushroom. This further acceleration leads to higher speed of the mushroom and the increase of the neck length [124]. The mechanism of the neck formation suggests that the initial breakup regimes of the mushroom and main spray body are quite different at the initial stage. The air drag force is mainly responsible for the mushroom breakup which is boosted by the accelerating effects of the air bubble. By contrast, the turbulent / cavitating flow regime is important for the breakup of the main spray.

It is noteworthy that lower injection pressure results in a longer neck, as presented in Figures 5-2, 5-3 and 5-4. It is quite likely that high injection pressure leads to large velocity of the main spray, leading to much smaller velocity difference between the mushroom head and the main spray. The further increased velocity of the main spray due to further injector opening enables the main spray to chase up and overtake the mushroom head, causing much shorter neck when compared with the one under low injection pressure. Besides, the lower absolute velocities (when injection pressure being less than around 60 MPa) for the mushroom and the main body lead to poorer primary breakup, giving sufficient time for the neck to increase in length. It can be also expected that the appearance of the neck and

mushroom suggests the existence of the fuel remains in the injector hole. It was reported that the remaining fuel of the previous injection and some gas come out before the fresh fuel, forming a intact spheroid [112, 113]. Cyril et al. [115] also found that the spheroidal mushroom appears at the immediate appearance of the fuel jet and it was pointed out that gas takes about 50 to 83% of the hole volume. Low injection pressure leads to higher possibility of the existence of the fuel residual and thus higher possibility of the appearance of the neck. This is understandable as low injection pressure contributes to lower velocity for the ligament released at the end of the injection. The lower velocity possibly leads to the fact that the inertial force fails to overcome the fluid friction.

(5) Spray characteristics

The spray area is a good indicator to denote the spray propagation rate. As shown in Figure 5-8 (a), higher pressure leads to a higher increase of area, meaning quicker fuel propagation. The area dips after it peaks. This may be attributed to the fact that the dispersed fuel ligaments or droplets around the spray tip move out of the view field, resulting in less fuel being observed. It is noteworthy that lower injection pressure causes larger magnitude of the area dip. This may be attributed to the larger area of the mushroom after breakup, as shown in Figure 5-3. In addition, after the area dip, the cases with 60 and 120 MPa injection pressure seem to show similar fuel areas, whilst the case under 90 MPa injection pressure tends to presents the highest fuel area. The assumed throttling effect under 90 MPa or fuel flipping across the injector hole under 120 MPa injection pressure may be responsible for the larger area than the other two cases. This can be further verified by

the development of cone angle, as shown in Figure 5-8 (b) where the 90 MPa injection pressure case has the largest cone angle due to throttling effect or strong cavitation [[105, 122]. Further discussion will be given in later section where the effects of fuel temperature are discussed.

Sou et al. [116] studied the water flow regimes in a 2D nozzle with sharp inlet edge by visualizing the cavitation in the nozzle hole. It was reported that when *Re* is higher than 68000, the flow is super cavitating, causing an obvious higher cone angle. The obvious radial velocity and strong turbulence of the ligaments and droplets are the main reasons for the larger cone angle. However, when *Re* is higher than 76000, the flow is in the hydraulic flipping regime, leading to complete detachment of liquid from the hole wall [116]. The cone angle is clearly smaller compared with the cavitating one. The injector structure used in their study shares some similarities with the one used in this study, namely, sharp hole inlet edge and no hole convergence,. The aforementioned two key values of *Re* (68000 and 76000) are therefore employed as thresholds to distinguish the flow regimes in this study although some inaccuracies may be invited. *Re* can be calculated through Equation 2-2. The actual flow velocity can be calculated through Equation:

$$V_{act} = \frac{\dot{m}}{\rho \pi d_0^2 / 4} \qquad \text{Equation 5-3}$$

Where: $\dot{m}$ is measured MFR, shown in Figure 5-1.

From the varying trend of *Re* during the opening phase under various injection pressures, shown in Figure 5-9, it can be found that 120 MPa injection pressure cannot lead to strong

cavitation, much less flipping before 50 μs ASOI. The throttling effect is therefore more possible to be the reason. The throttling effect under 60 MPa may not have appeared before the end of imaging due to relatively lower needle motion. However, 120 MPa injection pressure can lead to quick needle lift and the throttling effect is not as obvious as that under 90 MPa.

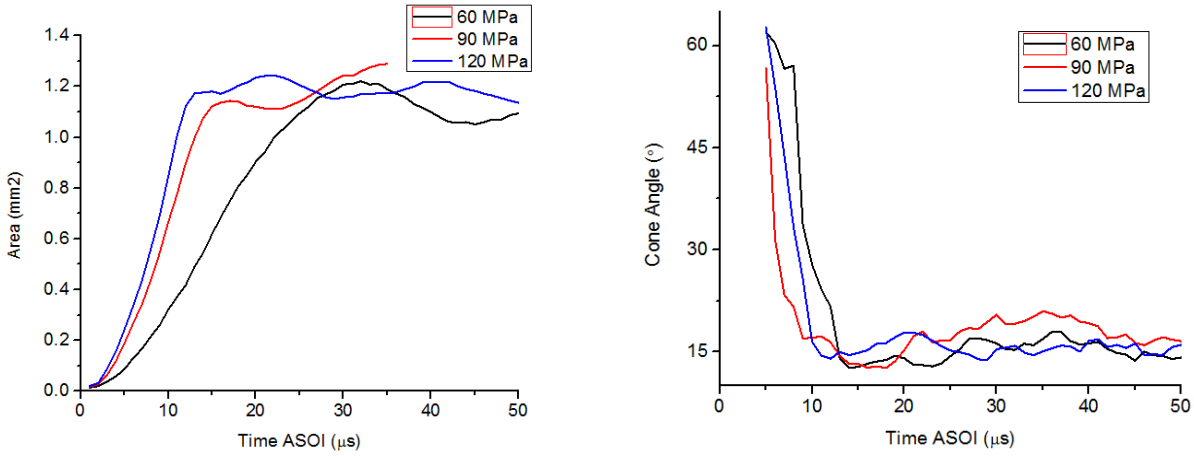

a b

Figure 5-8 (a) spray area and (b) cone angle under various injection pressures

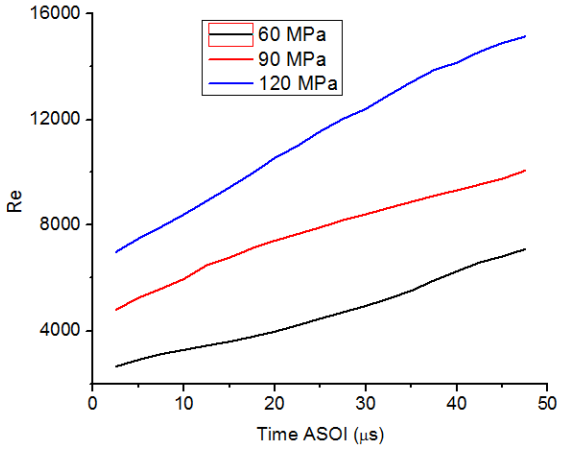

Figure 5-9 Re number at the initial stage

It is clearly seen that during the developing stage (before 15 μs), shown in Figure 5-8 (b),

the plume shows an obvious cone angle reduction. The development of the cone angle causes calculating inaccuracies and the varying trend of the cone angle during this stage is not deeply discussed in this study.

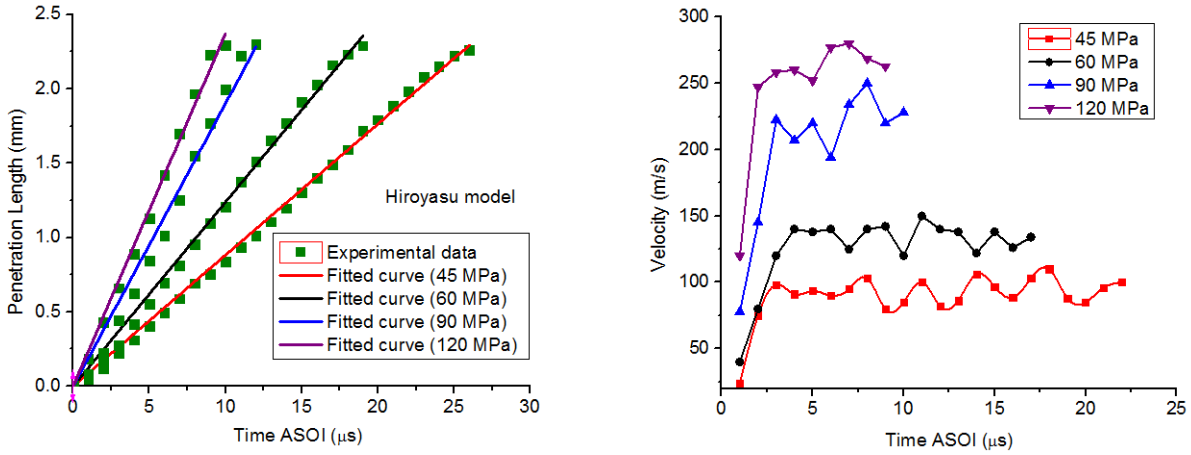

a b

Figure 5-10 (a) penetration length and (b) velocity for single injection under different injection pressures

The experimental jet penetration lengths under various injection pressures are presented in Figure 5-10 (a). It is worth noting that the penetration length shows an almost linear increase except for the first two or three microseconds, suggesting that the fuel jet has completed its acceleration at the very beginning of injection [23]. The corresponding velocities are shown in Figure 5-10 (b). Apparently, the fuel jet presents an obvious velocity increase within only a few microseconds, then shows an almost constant velocity with some fluctuations. However, it does not mean that the fuel plume has completely finished its acceleration for its whole movement. This is because the injector has not fully opened and the spray is still in the transition state.

The Hiroyasu model (Equation 2-6 to 2-8) is used to further study the varying trend of

penetration. As presented in Equation 2-7, before $t_{breakup}$, the plume length increases linearly with the escape of time *t*. The varying trend of penetration length suggests that *t* is smaller than $t_{breakup}$, therefore the first equation is used to fit the experimental data. Aim to get high fitting accuracy, the coefficient 0.39 is replaced by a variable "*A*" which can be changed according to different spray conditions, as shown in Equation 5-4. The fitted curves are shown in Figure 5-10 (a) and high accuracy is obtained. The values of variable coefficient *A* and R^2 under various injection pressures are shown in Table 5-3. The high accuracy (high value for R^2) further verifies the argument that the plume moves at an almost constant velocity during the initial stage.

$$S = \begin{cases} 0.39t\sqrt{\frac{2\Delta p}{\rho_f}} = At\sqrt{\frac{2\Delta p}{\rho_f}} & t < t_{breakup} \\ 2.95\left(\frac{\Delta p}{\rho_g}\right)^{1/4}\sqrt{d_0 t} & t \geq t_{breakup} \end{cases} \quad \text{Equation 5-4}$$

Table 5-3 The fitted values for Hiroyasu model

P_{inj} (MPa)	45	60	90	120
A	0.26431	0.32149	0.40287	0.4350
R^2	0.9975	0.9952	0.9827	0.9946

(6) Dispersion quantification

Generally, it is difficult to quantify the dispersion quality in the near nozzle field just with images. However, the combination of images and the measurement of fuel MFR makes this possible. In present study, the dispersion quality is quantified by the ratio of fuel mass and spray area (similar to fuel air ratio), shown as:

$$\lambda_{ratio} = \frac{\Delta m}{S}$$

Equation 5-5

Where: λ_{ratio} is fuel mass/spray area ratio, mg/mm^2; Δm is fuel mass seen in the image, mg; S is the spray area.

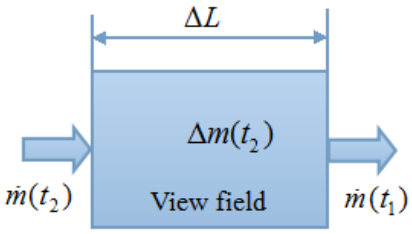

Figure 5-11 The schematic of the fuel mass equilibrium

The spray area S can be obtained from the images, as shown in Figure 5-8 (a). However, the fuel mass seen in the image needs to be calculated according to the equilibrium of the fuel mass, as shown in Figure 5-11. At time t_2, the fuel flows into the view field with MFR of $\dot{m}(t_2)$ and simultaneously fuel flows out of the view field with MFR of $\dot{m}(t_1)$. It should be noted that the MFR for $\dot{m}(t_2)$ and $\dot{m}(t_1)$ is the MFR at the outlet of injector at different time points. During the injector opening stage, the MFR is increasing, MFR $\dot{m}(t_1)$ therefore is smaller than $\dot{m}(t_2)$. The fuel mass in the view field can be calculated by Equation 5-6:

$$\Delta m(t_2) = \int_0^{t_2} \dot{m}(t)dt - \int_0^{t_1} \dot{m}(t)dt$$

Equation 5-6

Because the tests were carried out under atmospheric condition, the effects of air drag force on the spray in the near field can be ignored. The penetrating velocity of the fuel released at a certain time point is seen as constant in the view field. The time difference Δt between t_2 and t_1 is the duration of the fuel movement in the view field. The variation of

MFR leads to the variation of spray velocity, thus the variation of Δt. Δt therefore should be written as $\Delta t(t)$ and can be calculated through Equation 5-7, shown as:

$$\Delta t = t_2 - t_1 = \frac{\Delta L}{V(t_1)}$$

Equation 5-7

Where: ΔL is the length of the view field downstream of the injector tip, 2.3 mm.

The velocity of the spray can be obtained through the measured MFR, as shown in Equation 5-3. Equation 5-6 then can be written as:

$$\Delta m(t_2) = \int_0^{t_2} \dot{m}(t)dt - \int_0^{t_1} \dot{m}(t)dt = \int_{t_1}^{t_1+\Delta t} \dot{m}(t)dt = \int_{t_1}^{t_1+\frac{\Delta L \rho \pi d_0^2}{4\dot{m}(t_1)}} \dot{m}(t)dt, \qquad t_1 > t_{edge}$$

Equation 5-8

Where: t_{edge} is the time when the spray penetrates out of the view field.

When t_1 is smaller than t_{edge}, Δm should be obtained through Equation 5-9:

$$\Delta m = \int_0^t \dot{m}(t)dt$$

Equation 5-9

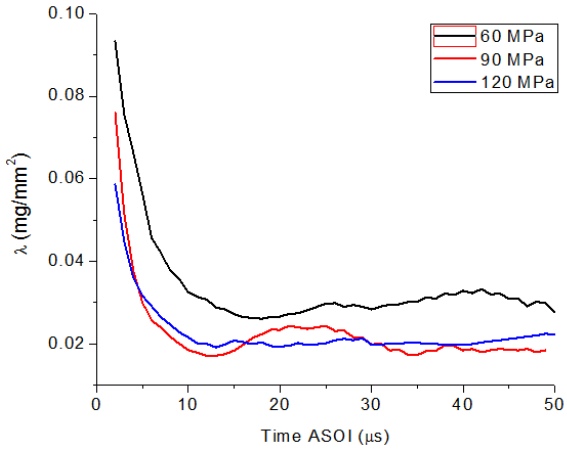

Figure 5-12 The development of fuel mass/spray area ratio

As shown in Figure 5-12, fuel mass/spray area ratio, λ, shows a sharp decrease before leveling off with the elapse of time. The continuous opening of the injector causes a dramatic increase of spray velocity, thus much better dispersion. According to the graph, it

can be assumed that the dispersion quality is greatly improved within 10 μs. Lower injection pressure (60 MPa) obviously leads to larger mass/spray area ratio than the cases under high injection pressures (90 and 120 MPa). This difference is quite obvious at the very start of injection. The leveling off the fuel mass/spray area ratio suggests that little improvement of fuel distribution in the near field can be expected although the injector continues to opening.

5.3.2 **Characteristics of split injection under room temperature**

For split injection strategy, the primary breakup of each split injection events tends to present some distinctions due to the interaction between splits. Under room temperature, the characteristics of the second and third split injections tend to vary significantly. This subsection mainly focuses on the second and third split injections. The characteristics of the first split injection will be discussed in the following section where the impact of fuel temperature is studied.

5.3.2.1 Two-Split injection

(1) Morphology development of the second split

The morphology evolution of the second split injection event with 0.2 ms dwell under 60 MPa is shown in Figure 5-13. It is shown that some fuel drops of the former split are still observable when the second split spray appears. These drops understandably collide with the spray tip and decrease the velocity of the second split, resulting in the disservice of dispersion. In addition, the mushroom was not found during the test. It can be argued that

the incomplete injector closing causes the existence of fuel flow in the injector hole, resulting in the destruction of the formation of the mushroom.

When the dwell increases to 0.3 ms, the droplets that can be observable are much fewer, as presented in Figure 5-14. Therefore the second split is less affected by the remaining fuel of the first split, meaning weaker collision for the second split injection event. It can be thought that shorter dwell causes stronger collision whilst longer dwell leads to weaker collision. It should also be noted that the spray with 0.3 ms dwell shows smaller cone angle, lower velocity and poorer dispersion. This lower penetration speed indicates lower fuel MFR. For the 0.2 ms dwell case in Figure 5-13, it takes just 16 μs for the spray to penetrate out of the view field. However, for the 0.3 ms dwell case in Figure 5-14, it takes more than 26 μs for the spray to penetrate out of the view field. This obviously lower penetration rate means considerably lower mass flow rate (thereby less fuel mass injected) for the 0.3 ms dwell case. This type of phenomenon is thought to be related to the injection conditions, injection strategy, needle movement and injector technology although the exact reason is still unclear so far. More studies need to be carried out to identify the exact reason. (This type of phenomenon is called lower mass flow rate (MFR) and employed as a reason to explain the spray characteristics in this study).

Less injected fuel than the second split with 0.3 ms dwell is also expected at the initial injector opening stage. The lower MFR results in poorer fuel atomization as at 26 μs ASOI, the compact liquid column is still in the view field with little dispersion. In addition, the intact jet at the very outlet of the injector is still clearly observed at 40 μs ASOI. By

contrast, the case with 0.2 ms dwell gives a quite different picture, with the spray moving out of the view field at 16 μs and showing dispersed spray at the start of injection.

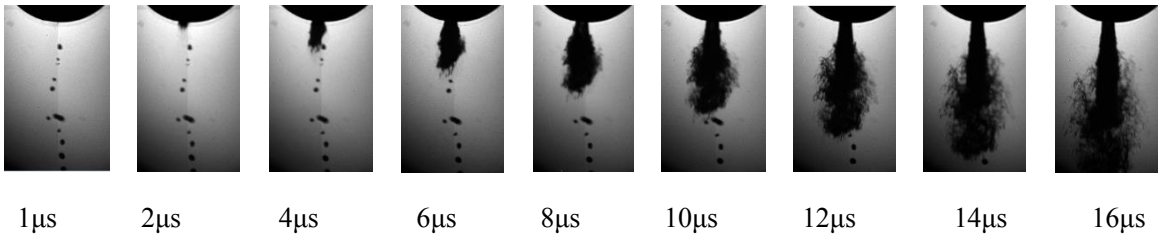

Figure 5-13 Morphology development of second split with 0.2 ms dwell under 60 MPa

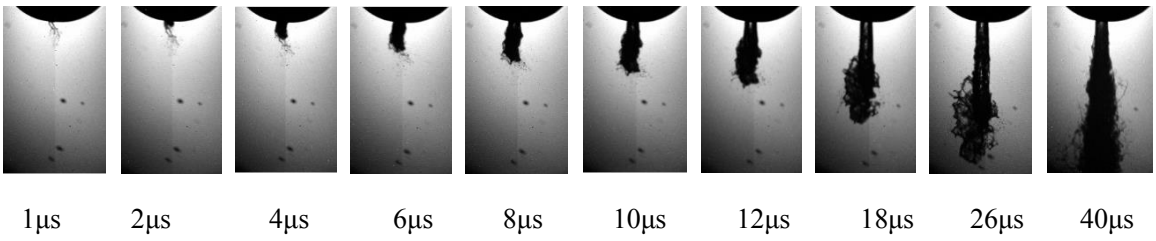

Figure 5-14 Morphology development of the second split with 0.3 ms dwell under 60 MPa

When the injection pressure increases to 120 MPa, some of the split injections with 0.2 ms dwell are actually single injections. However, some separated split injections were still successfully captured. Compared with the second split under 60 MPa with 0.2 ms dwell, the second split injection event under 120 MPa shows some distinctions, as shown in Figure 5-15. The large droplets left from the first split and the high inertial force of the second spray cause strong collision and high momentum loss. This strong collision contributes to a dramatic increase of the cone angle. It should be noted that this dramatic increase of cone angle may be caused by the air bubble collapse. By comparing the cone angle increase induced by collision or air bubble collapse under 60 MPa and 120 MPa, it is easy to find that higher injection pressure contributes to stronger collision or collapse due to higher inertial force and higher momentum.

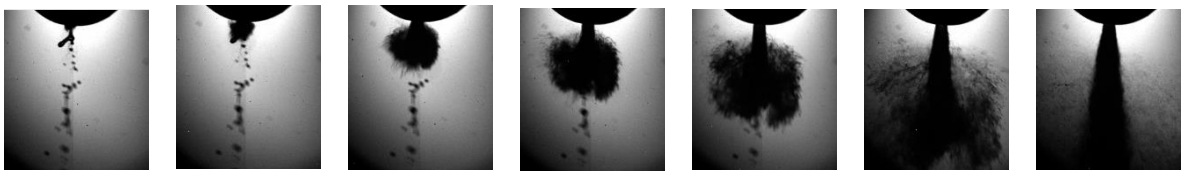

1μs 2μs 4μs 6μs 8μs 10μs 20μs

Figure 5-15 Morphology development of the second split with 0.2 ms dwell under 120 MPa

(2) Spray characteristics of the second split injection event

Morphology development of the second split suggests that spray characteristics of the second split injection event with different time intervals of dwell are quite different, as shown in Figure 5-16. Under low injection pressure (60 MPa), the 0.3 ms dwell case is the most special one. It has the slowest increasing rate for the area and the penetration length. The slow development trend for the area shows poor fuel dispersion, and the slow variation of penetration length means low spray tip velocity, thus low fuel MFR. It is quite likely that lower MFR at the initial injector opening stage is responsible for the distinctive characteristics.

Except for the 0.3 ms dwell case, the rest of cases show much quicker rates of area increase and slightly higher increasing rates of penetration length than the single injection. These higher penetrating rates may result from the quicker air movement induced by the first split [11]. The plume of the first injection event pushes the air forward, and the air at the spray periphery is simultaneously driven forward, flowing both radially and axially. This axial movement of air leads to lower front air resistance force and lower side drag force for the second split. Although this moving air cannot actually drive and accelerate the second split spray due to its lower velocity compared with that of the fuel penetration velocity, it can

"boost" the penetration rate of the second split injection event when compared with the penetration rate of the first split. This kind of effect can be called "induced air driving force" (for the second split spray or third split spray when applicable). This undoubtedly contributes to quicker fuel propagation and penetration. It can be understood that shorter dwell contributes to stronger induced driving force while longer dwell leads to weaker driving force for the upcoming split injection event. Christian et al. [125] studied the air entrainment at the view field of 2x2 mm^2 downstream of the injector tip by employing the PIV technique. It was reported that the radial induced air velocity could reach up to 9 m/s (at 0.8 mm radial position, 1.8 mm downstream of the injector) for a sharp edged inlet injector under 80 MPa injection pressure.

Special attention should be paid to the 0.2 ms dwell case which shows the strongest collision and driving force. The collision leads to an observable increase of the cone angle and area but without the decrease of penetration length. The collision may not be sufficiently strong to cause an obvious reduction of penetration.

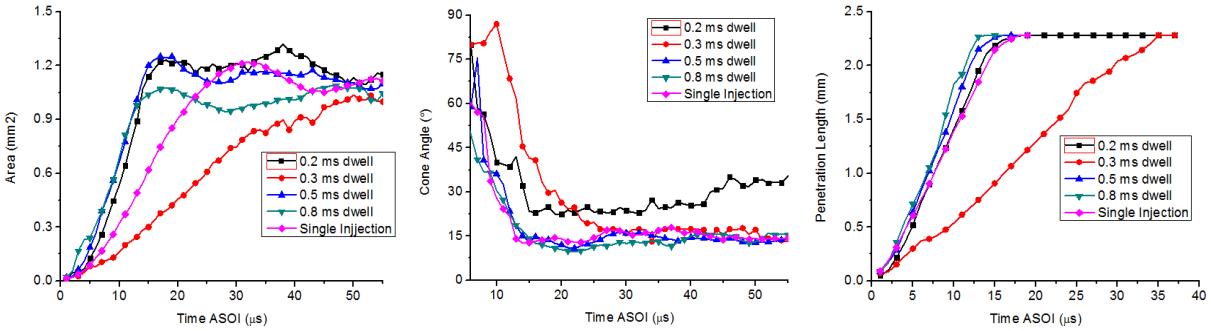

a b c

Figure 5-16 Spray characteristics of second split for 2-split injection under 60 MPa

Under high injection pressure (120 MPa), a different picture for the second split is

observed. The case of 0.2 ms dwell is the most distinctive one which shows the quickest increasing rate of area and the largest cone angle but the lowest increasing rate of penetration, as shown in Figure 5-17. The strong collision is likely to be responsible [11, 19]. This type of strong collision occurs at the near field of the spray and can be called "primary collision". It is worthy to distinguish the different reasons for the low penetration between the 0.2 ms dwell case under 120 MPa and the 0.3 ms dwell case under 60 MPa. Under the low injection pressure lower fuel MFR is mainly responsible for low penetration while under higher injection pressure the primary collision is the probably the root reason. Higher injection pressure leads to earlier injector opening for the second split, which means that the effects of lower MFR on the spray characteristics under higher pressure are not as obvious as those under low injection pressure. Therefore no distinctive characteristics similar to those at the 0.3 ms dwell case under 60 MPa are observed under 120 MPa.

In addition, it is clearly shown that the single injection shows smaller cone angle than the second injection for split cases at all dwells, but similar penetration length to all cases except for the 0.2 ms dwell. The weak primary collision is thought to be responsible for the slightly larger cone angle for the second split with 0.3, 0.5 and 0.8 ms dwells. It is also interesting to find that the 0.8 ms dwell case, expected to show the weakest primary collision, surprisingly presents larger cone angle than the 0.3 and 0.5 ms dwell cases, as shown in Figure 5-17 (b). The longest dwell results in the weakest interaction between splits and the second split should present similar spray characteristics to the single injection, however, the cone angle with 0.8 ms dwell is larger. This phenomenon is somewhat strange and the reason is unknown.

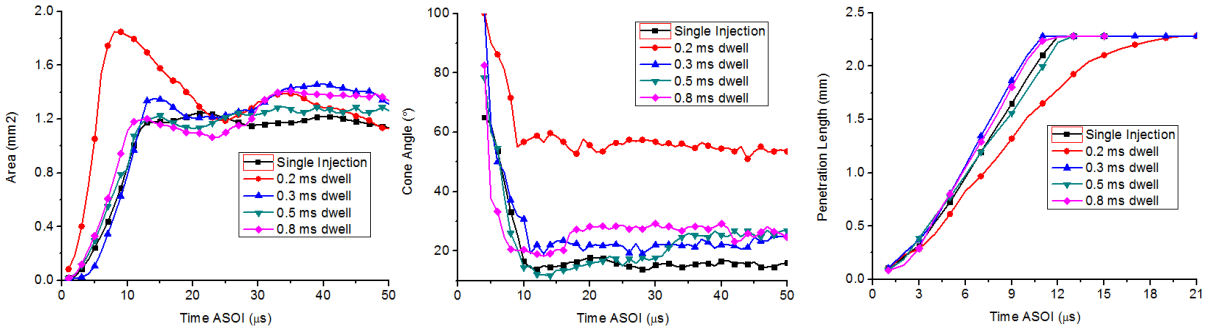

a b c

Figure 5-17 Spray characteristics of second split for 2-split injection under 120 MPa

(3) Impact of injection duration distribution between split injections

The impact of the injection duration distribution between splits was studied under 90 MPa injection pressure.

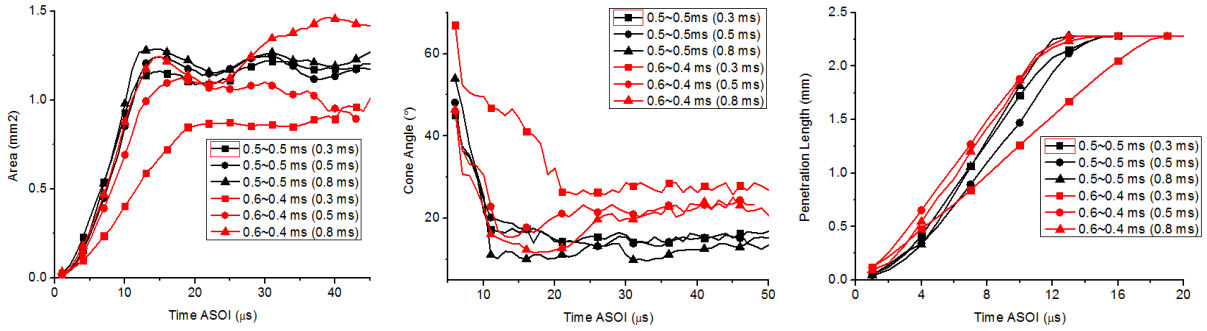

a b c

Figure 5-18 Impacts of injection duration distribution between splits

The second split with different duration distributions of injection energization presents distinctive characteristics, as shown in Figure 5-18. The second split for 0.6+0.4 ms cases has smaller area but larger cone angle than the 0.5+0.5 ms cases, especially for the 0.3 ms dwell case. The stronger influence of the primary collision for the 0.6+0.4 ms cases is believed to be mainly responsible for these spray distinctions. The effects of thresholds for image processing on the obvious spray distinctions may need to be taken into consideration.

For the first split injection, longer duration leads to higher needle lift thus to larger injector opening area. Consequently, more time is required for the needle to move back to close the injector. This contributes to the fact that larger liquid ligaments still exist at the injector tip when the second split injection arrives. The spray tip of the second injection tends to be more apparently affected by the presence of these large liquid features.

It should be noted that the stronger collision for 0.3 ms dwell case does not cause larger fuel spray area but mainly a much smaller one. This contradicts with the aforementioned findings which show a sharp increase of cone angle in Figure 5-15. The penetration length for the 0.3 ms dwell case is also apparently lower than that for the longer dwells. It can be speculated that the momentum of the spray tip of the second split injection is not sufficiently high to push the remaining fuel of the first injection and to move axially without little interference. However, this case shows some contradictions to the cases with strong collision where a much larger spray area is observed, for instance, the 0.2 ms dwell case under 120 MPa (Figure 5-17). The author believe that another reason is also responsible for the smaller spray area for the 0.6+0.4 ms cases and the lower MFR is thought to be the reason. This can be verified in Figure 5-19 where the second split injection (0.3 ms dwell) with 0.5 + 0.5 ms shows normal morphology while the one with 0.6 + 0.4 ms shows much lower MFR and stronger collision.

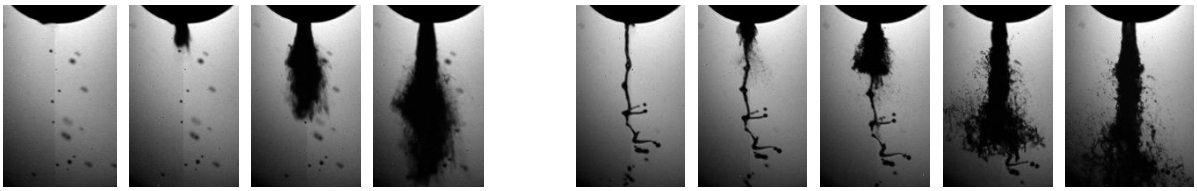

0 μs 2 μs 6 μs 10 μs 0 μs 10 μs 20 μs 35 μs 45 μs

a b

Figure 5-19 The morphology of the second split (0.3 ms dwell) with (a) duration of 0.5 + 0.5 ms and (b) 0.6 + 0.4 ms

In addition, the cases for 0.6+0.4 ms split injections except for the one with 0.3 ms dwell show higher penetration length than those of 0.5+0.5 ms cases. This can possibly be attributed to the stronger induced driving force by the first split. Longer injection duration for the first split results in more injected fuel, and more air being pushed forward. Stronger air driving force and quicker air movement enable the second split to move faster.

5.3.2.2 Three-split injection

The increase of the number of splits is thought to significantly affect the primary breakup characteristics. 3-split injection cases are expected to present different injection characteristics from those of the 2-split injection.

(1) Injection characteristics under low injection pressure

The fuel spray area development for each split with various dwells under 60 MPa is shown in Figure 5-20. It can be seen that the first split has spray area comparable with single injection for all cases, meaning that the first split is not apparently affected. With 0.2 and 0.3 ms dwell, the second split shows much lower spray area than single injection, whereas the third split injection presents apparently higher spray area than the single injection. This shows a difference with the 2-split injection where the second split has much higher area than the single injection when the dwell is 0.2 ms, as shown in Figure 5-16 (a). For the 0.2 ms dwell case with 3-split injection, the spray characteristics of the second split injection can be

attributed to its much lower MFR (shown in Figure 5-21) compared with the 0.2 ms dwell case of 2-split injection strategy where primary collision is more important. This suggests that the increase of the number of the splits can seriously affect the second split. However, it is still unknown how the increase of the number of splits impacts the spray behavior of the second split. For the third split injection, because the dwells are short throughout, the fuel still flows out continuously when the energization of the third split injection starts. This leads to earlier injector opening for the third split, consequently higher fuel momentum due to higher effective injection pressure.

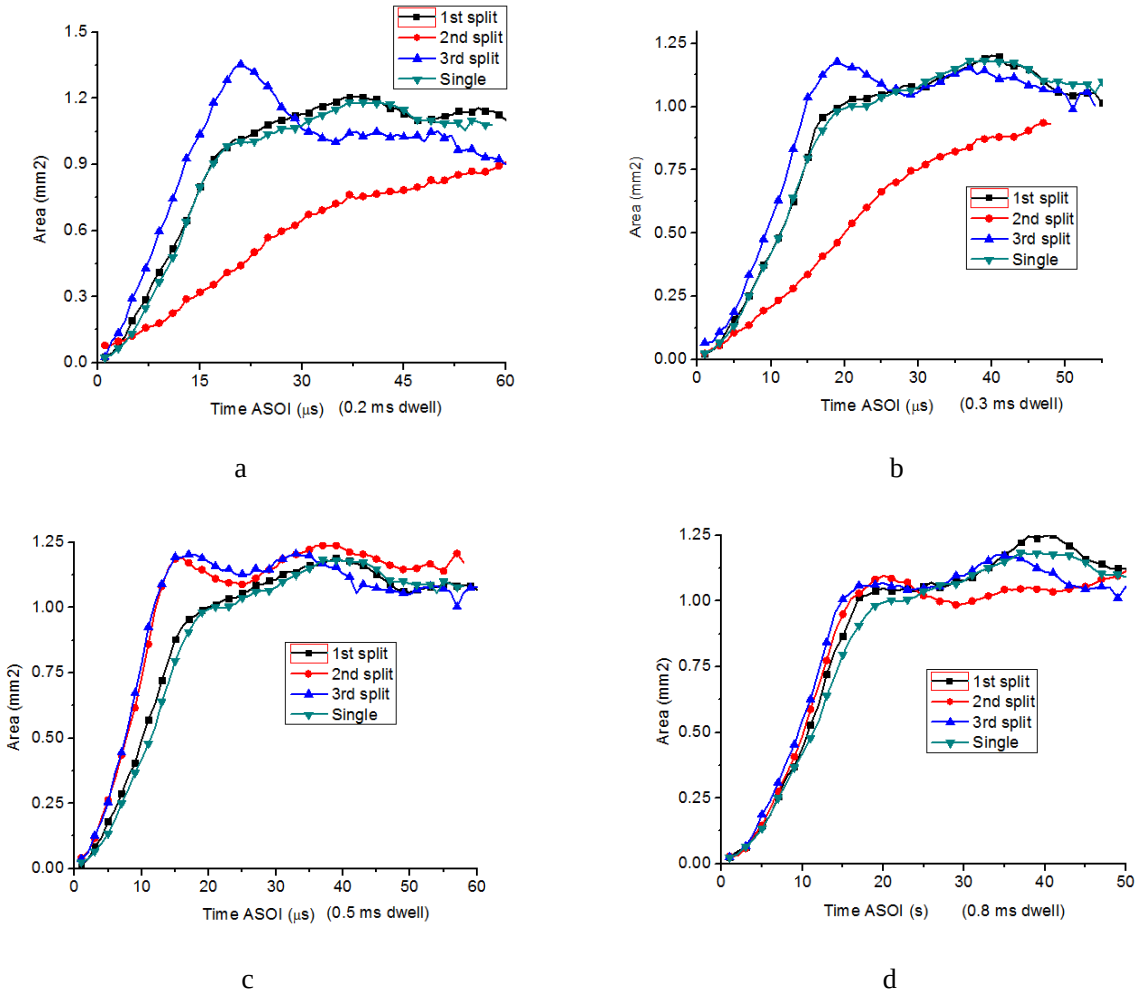

Figure 5-20 Fuel spray area for each split with various dwells for 3-split injection under 60 MPa

With 0.3 ms dwell, the fuel spray has smaller area, showing similar characteristics to its counterpart with 2-split injection, as shown in Figure 5-16 (a). The lower MFR is again considered to be responsible. When the dwell rises to 0.5 ms, the areas of the second and third splits are similar and they are clearly higher than the single injection, shown in Figure 5-20 (c). This suggests that the second split recovers from the influence of the first split. Further increased dwell (0.8 ms) causes comparable areas for all splits.

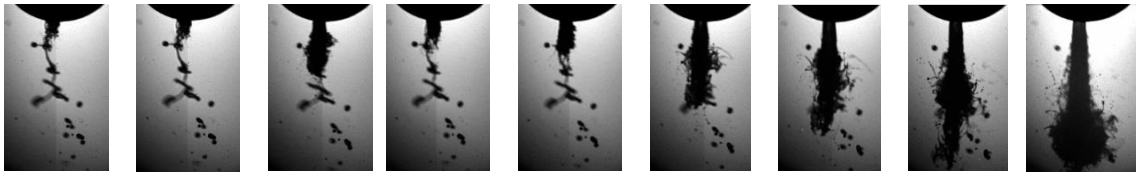

Figure 5-21 Morphology of the second split with 0.2 ms dwell for 3-split injection under 60 MPa

The varying trend of cone angle and penetration length can also effectively reflect the reasons for the distinction of these spray characteristics. As presented in Figure 5-22 and 5-23, with 0.2 ms dwell, the obviously higher angle and lower penetration rate for the second and third splits means that strong collision occurs. The penetration of the third split is not shown due to the difficulty of identifying the tip of the third split spray, as shown in Figure 5-24. The continuous compact fuel liquid can be clearly observed at the outset of the third spray. The resultant strong collision contributes to the larger cone angle of the third split than that of the second split.

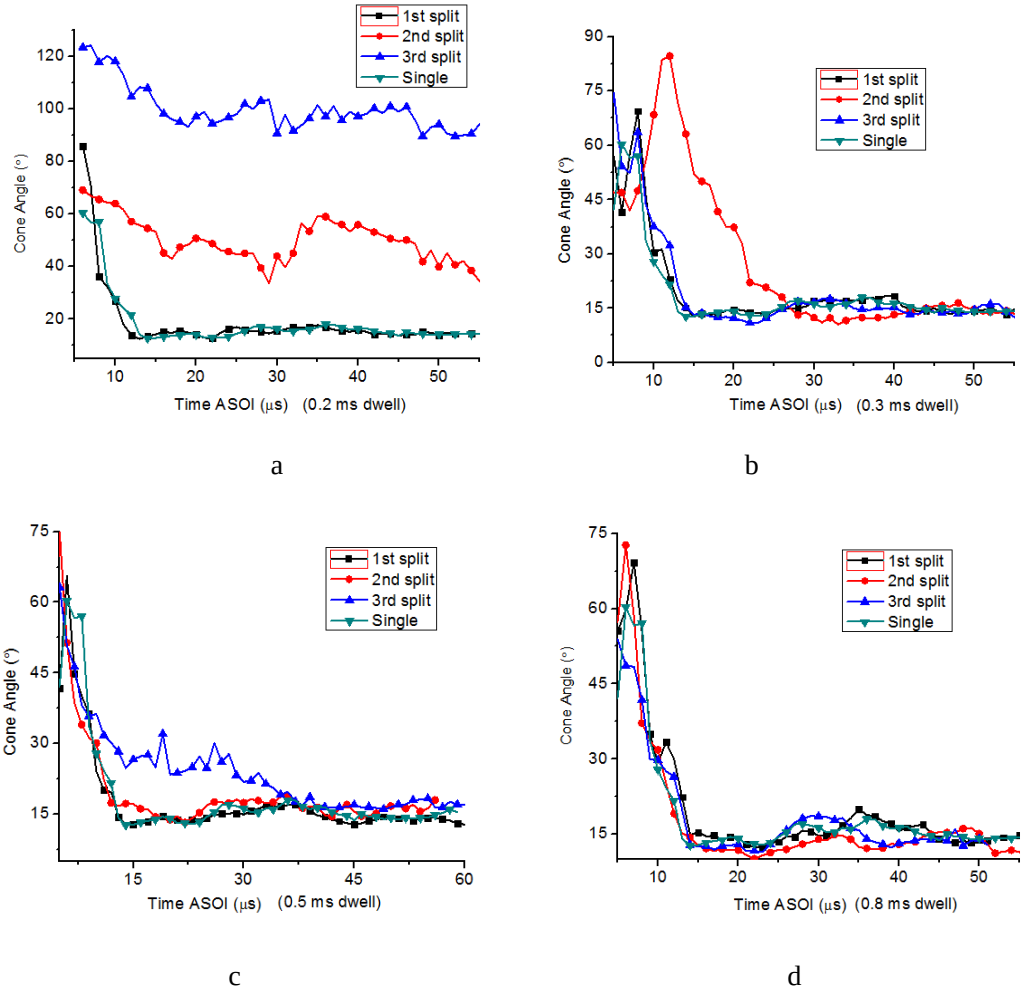

Figure 5-22 Spray cone angle of each split injection with various dwells for 3-split injection under 60 MPa

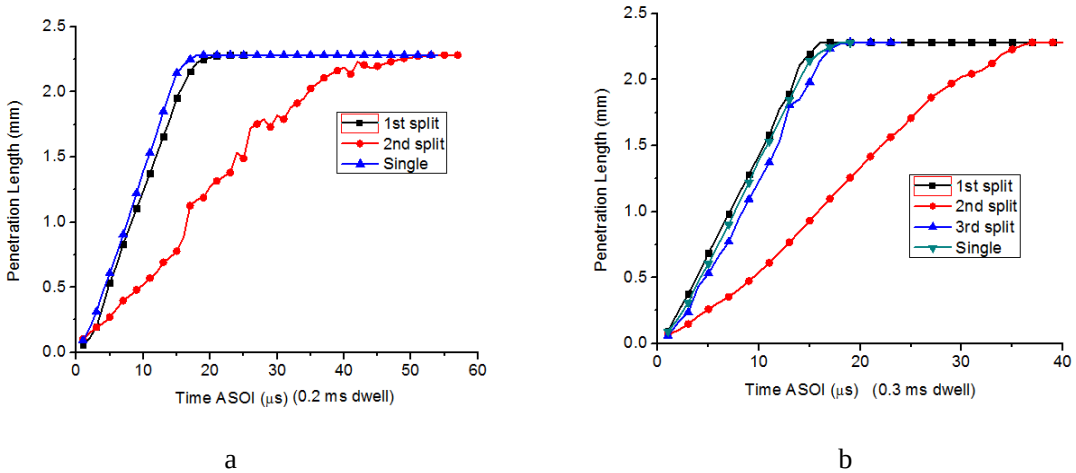

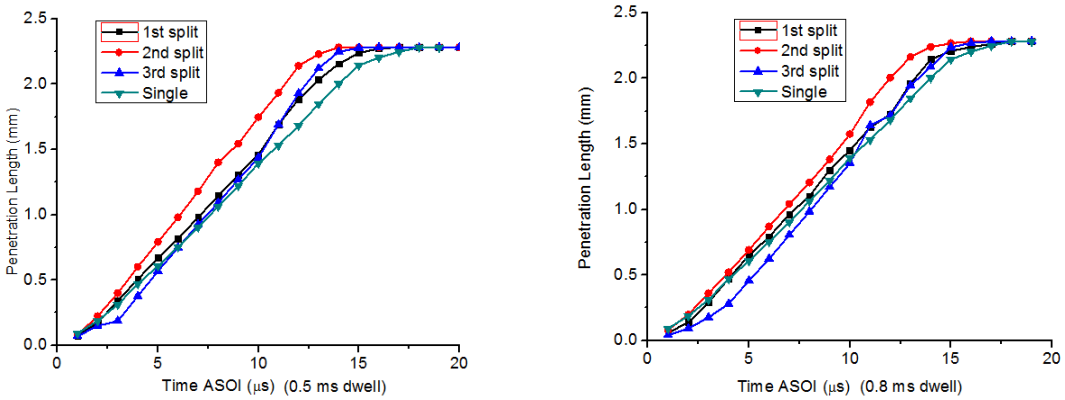

c d

Figure 5-23 Penetration length of each split injection with various dwells for 3-split injection under 60 MPa

For the 0.3 ms dwell case, only the second split shows higher cone angle at the early stage and lower penetration inc6reasing rate, while the third split surprisingly presents similar characteristics with single injection. By contrast, when the dwell is increased to 0.5ms, only the third split presents higher fuel spray cone angle at the early stage, whereas the second split presents slightly higher penetrating rate than the other split injections (Fig 5-22 (c)). When the dwell rises to 0.8 ms, fewer differences are discovered for the split, suggesting that the interaction between splits is quite weak.

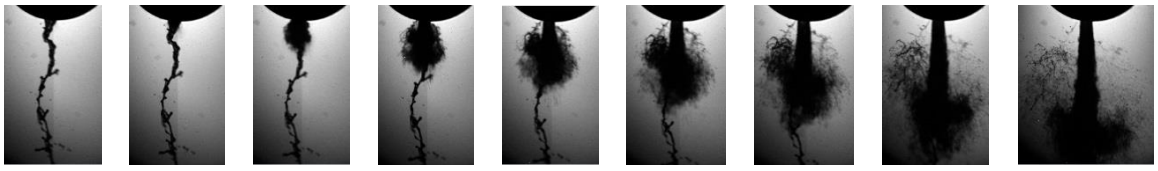

1μs 2μs 4μs 6μs 8μs 10μs 12μs 16μs 20μs

Figure 5-24 Morphology of the third split with 0.2 ms dwell for 3-split injection under 60 MPa

According to the aforementioned discussion, it seems that the increase of the number of the split makes the split injection characteristics more complex and more unpredictable. Some phenomena cannot be clearly explained with information available in this study. The

MFR characteristics in chapter 4 cannot be used to explain these phenomenon as the two injectors used in chapter 4 and this chapter are different. The injector technology (the electric-magnetic characteristics) is assumed to significant influence the spray behavior. More studies need to be carried out.

(2) Characteristics comparison of the second split between 2-split and 3-split

The aforementioned discussion suggests that the second split seems to be influenced by different phenomena and presents distinct injection features when the numbers of the splits are different. To outline these differences, the characteristics of the second split with 2-split and 3-split injections are compared, presented in Figure 5-25 and Figure 5-26. It can be seen that for the case with 0.2 ms dwell, significant differences are shown although almost no distinctions can be found for longer dwell cases (0.3, 0.5 and 0.8 ms). The second split for 2-split injection case has much higher fuel spray area and penetration length but much smaller cone angle than the second split for a 3-split injection. This suggests that the main factors that affect the second split with different number of splits of injection are different.

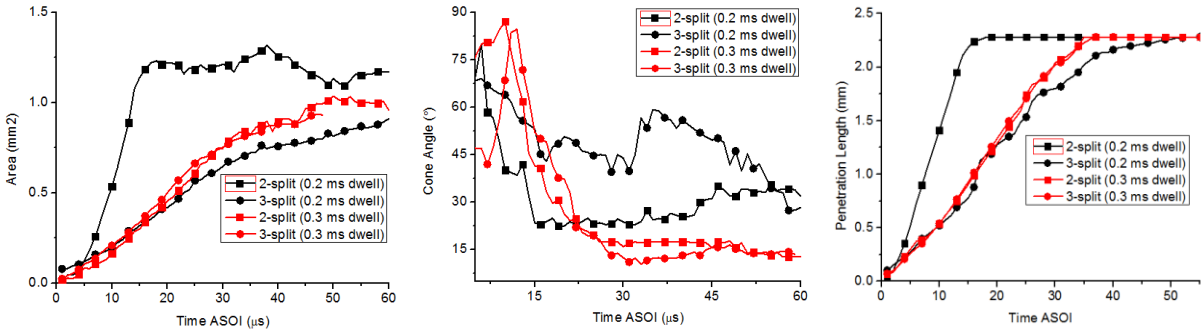

a b c

Figure 5-25 Comparison for the second split injection between 2-split and 3-splits with short dwell

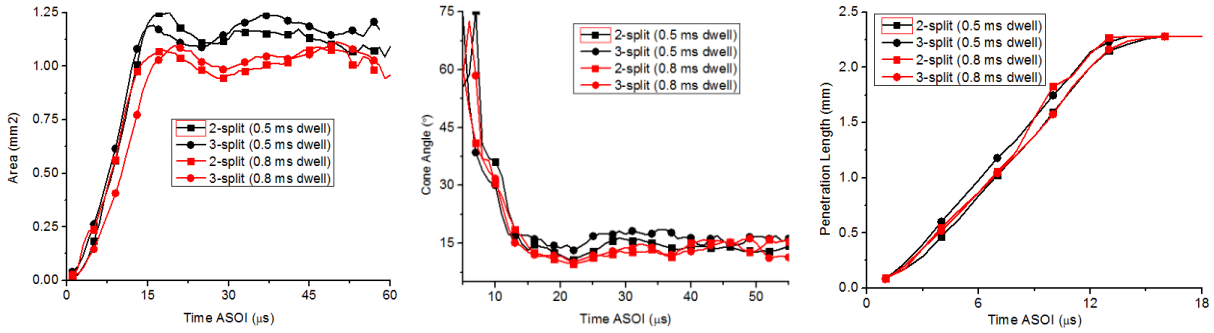

a b c

Figure 5-26 Comparison between 2-split and 3-split for the second split with long dwell

To the author's best knowledge, there are three main factors or effects that impact the spray characteristics, namely: primary collision, air driving force and lower MFR. From the aforementioned explanation, collision leads to higher increase of the fuel spray cone angle and area but lower penetration. Air driving force causes higher increase of penetration and fuel area. However, lower MFR contributes to lower increase of fuel area, cone angle and penetration. It should be also noted that short dwell causes the strong simultaneous effects of the three factors. Therefore the combined influences of the three factors are quite complex. Fortunately, by comparing the spray characteristics, the dominant factors for the characteristics of the second split injections can be identified. When the dwell is set to 0.2 ms, for the 2-split case, lower cone angle means weaker collision, and higher area and penetration length suggest higher air driving force. Consequently, given the three spray characteristics, the stronger air driving force tends to be the main factor that dominates the spray behavior of the second split injection event for 2-split injection case. For the 3-split injection case, lower fuel spray area and smaller penetration length means lower MFR. By contrast, the much higher fuel spray cone angle than for the cases with longer dwell (0.5 and

0.8 ms) means that strong collision exists. Therefore, it is argued that the lower MFR and strong collision are mainly responsible for the spray characteristics of the second split injection for 3-split case.

(3) Injection characteristics under high injection pressure

As presented in Figure 5-27, higher injection pressure (90 MPa) causes similar varying trends of the injection characteristics to those under lower injection pressure (60 MPa) but with larger magnitudes of variation when injection dwell is short. With 0.2 ms dwell, the second split shows a higher area and cone angle of the fuel spray than the first split injection event and also than the single injection. By contrast, the third split injection event presents a much higher rate of increase of the spray area and a much larger spray cone angle than the other split injections. The extremely strong collision is perhaps responsible, as shown in Figure 5-28 where the spray morphology development for the third split with 0.2 ms dwell is shown. It can be seen that the fuel of the second split is continuously flowing out at high MFR when the spray tip of the third split comes out (see the 2μs frame). The fuel spray area after it peaks presents a reduction to a value which is much lower than that of single injection. The reason for this reduction is unknown as the reduction seems to be abnormal. The moving out of the dispersed fuel due to collision would be expected to just lead to the reduction of liquid area to the value which is similar to that of the single injection. However, the resultant area is much lower than that of single injection, leading to an over exaggerated area difference. The cone angle of the third split shows an average value of 120° which is much higher than that of the second split (around 25°).

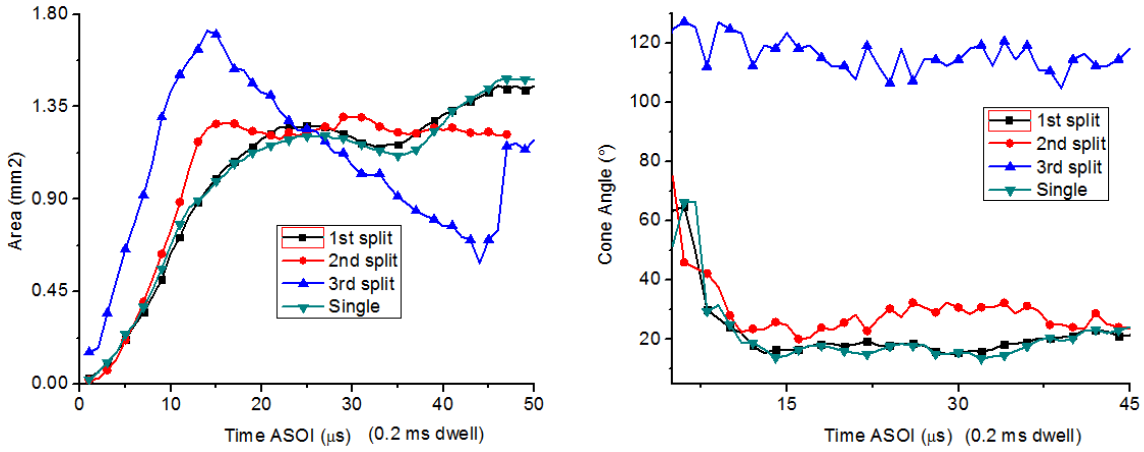

a b

Figure 5-27 (a) area and (b) cone angle for each split with 0.2 ms dwell for 3-split under 90 MPa

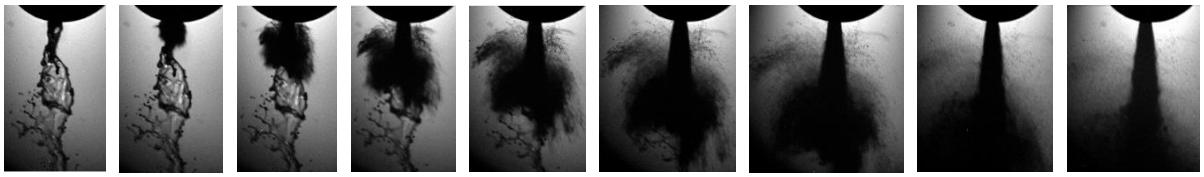

1μs 2μs 4μs 6μs 8μs 10μs 12μs 16μs 20μs

Figure 5-28 Morphology of the third split with 0.2 ms dwell for 3-split injection under 90 MPa

As the dwell rises to 0.3 ms, the interaction among splits seems to disappear, as shown in Figure 5-29. Only the second split injection event shows slight higher fuel spray area and the third split injection event presents marginally larger cone angle than the rest, suggesting that the collision is quite weak. The interaction tends to weaken as quickly as for the case under low injection pressure (60 MPa). In addition, the penetration length of the first split is marginally higher than the rest, which means that the split injection strategy can still affect the first injection event although the influence is weak.

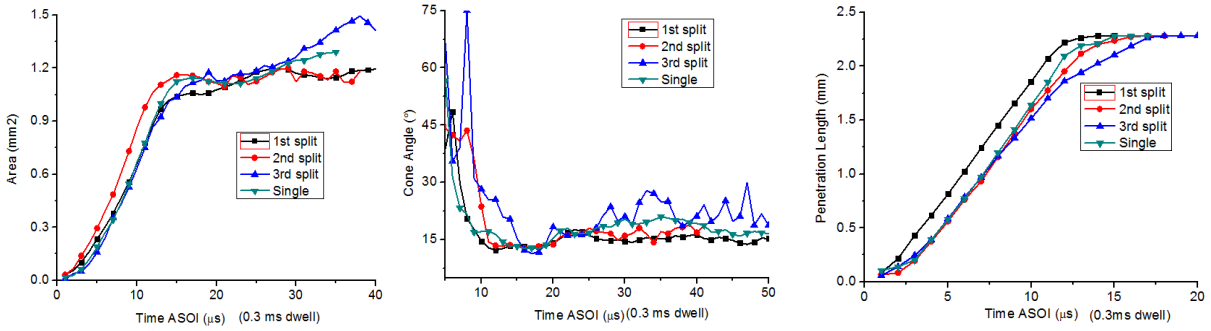

a b c

Figure 5-29 Spray characteristics for each split with 0.3 ms dwell for 3-split under 90 MPa

5.4 Influence of fuel temperature

5.4.1 Single injection

(1) The initial spray stage

The varying trend of spray area (Figure 5-30) is further discussed for both RT and LT under low and high injection pressures. Several letters are used to denote different cases, "A" for RT under high injection pressure, "B" for LT under high injection pressure, "C" for RT under low injection pressure, "D" for LT under low injection pressure. Area developing stages are numbered, 0-1 for quick increasing stage from ASOI (0 point) to the first peak (1 point), 1-2 for the first decreasing stage to the first valley (2 point), 2-3 for the second increasing stage to the second peak (3 point). Connected by dash lines are the corresponding key points under high injection pressure, whilst connected by solid thin lines are those under low injection pressure. Images at these key timing points are also attached so that the area developing trend can be illustrated more clearly.

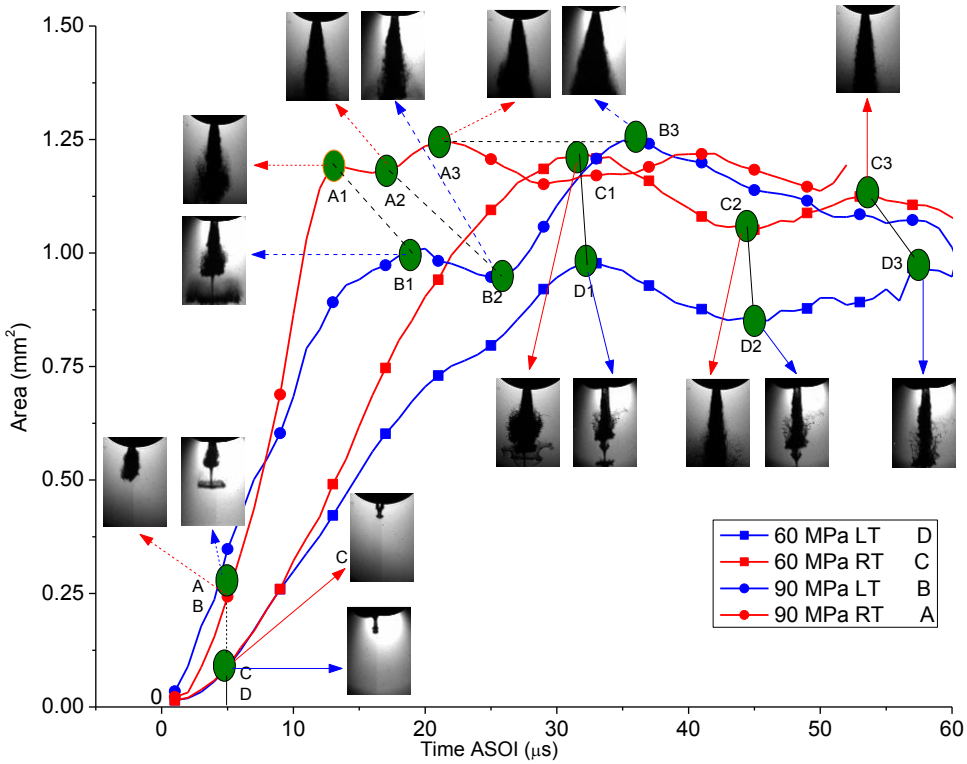

Figure 5-30 The development of spray area with single injection ASOI

Under low injection pressure (60 MPa), area varying trend under LT shows good consistency with that under RT but with lower values. ASOI, observed is a spheroid head which develops into a "mushroom", shown at points at C and D. The plume area increases drastically to the first peak at points C_1 and D_1 largely due to the breakup of the liquid column and the enlargement of the mushroom through the air drag force. At points C_1 and D_1, it can be seen that the "stem" of the mushroom is the longest in the view field. From then on, the area shows an obvious dip to the first lowest points C_2 and D_2 because of the aforementioned moving out of the whole enlarged mushroom. An observable increase is then observed due to the continuous breakup of the liquid column. The consistently lower fuel area for LT than RT is due to the poorer breakup and dispersion. More apparent mushroom enlargement for RT than LT clearly suggests better dispersion for RT case. The raised viscosity and surface

tension under LT cause lower jet velocity, lower air drag force and lower chances of breakup [113]. Large ligaments at the wavy sides of column for LT case are observed while better dispersed droplets are seen for the RT case.

Under high injection pressure (90 MPa), although overall similar varying trends for RT and LT cases are found, various distinctions can be clearly seen. For the initial increasing stage, the LT case surprisingly shows obviously higher area than the RT case. Besides, a large mushroom and a long stem are observed for LT case, however, a better dispersed spray without obvious mushroom or stem under RT is found. Approximate at 8 μs ASOI, the area of RT outstrips that of LT, and the difference is then quickly widened even until the first area peak points appear at A_1 and B_1. The area difference is further enlarged to the first lowest area points A_2 and B_2. Before the lowest fuel area points, the LT case consistently presents poorer dispersion than the RT case. After this key point, an observable area rise for RT can be seen, while a sharp area increase for LT case is found. From the images at points A_3 and B_3, the plume at this moment has much larger cone angle than those before this timing point. The plume also shows high asymmetry for both LT and RT cases. It can be expected that this sharp area increase is likely to result from the oscillation of the needle during the opening stage or the throttling flow or even both [112]. A clear time lag (approximate 15 μs) for the appearance of the second peak between LT and RT suggests slower injector opening under LT.

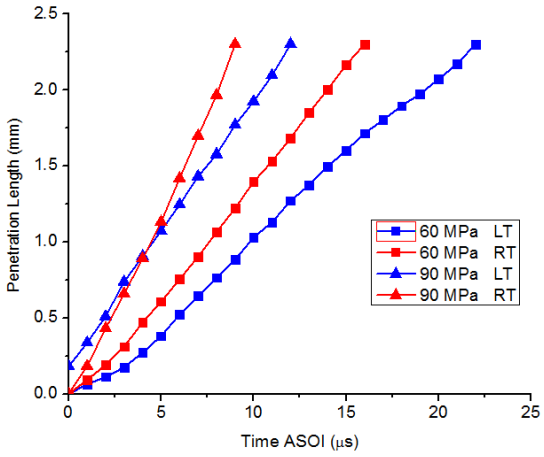

Figure 5-31 Spray penetration under various conditions

From Figure 5-31, it can be seen that the LT case shows much lower penetrating rate than the RT case when injection pressure set to 60 MPa. Higher viscous force under LT tends to be the reason. By contrast, a slightly higher penetrating velocity for LT than RT is observed for the initial injection stage under high injection pressure. After approximate 5 μs, RT case presents higher penetration velocity. This phenomenon seems to be unreal as the increased viscosity under LT decelerates the spray, and lower penetrating rate for LT is expected. However, if the formation regimes of the mushroom and stem are taken into consideration, the results seem to be reasonable.

According to the aforementioned regimes for the formation and development of the mushroom and stem, it can be expected that under high injection pressure, the LT case has higher chances of forming the mushroom than RT case due to higher possibility of the laminar flow. This also means that higher initial velocity of the mushroom because of the accelerating effect of the compressed air leads to higher penetrating velocity for LT, thereby larger fuel area during the initial injection stage, as shown in Figure 5-30 and Figure 5-31.

Further needle lift enables the fuel to break up and disperse instantly at the outlet of the nozzle due to higher inertia under high injection pressure. The instant dispersion of the spray causes larger fuel area for RT case [113]. By contrast, under low injection pressure, much lower spray inertia cannot disperse the spray instantly and compress the sucked air sufficiently. The insufficiently compressed air fails to accelerate the mushroom as effectively as that under high injection pressure. The resultant mushroom acceleration tends to be weak when compared with the effects of raised viscosity and surface tension, which causes low inertia and penetrating velocity.

(2) The end of the injection

The shape of MFR (Figure 5-1) shows that the injection duration for the end of injection is much longer than the duration of the start of injection. The resultant large amount of fuel with low velocity is thought to inevitably significantly influence the spray characteristics.

The spray morphology during the end of injection for RT and LT under 60 MPa (Figure 5-32 and Figure 5-33 respectively) shows similar varying trends, namely, presenting a sharp cone angle increase from a value of steady state, then decreasing drastically with poor dispersion. The timings shown are the time points before the end of injection (BEOI (the end of injection gained from MFR (Figure 5-1) is used as the time baseline)). During the injector closing stage, the larger cone angle than that at quasi-steady stage can be attributed to the aforementioned throttling effect due to low needle lift [112]. At the end of injection, the reduction of effective injection pressure slows down the breakup of the droplets, leading to

much larger ligaments than those during the main injection [113].

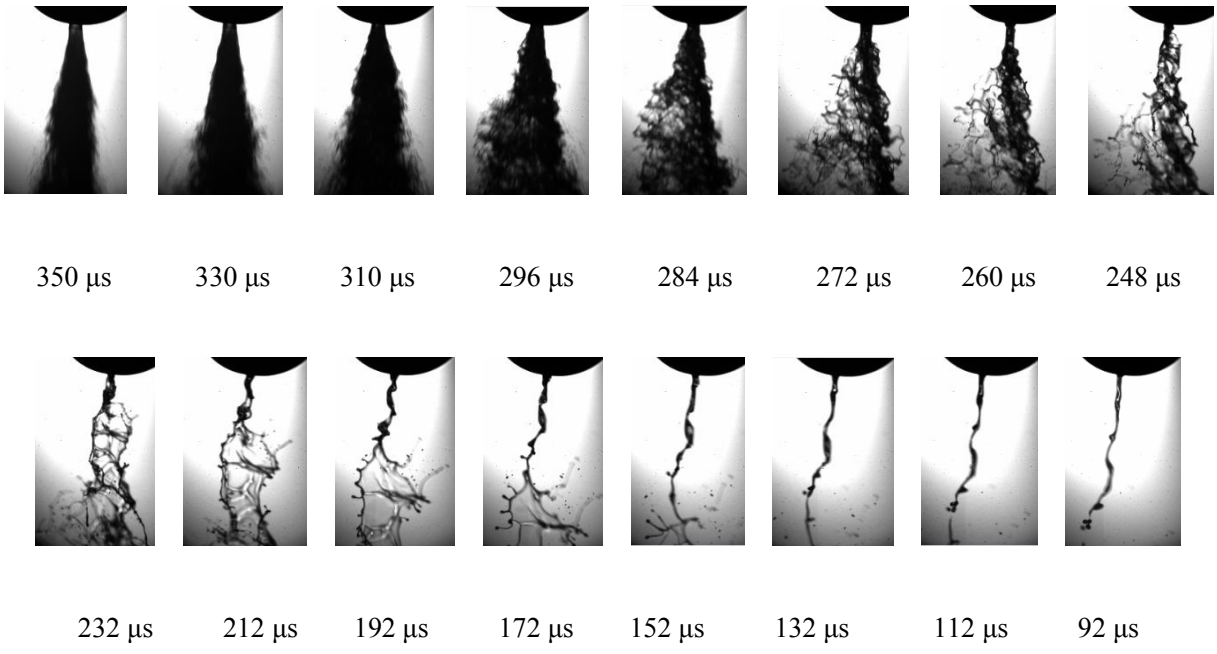

Figure 5-32 Spray morphology at the end of injection for single injection under RT and 60 MPa (BEOI)

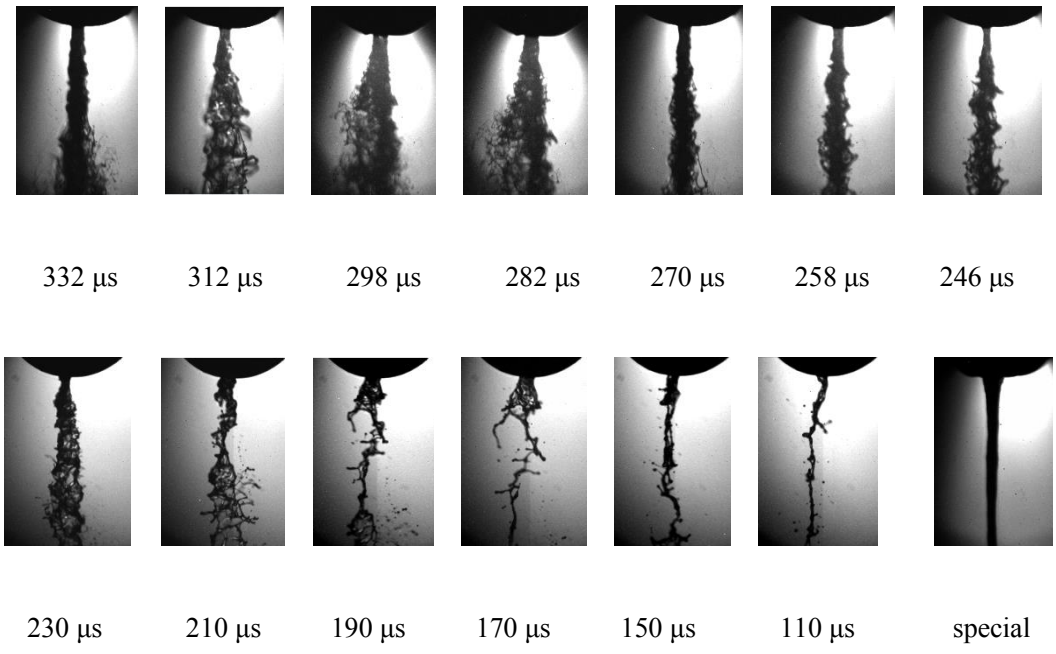

Figure 5-33 Spray morphology at the end of injection for single injection under LT and 60 MPa (BEOI)

From the microscopic point of view, spray under RT transits from full atomization with

fine droplets to continuous intertwined ligaments then to thin sheets or membranes and finally to compact liquid column. By contrast, spray under LT transits from poor atomization with large droplets to continuous intertwined large ligaments then directly to compact liquid column. Thin sheets or membranes are rarely observed under LT. This means that the breakup regimes under LT transit obviously quicker than those under RT, and the much quicker flow regime transition in nozzle hole under LT seems to be responsible. Surprisingly observed sometime is a total smooth liquid column without droplets or ligaments at its periphery, shown in Figure 5-33, marked as "special" (200μs BEOI). The disappearance of the large ligaments and droplets is considerably advanced under LT by increase of viscosity through its stabilizing effect [113]. Besides, LT case presents larger ligaments than the case under RT after the formation because of the stabilizing effect of the fuel properties. In addition, the higher surface tension may lead to the recombination of the ligaments. Particles under LT present more spherical shape than the same sized counterparts under RT as its high surface tension enhances the retention of the spherical shape [113].

Lower spray velocity under LT can be expected at the end of injection thus higher chances of the existence of residual fuel in nozzle hole. The existence of residual causes higher chances of formation of mushroom and stem under LT. Higher chances of the existence of deposit in the nozzle hole can also be expected, and higher concentration of HC and CO is likely to ensue under LT [1].

(3) Breakup regimes

From the above description, it suggests that the increased fuel viscosity and surface tension are the main factors that lead to the difference of spray characteristics between LT and RT. Besides, the opening and closing of the injector lead to dramatic variation of effective injection pressure and the flow regimes. The complicated spray behavior is dominated by the combination of these factors and regimes. How the combined impacts of fuel properties and transition of flow regimes affect the spray breakup and droplets formation needs to be quantified. This subsection discusses the break regimes by employing the cases under 60 MPa injection pressure.

The *Re* number can effective denote the significance of injection pressure, flow regimes in nozzle hole and the energy responsible for breakup. Inherent energy of spray strongly impacts the formation of wavy surface and the magnitude and length of peripheral waves [126]. Higher *Re* means higher flow turbulence, higher energy for vortexes at the spray periphery and higher spray velocity. The high energy of vortexes enables the surface to form small waved structures [109].

Combining Equation 3-7 and Equation 5-3, the Reynolds number can be expressed as:

$$\mathrm{Re} = \frac{d_0 \dot{m}(t,T)}{\rho_l \nu(T) \pi d_0^{\,2} / 4} \qquad \text{Equation 5-10}$$

Given the effect of temperature on fuel properties, shown in Figure 3-13, new expression of *Re* can be obtained, shown as:

$$\mathrm{Re} = \frac{\dot{m}(t,T)}{\rho_l (1.0227 * e^{1.14-0.031*T} + 1.043) * \pi d_0 / 4}$$

Equation 5-11

It should be noted that both viscosity and actual MFR vary with the variation of fuel temperature. In addition, during the opening and closing stages, the actual MFR also changes with the elapse of time. The varying trend of *Re* during the opening stage under various temperatures is shown in Figure 5-34. The calculation of *Re* is carried out within 100 μs ASOI, with temperature varying from -18 to 48 degC. It can be seen that during the initial opening stage under LT, *Re* is very low, leading to low spray velocity. Under higher temperature condition, *Re* is higher than its counterparts under lower temperature. It is noteworthy that *Re* difference between LT and RT is more obvious at 100 μs after start of injection. The exponential varying rate of viscosity denotes that under low injection pressure and LT, fuel viscosity can affect the flow speed in nozzle hole to a staggering degree. 100 μs ASOI, fuel flow in the nozzle under LT tends to be lamina, with *Re* being less than 4000, whereas the corresponding flow under RT is highly turbulent or even cavitating, with *Re* being approximate 16000. This huge disparity shows much lower spray breakup possibility and lower spray penetrating velocity for LT case, as illustrated in Figure 5-30.

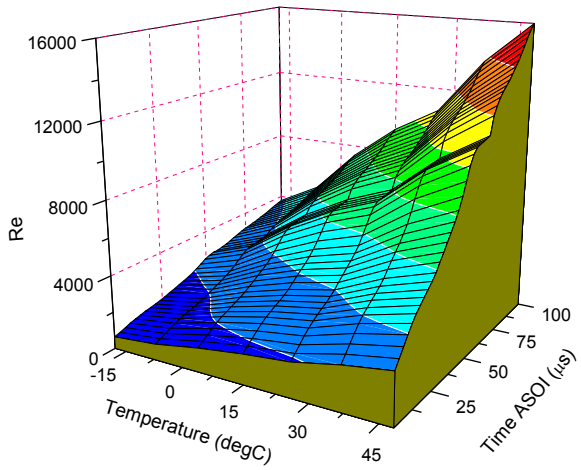

Figure 5-34 Development of Re ASOI under various temperatures (60 MPa)

We (*We*$_l$ and *We*$_g$), showing the possibility of spray breakup and droplet formation can be gained from Equation 5-12 (*We*$_l$) and Equation 5-13 (*We*$_g$) :

$$We_l = \frac{\rho_l V^2 d_0}{\sigma} = \frac{16\dot{m}(t,T)^2}{\pi^2 \sigma \rho_l d_0^3} = \frac{16\dot{m}(t,T)^2}{\pi^2 \rho_l d_0^3 (-0.09923 * T + 27.95261)} \quad \text{Equation 5-12}$$

$$We_g = \frac{\rho_g V^2 d_0}{\sigma} = \frac{16\rho_g \dot{m}(t,T)^2}{\pi^2 \sigma \rho_l^2 d_0^3} = \frac{16\rho_g \dot{m}(t,T)^2}{\pi^2 \rho_l^2 d_0^3 (-0.09923 * T + 27.95261)} \quad \text{Equation 5-13}$$

The varying trends of *We*$_l$ and *We*$_g$ under a wide range of temperatures are shown in Figure 5-35. Both present similar developing trends. During the initial spray stage, *We* number is considerably low, and the increase of MFR leads to a dramatic increase of *We*, suggesting much higher possibility of breakup of jet. It is interesting to find that *We* difference between LT and RT at 80 μs ASOI is more obvious than that at the initial stage. This similarly supports that LT results in much lower possibility of spray breakup by both lower spray velocity and higher surface tension. Higher stabilizing and retaining effects under LT tend to result in larger sized droplets, as presented in the images in Figure 5-30. The reciprocal

varying trend of *We* shows that the impact of raised surface tension on *We* is not as obvious as that of viscosity on Re (Equation 5-11).

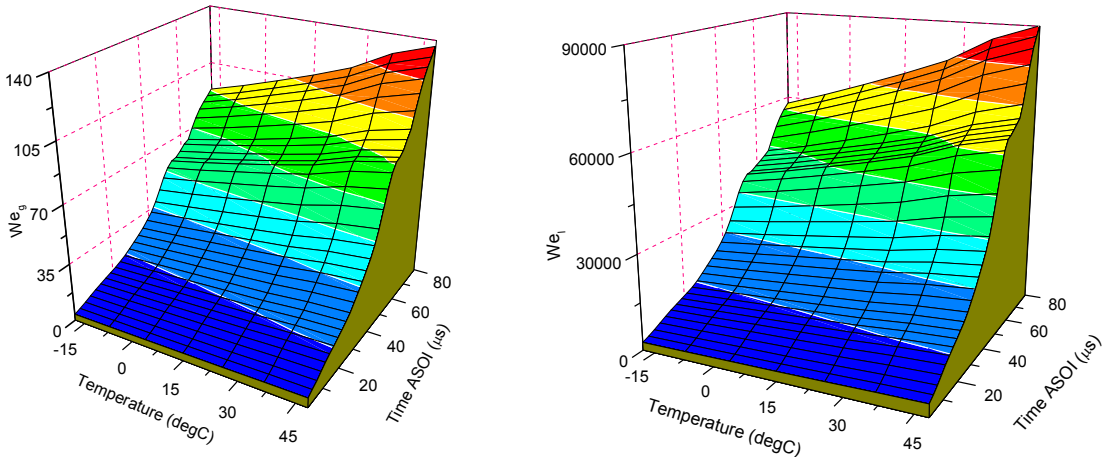

a b

Figure 5-35 Development of *We* ASOI under various temperatures (60 MPa)

The stability of the jet itself can be expressed through Ohsornge number (*Oh*) which is shown as:

$$Oh = \frac{\sqrt{We_l}}{\mathrm{Re}_l} = \frac{\nu_l}{\sqrt{\rho_l \sigma d_l}} = \frac{1.0227 * e^{1.14-0.03\Gamma * T} + 1.043}{\sqrt{\rho_l d_l * (-0.09923 * T + 27.95261)}}$$

Equation 5-14

Smaller *Oh* suggests lower stability and higher possibility of breakup. From Equation 5-14 and Figure 5-36, it can be expected that *Oh* is significantly affected by temperature, and lower fuel temperature results in considerably higher stability of the jet.

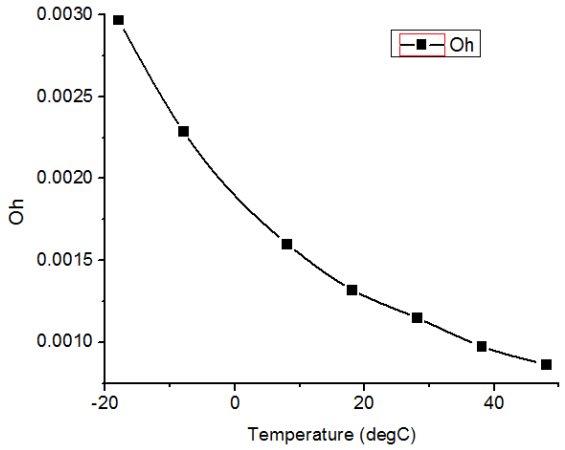

Figure 5-36 *Oh* under various temperatures

These dimensionless numbers can be employed to denote the breakup regimes which have been deeply investigated in various studies by different defining methodologies. Basing on the breakup regimes proposed by Ohnesorge [127], Reitz [32] defined the boundary conditions (Table 5-4) to distinguish the breakup patterns. These boundary conditions are employed to define the timings of the start of corresponding breakup regimes in this study. All regimes except Rayleigh exist under low injection pressure (60 MPa) according to the values of We_g. During the initial injection stage, the start timings of the breakup regimes (Figure 5-37 (a)) decrease with the rise of temperature. Under various temperatures, the start timings of second wind present small difference while the timings of atomization show more obvious difference, meaning that LT exerts more profound influence on atomization regime. As for the end of injection, the rise of temperature retards the transition of breakup regimes from atomization to second wind induced and to first wind induced (Figure 5-37 (b)). It also clearly shown that the durations of first and second wind induced breakup regimes for the end of injection is much longer than those of initial injection

stage, again meaning much more poorly dispersed liquid fuel during this stage.

Table 5-4 Boundary conditions for breakup regimes [32]

Rayleigh	First wind induced	Second wind induced	Atomization
$We_g < 0.4\,(1.2+3.4Oh^{0.9})$	$1.2+3.4\,Oh^{0.9} < We_g < 13$	$13 < We_g < 40.4$	$We_g > 40.4$

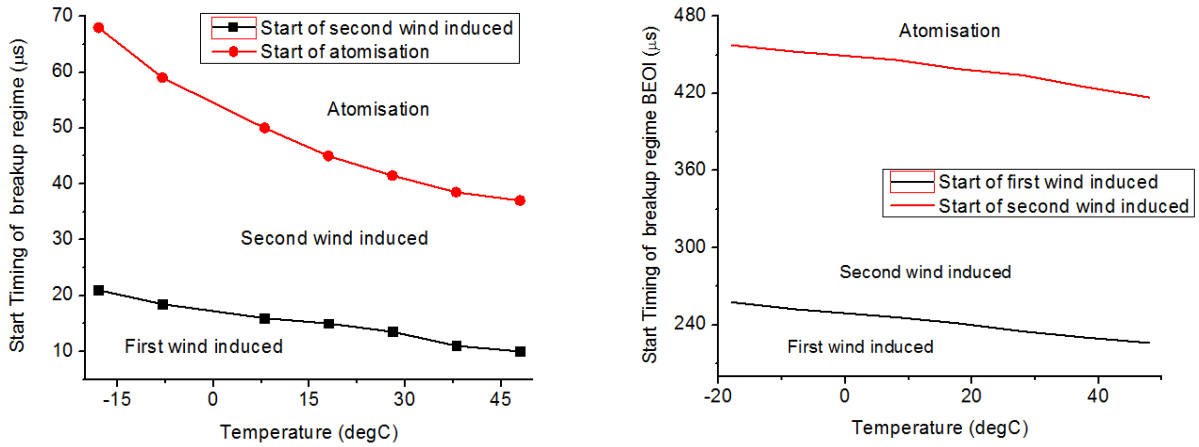

a b

Figure 5-37 Start of variation of breakup regimes for (a) the initial stage and (b) the end of injection

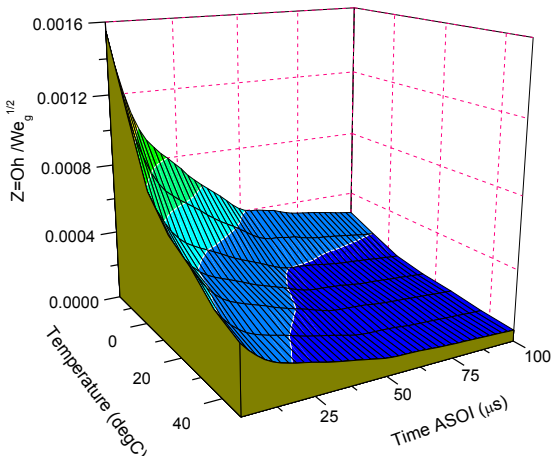

Figure 5-38 Z vs ASOI under various temperatures

Although *Oh* can denote the droplet stability by taking the fuel properties into

consideration, the influences of ambient gas are nearly ignored. To outline the impacts of gas properties on the spray of rocket engine where a coaxial gas flow is employed, an equation, shown in Equation 5-15, was employed [126, 128]. It was proven to effectively denote the impacts of ambient gas.

$$Z_{coaxial} = Oh * (We_g^{1/2})$$ Equation 5-15

However, the aforementioned equation is not suitable for the case in this study because the coaxial gas flow can stabilize the spray but no coaxial gas flow is employed in this study. By contrast, the stagnant gas actually boosts the spray breakup due to air drag force. A new equation based on the same idea is proposed in this study to take the effects of ambient gas into consideration, shown in Equation 5-16:

$$Z = Oh / (We_g^{1/2})$$ Equation 5-16

Compared with *Oh*, the new dimensionless number *Z* can express the stability of the droplet more effectively. As presented in Figure 5-38, the spray jet at the beginning of the injection under LT is highly stable compared with the one under RT. The higher MFR thus higher spray velocity with the elapse of time can effectively lower the stability of the spray.

For the end of injection, these aforementioned dimensionless numbers used to evaluate the possibility of break up are similarly calculated, shown from Figure 5-39 to Figure 5-42. To make the varying trend to be clearer, the view angle of the graphs are changed, and this leads to the reverse of varying sequence for the two variables, namely, temperature and time

ASOI. Spray at the end of injection presents very low *Re* under LT. The blue part shows that fuel flow at the nozzle outlet (*Re*<2000) is completely laminar flow. The area of the blue part also suggests the duration of laminar flow. The area of blue part for the end of injection (Figure 5-39) is much larger than that of start of injection (Figure 5-34). This means that much longer injection duration at the end of injection than at the start of injection is in the state of laminar flow. The impact of temperature on *Re* for end of injection is more obvious than that on *Re* for the start of injection. For the end of injection, under the lowest temperature (-18 degC), the completely laminar flow lasts approximate 400 μs, while under the highest temperature (48 degC), the laminar flow is just seen for 75 us. This again suggests that the adverse effects of LT is significant under low effective injection pressure.

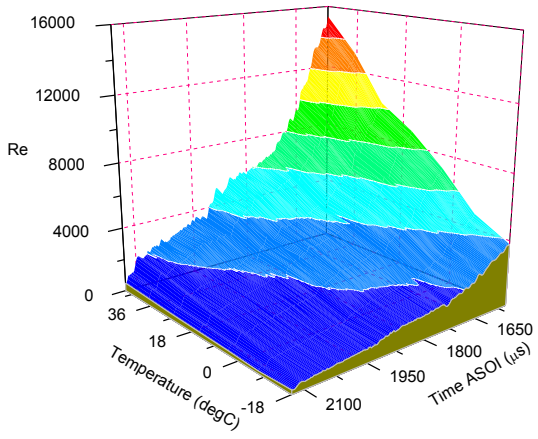

Figure 5-39 Re BEOI under various temperatures

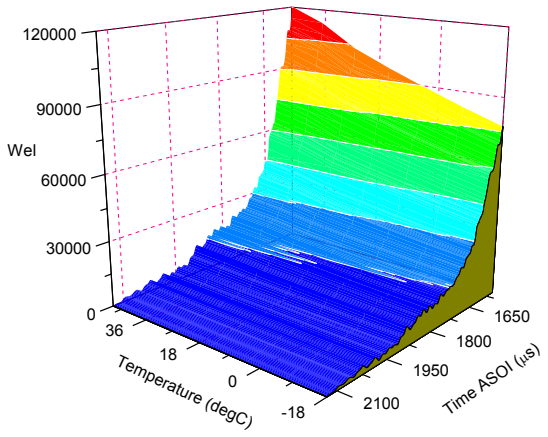

Figure 5-40 We_l BEOI under various temperatures

The corresponding We_l and We_g numbers show similar developing trend. Later at the end of injection and lower temperature cause lower *We* numbers. The extremely low chances of breakup of the spray can be confirmed through the image shown Figure 5-33.

Z similarly shows the drastic increase of spray stability at the end of injection, especially under LT. Temperature is of great importance for the droplet breakup as it can be seen that at the very end of injection, the droplets under LT show much higher stability than the one under RT. The aforementioned results and discussion suggest under cold start condition, a relatively higher injection pressure is required to get acceptable spray quantity. It can be expected even higher injection pressure is employed under cold start condition, poor spray quantity inevitably ensues due to the larger ligaments or droplets at the end of injection caused by lower effective injection pressure.

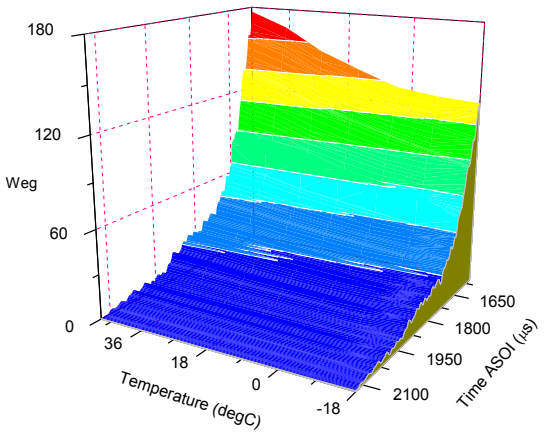

Figure 5-41 We_g BEOI under various temperatures

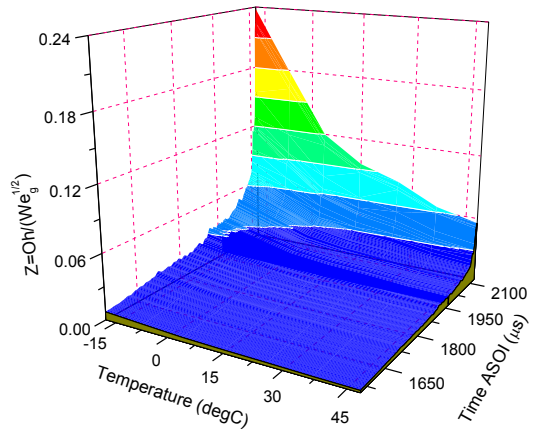

Figure 5-42 Z BEOI under various temperatures

5.4.2 **Two-split injection**

In this section, only several simple cases were selected to study the effects of temperature on primary breakup characteristics with split injection strategy. The injection duration was set to $0.5 \sim \tau \sim 0.5$ ms, τ ranging from 0.2 to 0.8 ms.

From the breakup characteristics with single injection strategy, it can be seen that spray behaves significantly different under different injection pressures. The effects of low fuel temperature on spray characteristics spray under high injection pressure tend to be weak. In

this subsection, the injection pressure is set to low injection pressure (60 MPa).

(1) Breakup characteristics of the first split injection

As presented in Figure 5-43, the first split injection shows distinctive characteristics. The spray characteristics of single injection under RT are employed as the reference in this study. Under RT, the first split injections with various dwells show slightly higher dispersed fuel areas than single injection although small area variations are observed when dwell varies. Suggested is that the first split injection seems to be almost independent on injection dwell under RT, meaning that effects of fuel properties and dwell can almost be ignored.

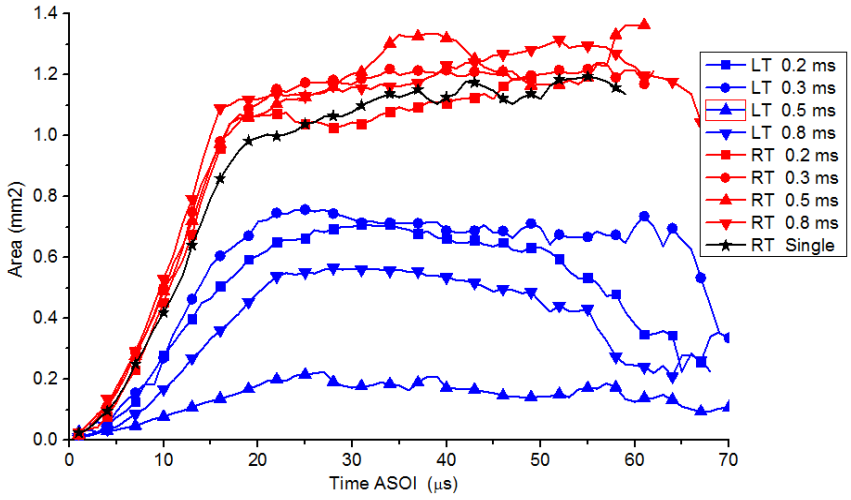

Figure 5-43 Spray area comparison of the first split injection between RT and LT under 60 MPa

By contrast, under LT, dramatic differences between cases with different dwells are clearly shown. The case with 0.3 ms dwell has the largest fuel area, closely followed by the case with 0.2 ms dwell. When dwell rises to 0.5 ms, the lowest fuel area is seen. An obvious recovery appears when dwell prolongs to 0.8 ms, meaning that the effects of split injection strategy weaken. Besides, it is obviously shown that fuel areas under LT are much

lower than those under RT, which can largely be attributed to raised viscosity and surface tension. It is also interesting to find that nearly all cases under LT present a sharp area reduction after 60 μs ASOI, suggesting the end of injection. Expected is that the first split injection duration under LT is much shorter than that under RT.

The corresponding spray penetration length varies significantly as shown in Figure 5-44. The spray of all cases under RT penetrates slightly faster than the single injection whereas the spray of all cases under LT penetrates much slower than single injection. Apart from that, RT causes a nearly linear increase of the plume penetration length, suggesting almost constant velocity for plume. By contrast, LT results in nonlinear increase of penetration length and more importantly a much lower penetration rate after approximate 20 μs ASOI. This actually suggests that the injection begins to end, similar to the expected trend from the varying trend of fuel area (shown in Figure 5-43), although an obvious time disparity in terms of the timing points for the reducing trends is observed from the two graphs. The 0.5 ms dwell case under LT presents the most distinctive spray penetration characteristic, shown in Figure 5-44 (b). Two nearly linear varying stages are observed, and the penetrating rate is surprisingly much lower than that of counterpart (0.5 ms dwell) and that of single injection under RT.

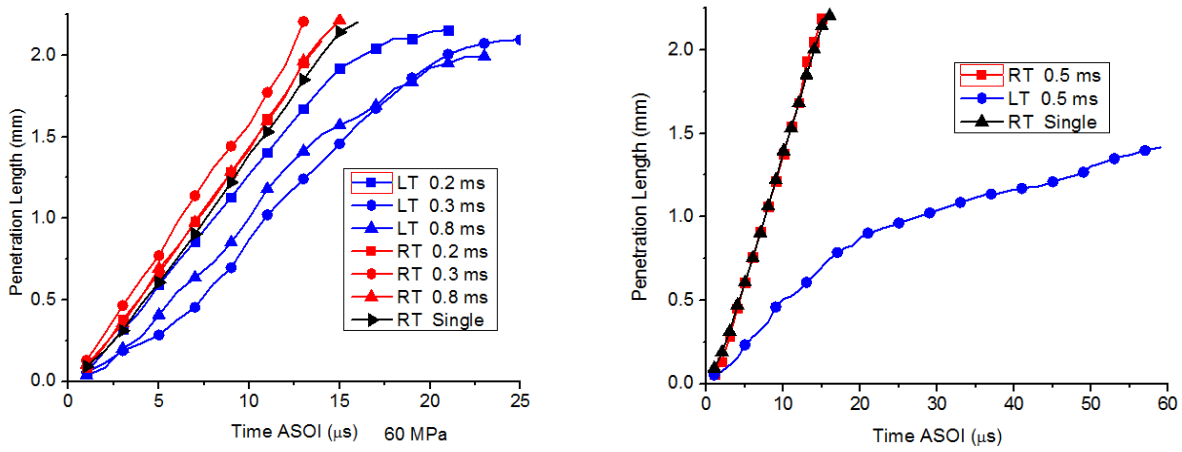

a b

Figure 5-44 Penetration comparison of the first split injection between RT and LT under 60 MPa

The spray morphology development for the first split injection with 0.5 ms dwell under RT and LT are shown in Figure 5-45 and Figure 5-46 respectively. It can be seen that the spray under RT shows good fuel dispersion although dispersed mushroom is observed. Surprisingly, the plume under LT is actually compact liquid column with intact spheroid head. The lower chances of breakup partly lead to the absence of separated ligaments and droplets, even though the spray shows higher velocity and higher potential of breakup with the rise of needle [113]. At 72 μs ASOI, the end of injection tends to start as the width of the liquid column at the very outlet of the injection obviously reduces, and this leads to the reduction of fuel area, corresponding to the fuel area varying trend presented in Figure 5-43.

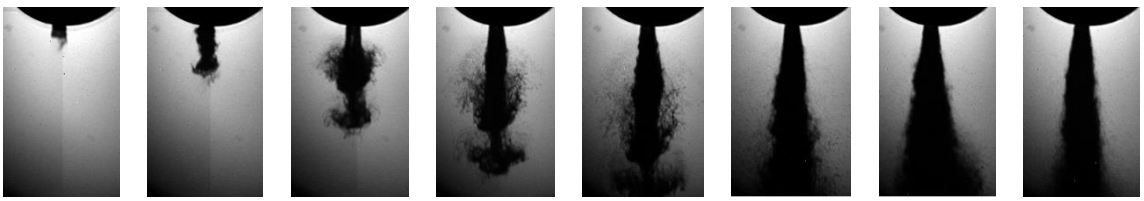

2 μs 5 μs 10 μs 15 μs 18 μs 30 μs 45 μs 55 μs

Figure 5-45 Morphology development of the first split injection with 0.5 ms dwell under RT and 60 MPa

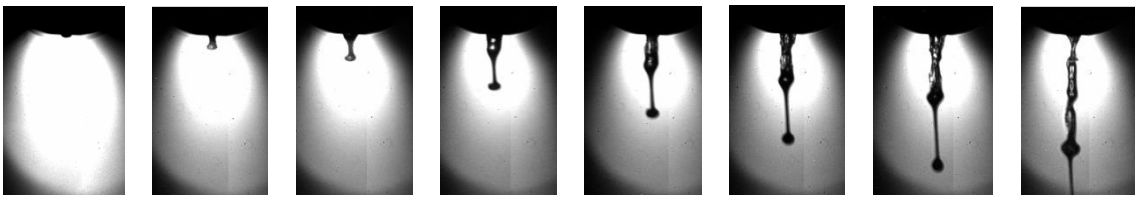

2 μs 7 μs 12 μs 22 μs 32 μs 42 μs 52 μs 72 μs

Figure 5-46 Morphology development of the first split injection with 0.5 ms dwell under LT (60 MPa)

The first split injection is thought to be the most independent split injection and its spray characteristics are thought to resemble to the ones of single injection [15, 129]. According to above area developing trends, the first split injection is impacted by both temperature and dwell simultaneously under same injection pressure, although under RT, the spray characteristics seem to be dominated by the injection pressure and dwell exerts slight influences. The effects of fuel properties are easy to understand through the much lower spray area and much slower penetrating velocity under LT. The influences of dwell are quite likely to be attributed to the electric-magnetic characteristics of the injector [11]. The employed injector is a solenoid injector and the strong interaction between a train of closely coupled energizing signals and the electrically induced resistance tends to significantly affect the needle lift and the effective injection duration. Although how the movement of the needle is impacted by this interaction is unknown, the effective injection duration seems to be shortened. Kourosh [11] studied the MFR of split injection reported that the first split injection showed 19% of less injected fuel than single injection. Although the reason was not given, it is suggested that the actual injection duration of the first split injection can be

considerably influenced by split injection strategy with various dwells.

(2) Breakup characteristics of the second split

The area development for the second injection under both RT and LT is shown in Figure 5-47. As discussed before, the RT cases show significant variation of spray characteristics due to strong interaction between split injections. However, similar varying trends and comparable plume areas for the cases with various dwells under LT are clearly shown. This suggests the dwell slightly affects the second split injection, that is, the second split injection is quite independent on the interaction between splits.

It is worth noting that LT cases have much smaller area than the RT cases when the fuel area reaches the stable stage. Raised fuel viscosity under LT can severely shorten the effective injection duration for each split injection, as discussed for the aforementioned first split injection. This means that split injections energized by a train of closely coupled energizations become more independent and separated under LT, resulting in longer actual dwell intervals between split injections compared with the cases under RT. The interaction between split injections under LT is significantly weakened and the second split injections are not obviously influenced by the first split injections. The split injections with various dwells are expected to demonstrate similar breakup characteristics under LT.

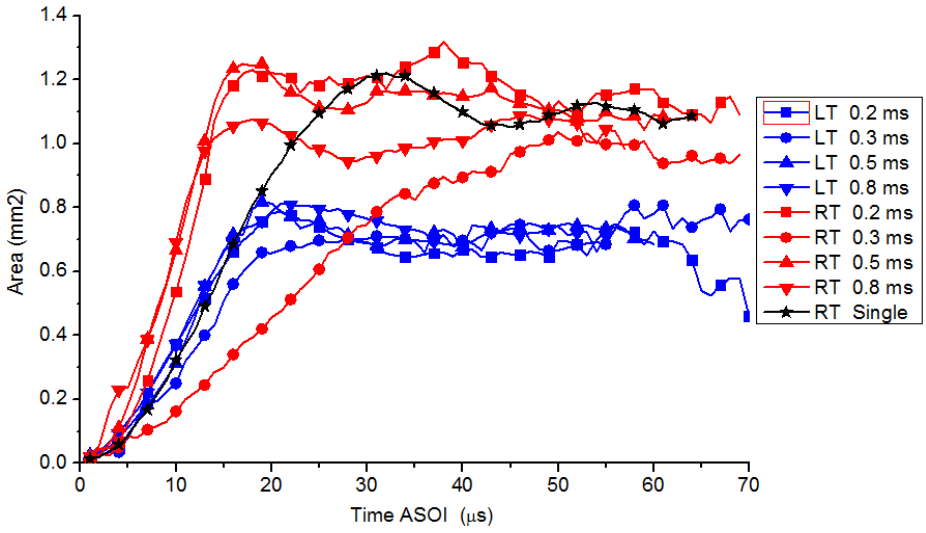

Figure 5-47 Spray area comparison of the second split injection between RT and LT under 60 MPa

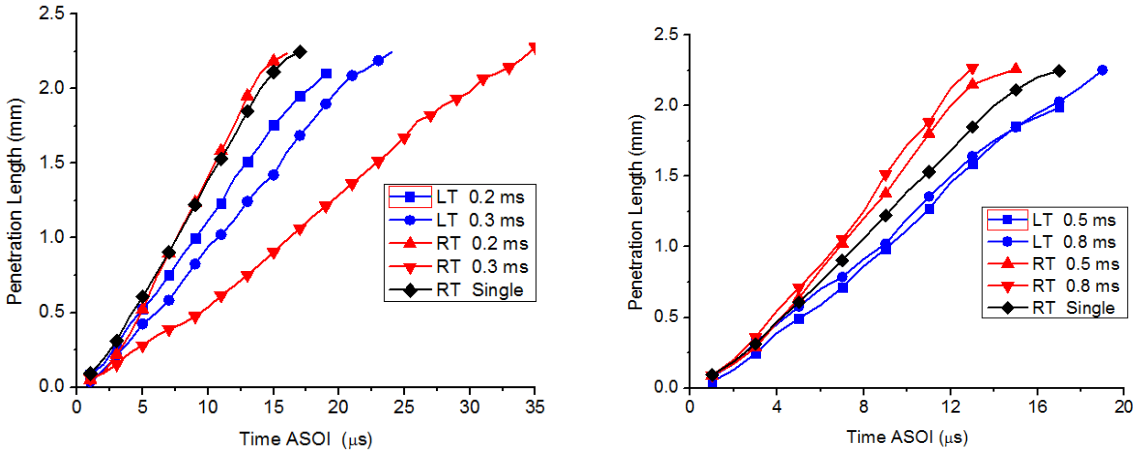

a b

Figure 5-48 Penetration comparison of the second split injection between RT and LT under 60 MPa

The plume of all cases under LT penetrates obviously lower than the single injection (Figure 5-48). The morphology development and area developing trend of the first split injection under LT (shown in Figure 43 and Figure 46 respectively) suggest that the air induced driving force can be ignored and the collision is unlikely to occur. Therefore, features of the second split injection tend to be governed by fuel properties (viscosity and

surface tension), penetrating apparently slower than single injection.

5.5 Conclusion and summary

This chapter focused on the primary breakup of spray at the initial injector opening stage and the end of injection with single and split injection strategies at injection to atmospheric conditions. The influence of low fuel temperature was also investigated. The following conclusions can be drawn.

(1) The formation of the mushroom shaped spray head can be attributed to the laminar flow regime in the injector hole, while the development of the mushroom results from the ambient air drag force. The appearance of the mushroom is expected to predict the existence of residue of the former injection. Lower injection pressure is thought to result in higher chances of the existence of mushroom.

(2) During the initial spray stage, the spray penetrated almost linearly with respect to time. The quantification of the fuel mass/spray area ratio suggests that the dispersion of the spray is greatly improved within a very short time, which is assumed to be caused by the further opening of injector.

(3) The injection pressure, dwell duration, distribution of injection duration between split injections and the number of the splits significantly affect the strength of primary collision and thus the primary breakup characteristics. Besides, the spray characteristics of the split injections except those of the first split injection are simultaneously affected by three main factors, namely, induced air driving force, lower MFR and primary collision. The combined

influences of the injection pressure, injection duration distribution and dwell duration determine the main effect on the affected split injections.

(4) It was shown that under low injection pressure and low temperature, raised viscosity and surface tension caused slower penetration and poorer breakup. Under high injection pressure, higher chances of mushroom formation under low temperature due to higher viscosity surprisingly lead to quicker penetration but still poorer dispersion during the initial spray stage. Low temperature retarded the start of atomization as the needle rose. The end of injection showed a large amount of compact liquid fuel with little dispersion, which was deteriorated by low temperature. The dimensionless parameters, namely, *Re*, *We*, *Oh* and the newly proposed Z, suggest that both inertia and viscosity were of great importance for the breakup regimes and spray stability.

(5) Under low injection pressure when split injection strategy employed, the first split injection was unexpectedly severely affected by both temperature and dwell, with significant breakup characteristic differences when dwell varied. By contrast, the second split under low injection pressure tended to be affected only by temperature rather by dwell.

Chapter 6 **Macroscopic characteristics of spray**

6.1 Introduction

The macroscopic spray characteristics of split injection are thought to depend on various factors. Although the impact of dwell, ambient temperature and fuel quantity ratio between injections on the spray characteristics has been widely studied, the effects of injection pressure and back pressure on the interaction between split injections are still not very clear. More importantly, the influences of fuel temperature on the characteristics of split injection and the interaction when dwell varies need to be investigated. The spray in this chapter is mainly characterized by the plume 2D fuel area and penetration.

6.2 Test conditions

To study the spray characteristics of single and split injection strategies under room temperature, the injection pressure varied from 60 to 120 MPa while the back pressure ranged between atmospheric and 3.5 MPa. The injection durations are shown in Table 6-1.

Table 6-1 Test matrix for macroscopic characteristics

	Single	2-split	
Injection duration (ms)	1	0.5 + 0.5	0.6 + 0.4
Dwell (ms)	----	0.2, 0.3, 0.5, 0.8	0.3, 0.5, 0.8

To study the influence of fuel temperature, the injection pressure was set to 60 and 90 MPa and the back pressure was set to atmospheric condition. The corresponding injection durations are shown in Table 6-1 (blue color)

6.3 Spray under room temperature

6.3.1 **Single injection under room temperature**

(1) Spray morphology

The spray morphology development under low injection pressure (60 MPa) with 3.5 MPa of back pressure is shown in Figure 6-1. Observable asymmetry for the plume morphology with wavy edges is shown, and this may be attributed to the air drag forces, internal turbulence in the spray and injector technology. After the initial injection stage (128 μs ASOI), the plume in the near field shows small cone angle. The morphology development under high injection pressure is not shown due to its great similarity to that under low injection pressure.

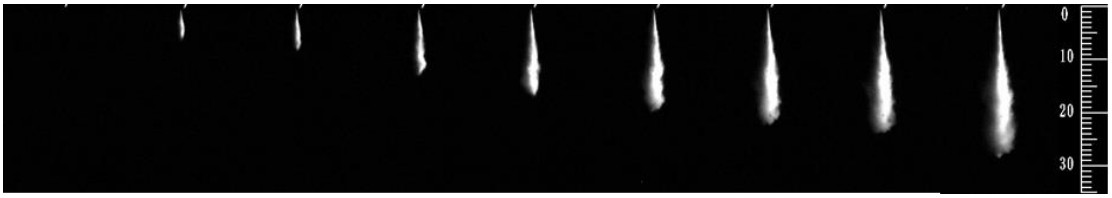

0 32 64 96 128 160 192 224 288

Figure 6-1 Spray morphology development (time inμs ASOI) under 60 MPa Pinj and 3.5 MPa Pb

(2) The influence of injection pressure and back pressure

The influence of injection pressure and back pressure on penetration is shown in Figure 6-2. It can be seen that higher back pressure considerably decelerates the penetration of plume by transfering the spray momentum to the ambient gas quickly. Stronger air drag force is expected with higher back pressure [85]. In addition, the difference in penetrating rate at the end of injection under low and high injection pressures is widened by the reduction of back pressure. This can be argued that the cases with low injection pressure show higher sensitivity to the variation of back pressure due to its lower initial force [34, 85, 130]. However, penetration shows small difference at the early spray stage under the same injection pressure. This can be attributed to the fact that the early injection stage is mainly governed by the injection pressure [11, 85].

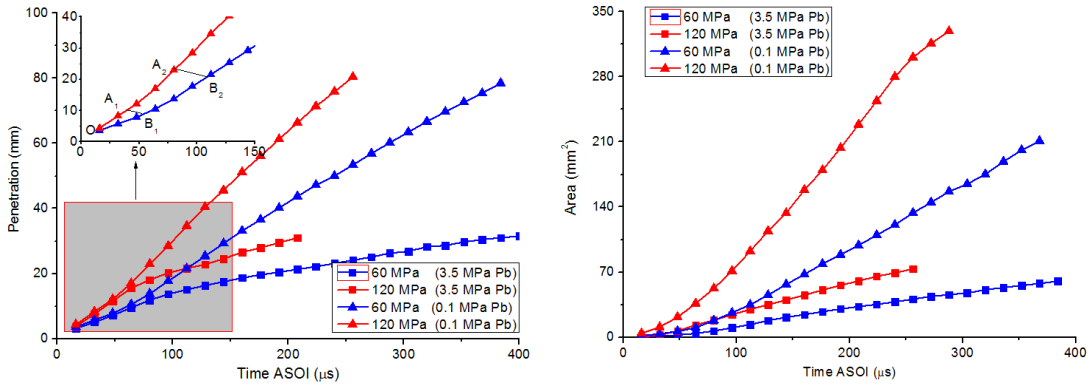

Figure 6-2 (a) spray penetration and (b) plume area under various injection conditions

Two stages with an obvious turning point can be clearly seen under high back pressure (3.5 MPa). This agrees well with the results of many studies [25, 131, 132]. The rise of MFR resulted from the further injector opening is the dominant factor for the first stage, while the ambient conditions tend to be more important for the later stage. Yanfei [85] reported

that within 100 us, the effects of back pressure on the penetration and cone angle are not obvious, suggesting that the initial spray stage is mainly dominated by the injection pressure. However, further from the injection tip, the impacts of ambient pressure is apparent, meaning the dominance of the back pressure [85]. It can be expected that with high back pressure the movement of plume quickly transfers from penetrating stage to diffusing stage where significant gas-fuel mixing effectively takes place.

However, three stages are observed under low back pressure (0.1 MPa), shown in the magnified graph in Figure 6-2 (a). From O to A_1 (or B_1), a nearly linear increasing stage is observed, showing good agreement with the result in the study of primary breakup. The aforementioned existence of the residual fuel in nozzle hole tends to be responsible for this linear varying stage. Then an acceleration stage follows (from A_1 to A_2 or B_1 to B_2), which possibly results from the further opening of injector. This result shows high agreement with other studies where an acceleration was reported [85, 115, 133, 134]. From then on (after A_2 or B_2), a linear varying stage is observed again.

Combining the varying trend of penetration under high back pressure, it can be expected that another linear varying trend will turn up after the aforementioned linear varying stage (after A_2 or B_2). Under high back pressure condition, the acceleration stage is also reported in many studies [85]. The decrease of the back pressure rises the time t_{peak} when the peak velocity appears. Spray has shorter t_{peak} when injection pressure is raised because of better atomization, thus faster momentum transfer to ambient gas and quicker velocity reduction.

The effects of back pressure on the transition length are significant. Generally, a raised back pressure leads to a reduced transition length [85]. It therefore can be concluded that there are at least 4 stages for the penetration development, namely, in timing sequence, a linear stage, an accelerating stage and two linear stages with different varying rate.

The plume area shows that more fuel mass and better dispersion under high injection pressure lead to much larger plume area. According to $We_l = \rho_l V^2 d_l / \sigma$, higher injection pressure leads to higher spray velocity thus higher *We*, meaning higher possibility of breakup and dispersion. The rise of injection pressure also raises the potential of cavitation which boosts the breakup of the liquid jet at the very outlet of the injector. Increased back pressure under a certain temperature raises the density of ambient gas and friction for the movement of plume, leading to much quicker decelerating effect and smaller fuel area. It can be observed that the rise of back pressure bridges the area difference caused by the variation of injection pressure.

6.3.2 **Two-split injection under room temperature**

(1) Spray morphology under high back pressure

The morphology development of spray under low injection pressure (60 MPa) with 3.5 MPa back pressure when split injection strategy (dwell of 0.3 ms) is employed is presented in Figures 6-3 and 6-4. The red dot lines denote the tip of second split injection. The plume development of the first split injection (0.3 ms dwell) shows great similarity to that with

single injection strategy in terms of penetrating rate and plume shape at the initial injection stage. It can be seen that the end of injection appears early at 306 μs ASOI. Such a short injection duration suggests that the whole injection process is in the transient stages, namely injector opening and closing stages. The throttling effect of flow, needle oscillation and radial vibration due to the transient injection characteristics tend to cause obvious spray radial expansion and propagation in the near field. However, this radial propagation in the near field is no obvious for the second split injection with the same energization duration (Figure 6-4). This can be reasoned that with short dwell, the injector opening for the second split injection tends to be earlier than that of the first split injection. This earlier injector opening results in shorter transient injection duration, thereby less throttled injection and relived needle radial vibration. The resultant smaller cone angle near the nozzle tends to appear. More importantly, noticeably observed is that the plume of the second split injection catches up and collide the wake of the first split injection. The collision is expected to be strong since the existence of the high density of the wake makes the boundary between the first split injection and the second split injection difficult to distinguish.

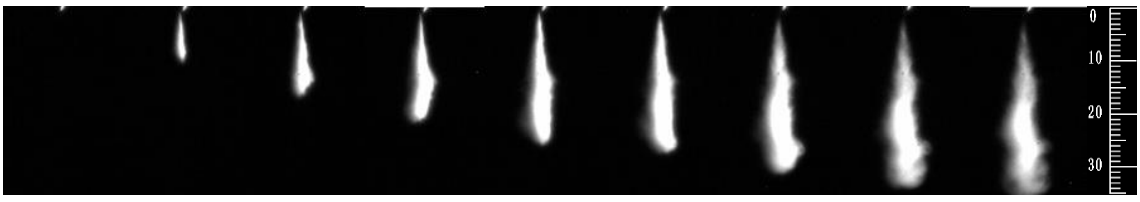

0 64 128 192 258 306 (end) 386 466 546

Figure 6-3 Spray morphology of the first injection (time inμs ASOI) under 60 / 3.5 Mpa with 0.3 ms dwell

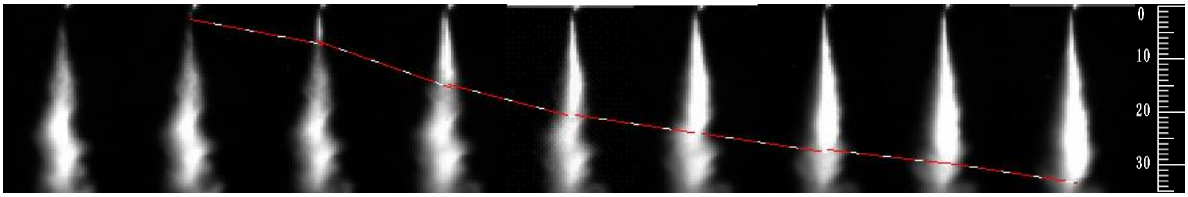

0 16 64 112 160 224 288 320 368

Figure 6-4 Spray morphology of the second injection (time inμs ASOI) under 60 / 3.5 Mpa with 0.3 ms dwell

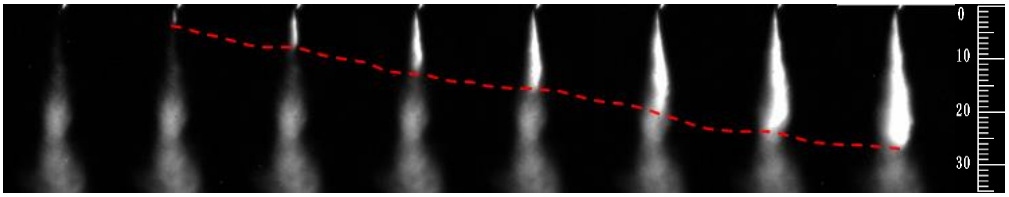

0 16 48 80 112 160 208 256

Figure 6-5 Spray morphology of the second injection (time inμs ASOI) under 60 / 3.5 Mpa with 0.8 ms dwell

The rise of dwell leads to a different picture for the second split injection (the morphology of the first split injection with 0.8 ms dwell case is not presented due to great similarities to that of the case with 0.3 ms dwell.). Much less fuel can be observed in the wake of the first split injection when the tip of the second split injection catches up (Figure 6-5). It can be expected that weaker collision tends to occur, exerting weaker influences on the characteristics of the second split injection. It is noteworthy that the plume of the second split injection follows the wake of the first injection split, leading to the distortion and asymmetry of the spray plume, shown at 160 and 208 μs ASOI. This is not obvious in the case with shorter dwell (0.3 ms).

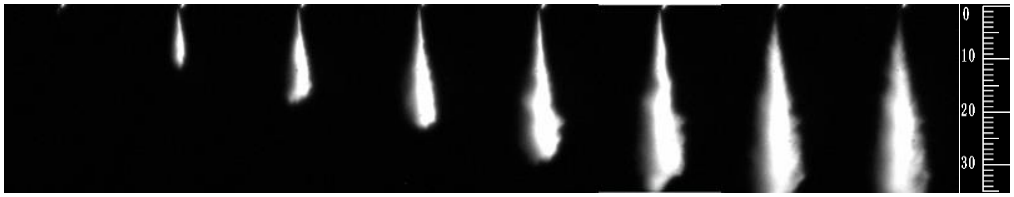

0 64 128 192 272 352 432 512

Figure 6-6 Spray morphology of the first injection (time inμs ASOI) under 90 / 3.5 Mpa with 0.3 ms dwell

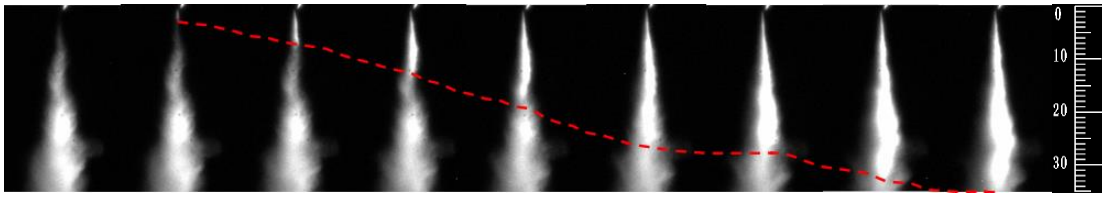

0 16 48 80 112 160 208 256 288

Figure 6-7 Spray morphology of the second injection (time in μs ASOI) under 90 /3.5 Mpa with 0.3 ms dwell

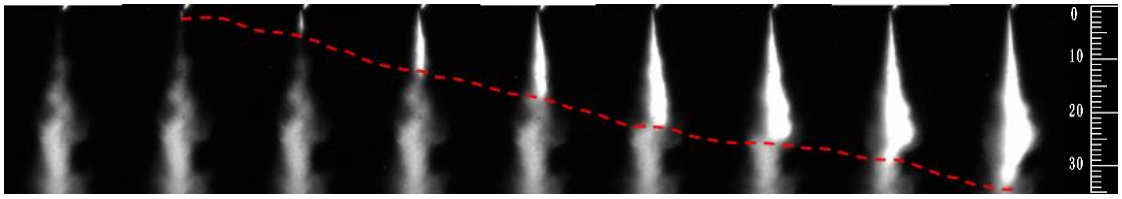

0 16 48 80 112 160 224 256 304

Figure 6-8 Spray morphology of the second injection (time in μs ASOI) under 90 3.5 Mpa with 0.8 ms dwell

For the case with higher injection pressure (90 Mpa), similar characteristics to those under low injection pressure (60 MPa) in terms of morphology are also observed. The obvious difference is that higher injection pressure leads to more symmetric shape of the plume than that under lower injection pressure, presenting less distorted plume. This suggests that lower injection pressure contributes to longer duration of throttling effect or longer transient injection duration due to slower needle movement and injector opening.

When chased up by the second split injection, the wake of the first split injection has obviously more observable fuel than that under lower injection pressure (Figure 6-7). More injected fuel mass under higher injection pressure is an important reason for showing more fuel mass in the wake. The later injector closing under high injection pressure should also be responsible because the actual dwell interval between the two split injections is reduced and the time for the first split injection to disperse and evaporate is also shortened. It is therefore can be expected that stronger collision occurs under higher injection pressure.

More noticeably seen is that for the long dwell case, the plume of the second split injection tends to be more seriously distorted by the wake of the first split injection as shown from 224 to 304 μs ASOI in Figure 6-8. The gas-liquid interacting surface and the droplet flowing stream seem to be important for the apparent distortion of the plume. The droplets in the wake move at a much higher velocity than the gas stream at the periphery. This higher moving velocity for droplets leads to smaller friction for the movement of the second split injection plume, meaning a so called " wake driving force" exerted by the moving droplet for the plume of the second plume. The second plume understandably moves in the direction where lower fiction or so called wake driving force exists, resulting in the distortion of the second plume. The transient injection characteristics inevitably lead to the asymmetry of the first plume, therefore high possibility of the occurrence distortion is expected.

It should be noted that the assumed wake driving force is different from the air driving force because the aforementioned air driving force in chapter 5 is produced by the plume

through momentum transfer. Noteworthy is that the wake driving force tends to be stronger than the air driving force at the same time point due to the higher velocity of the wake. With short dwell, the strong air driving force and the wake driving force enhance the second plume to move forward and the distortion at the periphery can be considerably weakened by the strong forward air driving force. By contrast, when dwell is long, the air driving force is too weak to constrain the distortion of the second plume at the periphery when wake driving force is still strong.

(2) Spray morphology under low back pressure

The morphology of the second injection under 60 MPa injection pressure and 2 MPa Pb is shown in Figure 6-9.

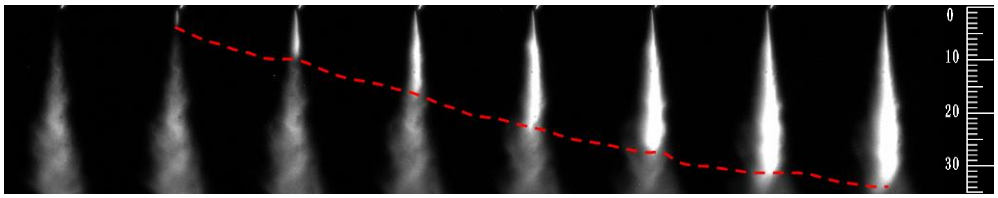

0 16 64 112 160 224 288 320

Figure 6-9 Spray morphology of the second injection (time in μs ASOI) under 60 /2 Mpa with 0.3 ms dwell

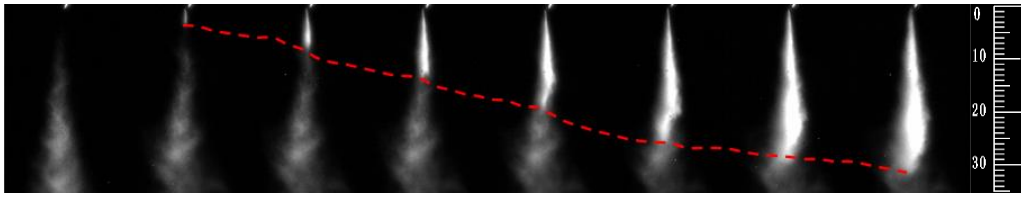

0 16 48 80 112 160 208 256

Figure 6-10 Spray morphology of the second injection (time in μs ASOI) under 60 /2 Mpa with 0.8 ms dwell

The variation of back pressure tends to considerably impact the development of plume shape and the collision with the wake of the first plume. For cases under 60 MPa injection pressure, the reduction of back pressure from 3.5 to 2 MPa causes substantial reduction of fuel mass left the wake of the first plume when chased up by the tip of the second plume (Figure 6-9 and 6-10). Low back pressure means weaker air drag force for plume and less momentum transfer between ambient gas and spray. Expected is the weaker interaction between the two plumes, meaning smaller contacting area between the two plumes. It is noteworthy that the effects of the variation of dwell on the remains of fuel droplets in the wake are not significant. Under the same injection and back pressure, the 0.3 ms and 0.8 ms dwell cause little difference in the existence of droplets in the wake, as clearly seen Figure 6-9 and 6-10.

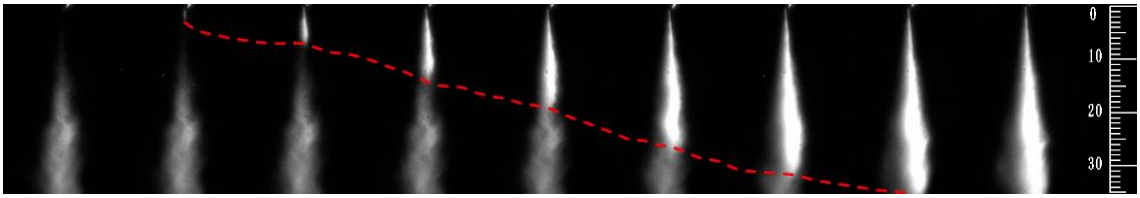

0 16 48 80 112 160 208 256 288

Figure 6-11 Spary morphology of the second injection (time in μs ASOI) under 90 / 2 Mpa with 0.3 ms dwell

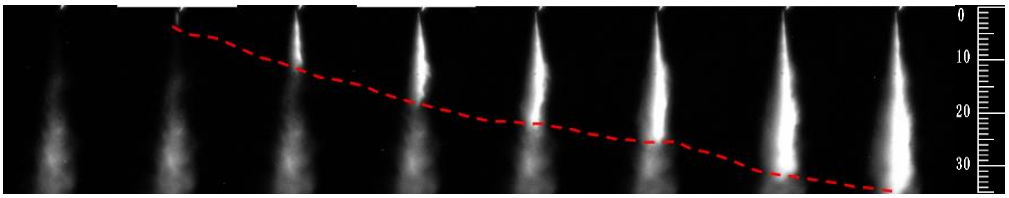

0 16 48 80 112 160 224 256 304

Figure 6-12 Spray morphology of the second injection (time in μs ASOI) under 90 /2 Mpa with 0.8 ms dwell

Surprisingly observed under high injection pressure (90 MPa) with short dwell in Figure 6-11 is that the plume does not totally follow the wake of the first plume as mentioned before, but actually deviates from the wake. It appears that the assumed "wake driving force" disappears and a new resistant force turns up. It should be kept in mind that most of droplets with high velocity move forward under low ambient back pressure condition due to weak air resistant force, leaving the ones behind with very low velocity. The existence of the droplets with very low velocity causes weak "wake driving force" for the coming plume but actually higher resistance for the second plume due to higher density. Consequently, the resistances between the two sides of the second plume is unbalanced, causing the moving deviation of the plume if get disturbed. In addition, the retarded second plume (0.8 ms dwell) shows unobvious deviation (Figure 6-12). Increased dwell allows the wake of the first plume to obtain sufficient time to propagate and vaporize. More evenly distributed air-fuel mixture tends to present more balanced resistance for the second plume. The more balanced air drag force is unlikely to significantly deviate the second plume.

(3) Spray characteristics

Split injection strategy with short injection duration inevitably causes highly transient characteristics for split plumes, leading to high variation of cone angle. Consequently, cone angle is not studied in this section. According to the images of plume shown before, high back pressure makes it difficult to define the boundary between the wake of the first plume

and the tip of the second plume. To avoid the blur when employing Matlab program to quantify the characteristics, low back pressure (2 MPa) cases are adopted.

1) Spray characteristics under low injection pressure

The area development of the first and second plumes under 60 MP injection pressure with various dwells suggests significant difference (Figure 6-13). The second split plume with 0.2 ms dwell persistently presents larger area than the corresponding first plume. The strong collision due to the existence of large amount of fuel in the first plume wake tends to be mainly responsible because lower penetration rate is found at the initial spray stage (Figure 6-13 (b)) [11]. The 0.5 ms dwell case similarly shows larger area than its corresponding first plume and higher penetrating rate. This probably can be attributed to the dominant air and wake driving forces. The collision tends to be significantly reduced when compared with 0.2 ms dwell case. When dwell further increases to 0.8 ms, overall similar areas for the first and second split sprays are found, however, the second plume still tends to shows quicker penetrating rate than the first one. It suggests the interaction between the two split sprays still exists although expected to be weak.

The results agree well with the findings in other studies [11, 130, 135]. All reported that the second spray plume penetrates quicker than the first one, and the penetration difference becomes more obvious at the later stage. This difference is enhanced by the reduction of dwell. The difference of the tip velocity between consecutive split injections was as high as 10 m/s which approximated the velocity of the wake of the first split injection [11].

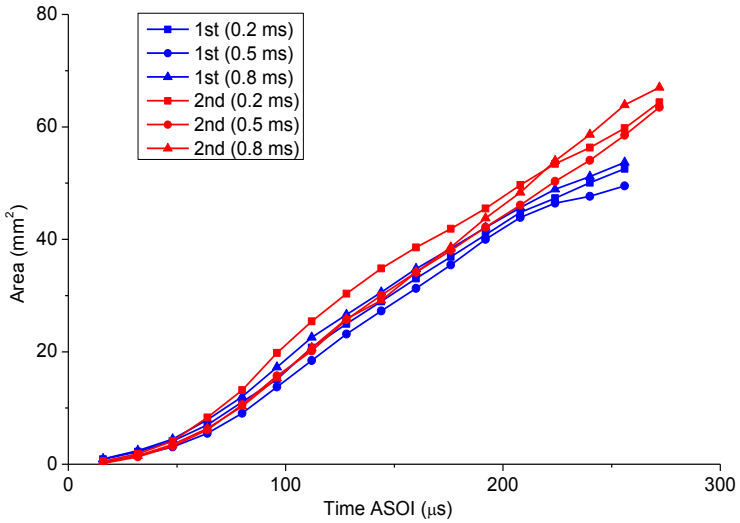

a

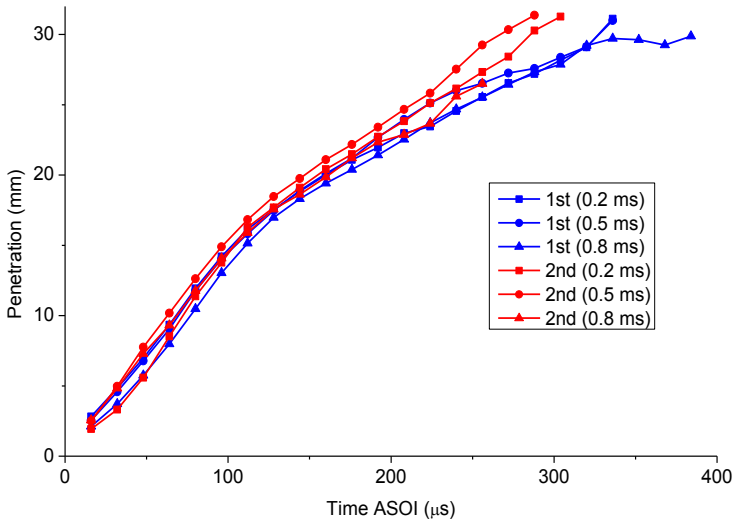

b

Figure 6-13 (a) area and (b) penetration development under 60 MPa / 2 Mpa with various dwells

It is interesting to find that the second plume presents larger area and higher penetration than the first plume after 200 μs ASOI for all cases with various dwells. The shorter injection duration for the first split injections fail to provide sufficient fuel with high velocity to push forward the decelerated fuel by the air drag force at the tip of the plume. By contrast the earlier opening of the second split injections leads to longer injection duration and

sufficient fuel continuously pushing the liquid fuel forward. It should be noted that dwell can also impact the spray characteristics of the first plume although collision, wake driving force and air driving force do not exist. Assumed variation of MFR due to needle oscillation and stagnation is the main reason when dwell ranges from 0.2 to 0.8 ms. The magnetic characteristics of the injector are expected to strengthen the variation of needle movement when closely coupled energization signals are employed.

2) Spray characteristics under high injection pressure

Under high injection pressure (90 MPa), smaller fuel area and slower penetration for the second split plumes than the first one are clearly found at the early stage of injection (Figure 6-14). During the later injection stage, apparently larger fuel area and higher penetration rate for the second plume are observed. This phenomenon is quite different from that under low injection pressure (60 MPa). Stronger collision is thought to be responsible during the early stage. High injection pressure leads to retarded injector closing, thus the existence of large amount of compact liquid fuel with low velocity near the injector at the end of the first split injection. This inevitably entails the occurrence of strong collision between the tip of the second plume and the wake of the first plume. Short dwell can considerably deteriorate this undesirable collision. When strong collision and coalescence appear, the second plume is expected to be considerably decelerated and poor dispersion ensues.

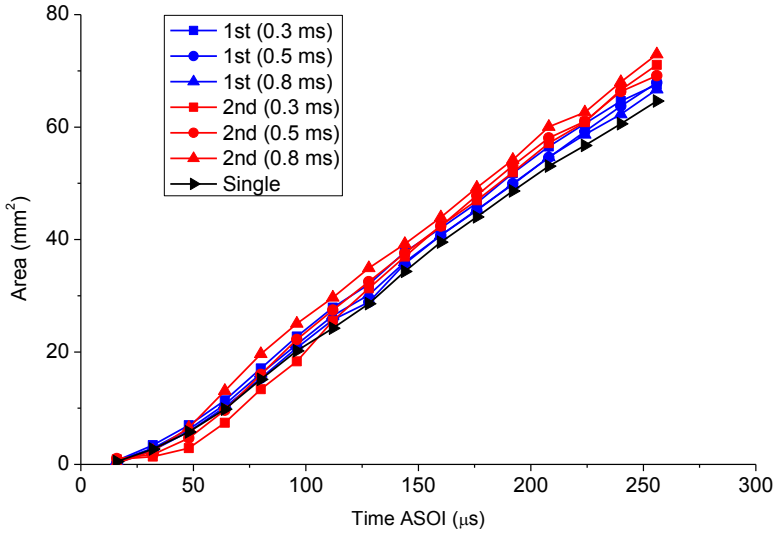

a

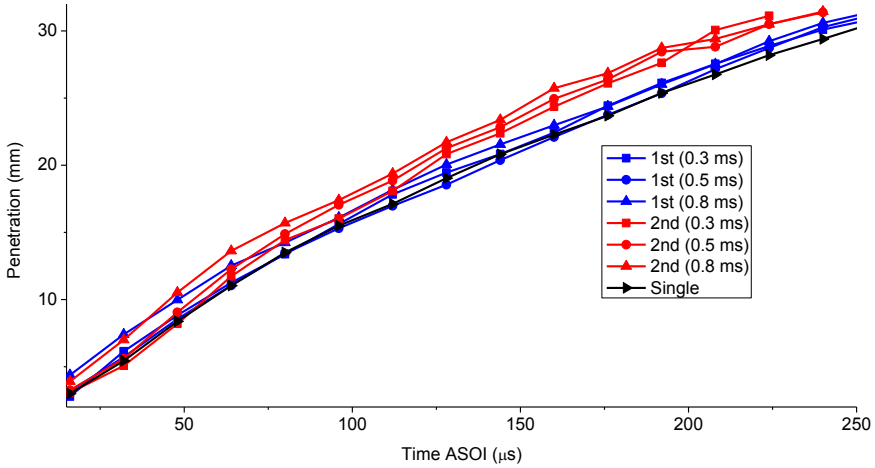

b

Figure 6-14 (a) area and (b) penetration development under 90 MPa / 2 Mpa with various dwells

It should be noted that the varying trend of the area at the initial stage is contradict to the varying trend found in primary breakup. In primary breakup, the view field is very small and the light employed to illuminate the view field is strong. The primary collision which results in an obvious area increase can be clearly observed. However, for high speed photography, the view field is much larger and the light density is relatively much lower.

Consequently, the primary collision is not captured, and the spray characteristics mainly depend on the macroscopic spray behavior.

The elapse of time allows sufficient fuel with high inertia and velocity to push the decelerated fuel progressively forward to the positions where the wake driving force and air driving force are relatively much stronger. The second plume can get significantly "accelerated", thereby obviously larger fuel area and penetration rate [11].

6.3.3 **Influence of injection duration distribution**

Macroscopic characteristics are expected to depend on the variation of energizing duration distribution. The injection pressure in this subsection was set to 90 MPa. The comparison of macroscopic characteristics for the first split injection between two different injection duration distributions is shown in Figure 6-15.

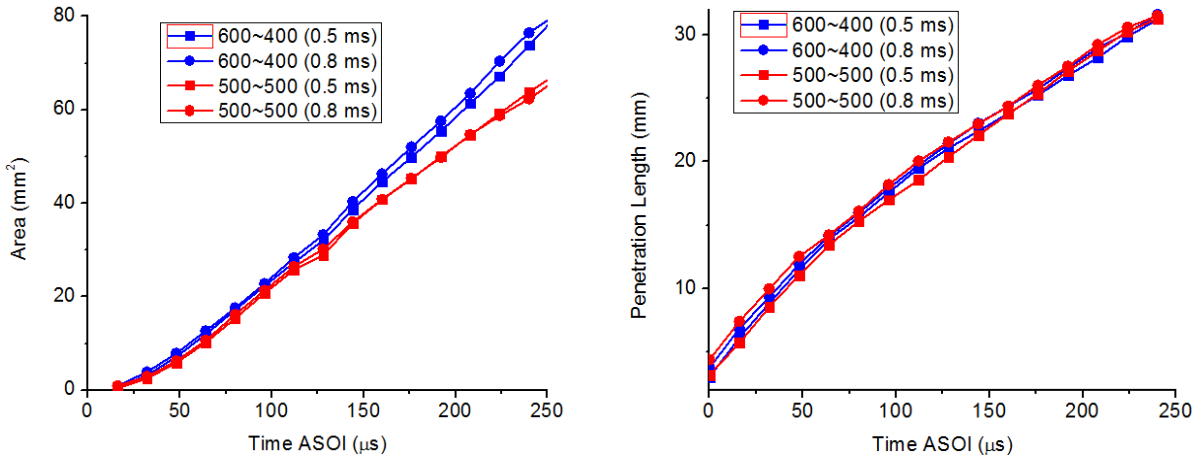

a b

Figure 6-15 (a) area and (b) penetration of the 1st injection with different energization distributions

The first plume with 0.6~0.4 energizing duration tends to consistently show larger area than the case with 0.5~0.5 ms. However, comparable penetration rates between the two cases are observed. Longer energizing duration enables the needle of the injector to move to a higher degree, leading to larger opening area and more fuel mass to be injected. Larger fuel area therefore can be expected partly owing to more fuel mass and partly due to better fuel dispersion (larger injector opening due to longer energizing duration weakens the throttling effect).

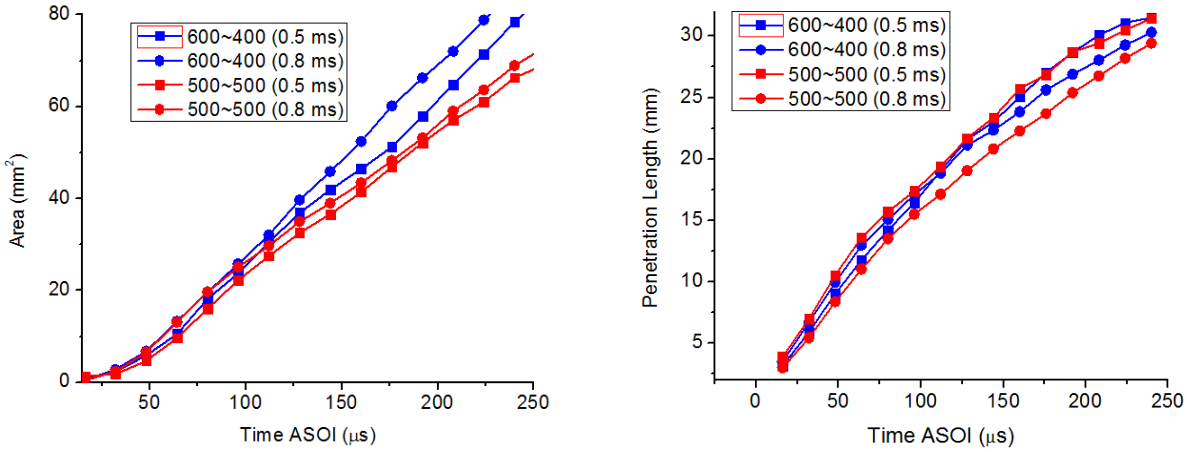

a b

Figure 6-16 (a) area and (b) penetration of the 2nd injection with different energization distributions

The second plume with various energizing distributions presents more noticeable variation of spray characteristics (Figure 6-16). The cases with shorter injection duration for the first one have smaller fuel area. Again, the quality of dispersion and the difference of injected fuel mass tend to be responsible. Longer first energizing duration enables larger injector opening for the second split injection, therefore better fuel dispersion. More injected fuel mass is also likely to ensue for the 0.6~0.4 cases although shorter energizing duration for

the second split injection (0.4 ms) is employed. The dwell is a dominant factor when various injection distributions are employed. 0.3 ms dwell makes the boundary distinction between the two split injections considerably difficult when 0.6~0.4 ms injection strategy is employed, and therefore is not shown in this study. The area of 0.6~0.4 ms injection strategy shows higher sensitivity to the variation of dwell possibly due to stronger collision than wake driving force and air driving force. By contrast, the penetration of 0.5~0.5 ms injection strategy is more sensitive to the difference of dwell, and the relatively stronger impact of wake and air driving force than that of collision is possibly the main reason.

6.4 Spray characteristics under low fuel temperature

6.4.1 Spray characteristics under low temperature with single injection

The fuel properties can be significantly affected by the reduction of temperature, namely increased viscosity and surface tension. The macroscopic spray characteristics are thought to be correspondingly considerably impacted.

LT results in an obvious reduction of fuel area under low injection pressure cases (Figure 6-17). The raised viscosity increases the friction for the movement of needle, thus retarded injector opening. Shortened injection duration and reduced injected fuel mass are expected, as a result, smaller plume area and penetration ensue. Furthermore, the inertia of the injected fuel is considerably reduced in the nozzle hole because of the raised viscous force. The decrease of fuel temperature effectively reduces the discharge coefficient under low

injection pressure, thus lower velocity and fuel MFR. This inevitably reduces the initial velocity of the plume. Bernoulli's equation, $u = C_d\sqrt{2\Delta p/\rho}$ suggests that higher fuel density results in lower penetrating rate. LT can slightly increase the fuel density, leading to lower initial velocity and penetration. More importantly, higher surface tension can greatly enhance the stability of the droplets and lower the possibility of breakup (both primary and secondary breakup). When injection pressure rises to 90 MPa, the penetration length shows slight difference under RT and LT although apparent area difference is still observed. The effect of fuel surface tension again tends to be one of the reasons for the area difference.

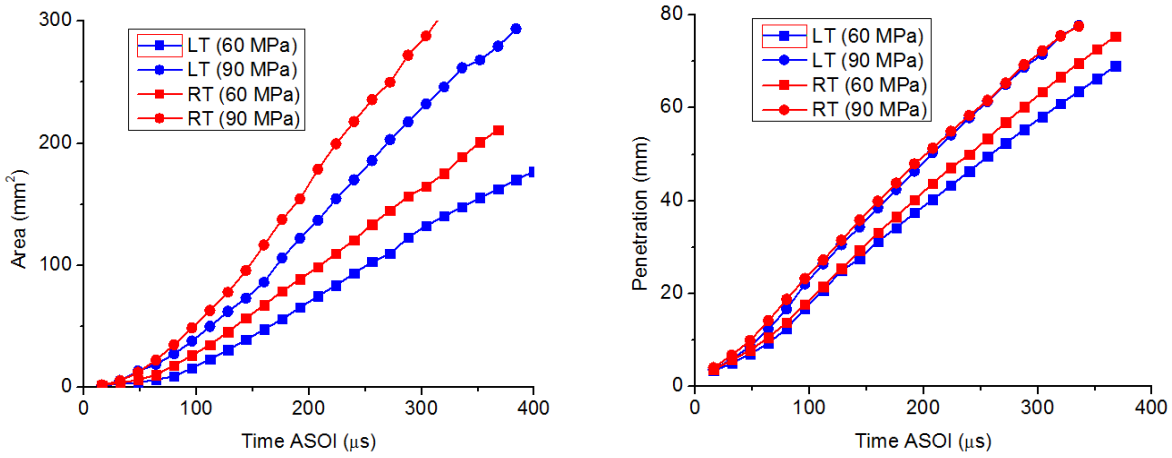

a b

Figure 6-17 Comparison of (a) area and (b) penetration between RT and LT with single injection

Hiroyasu et al. [136] estimated the time for the primary breakup, shown as:

$$t_b = \frac{15.8\,\rho_f d_0}{C_d\sqrt{2\rho_g \Delta p}} \qquad \text{Equation 6-1}$$

t_b generally varies between 20 and 50 us [137]. Before t_b, the spray increases linearly with the square root of time elapse, and then it keeps almost stable, show as:

$$\begin{cases} 0 < t < t_r : LL(t) = \alpha\sqrt{t} \\ t > t_r : LL(t) = LL_{\max} \end{cases}$$ Equation 6-2

Coefficient α depends on various factors and is presented as:

$$\alpha \propto d_h^A \rho_g^B p_{inj}^C C_d^D$$ Equation 6-3

Where A, B, C and D are coefficients.

According to the results, the author pointed out that the time limit t_b can be expanded with quite high accuracy. In this study, the coefficients need to be modified to meet various injection conditions, and the spray penetration correlation is expressed as:

$$LL(t) = Kd_0^a \rho_g^b p_{inj}^c C_d^d t^e$$ Equation 6-4

The varying trend of the correlation between calculated penetration and experimental penetration under RT and LT shows high linearity (Figure 6-18). The low back pressure leads to rather poor dispersion and the spray with large ligaments or large droplets can survive for a rather long time. This penetration correlation can predict the development of spray with high accuracy, with R^2=0.995 for LT and R^2=0.989 for RT. The LT case presents poorer dispersion thus higher fitting accuracy than the RT case. The discrepancy between calculated and experimental penetration becomes larger at the end of spray partly possibly because of the effects of finer breakup of the spray caused by the ambient gas. The variance can also be attributed to various factors, for instance, the variation of fuel temperature, injection pressure and liquid properties.

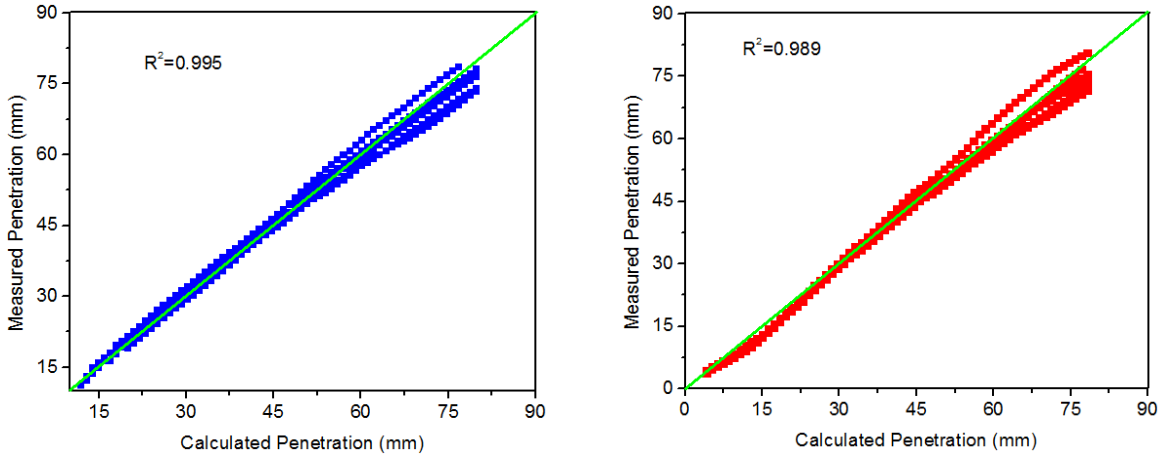

a b

Figure 6-18 Correlation of predicted and measured penetration under (a) LT and (b) RT (60 /0.1 (MPa))

The gas/liquid density ratio, *We* and *Re* are important for spray breakup. The macroscopic characteristics show higher dependence on *We* and air/liquid density ratio than on *Re* [31]. The variation of temperature causes significant variation of vapor pressure, and significant variation of flow regimes in the injector nozzle. In addition, low injection pressure and low temperature cause low *We* and *Re*. Low momentum and inertia are expected to lead to weak interaction between plume and ambient gas. Poor dispersion and short penetration are likely to occur [31].

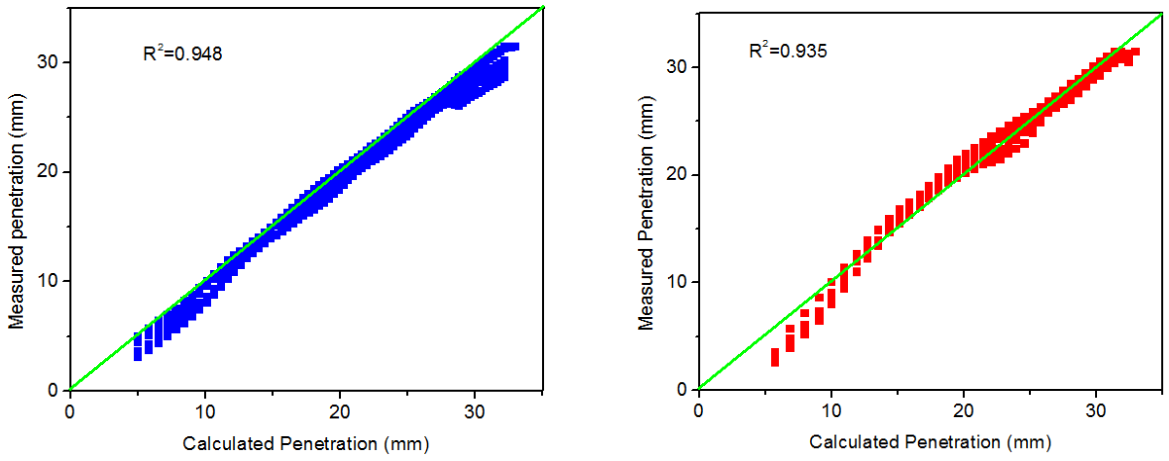

a b

Figure 6-19 Correlation of predicted and measured penetration under (a) low and (b) high P_{inj} (Pb=3.5 MPa)

The rise of back pressure results in the reduction of fitting accuracy (R^2=0.948 for 60/3 MPa and R^2=0.935 for 120/3.5 MPa) probably due to the boosted breakup of spray (Figure 6-19). The ligaments or droplet breakups quickly, leading to the failure of meeting the requirement for the correlation to precisely predict the spray penetration. It also can be observed that the predicted penetration is higher than the measured one especially for the 60/3 MPa case.

Raul [87] thoroughly analyzed the penetration correlations proposed by other researchers and found that various factors are involved during the whole spray developing process. The injection pressure (Δp), ambient gas density (ρ_g), injector hole diameter (d_0), cone angle (θ) and the elapse of time (t) are found to be related to the penetration. In present study, the fuel viscosity is expected to influence the initial velocity, and surface tension is thought to affect the spray breakup and dispersion. Taking these factors into consideration, the following correlation is put forward to predict the penetration.

$$S(t) = K\Delta p^a \rho_g^b \tan^c(\theta/2) t^d d_0^e \upsilon^f \sigma^g$$ Equation 6-5

The coefficients of this correlation under low and high back pressure are shown in Tables 6-2 and 6-3 respectively. Overall higher accuracy is obtained with this correlation when compared with the one proposed by Martinez et. al. [137], especially for the cases under high back pressure (Figure 6-20). This maybe because the influences of fuel properties are taken into consideration although they are not as important as the injection pressure and back pressure.

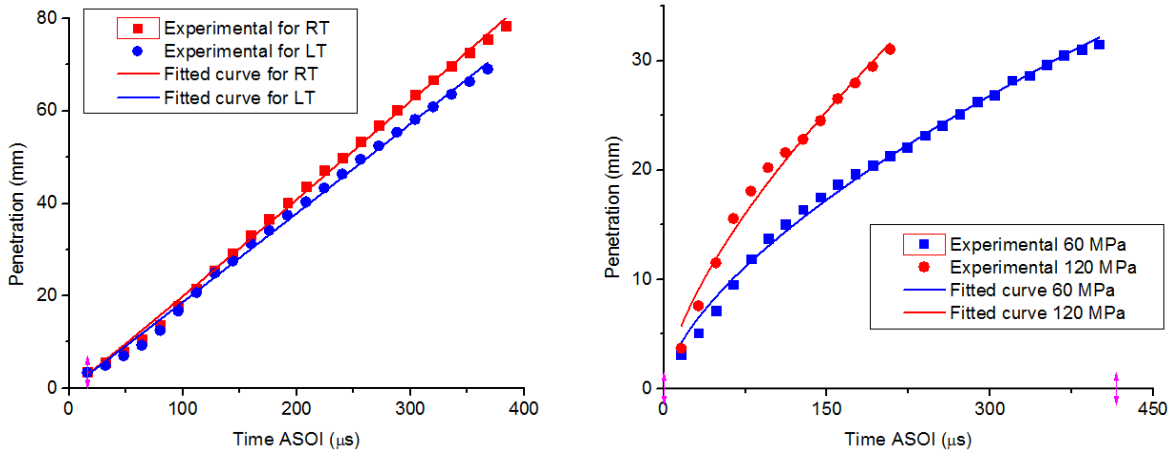

(a) (b)

Figure 6-20 Penetration fitting with Raul's model under (a) low P_b (60 MPa) and (b) high P_b (60 and 120 MPa)

Table 6-2 Coefficients for Raul's model under low P_b (under 60 MPa)

	K	a	b	c	d	e	f	g	R^2
RT	0.14785	0.25762	-0.7914	0.05014	1.03343	0.25361	-0.1047	0.02695	0.99712
LT	0.1520	0.2172	-0.589	0.0372	1.0185	0.2606	-0.034	0.016	0.99565

Table 6-3 Coefficients for Raul's smodel under high P_b

	K	a	b	c	d	e	f	g	R^2
120 MPa	0.7077	0.9329	0.9140	1.0171	0.6648	1.1890	0.6294	1.0917	0.96523
60 MPa	0.7620	0.9385	0.9333	1.1325	0.6316	1.1468	0.7123	1.0713	0.9926

6.4.2 **Spray characteristics under low temperature with split injection**

(1) Spray characteristics under low injection pressure

The first split injection with a wide range of dwells under both RT and LT presents dramatic variation of spray characteristics (Figure 6-21). The fuel area for all cases shows an increase and then a decrease. The increase of MFR with the opening of the injector is thought to be responsible for the increase of spray area. However, the dispersion, evaporation and the fact that the spray moves out of view field are assumed to be the reasons for the reduction of the spray area. It is shown that LT can decrease the dispersed fuel area to an astonishing degree. This means that the varied fuel properties can further deteriorate the spray characteristics when split injection strategy is employed. The aforementioned less fuel mass and poorer dispersion quality are mainly responsible for the much lower spray area.

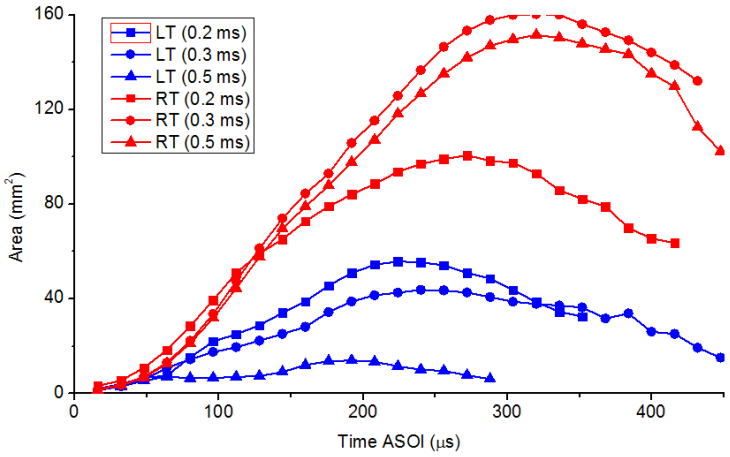

Figure 6-21 The area comparison of the 1st injection between RT and LT under low Pinj

Attention should also be paid to the influence of dwell interval on the spray characteristics. Under RT, the difference among cases with various dwells is dramatic under low back pressure condition. This is obviously different from the result under high back pressure as reported before. The increase of back pressure significantly boosts the interaction between splits and obscure the difference caused by the variation of dwell. High back pressure thus high ambient gas density inhibits the propagation of plume and narrows the differences. It is seen that under low back pressure, the 0.2 ms dwell case has the lowest fuel area thus assumed lowest injected fuel mass. This phenomenon is quite unique because short dwell tends to cause earlier injector opening and more fuel mass injected. This may be ascribed to the electric-magnetic characteristics of the solenoid driven injector when the closely coupled energizing signal is employed. This contradicts with the findings in Chapter 4 and this again suggests that the spray characteristics greatly depend on injector technology. Further study should be carried out to investigate this phenomenon.

By contrast, under LT, the 0.5 ms dwell case presents the lowest fuel area (Figure 6-21), which is different from the lowest case under RT (0.2 ms dwell). It should be noted that the 0.2 ms dwell case shows the highest value, closely followed by the 0.8 ms dwell case, which is also different from the highest case (0.3 ms dwell) under RT. This suggests that the interaction between the variation of fuel properties and the electric-magnetic characteristics exist.

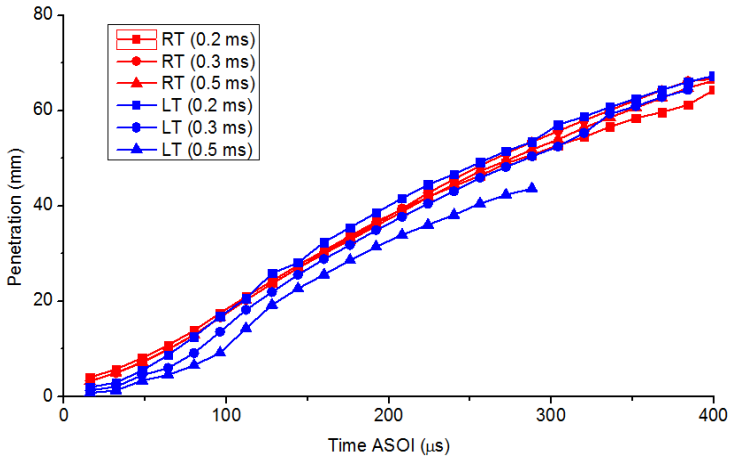

Figure 6-22 Penetration comparison of the 1st between RT and LT under low Pinj

The penetration rate also varies significantly. The 0.2 and 0.3 ms cases under LT initially present obviously lower penetration rate and then show a trend to overtake their counterparts under RT. This shows contradiction to the single injection in Figure 6-17 where LT shows lower penetration under 60 MPa. This contradiction may be attributed to the transiting characteristics of split injection (injector is not fully open). Reduced initial velocity under LT appears to be the main reason for the lower penetration rate at the early spray stage, however, the weaker momentum transfer and smaller velocity reduction enables the plume to penetrate faster at the late stage.

Interestingly, much lower penetration rate for the 0.5 ms dwell case under LT is observed, and the plume never gets to the boundary of the view field. This can be further verified through the morphology development of the plume, shown in Figure 6-23. It can be observed that only a small amount of fuel is injected for the first split injection when compared with the second split injection, agreeing very well with the microscopic morphology in Figure 5-45.

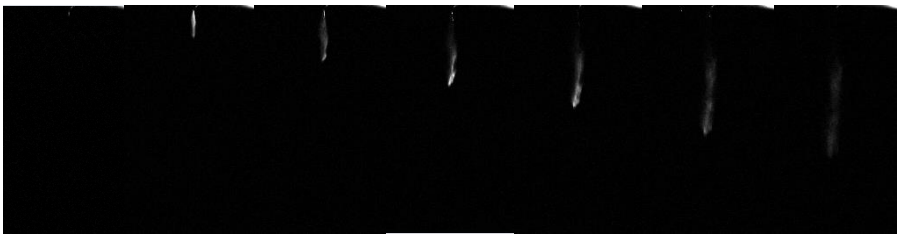

0 48 96 144 192 272 352

a

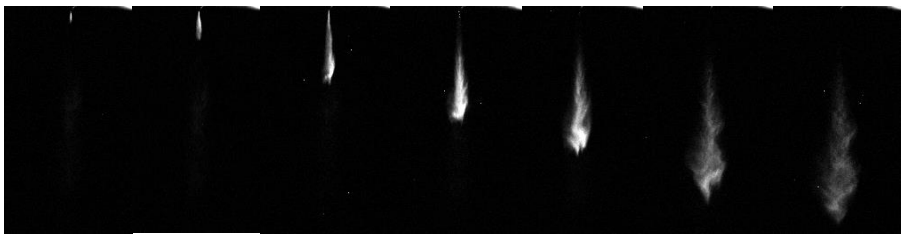

16 64 144 224 304 624 688

b

Figure 6-23 Morphology of the 1st (a) and 2nd (b) injections under LT with 60 MPa P_{inj} and 0.5 ms dwell.

Obvious area difference among cases with a wide range of dwells under RT and LT is also seen for the second split injection (Figure 6-24), however, the difference is not as significant as that for the first split injection. Under RT, the varying trend of the second split injection (0.5 ms dwell case has the highest fuel area followed by 0.2 ms dwell and 0.3 ms

dwell) does not consistently echo with that of the first split injection (0.3 ms dwell case has the highest fuel area followed by 0.5 ms dwell and 0.2 ms dwell). The area variation for the second injection with different dwells under LT is narrowed when compared with the first one. The earlier opening of the injector allows more fuel to be injected, compensating the reduced injected fuel mass caused by the variation of fuel properties.

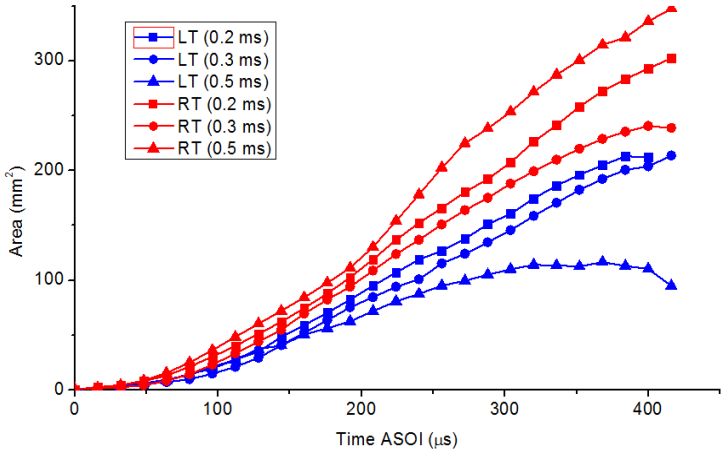

Figure 6-24 Area comparison of the 2nd injection between RT and LT under low P_{inj}

The penetration of the second plume under various conditions shows similar developing trend to that of the first one but with smaller difference, as shown in Figure 6-25. It is noteworthy that at the later stage of spray, only the penetration of 0.2 ms dwell case shows the potential to overtake those under RT. Two possible reasons can explain this small difference. Under RT, sufficiently injected fuel mass pushes the plume forward and the effect of the reduction of velocity due to better dispersion can be dampened. Under LT, increased amount of injected fuel mass for 0.2 dwell case (because of larger injector opening) contributes to better dispersion and higher momentum transfer to the ambient gas, weakening the retaining effect for the droplets to keep stable (caused by the variation of fuel properties).

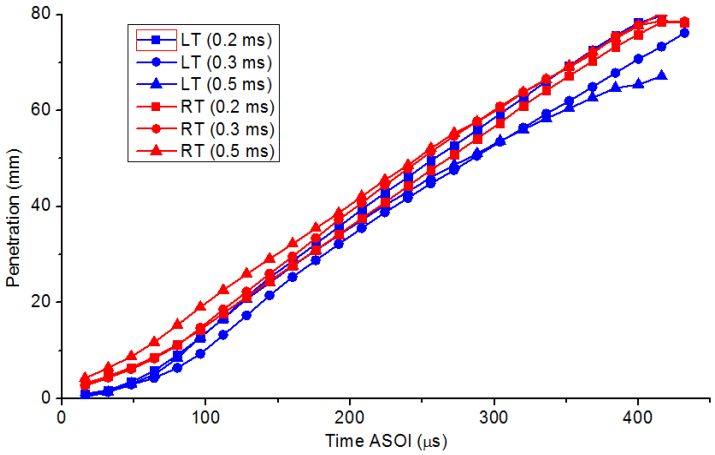

Figure 6-25 Penetration comparison of the 2nd injection between RT and LT under low P_{inj}

(2) Characteristics under high injection pressure

1) Spray characteristics of the first split injection

The hydraulic force is a dominant factor for the characteristics of the spray, and increase of injection pressure tends to change the behavior of the spray. Under 90 MPa, the first split injection shows much smaller injection character variation than that under low injection pressure (60 MPa), although small difference are still observed (Figure 6-26). The LT case tends to have similar plume area to the RT case even though dwell varies. Under high injection pressure, the hydraulic force tends to be dominant and the influence of LT is not obvious. In addition, the effects of dwell are still observed although much weakened by the increase of injection pressure. The 0.2 ms dwell case presents observably lower fuel area under both LT and RT.

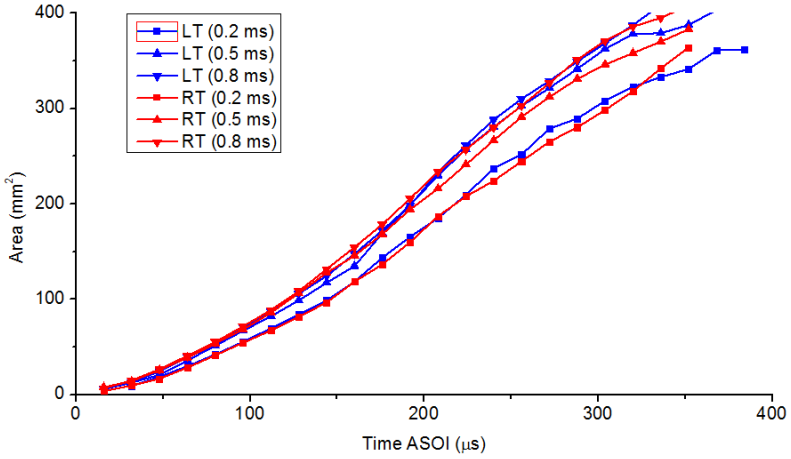

Figure 6-26 Area comparison of the 1st injection between RT and LT under high P_{inj}

The penetration similarly shows comparable values under LT and RT for various cases with a host of dwells except the one with 0.5 ms under RT (Figure 6-27). This suggests that the influences of fuel properties on penetration can be effectively dampened by the rise of injection pressure and the reduction of back pressure. The higher penetration at the later spray stage for the 0.5 ms dwell case under RT may be attributed to the electric-magnetic characteristics which may lead to earlier injector opening.

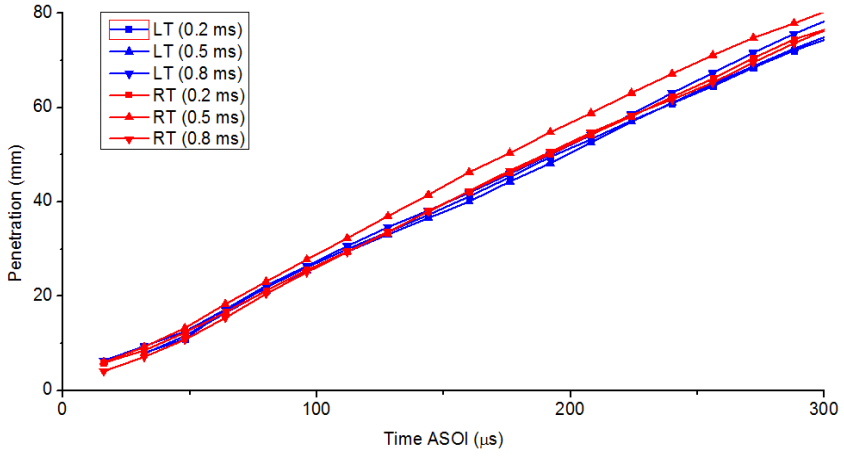

Figure 6-27 Penetration comparison of the 1st injection between RT and LT under high P_{inj}

2) Spray characteristics of the second split injection

As presented in Figure 6-28 the second split injection tends to show larger fuel area variation when compared with the first split injection under the same injection pressure, but relatively smaller variation when compared with the second ones under low injection pressure (60 MP). Under high injection pressure, as mentioned before, the interaction between split injections is considerably enhanced by collision, wake driving force and air driving force. Under LT, the raised viscosity retards the injector opening and stops the injection quicker (as seen from the MFR graph), effectively weakening the degree of interaction between split injections. Consequently, the fuel area variation is smaller under LT when dwell changes. More importantly, the reduction of back pressure can further significantly weaken the interaction between split injections.

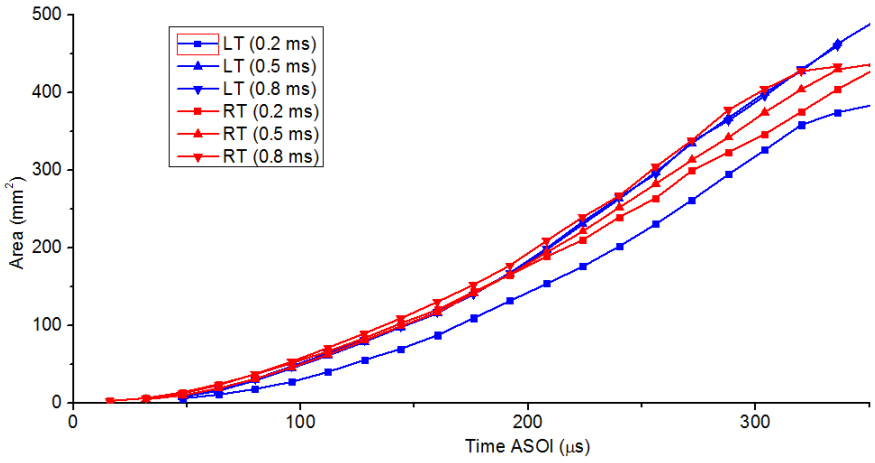

Figure 6-28 Area comparison of the 2nd injection between RT and LT under high P_{inj} with split injection

The plume under LT again penetrates slightly slower except the case of 0.2 ms dwell due to slightly lower initial velocity (Figure 6-29). When the dwell is set to 0.2 ms, the collision under LT is expected to be weaker than that under RT, and the wake and air driving forces are assumed to be comparable.

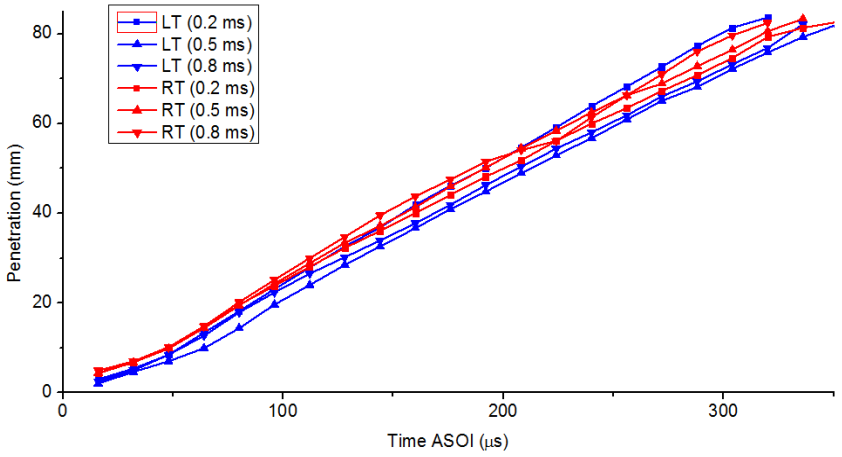

Figure 6-29 Penetration comparison of the 2nd injection between RT and LT under high P_{inj}

6.5 Conclusion and summary

Macroscopic characteristics were studied in this chapter. The effects of low fuel temperature were also investigated.

(1) Four stages, namely, a linear stage, an accelerating stage and two consecutive linear stages with different slopes are expected for the development of penetration. The existence of the four stages greatly depends on the back pressure and injection pressure.

(2) The transient characteristic of the first split injection leads to the asymmetry of the spray morphology, while the earlier start of injection of the second split injection causes more symmetric morphology. The "wake driving force" caused by the higher speed of wake than that of periphery gas tends to distort the second split injection because of the transient characteristics, whereas the air driving force caused by the first split injection tends to make the second plume symmetric by pushing the fuel at the periphery forward.

(2) Injection pressure, dwell interval and back pressure strongly affect the interaction between split injections. Generally, high injection and back pressures and short dwell lead

to strong interaction

(3) The second split injection tends to show smaller observed spray area and slower penetration during the early stage due to the primary collision. However, obviously larger spray area and higher penetration at the later stage are found due to ‘wake driving force’ and ‘air driving force’.

(4) Longer the first injection duration causes larger spray area than that with shorter the first injection duration. More injected fuel and better dispersion due to larger injector opening tend to be responsible.

(5) With single injection strategy, LT results in smaller spray area and slower penetration than that under RT due to less injected fuel and poorer dispersion under LT.

(6) Under low injection pressure, split-injection is severely affected by LT. Split injection under LT shows much lower spray area and slower penetration than those under RT. When injection pressure is raised, the differences are effectively narrowed.

Chapter 7 **Microscopic characteristics of spray**

7.1 Introduction

The size and velocity of droplets can be employed to denote the atomization quality. The evaporation of spray greatly depends on droplet size. The radial and axial distributions of droplet size and droplet velocity have been widely studied. The tip of spray presents the smallest droplets because of strong air interaction, while the tale shows the largest drops resulted from low velocity [49, 90, 138]. The coalescence and collision of droplets at the further positions along the plume lead to an increase of SMD [49, 52, 139].

The impact of injection pressure, back pressure, ambient temperature has also been widely studied. It is well known that enhanced atomization under high injection and ambient pressures leads to smaller SMD [40, 139]. This is because the effects of raised back pressure in terms of boosting the break up outbalance the effects of coalescence. The increase of back pressure significantly narrows the velocity difference between the head and the tail as all the droplets are decelerated [139]. Many studies also show that high viscosity and surface tension cause large SMD [40].

It was reported that the influences of ambient temperature on SMD under low injection pressure outstrip those under high injection pressure. When the ambient temperature is raised, the influences of injection pressure seem to be weak. The evaporation of small droplets causes the existence of the large droplets, thus detection of higher SMD [140].

However, the microscopic spray characteristics when split injection strategy is employed are still not sufficiently studied. In addition, the influence of reduced fuel temperature is still unknown, especially when multiple injection strategy is used.

7.2 Test conditions

To study the spray characteristics of single and split injection strategies under room temperature, the injection pressure varied from 60 to 120 MPa while the back pressure was set to atmospheric condition. The injection durations are shown in Table 7-1. To study the influence of fuel temperature, the injection pressure was set to 60 and 90 MPa and the back pressure was set to atmospheric condition. The corresponding injection durations are shown in Table 7-1(blue color). The measuring position significantly affects the droplet velocity, size and data rate. In this study, the measuring positions are located along the plume axis. Data were acquired for 240 injections or 20,000 validated particles detected.

Table 7-1 Test matrix for macroscopic characteristics

	Single	2-split	3-split
Injection duration (ms)	1	0.5 + 0.5	0.5 + 0.5 + 0.5
Dwell (ms)	----	0.2, 0.3, 0.5, 0.8	0.2, 0.3, 0.5, 0.8

7.3 Microscopic characteristics under room temperature

7.3.1 Microscopic characteristics with single injection

(1) Spray structure

The distributions of the captured droplets with a wide range of velocities at various positions under 60 and 120 MPa are illustrated in Figures 7-1 and 7-2. The mean velocity of the droplets at 20 mm under 60 MPa injection pressure is also presented. All cases at different positions show the same structure as shown in Figure 7-1 although some differences are observed. The arrival time includes the injection delay and the time for the spray to travel from the injector tip to the measuring positions [50, 85]. The time point when a drastic velocity reduction is seen divides the spray into head and tail [50, 139]. Only a small number of droplets were captured for the head while a large number of droplets were obtained for the tale.

One-droplet principle of PDPA causes the failure of detection when more than one droplets are in the measuring volume. The simultaneous existence of several droplets in the measuring volume due to high density or the existence of unbroken liquid jet can cause this failure. A blank area ensues when this failure appears, and this generally takes place near the nozzle, 20 and 30 mm [26, 85, 141]. The increase of injection pressure contributes to the increase of the distance of the positions far from the injector where the blank area still exists. In addition, high velocity for droplets is expected for diesel spray due to the hydraulic force.

Strong air resistance distorts the droplets into ellipsoids, consequently, the software of PDPA rejects these non-spheroids.

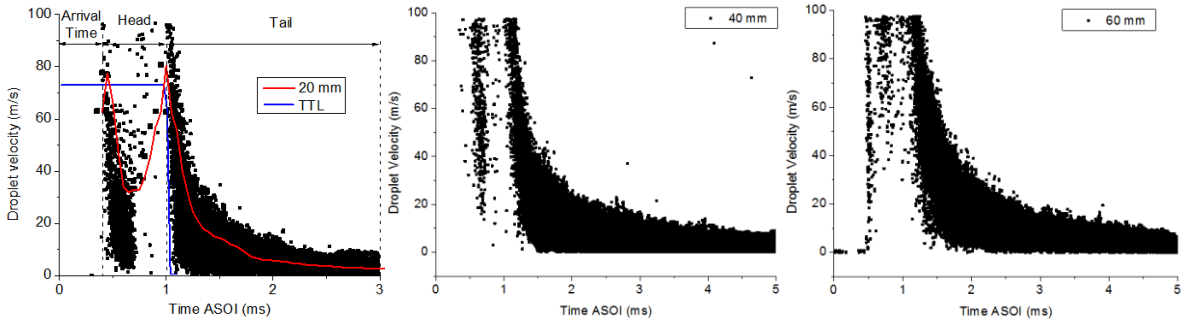

20 mm 40 mm 60mm

Figure 7-1 Droplet axial velocity at various positions under 60 MPa P_{inj}

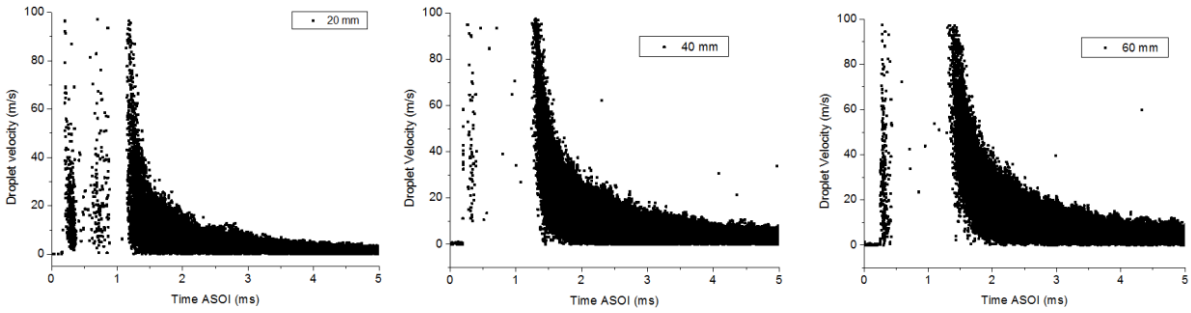

20 mm 40 mm 60 mm

Figure 7-2 Droplet axial velocity at various positions under 120 MPa P_{inj}

(2) Mean velocity

The axial mean velocity distributions along the plume axis for both 60 and 120 MPa cases are shown in Figure 7-3 and 7-4. Low injection pressure case and high injection case show similar varying trend except that no head is observed under high injection pressure. Specifically, low injection pressure leads to appearance of “head” where a “velocity dip” is

observed, while high injection pressure fails to show this phenomenon. The positions further from the injector tip tend to show smaller velocity "dip" and present lower varying rate of velocity with the elapse of time. Higher injection pressure entails higher velocity for droplets and higher air resistance, thus severer deformation. Except for the aerodynamic shearing force, the coalescence is another reason for the appearance of non-spherical ellipsoids. More importantly, higher injection pressure causes better dispersion, and more small particles are expected. The larger number of droplets increase the chances of the existence of droplets in the measuring volume [139]. These factors lead to the failure of the detection of the droplets for the head under high injection pressure.

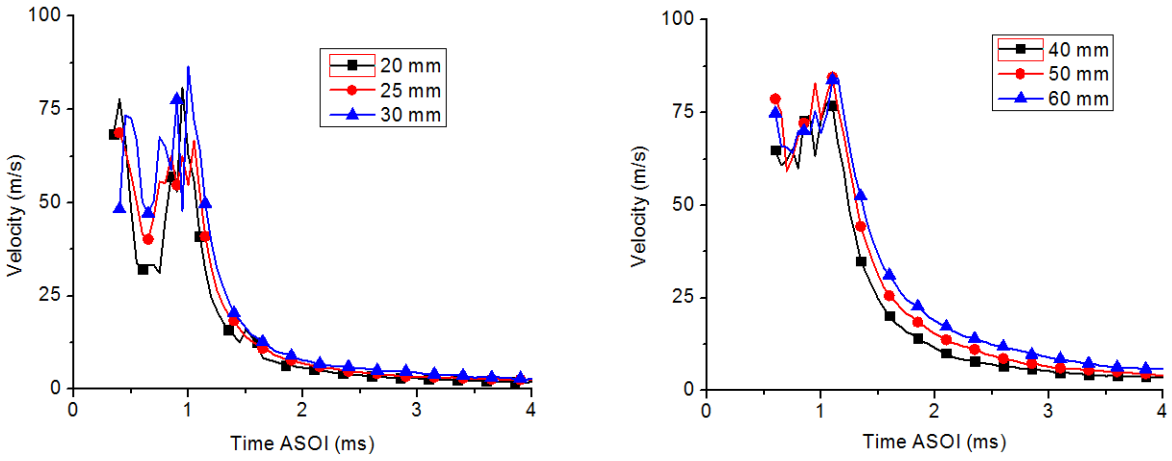

(a) (b)

Figure 7-3 Mean velocity at various axial positions under 60 MPa P_{inj}

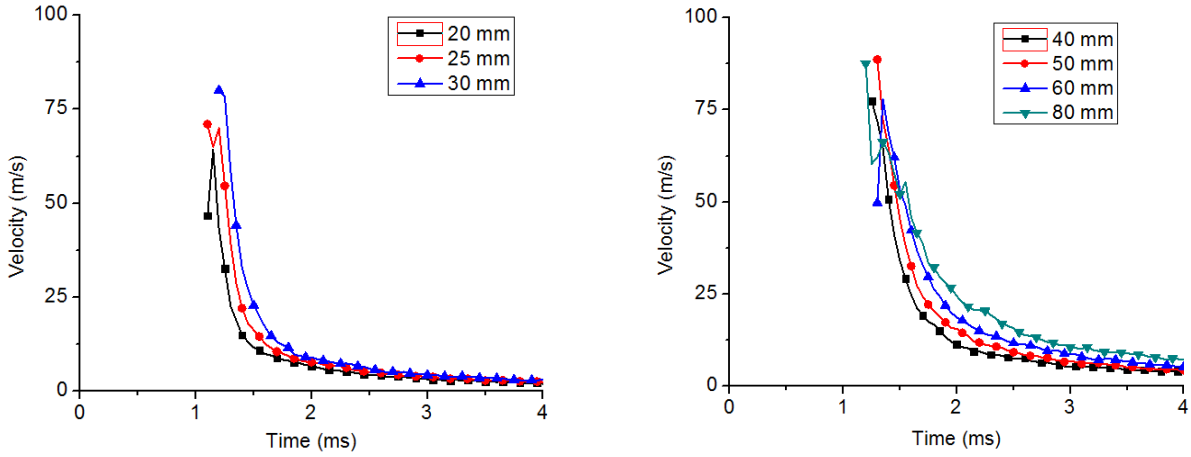

Figure 7-4 Mean velocity at various axial positions under 120 MPa P_{inj}

It is noteworthy that the further positions show higher velocities. For 60 MPa case, the velocity difference between positions is small whereas that for 120 MPa is quite obvious. This can be attributed to the progressively pushing effect of the coming fuel. The fast movement of initial droplets accelerates the ambient gas by momentum transfer, resulting in the deceleration of the initial droplets. Slightly lower air resistance for the coming droplets is expected. The coming droplets with a slightly higher velocity due to reduced air resistance catch up and outstrip the decelerated ones. The repetition of this process causes the consistent reduction of air resistance along the plume axis, thus the consistent increase of velocity of the plume tip if the injection still continues [139].

(3) Particle size

As presented in Figure 7-5, the droplet size is dominated by the injection pressure. The rise of injection pressure drastically decreases the SMD [85]. Higher droplet inertia under higher injection pressure increases the air drag force thus reducing the stability, meaning better dispersion. Overall, the droplets show an apparent size reduction then present an

increase along the plume axis under a wide range of injection pressures. The secondary breakup is supposed to cause the initial size reduction, while the rise of size can be attributed to the coalescence due to droplet collision [49, 52, 139]. It should be noted that the position where the smallest droplets are obtained is further downward as the injection pressure rises. The higher inertial energy enables the droplets to breakup for "longer duration" (in terms of penetration length).

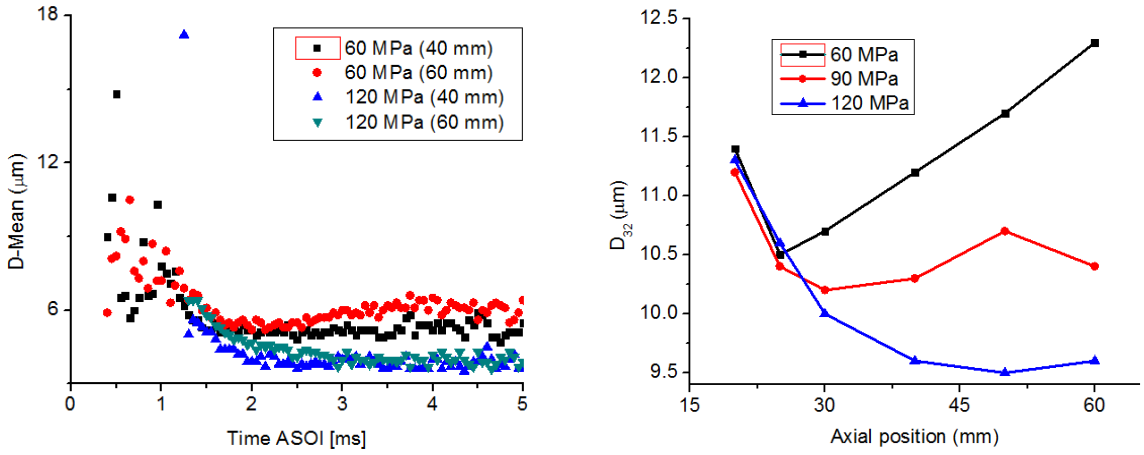

(a) (b)

Figure 7-5 Droplet diameter under various injection pressures with single injection

7.3.2 **Microscopic characteristics for two-split injection**

(1) Spray structure

The spray structure when split injection strategy is employed is very different from that of single injection, as shown in Figure 7-6 for 2-split injection. The first split injection just show the dramatic decrease phase without the tail which is overtaken by the second split injection. For 2-split injection, the blank area is still observed between the first and second

split injections at the positions close to the injector. The increase of distance from the injector tip enables more droplets to be detected and the blank area to be decreased. The increase of dwell is very important for the detection of the droplets belonging to the first injection, leading to the detection of more droplets with low velocity.

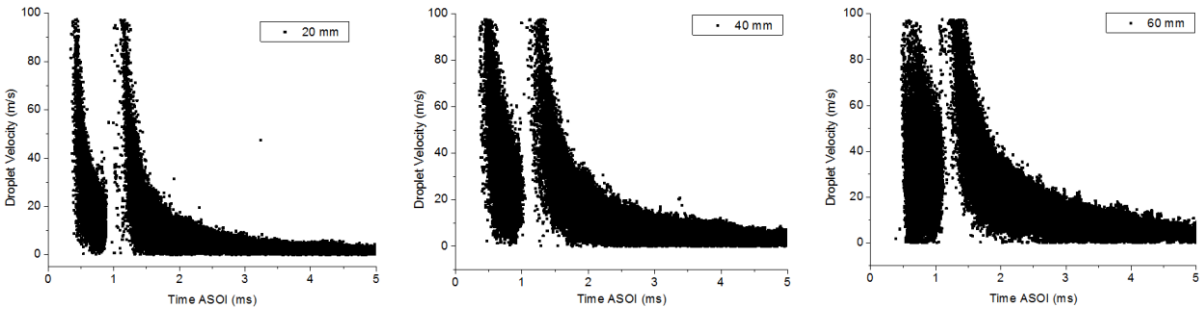

a (2-split with 0.2 ms dwell)

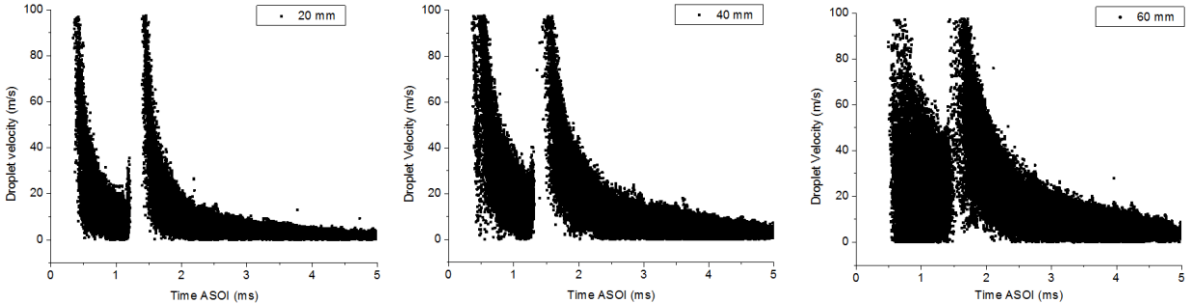

b (2-split with 0.5 ms dwell)

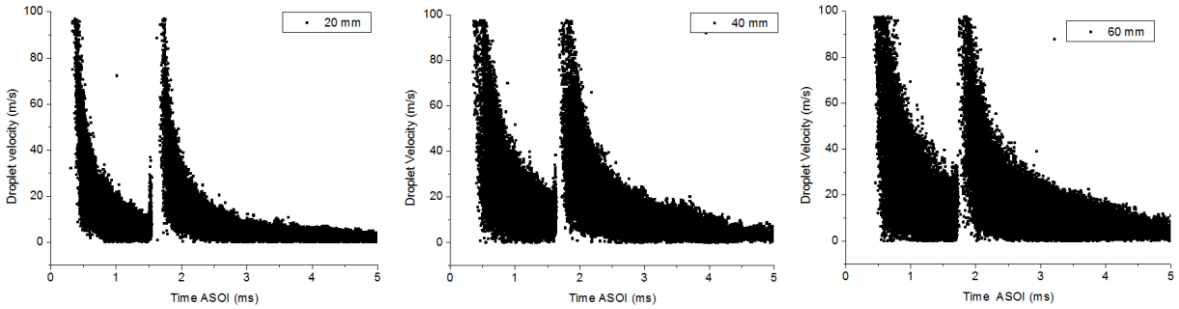

c (2-split with 0.8 ms dwell)

Figure 7-6 Droplet axial velocity of 2-split injection at various positions under 60 MPa

(2) Mean velocity

The mean velocities for 0.5~0.5 ms injection with various injection dwells under 60 MPa are shown in Figure 7-7, while these under 90 MPa injection pressure are shown in Figure 7-8. Apparently, almost all curves under 60 MPa show a similar trend, namely, the mean velocity decreases drastically and then shots to a certain point before showing a dramatic reduction. The two decreasing phases denote the end of the two injection events. Generally, the second split injection presents lower peak velocity than the first one. The duration of the second injection with high mean velocity increases with the reduction of dwell. It is likely that short dwell results in longer injector opening for the second injection, thereby more injected fuel with higher velocity.

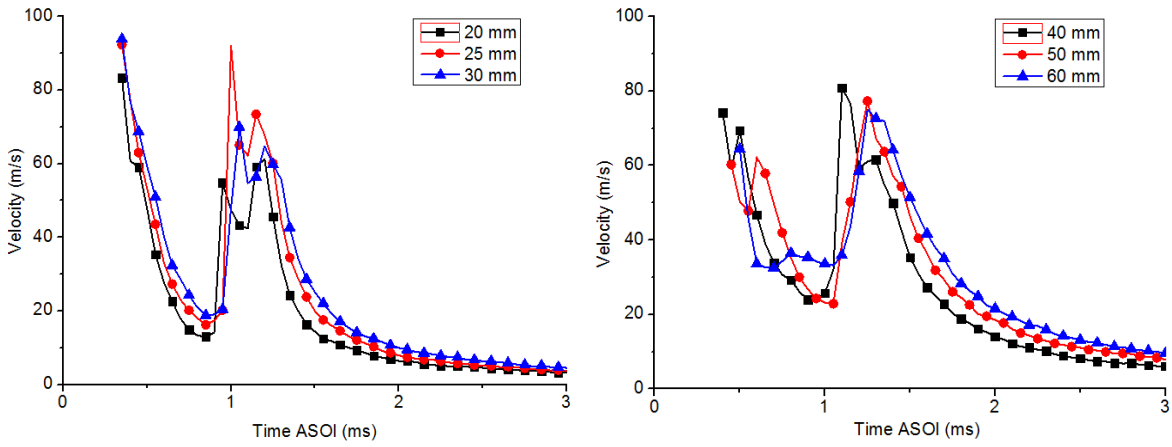

a (0.2 ms dwell)

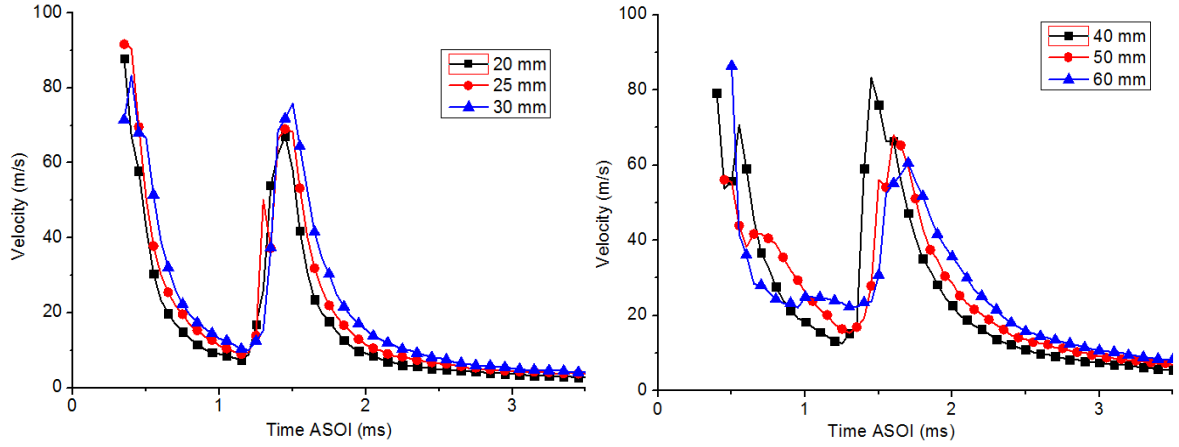

b (0.5 ms dwell)

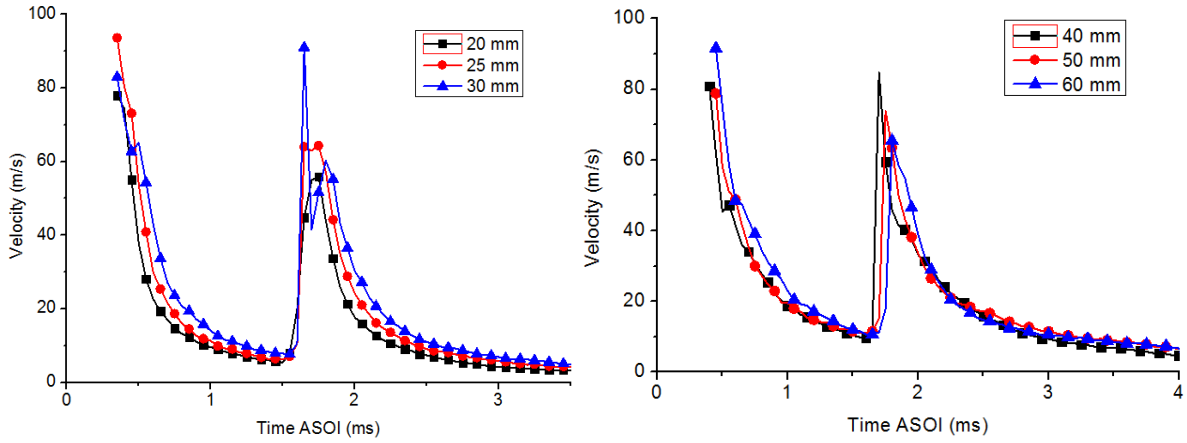

c (0.8ms dwell)

Figure 7-7 Mean velocity at various positions with different dwells under 60 MPa

When injection pressure is elevated to 90 MPa, the injection event for the second split at all tested positions with short dwell are not very clear compared with the ones under 60 MPa. The higher initial momentum and velocity (thus high droplet density and severer deformation) under higher injection pressure should be partly responsible.

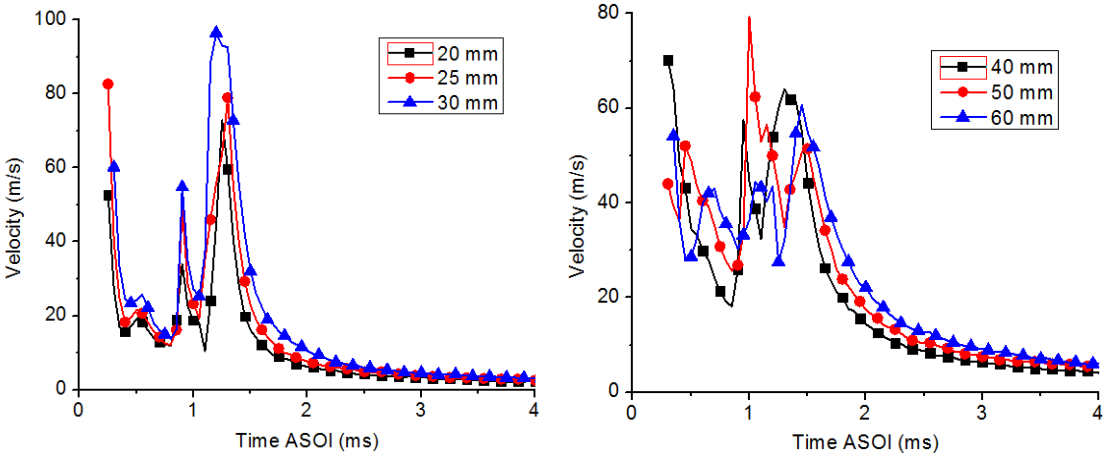

a (0.2 ms dwell)

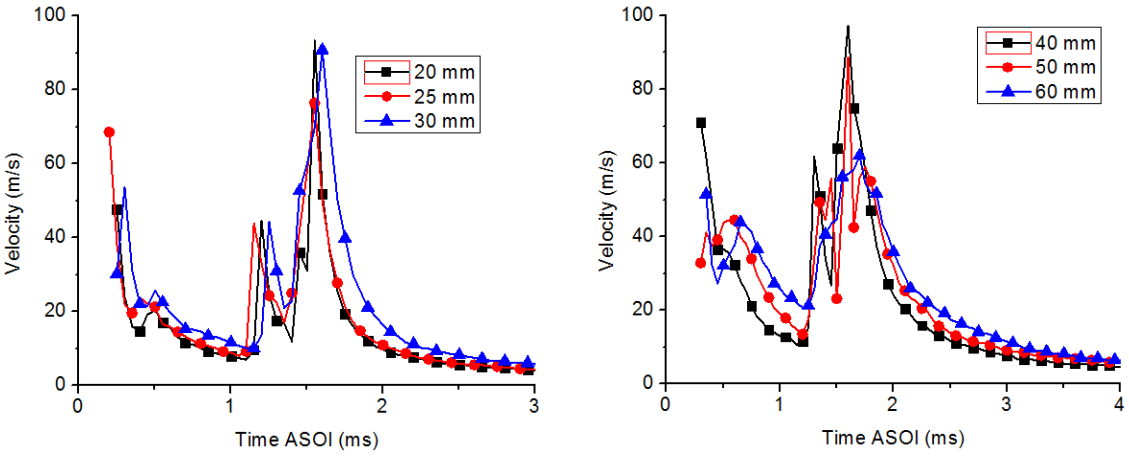

b (0.5 ms dwell)

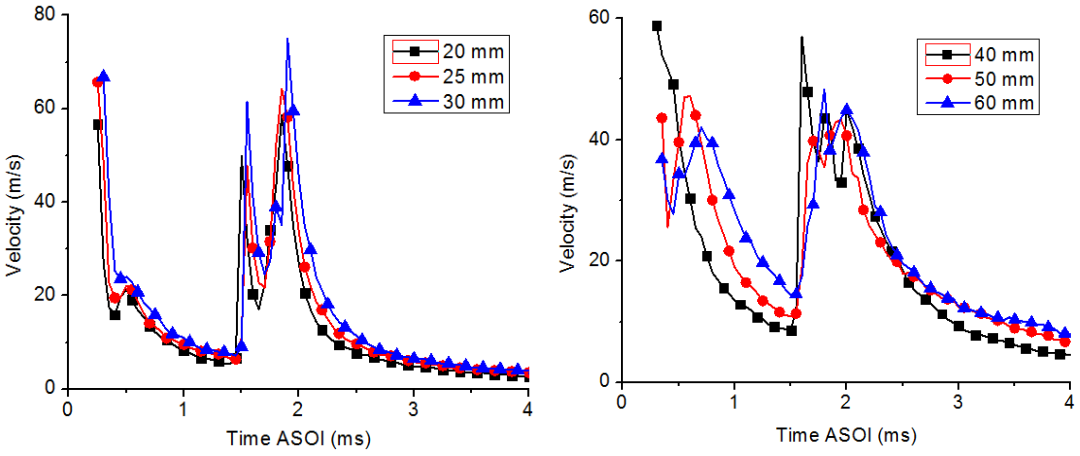

c (0.8 ms dwell)

Figure 7-8 Mean velocity at various positions with different dwells under 90 MPa

Besides, it is worth noting that droplet velocities when the second splits arrive (this is called “Valley velocity” and this term is used for the rest of the thesis) rise along the spray. The valley velocity is quite useful as it can denote the coalescence degree. This is because higher valley velocity shows more particles chased by the following ones. It is also interesting to find that longer injection dwell leads to lower valley velocity, therefore, lower coalescence degree. This is reasonable as more time is given to the first split to disperse before the arrival of the second.

(3) Influence of dwell

The mean velocity comparison among the cases with different dwells under 60 and 90 MPa fuel pressure is carried out to outline the effects of dwell, presented in Figure 7-9 and Figure 7-10 respectively. According to the graphs, the injection interval has insignificant effects on the velocity of first split but significant influence on the second split at both 20 and 60 mm points. Under 60 MPa injection pressure , the 0.5 ms dwell case at 20 mm shows the highest peak velocity for the second split, while the 0.2 ms dwell case at 60 mm presents the highest peak velocity for the second split.

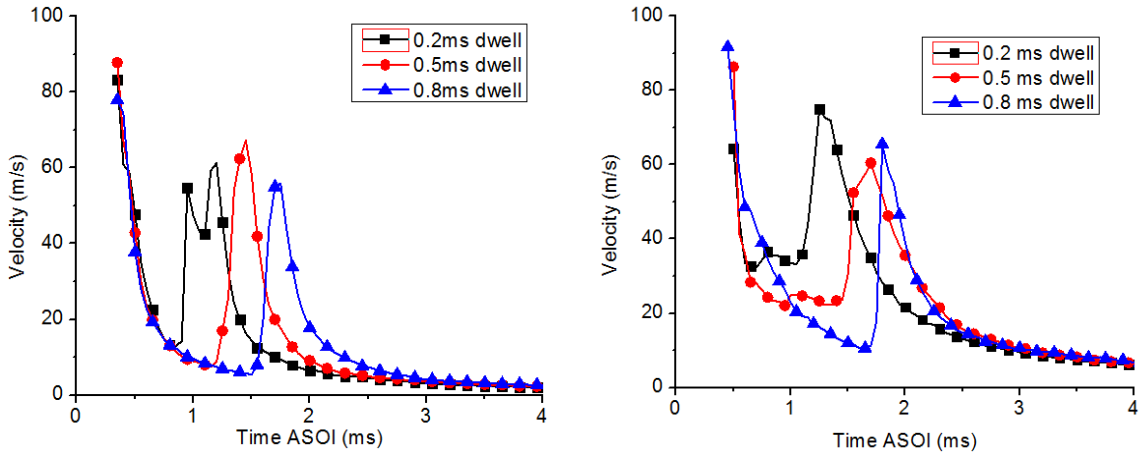

a (20 mm) b (60 mm)

Figure 7-9 Mean velocity comparison for 2-split with various dwells under 60 MPa

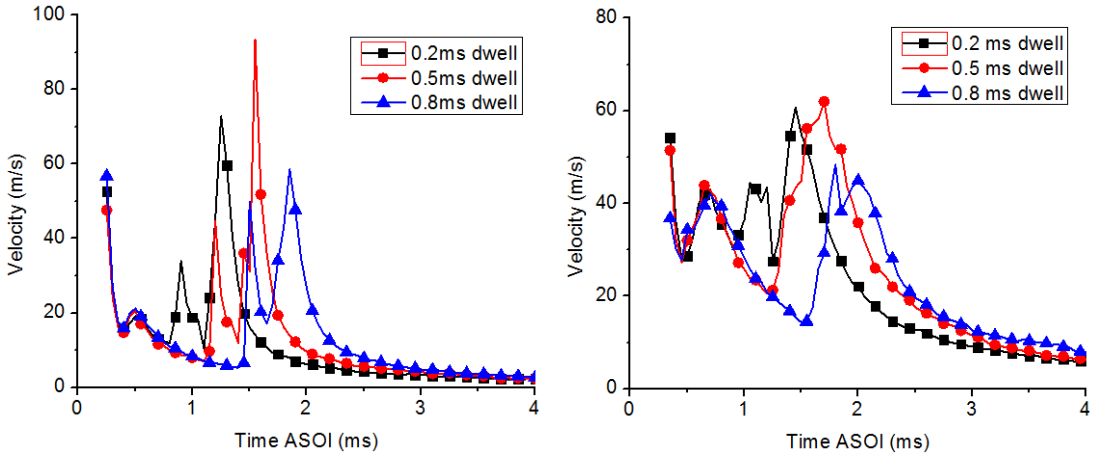

a (20mm) b (60 mm)

Figure 7-10 Mean velocity comparison for 2-split with various dwells under 90 MPa

However, under 90 MPa injection pressure, the 0.5 ms dwell case shows observably higher peak velocities than the case with 0.2 ms interval, especially at 20 mm. Due to the air flow induced by the first split, the second ones show higher penetrating speed. The increase of dwell weakens this accelerating effect, and if the dwell is too long the splits actually become single ones. On the other hand, too short interval leads to strong collision and coalescence. This means that a time point where the second split shows the highest peak

velocity tends to exist. At the same time, the influence of injection dwell on the injected fuel mass needs to be considered. According to aforementioned injection tests (Figure 6-26), the occurrence of the least spray area happens with dwell being 0.2ms, while the 0.3 and 0.5 ms dwell cases present obviously larger spray area (possibly more injected fuel mass). Therefore, the velocity of the particles is controlled by the two effects. The second split injection with 0.5 ms dwell gets stronger accelerating effect induced by the ambient gas. Meanwhile, it tends to show higher velocity due to more fuel mass that can continuously push the air outward and forward.

(4) Valley velocity

As mentioned before, the valley velocity is very interesting and quite important to study the influence of injection interval on the coalescence, as presented in Figure 7-11. It is seen that shorter dwell contributes to higher valley velocity under all injection pressures due to insufficient time for the first split to disperse and evaporate. With low injection pressure (60 MPa), the valley velocity rises and then decreases gradually along the plume axis when dwell is long. This means that higher proportion of fuel of the first split is chased up by the second one at around 40 mm downwards the injector tip. When dwell is short, the strong collision causes an increasing trend for the rise of valley velocity along the plume. By contrast, when pressure is raised to 90 MPa, the valley velocity rises gradually alone the plume. This is because higher injection pressure enables the particles of the first split injection to move faster and further when they are caught up by the second one.

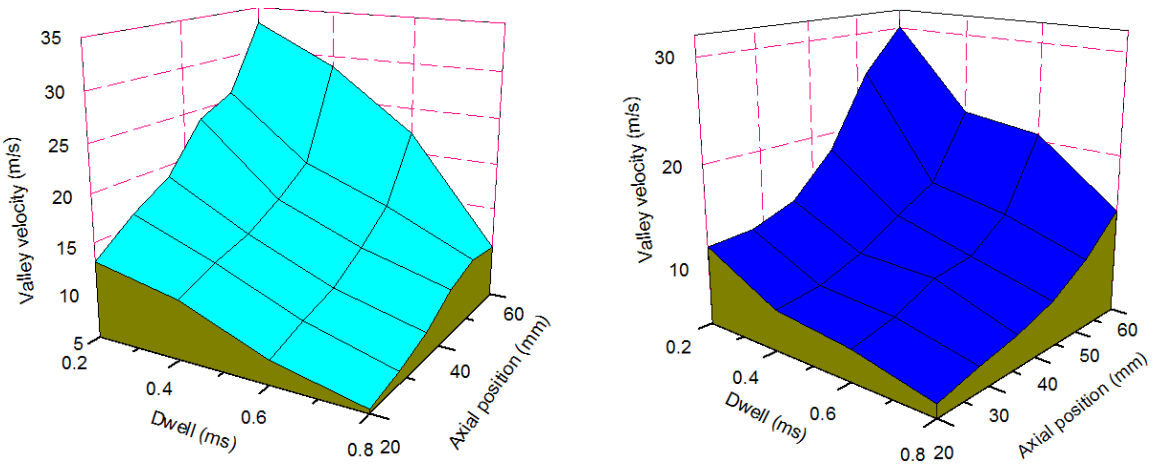

a (60 Mpa) b (90 MPa)

Figure 7-11 Valley velocity under (a) low and (b) high injection pressures with various dwells

(5) Droplet diameter

The droplet diameter against time for split injection is different from that of single injection, as seen for an example in Figure 7-12. Similar varying trend of diameter to that of velocity, namely, two peaks followed by a reduction, is observed for all cases. The diameter for split injection therefore is expected to be different from that of single injection.

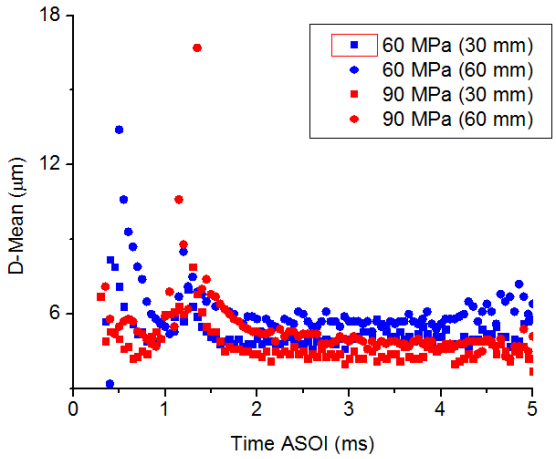

Figure 7-12 Droplet diameter for 2-split injection (0.2 ms dwell)

The D_{32} along the plume axis with various injection intervals under a wide range of injection pressures are presented in Figure 7-13. The injection event with 0 ms dwell means single injection. It is worth noting that all cases with split injection strategy show higher SMD than the single ones. The strong collision between splits which does not occur with single injection strategy should be responsible. More importantly, the higher effective injection pressure for single injection strategy due to fully injector opening leads to better dispersion and smaller SMD.

It is also interesting to find that the cases with 0.4 or 0.5 ms interval show smaller SMD among the split injections. Lower fuel mass for the split with dwell be around 0.5 ms probably leads to shorter penetration and less collision and coalescence. This understandably causes smaller SMD. Too short dwell (0.2 and 0.3 ms interval) or too long interval (0.8 ms) contributes to clearly larger particles, especially under low injection pressure.

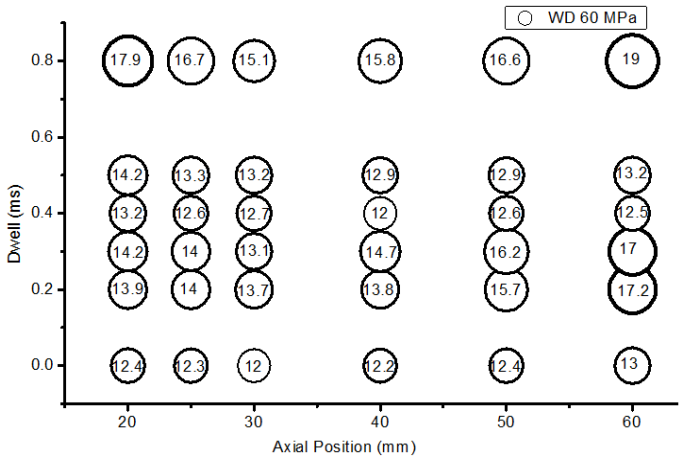

a

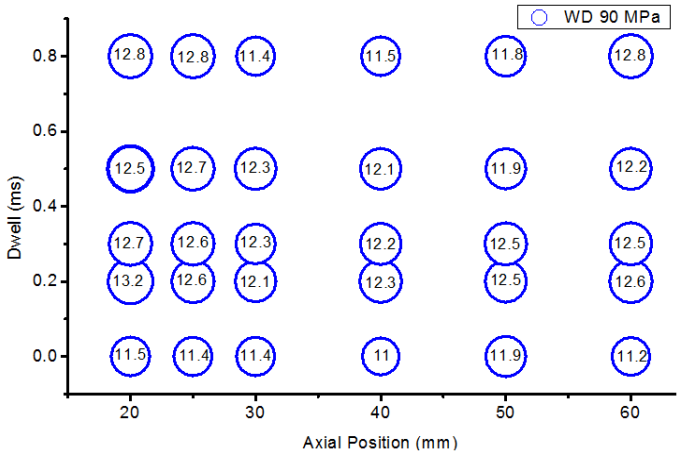

b

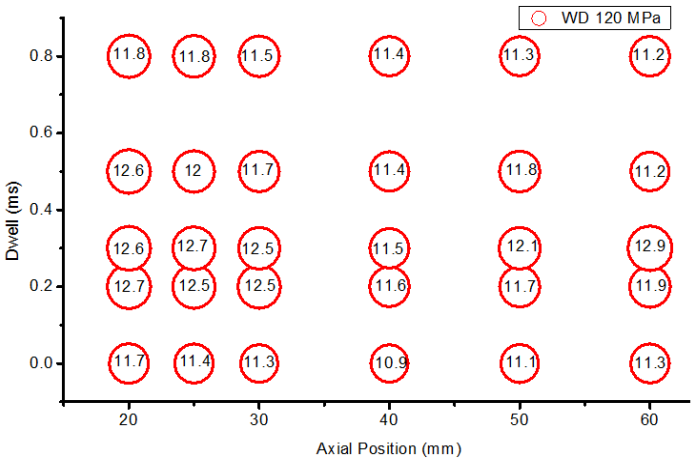

c

Figure 7-13 SMD with split injection under various injection pressures

The influence of injection pressure on SMD is very profound. High injection pressure can effectively bridge the SMD difference between single and split injection strategies. Low injection pressure (60 MPa) leads to much larger droplets with low velocity, and these droplet are quite stable. Higher pressure leads to much quicker injector opening and much higher effective injection pressure. Apart from that, strong cavitation which enables the spray to disperse better and evaporate quickly is more likely to occur under high injection pressure.

Along the plume axis, the SMD tends to show an overall decrease at 30 or 40 mm and then rises. That is to say SMD is relatively lower (not the lowest) for all cases, especially for the injection events with 60 MPa injection pressure. It can be concluded that the secondary breakup may finish at 30 to 40 mm downstream of the injector for split injection in this study.

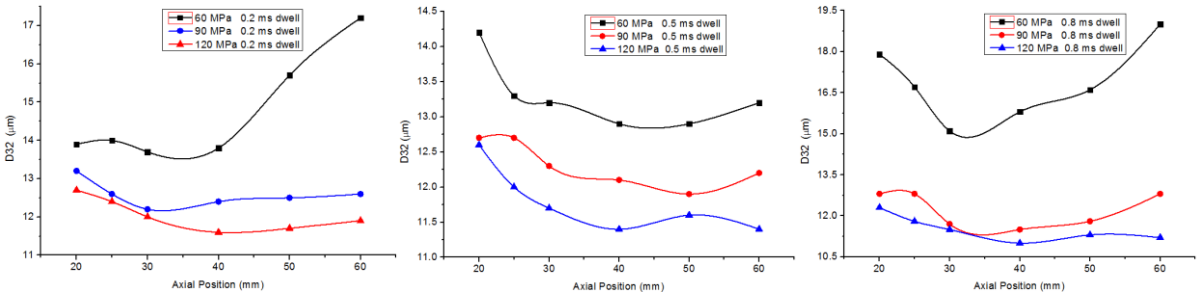

a b c

Figure 7-14 SMD at different positions with various dwells

7.3.3 **Microscopic characteristics with three-split injection**

(1) Spray structure

Compared with 2-split injection, 3-split injection tends to strengthen the interaction between split injections although similar spray structure is observed (Figure 7-15). The blank area disappears and the boundary between split injections becomes obscure and difficult to distinguish. The disappearance of the blank area suggests less deformation of the droplets or lower droplet density (less droplets in the measuring volume). The increase of dwell leads to clearer boundary between split injections while the rise of the distance from the injector obscures the boundary.

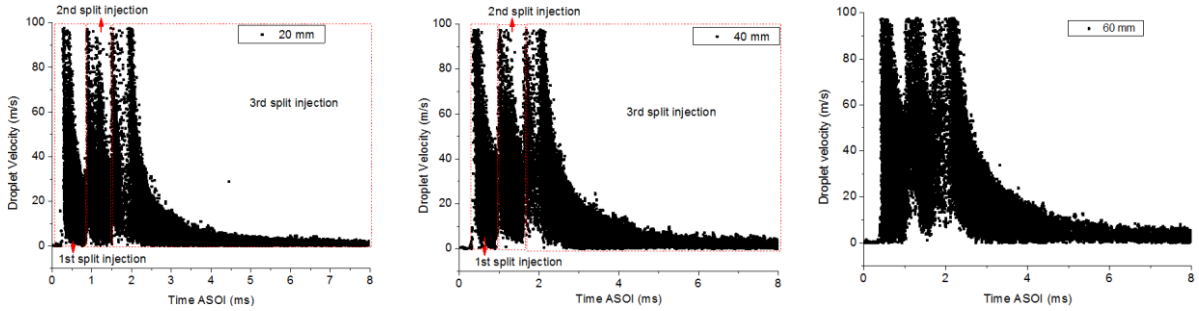

a (3-split with 0.2 ms dwell)

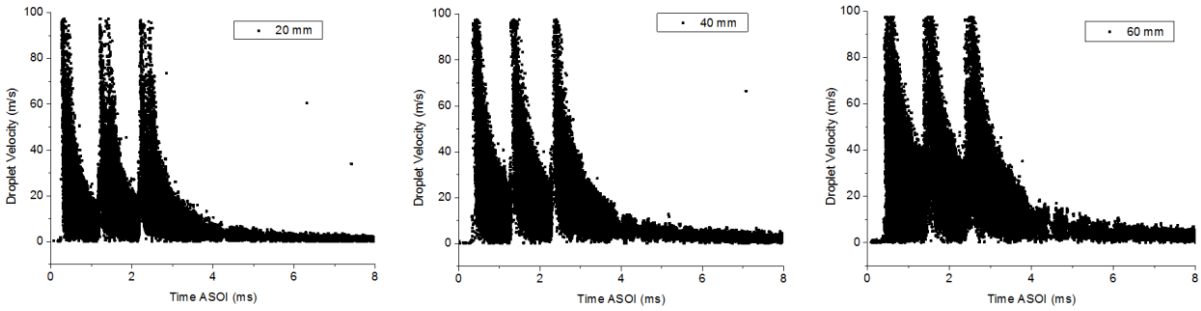

b (3-split with 0.5 ms dwell)

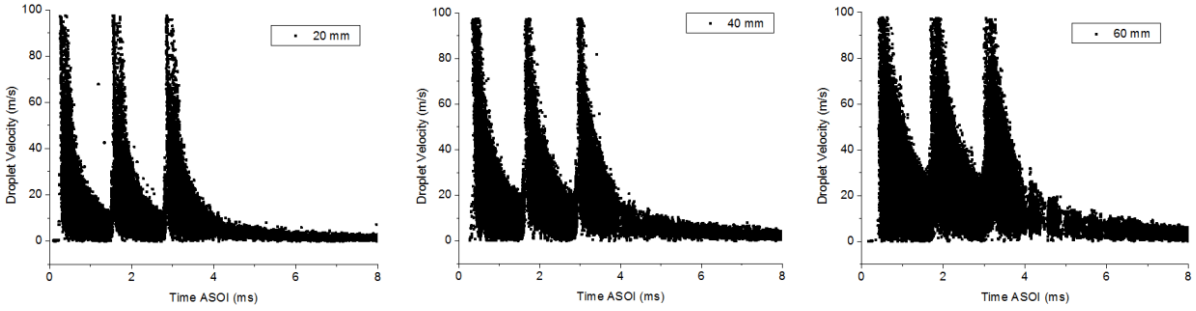

c (3-split with 0.8 ms dwell)

Figure 7-15 Droplet axial velocity of 3-split injection at various positions under 60 MPa

(2) Mean velocity

The increase of the number of split injections is thought to strengthen the interaction. When the dwell is short and injection pressure is high, split injection becomes single injection

and the plume is very dense. The injection pressure in this section was therefore set to 60 MPa.

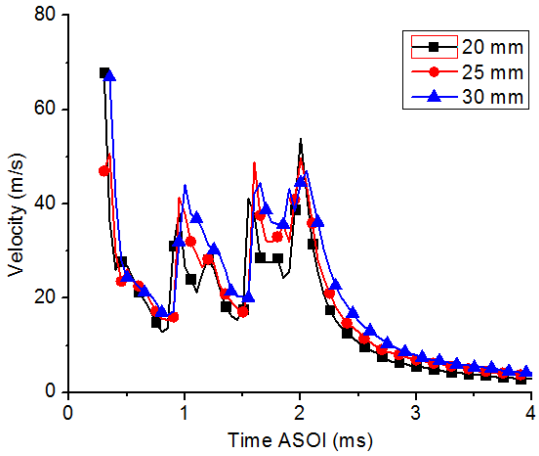

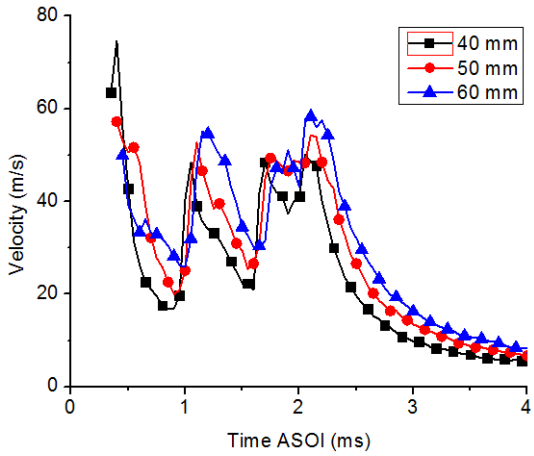

a (3-split with 0.2 ms dwell)

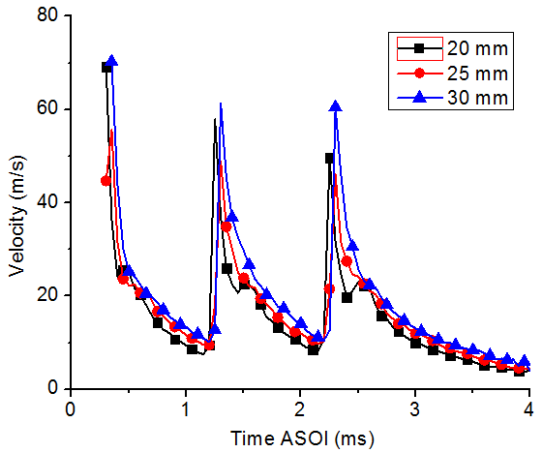

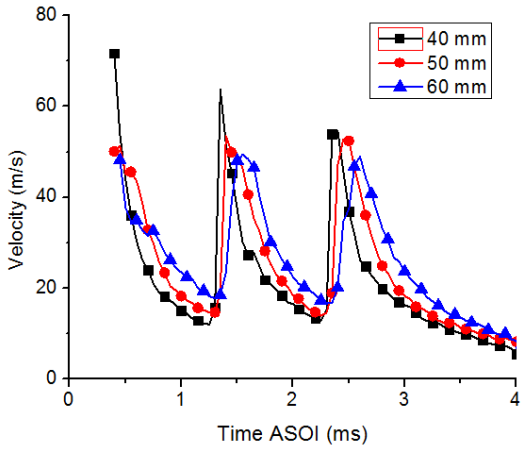

b (3-split with 0.5 ms dwell)

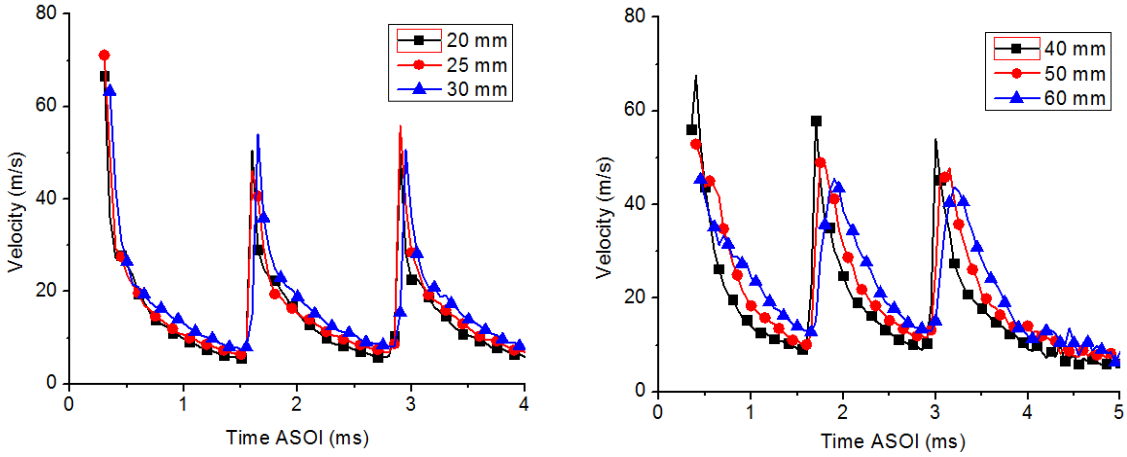

c (3-split with 0.8 ms dwell)

Figure 7-16 Mean velocity comparison for 3-split with various dwells under 60 MPa

The microscopic spray characteristics are also quite distinctive compared with 2-split injection, as shown in Figure 7-16. For short dwell (0.2 ms) case, the boundaries between split injections are quite obscure although distinguishable. The strong interaction through collision leads to the increase of the contact area between split injections. This means numerous droplets are chased up by the coming injection when their velocities are still high. When dwell is longer than 0.5 ms, 3 obvious peaks at all tested positions are observed. It is interesting that the second valley velocity is clearly higher than the first one, meaning that more fuel for the second split is chased up by the third split than that of first split by the second one. The rise of injection dwell leads to smaller valley velocity difference between the two valleys as the interaction is weakened.

It is noteworthy that, for short dwell case, the second split injection tends to show the lowest peak velocity at all measuring positions. By contrast, for long dwell cases, a gradual reduction of peak velocity with the rise of sequence of injections is observed, especially far

from the injector tip. These results contradict to the results of the penetration development. This is assumed to be caused by the strong collision and coalescence, leading to the formation of large droplets and reduction of the velocities of the droplets that are detectable. The split injections tend to be more interactive and the following split injections tend to chase up the former ones with higher speed, leading to higher deceleration for the following splits. Consequently, later splits show lower peak velocity. High droplet density is also thought to be responsible for this contradiction.

(3) Droplet size

The particle mean diameters under 60 and 120 MPa injection pressure with a wide range of dwells are shown in Figure 7-17. Similar to 2-split injection, the 3-split injection contributes to higher SMD than the single injection strategy. The collision and coalescence once again are thought to be the main reasons for the higher diameter. Similar overall distributing profile along the plume axis to that of single injection, namely decreasing and then increasing along the plume, can be observed.

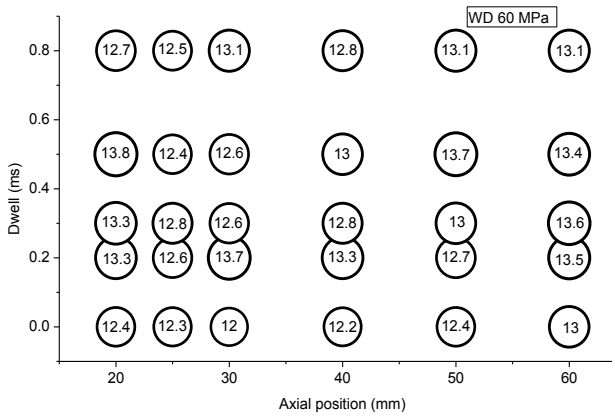

a

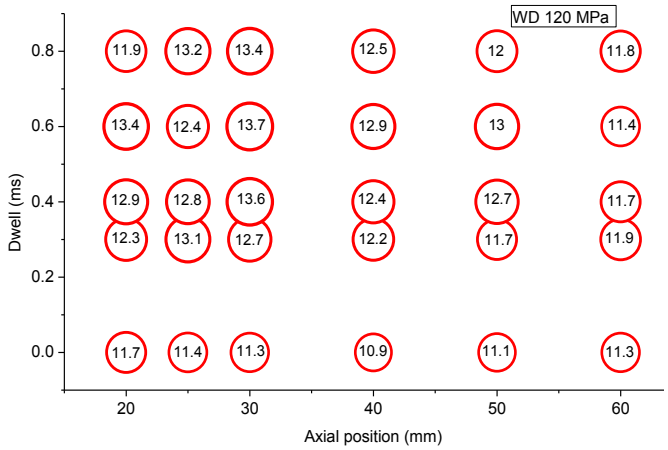

b

Figure 7-17 SMD of 3-split under (a) low and (b) high injection pressures under various dwells

The SMD comparison between 2-split (Figure 7-13) and 3-split (Figure 7-17) under different conditions can outline the influence of increased number of split injections. When injection pressure is low, the 2-split injection strategy with short dwell (0.2, 0.3 and 0.5 ms) leads to higher SMD than the 3-split injection strategy, however, when dwell rises to 0.8 ms, both strategies present similar SMD. The increase of the number of split injections strengthens the interaction between injections. The injector opening of the third split injection is thought to be further shortened when the dwell is short. The shorter injector opening means less throttling effect and higher effective injection pressure, thus expected better secondary breakup and dispersion, therefore smaller SMD is expected for 3-split injection compared with 2-split injection.

It should also be kept in mind that the increase of the number of the split injections leads to stronger collision and coalescence. From this perspective, 3-split injection is expected to show larger droplets than 2-split injection. The actual results suggest that the influence of

the rise of effective injection pressure outbalances the countering influence of collision and coalescence.

For high injection pressure case, the 3-split injection tends to present slightly larger droplets than 2-split injection when dwell varies from 0.4 to 0.6 ms. High injection pressure leads to much quicker injector opening and the influence of throttling effect can be ignored. In this case, the influence of collision and coalescence is assumed to be important. The stronger collision and coalescence for 3-split injection result in larger droplets.

7.4 Influence of temperature

7.4.1 Single injection

(1) Mean droplet velocity

Under low injection pressure (60 MPa), droplets at 20 mm show slightly higher velocity under LT than under RT, while droplets at 60 mm under RT show slightly higher velocity than under LT, as shown in Figure 7-18 (a). However, high injection pressure (90 MPa) surprisingly leads to obviously higher droplet velocity under LT than under RT at all positions along the plume axis (Figure 7-18 (b)). RT is expected to show higher penetration velocity and droplet velocity due to lower fuel viscous force. There are three assumed reasons for the higher velocity under LT. Higher viscosity and surface tension under LT boost the stability of the droplets, and droplets tend to present higher velocity due to poorer breakup and less reduced momentum transferred to the ambient gas, especially at positions further from the

injector tip. Another possibility is that the higher surface tension under LT enables droplets to retain spherical shape, whereas droplets with higher velocity and lower surface tension under RT fail to keep the spherical shape due to the strong gas resistance. PDPA fails to detect the deformed droplets with high velocity. In addition, the poorer breakup under LT leads to lower droplet density, and this increases the possibility for the droplets to be detected nearer to the nozzle where the velocity of droplets is high.

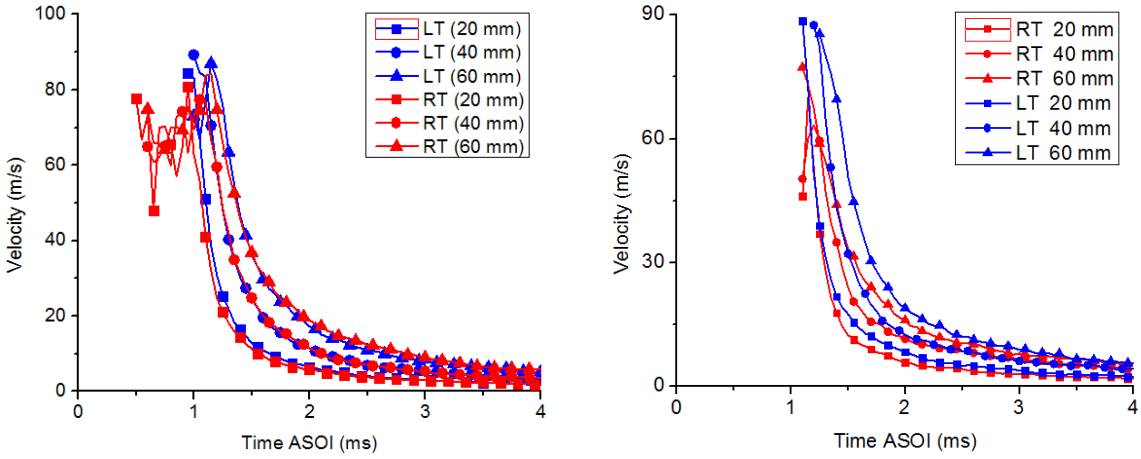

a b

Figure 7-18 Droplet velocity for RT and LT with single injection under (a) low and (b) high pressure

(2) Particle size

The cases under LT present apparently larger droplets than those under RT (Figure 7-19). Higher surface tension which can considerably reduce the possibility of breakup is likely to be responsible. In addition, higher viscosity results in larger energy loss when fuel flows through the nozzle hole. The resultant lower initial droplet velocity is another reason for the larger sizes under LT. The larger particle size can also be attributed to the weakened

cavitation under low temperature as the vapor pressure is decreased [135]. The study on the influence of temperature on the discharge coefficient suggests that LT can effectively curb the inception of cavitation.

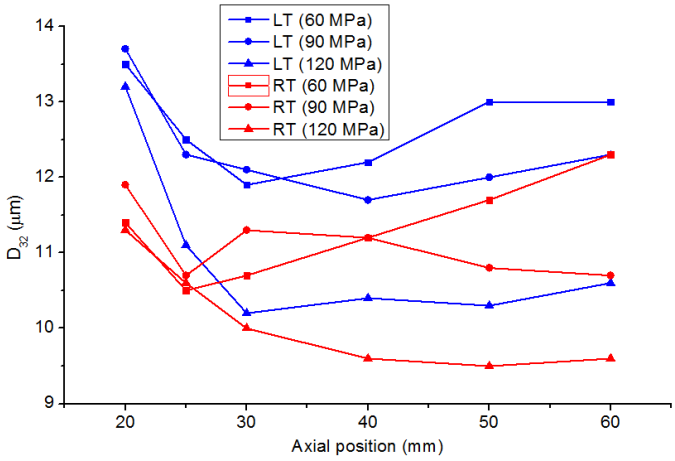

Figure 7-19 SMD for single injection under RT and LT

(3) Correlation for particle size

It can be expected that many factors influence the particle size. In this study some correlations proposed in other studies are employed to investigate the influence of various factors. Lacoste [139] found that Elkotb's correlation [142] can predict the SMD quite precisely, and the author modified the correlation by taking a host of factors into consideration. The modified correlation is shown as:

$$d_{32} = 3.08\times10^{6}\Delta p^{-0.54}\rho_g^{\ 0.06}\rho_l^{\ 0.737}\nu^{0.385}\sigma^{0.737} \qquad \text{Equation 7-1}$$

The calculated particle sizes under various conditions according to Equation 7-1 are shown in Table 7-2. Different testing positions present different droplet sizes. In this study,

the smallest droplet size along the plume axis is employed to compare with the calculated ones.

Table 7-2 Calculated SMD under various conditions with Lacoste's correlation

Temperature	RT			LT		
Δp (MPa)	60	90	120	60	90	120
Predicted SMD (μm)	13.6	10.9	9.3	17.9	14.4	12.3
Measured SMD (μm)	12.3	10.7	9.3	13.5	12	10.9

Good predicting trends when injection pressure varies are gained with this correlation. High accuracy can also be obtained under RT, especially under high injection pressure. Larger discrepancy under LT than RT can be found. Under RT, slightly larger discrepancy for low injection pressure than for high injection pressure is also observed. For these two cases with relatively large discrepancy, the effects of fuel properties tend to be significant. Tuning the coefficients for the viscosity and surface tension may lead to more accurate prediction.

Hiroyasu et al [136] also proposed an empirical correlation by taking the important dimensionless parameters into consideration, shown as:

$$\frac{SMD}{d_0} = 0.38\,\mathrm{Re}^{0.25} We_l^{-0.32} \left(\frac{\upsilon_l}{\upsilon_g}\right)^{0.37} \left(\frac{\rho_l}{\rho_g}\right)^{-0.47} \qquad \text{Equation 7-2}$$

This correlation is expected to show good prediction as *Re* and *We* dimensionless numbers take the influence of some fuel properties and injection conditions into consideration.

However, poor predicting accuracy is obtained although the varying trends are acceptable, as shown in Table 7-3. The failure of the accurate prediction may be attributed to the inaccuracy of the coefficients for the variables and good tuning may be a good way to get high accuracy.

Table 7-3 Calculated SMD under various conditions with Hiroyasu's correlation

Temperature	RT			LT		
Injection pressure (MPa)	60	90	120	60	90	120
Predicted SMD (μm)	23.8	20.0	19.3	27.9	25.1	23.9
Measured SMD (μm)	12.3	10.7	9.3	13.5	12	10.9

7.4.2 **Two-split injection**

(1) Mean velocity

Some distinct features are observed for split injections under LT. Under 60 MPa, all cases under LT show slightly higher velocity than the cases under RT except the second split injection of the 0.5 ms dwell case far from the injector tip (Figure 7-20). This suggests that the particles under LT are easier to be detected. The retaining effect of the raised fuel surface tension under LT again is seen as the main reason. This retaining effect is prominent when the velocity is high for droplets, as shown in the 0.2 ms case where LT contributes to more obviously higher velocity than RT. One interesting phenomenon should be noted that for short dwell cases, the valley velocity under LT is much lower than that of RT.

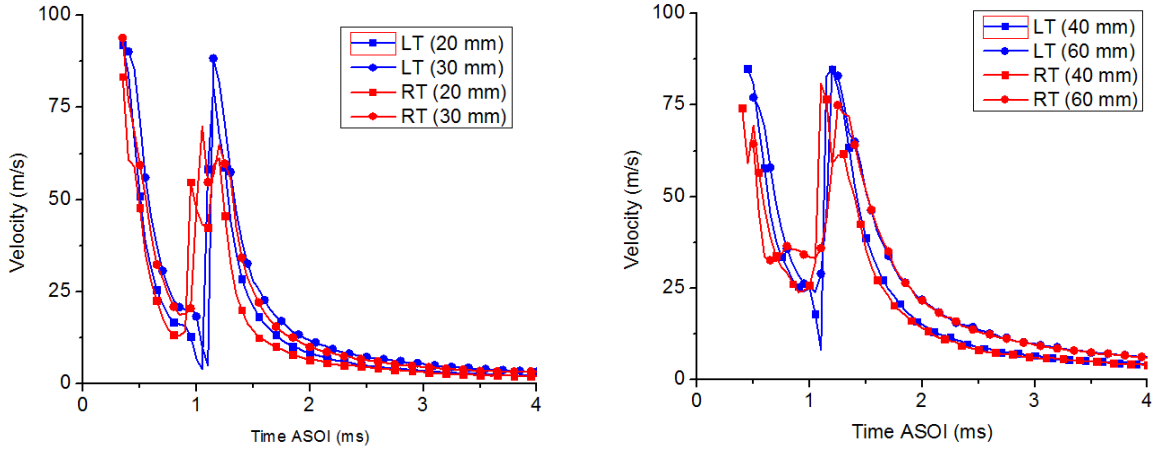

a (0.2 ms dwell)

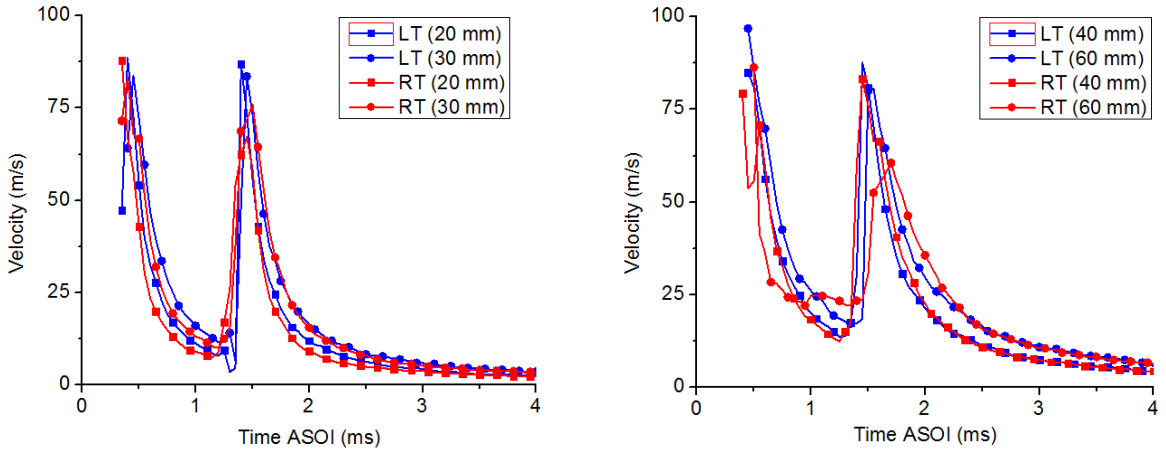

b (0.5 ms dwell)

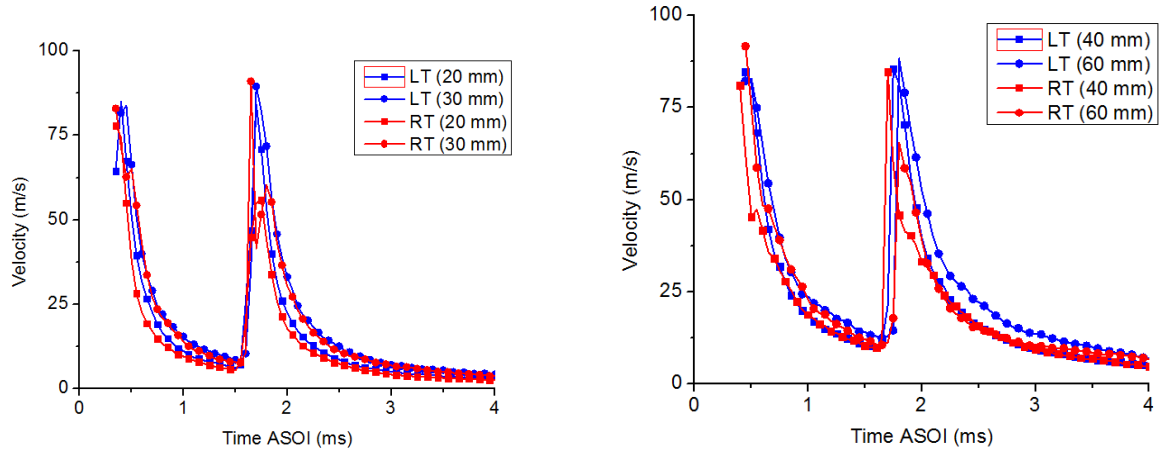

c (0.8 ms dwell)

Figure 7-20 Droplet velocity for RT and LT with split injection under 60 MPa

When injection pressure rises to 90 MPa, similar trends to those under 60 MPa injection are also found but with much larger difference for the magnitude (Figure 7-21). The velocity difference between LT and RT is very apparent when dwell is short. The high injection pressure leads to high droplet velocity and resultant obvious shape deformation. This huge velocity difference suggests the influence of changed fuel properties on droplet breakup under high injection pressure is also outstanding although the macroscopic characteristics (plume penetration and fuel area) show small differences. In addition, the valley velocity under LT is similarly much lower than that under RT when dwell is short. It can be assumed that this dramatic reduction of velocity can be attributed to the droplet collision. The large ligaments with low velocity at the tail of the first split injection seem to considerably reduce the velocities of droplets belonging to the second split injection.

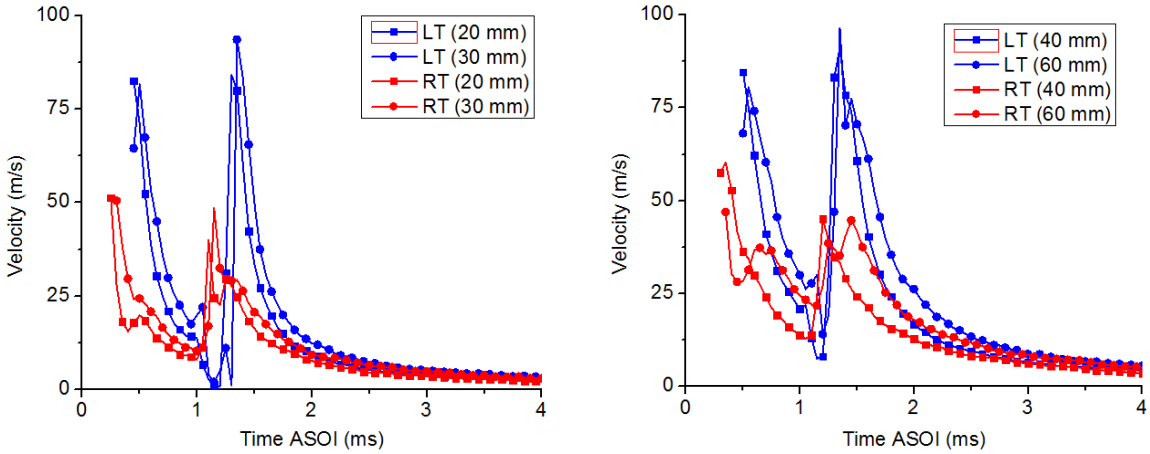

a (0.3 ms dwell)

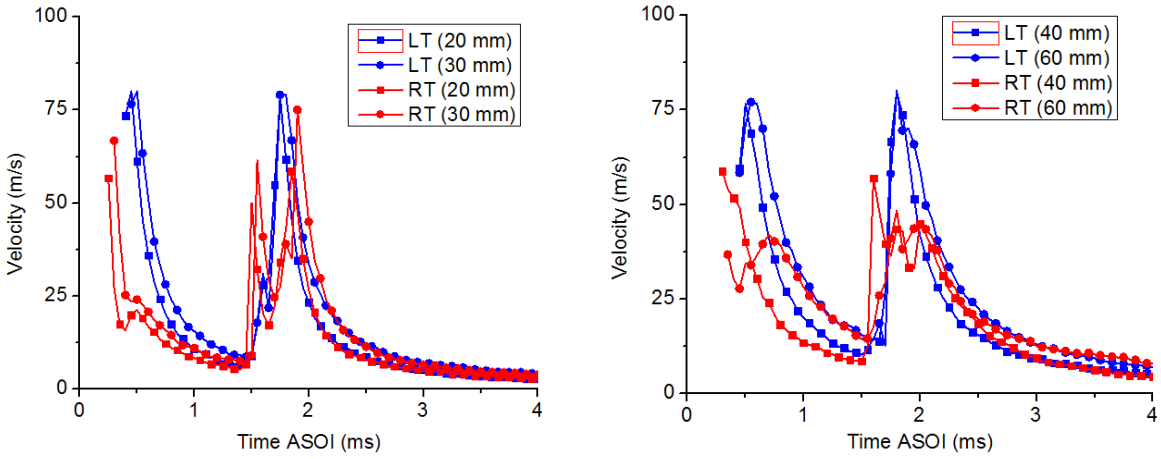

b (0.8 ms dwell)

Figure 7-21 Droplet velocity for RT and LT with split injection under 90 MPa

(2) Particle size

The droplet size ratio (droplet diameter under LT with various dwells/droplet diameter under RT with corresponding dwells) shows that LT results in much larger droplets, as presented in Figure 7-22. The droplets are very large both near the injector tip (possibly due to poorer dispersion) and far from the injector tip (probably due to collision and coalescence). The influence of dwell interval on droplet size is also obvious under low injection pressure (60 MPa, Figure 7-22(a)), with 0.3 and 0.5 ms cases showing relatively smaller sizes. High injection pressure (90 MPa, Figure 7-22(b)) tends to reduce the increasing rate of droplet size. This suggests that under LT, higher injection pressure is favorable to get fine droplets.

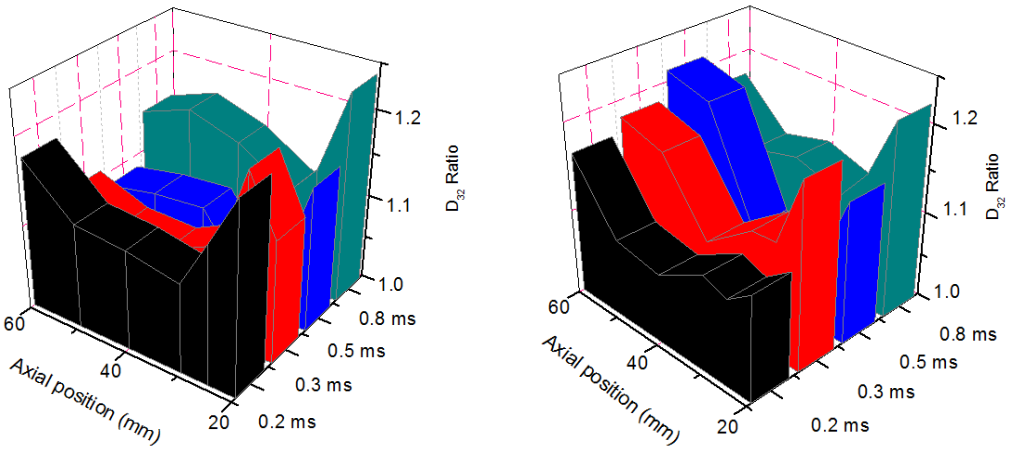

a b

Figure 7-22 SMD ratio between LT and RT with various dwells under (a) low and (b) high pressures

7.5 Conclusion and summary

The microscopic characteristics were studied in this chapter with PDPA technique. The following conclusions can be drawn.

(1) High injection pressure leads to small droplets. Droplets show an apparent size reduction followed an increase along the plume axis. The secondary breakup is believed to cause the initial size reduction, while the rise of size can be attributed to the coalescence.

(2) Strong collision causes the rise of valley velocity along the plume. However, long injection dwell leads to weaker coalescence thus lower valley velocity.

(3) It is worth noting that split injection strategy leads to higher SMD than the single injection. The strong collision between split injections tends to be responsible. Higher effective injection pressure for single injection strategy due to full injector opening leads to

better dispersion and smaller SMD. However, high injection pressure can effectively bridge the SMD difference between single and split injection strategies.

(4) The 2-split injection with short dwell (0.2, 0.3 and 0.5 ms) leads to higher SMD than the 3-split injection. The earlier injector opening means less throttling effect and higher effective injection pressure, thus expected better secondary breakup and dispersion, therefore smaller SMD is expected for 3-split injection compared with 2-split injection.

(5) Under low injection pressure LT leads to slightly higher droplet velocity than RT. However, high injection pressure surprisingly leads to obviously higher droplet velocity under LT than under RT. Higher viscosity and surface tension under LT boost the stability of the droplets, and droplets tend to present higher velocity due to poorer breakup and less reduced momentum transferred to the ambient gas.

(6) LT apparently increases droplet sizes due to poor dispersion and breakup.

(7) The valley velocity under LT is much lower than that under RT, which is assumed to be caused by droplet collision. Large ligaments with low velocity at the tail of the first split injection seem to considerably reduce the droplet velocities of the second split injection.

Chapter 8 **Conclusions and Recommendations**

The injection and spray characteristics with single and split injection were studied. The influence of low fuel temperature was also investigated. This thesis focuses on injection characteristics, primary breakup, macroscopic characteristics and microscopic characteristics. This chapter first concludes the findings and then gives advice for future work.

8.1 Conclusions

8.1.1 **Injection characteristics**

The fuel injection duration is longer than the injector energizing duration. Raised injection pressure shortens the injection delay and increases MFR. For split injection, injection pressure, the first injection duration, dwell and the number of injections dominate the interaction among splits. Low fuel temperature leads to lower MFR, longer injection delay, shorter injection duration and less injected fuel mass, especially under low injection pressure. The influence of fuel viscosity on discharge coefficient tends to be more significant than that of geometric structure under low temperature. The inception of cavitation can be effectively curbed by low temperature. Low temperature accelerates the transition of flow regime from cavitating to turbulent and then to laminar flow when the injection pressure difference decreases. The combination of low temperature and low injection pressure tends to increase the chances for laminar flow. The interaction degree between split injection events is considerably weakened by LT, contributing to much less

continuous MFR shapes for split injection compared with under RT. The qualitative effects of various factors on injection characteristics with single injection are summarized in Table 8-1, while the qualitative effects of the factors on injection characteristics with split injection (compared with those of single injection) are shown in Table 8-2. "+" means increasing effect, "-" means decreasing effect, "0" means no effect and "N/A" means not studied.

8.1.2 **Primary breakup**

The formation of the mushroom-shaped spray head can be attributed to the laminar flow in the injector hole, while the development of the mushroom results from the ambient air drag force. During the initial spray stage, the spray penetrates almost linearly with respect to time. The dispersion of the spray is greatly improved within a very short time, which is caused by the further opening of injector. The interaction strength between split injections affects the strength of primary collision and the primary breakup characteristics. Besides, the spray characteristics of the split injections except those of the first split injection are simultaneously affected by three main factors, namely, induced air driving force, lower MFR and primary collision. The interaction strength between split injections determines the main effect on the affected split injections.

Under low injection pressure and LT, raised viscosity and surface tension cause slower penetration and poorer breakup. Under high injection pressure, higher chances of mushroom formation under LT due to higher viscosity surprisingly lead to quicker penetration but still poorer dispersion during the initial spray stage. The end of injection shows a large amount

of compact liquid fuel with little dispersion, which has deteriorated at low temperature. Dimensionless parameters suggest that both injection pressure and temperature are of great importance for the breakup regimes and spray stability.

Under low injection pressure when split injection strategy employed, the first split injection is unexpectedly severely affected by both temperature and dwell. By contrast, the second split under low injection pressure tended to be affected only by temperature rather by dwell. High injection pressure considerably reduces the variation of breakup characteristics of the first split injection caused by temperature and dwell although the effects of fuel properties are still seen, leading to better dispersion and more predictable spray characteristics. The qualitative effects of various factors on primary breakup characteristics of the 2^{nd} or 3^{rd} split injection are summarized in Table 8-3.

8.1.3 **Macroscopic characteristics**

Four stages, a linear stage (constant velocity), an accelerating stage and two consecutive linear stages with different slopes (different velocities) are expected for the development of penetration. The existence of the four stages greatly depends on the back pressure and injection pressure.

The transient character of the first split injection leads to the asymmetry of the spray morphology while the earlier start of the second split injection causes more symmetric morphology. The wake driving force tends to distort the second split injection, whereas the air driving force tends to make the second plume symmetric.

Injection pressure, dwell interval and back pressure strongly affect the interaction between split injections for macroscopic characteristics. Generally, high injection pressure, high back pressure and short dwell lead to strong interaction. The second split injection tends to show smaller observed spray area and slower penetration during the early stage due to collision with the wake of the first injection. However, obviously larger spray area and higher penetration at the later stage are found.

With single injection strategy, LT results in smaller spray area and slower penetration than that under RT due to less injected fuel and poorer dispersion. Under low injection pressure, split-injection is severely affected by LT. Split injection under LT shows much lower spray area and slower penetration than those under RT. When injection pressure is raised, the differences are effectively narrowed.

8.1.4 **Microscopic characteristics**

High injection pressure leads to small droplets. Droplets show an apparent size reduction followed by an increase along the plume axis. The secondary breakup is supposed to cause the initial size reduction, while the rise of size can be attributed to the coalescence and collision.

Split injection strategy leads to higher SMD than the single injection due to strong collision between split injections. Higher effective injection pressure for single injection strategy due to fully injector opening leads to better dispersion and smaller SMD. However, high injection pressure can effectively bridge the SMD difference between single and split

injection strategies. 3-split injection strategy with short dwell leads to smaller SMD than the 2-split injection strategy. This is because of better dispersion caused by the larger injector opening and higher effective injection pressure for 3-split injection.

Under low injection pressure, LT leads to slightly higher droplet velocity. However, under high injection pressure, LT surprisingly leads to obviously higher droplet velocity. Higher viscosity and surface tension under LT boost the stability of the droplets, and droplets tend to present higher velocity due to poorer breakup and less reduced momentum transferred to the ambient gas.

LT leads to larger droplets due to poor dispersion and breakup. The valley velocity under LT is much lower than that under RT. It can be assumed that this much lower valley velocity can be attributed to the droplet collision. The large ligaments with low velocity at the tail of the first split injection seem to considerably reduce the velocities of droplets of the second split injection. The qualitative effects of various factors on macroscopic (for the 2^{nd} or 3^{rd} split injection) and microscopic characteristics are summarized in Table 8-4. It should be noted that the summarization of these effects with PDPA is based on the detected results and this does not mean the real results.

8.2 Recommendations

The primary breakup, macroscopic characteristics and microscopic characteristics need to be further studied under real engine working conditions, namely high back pressure and high temperature.

The flow regimes and primary breakup regimes require to be investigated by CFD simulation. The harsh conditions for the application of experimental measurement can be overcome by CFD simulation. Valuable results may be obtained and energy can be saved if the experimental results are further studied through CFD simulation.

The combustion characteristics of split injection strategy can be studied by injecting fuel into high pressure vessel filled with high temperature and high pressure air. The spray characteristics can be employed to further explore the combustion characteristics.

The influence of fuel temperature on combustion characteristics and emissions needs to be further studied. These important studies are expected to boost the engine design and engine calibration.

Table 8-1 Qualitative effects of various factors on injection characteristics with single injection

Single injection	MFR	Injection delay	Injection duration	C_d	Flow regime development
Increased P_{inj}	+ (higher effective injection pressure)	- (quicker injector opening)	+ (injector stays open longer)	+ (more turbulent flow)	+ (lower cavitation number)
Increased P_b	- (lower injection pressure difference)	+ (slower injector opening)	- (injector stay open shorter)	- (less turbulent flow)	- (higher cavitation number)
Increased Temp (RT)	+ (lower viscosity)	- (lower viscosity, quicker injector opening)	+ (injector stays open longer)	+ (more turbulent flow)	+ (lower cavitation number)
Decreased Temp (LT)	- (higher viscosity)	+(higher viscosity, slower injector opening)	- (injector stay open shorter)	- (less turbulent flow)	- (higher cavitation number)

Table 8-2 Qualitative effects of various factors on injection characteristics with split injection

Split injection	Fuel mass	Overall injection delay	Injection duration	Interaction
Short dwell	+ (injector keeps open during the dwell)	- (injector keeps open when the 2nd injection starts)	+	+ (positive)
Medium dwell	- (needle reverses its moving direction)	+ (injector continues to close when the 2nd injection starts)	-	+ (negative)
Long dwell	0	0	0	0
Duration of 1st injection	+ (higher degree of injector opening)	- (injector keeps open when the 2nd injection starts)	+	+
Number of injections	+(higher degree of injector opening)	- (higher degree of injector opening)	+	+

Table 8-3 Qualitative effects of various factors on primary breakup characteristics of the 2nd or 3rd injection

	Penetration	Cone angle	Spray area
Increased P_{inj}	+ (higher hydraulic force)	+ (better dispersion)	+
Increased temperature (RT)	+ (lower inertial loss)	+(better dispersion)	+
Decreased temperature (LT)	- (higher inertial loss)	- (poorer dispersion)	-
Short dwell	- (stronger collision)	+ (stronger collision)	+
Medium dwell	- (smaller injector opening, needle reverses its moving direction)	- (poorer dispersion)	-
Long dwell	0	0	0
Duration of 1st injection	- (stronger collision)	+ (stronger collision)	+
Number of injections	- (stronger collision)	+ (stronger collision)	+

Table 8-4 Qualitative effects of various factors on macroscopic (for the 2nd or 3rd split injection) and microscopic characteristics

	Penetration	Spray area	Droplet size	Droplet velocity
Increased P_{inj}	+ (higher hydraulic force)	+ (better propagation)	- (better dispersion)	+ (higher hydraulic force)
Increased P_b	-(lower hydraulic force)	- (poorer propagation)	N/A	N/A
Increased temperature (RT)	+ (lower inertial loss)	+ (better propagation)	- (better dispersion)	- (+ (actual))
Decreased temperature (LT)	- (higher inertial loss)	- (poorer propagation)	+ (poorer dispersion)	+ (- (actual))
Short dwell	+ + (strong wake and air driving force)	+ + (strong collision)	+ + (strong collision)	- - (strong collision)
Medium dwell	+ (weak wake and air driving force)	+ (weak collision)	+(weak collision)	-(weak collision)
Long dwell	0	0	0	0
Duration of 1st injection	+ (strong wake and air driving force)	+ (strong collision)	N/A	N/A
Number of injections	N/A	N/A	+ (strong collision)	- (strong collision)

References

1. MacMillan, D.J., *Influences on the cold start behaviour of a diesel engine at reduced compression ratio*. 2009, PhD thesis, University of Nottingham.
2. Sankar, S.V., et al., *Rapid characterization of fuel atomizers using an optical patternator.* Journal of engineering for gas turbines and power, 1999. 121(3): p. 409-414.
3. Rounce, P.L., *Engine performance and particulate matter speciation for compression ignition engines powered by a range of fossil and biofuels*. 2011, PhD thesis, University of Birmingham.
4. Heywood, J.B., *Internal Combustion Engine Fundamentals.* McGraw Hilled., 1988.
5. Heisler, H., *Advanced engine technology*. 1995.
6. Herzog, P.L., et al., *NOx reduction strategies for DI diesel engines*. SAE technical paper, 920470, 1992.
7. Ma, X., et al., *Co-evaporative multi-component fuel design for in-cylinder PLIF measurement and application in gasoline direct injection research.* Applied Energy, 2011. 88(8): 2617-2627.
8. Ramírez, A., et al. *Investigation of the effects of rate of injection on combustion phasing and emission characteristics: experimental and numerical study*. Spring technical meeting of the Central States section of the combustion institute. April 22-24, 2012.
9. Desantes, J.M., et al., *The modification of the fuel injection rate in heavy-duty diesel engines. Part 1: Effects on engine performance and emissions.* Applied Thermal Engineering, 2004. 24(17-18): p. 2701-2714.
10. Dolenc, A., *The Injection Equipment of Future High-Speed DI Diesel Engines with Respect to Power and Pollution Requirements.* Proceedings of the Institution of Mechanical Engineers, Part D: Journal of Automobile Engineering, 1990. 204(1): p. 49-58.
11. Karimi, K., *Characterisation of multiple-injection diesel sprays at elevated pressures and temperatures*. 2007, PhD thesis, School of Engineering, University of Brighton.
12. Birch, S., *New fuel injector technology from Delphi.* Automotive Engineering International Magazine, 2004. 112(2).
13. Li, T., et al., *Enhancement of stratified charge for DISI engines through split injection (effect and its mechanism).* JSME International Journal Series B, 2005. 48(4): p. 687-694.
14. Cung, K., et al., *Spray-combustion interaction mechanism of multiple-injection under diesel engine conditions.* Proceedings of the Combustion Institute, 2015. 35(3): p. 3061-3068.
15. Park, S.H.,et al., *Effects of multiple-injection strategies on overall spray behavior, combustion, and emissions reduction characteristics of biodiesel fuel.* Applied Energy, 2011. 88(1): p. 88-98.
16. Kuang, M., et al., *Numerical investigation on combustion and NOx emissions of a down-fired 350 MWe utility boiler with multiple injection and multiple staging: Effect of the air stoichiometric ratio in the primary combustion zone.* Fuel Processing Technology, 2013. 109(0): p. 32-42.

17. Yoon, S.H., et al., *An investigation of the effects of spray angle and injection strategy on dimethyl ether (DME) combustion and exhaust emission characteristics in a common-rail diesel engine.* Fuel Processing Technology, 2010. 91(11): p. 1364-1372.
18. Baniasad, M.S., *Analysis of fuel injection rate in diesel injection systems.* PhD thesis, University of London, 1994.
19. Arai, M., et al., *Experimental study on a diesel spray of multi-stage injection*. in *International Symposium COMODIA*. 1994.
20. Zhao, H., *Advanced Direct Injection Combustion Engine Technologies and Development: Diesel Engines*. Vol. 2. 2009: ISBN: 978-1-84569-389-3.
21. Herfatmanesh, M.R., *Investigation of single and split injection strategies in an optical diesel engine*. 2010, PhD thesis, Brunel University.
22. Alvaro, D. R., *Investigation of split injection in an optical diesel engine.* PhD thesis, Brunel University, 2009.
23. Kim, J.S., et al. *A Study on the In-Cylinder Flow Characteristics of GDI High-Pressure Fuel Injector Using a Transparent Engine System*. Seoul 2000 FISTA World Automotive Congress June.
24. Carlucci, P., et al, *Effects on combustion and emissions of early and pilot fuel injections in diesel engines.* International Journal of Engine Research, 2005. 6(1): p. 43-60.
25. Hiroyasu, H. et al, *Structures of fuel sprays in diesel engines*. 1990, SAE Technical Paper, 900475, 1990, doi:10.4271/900475.
26. Hung, C.C., et al., *Injection pressure effects upon droplet behavior in transient diesel sprays*. 1997, DTIC Document.
27. Zhu, J., et al., *An investigation of the effects of fuel injection pressure, ambient gas density and nozzle hole diameter on surrounding gas flow of a single diesel spray by the laser-induced fluorescence–particle image velocimetry technique.* International Journal of Engine Research, 2013. 14(6): p. 630-645.
28. Kawano, D., et al., *Fuel design concept for low emission in engine systems 3rd report: analysis of spray characteristics for mixed fuels*. SAE Technical Paper, 2002-01-0220, 2002, doi:10.4271/2002-01-0220.
29. Arcoumanis, C., et al., *Analysis of the flow in the nozzle of a vertical multi-hole diesel engine injector*. SAE Technical Paper, 980811, 1998, doi:10.4271/980811.
30. Afzal, H., et al., *Internal flow in diesel injector nozzles-modelling and experiments.* I.Mech.E, 1999. S492/S2/99.
31. Zeng, W., et al., *Macroscopic characteristics for direct-injection multi-hole sprays using dimensionless analysis.* Experimental Thermal and Fluid Science, 2012. 40: p. 81-92.
32. Reitz, R.D., *Atomization and other breakup regimes of a liquid jet.* PhD thesis, Princeton University, 1978.
33. Webber, C., *Disintegration of Liquid Jets.* Math. Mech., 1931. 11(2).
34. Hiroyasu, H., *Spray breakup mechanism from the hole-type nozzle and its applications.* Atomization and Sprays, 2000. 10(3-5).

35. Yule, A. et al, *On the distance required to atomize diesel sprays injected from orifice-type nozzles.* Proceedings of the Institution of Mechanical Engineers, Part D: Journal of Automobile Engineering, 1995. 209(3): p. 217-226.
36. Gulder, O., et al. *Internal structure of transient full-one dense diesel sprays*. in *Int. Symp. COMODIA*. 1994.
37. Bruneaux, G. et al., *Liquid and vapor spray structure in high-pressure common rail diesel injection.* Atomization and Sprays, 2001. 11(5).
38. Lee, C.S. et al., *An experimental and numerical study on fuel atomization characteristics of high-pressure diesel injection sprays.* Fuel, 2002. 81(18): p. 2417-2423.
39. Lee, S.W., et al., *Effects of diesel fuel characteristics on spray and combustion in a diesel engine*. JSAE review, 2002. 23(4): p. 407-414.
40. Shimizu, M., et al, *Measurements of breakup length in high speed jet.* Bulletin of JSME, 1984. 27(230): p. 1709-1715.
41. Wakuri, Y., et al., *Residual Fuel Sprays-Evaporation, Dispersion and Combustion Characteristics.* Proc. International Sympo. COMODIA, 1990. 90: p. 539.
42. Binder, J., *New generation of automotive sensors to fulfil the requirements of fuel economy and emission control.* Sensors and Actuators A: Physical, 1992. 31(1-3): p. 60-67.
43. Yule, A. et al., *On the break-up times and lengths of diesel sprays.* International journal of heat and fluid flow, 1992. 13(2): p. 197-206.
44. Mojtabi, M., *Optical analysis of multi-stream GDI sprays under various engine operating conditions*. PhD thesis, Loughborough University, 2011.
45. Mitroglou, N., et al., *Spray characteristics of a multi-hole injector for direct-injection gasoline engines.* International Journal of Engine Research, 2006. **7**(3): p. 255-270.
46. Arai, M., et al., *Disintegrating process and spray characterization of fuel jet injected by a diesel nozzle*., SAE Technical Paper, 840275, 1984, doi:10.4271/840275.
47. Crua, C., *Combustion processes in a diesel engine*. 2002, PhD thesis, University of Brighton.
48. Lefebvre, A., *Atomization and sprays*. Vol. 1040. 1988: CRC press.
49. Hiroyasu, H. et al., *Fuel droplet size distribution in diesel combustion chamber.* Bulletin of JSME, 1976. 19(135): p. 1064-1072.
50. Tian, G., et al., *Spray characteristics study of DMF using phase doppler particle analyzer.* SAE Int. 2010. 3(1): p. 948-958.
51. Lacoste, J., *Characteristics of diesel sprays at high temperatures and pressures.PhD thesis,* University of Brighton, 2006.
52. Levy, N., et al., *Non-reactive diesel spray computations supported by PDA measurements*. SAE Technical Paper.1997, 970046.
53. Desantes, J., et al., *Influence of cavitation phenomenon on primary break-up and spray behavior at stationary conditions.* Fuel, 2010. 89(10): p. 3033-3041.
54. Farrar-Khan, J., et al, *Influence of nozzle sac volume on diesel spray droplet sizes.* Proceedings of the Institution of Mechanical Engineers, Part A: Journal of Power and Energy, 1992. 206(4): p. 239-248.
55. Bae, C. et al, *The structure of a break-up zone in the transient diesel spray of a valve-covered orifice nozzle.* International Journal of Engine Research, 2006. **7**(4): p. 319-334.

56. Soteriou, C., et al, *Direct injection diesel sprays and the effect of cavitation and hydraulic flip on atomization*., SAE technical paper, 950080, 1995, doi:10.4271/950080.
57. Caprotti, R., et al., *Diesel injector deposits potential in future fueling systems*. SAE Technical Paper, 2006-01-3359, 2006, doi:10.4271/2006-01-3359 .
58. Schugger, C.R., *Experimental Investigations on the Primary Breakup Zone of High Pressure Diesel Sprays from Multi-Orifice Nozzles.* ICLASS conference, 2003.
59. Wang, X., et al., *Experimental and analytical study on biodiesel and diesel spray characteristics under ultra-high injection pressure.* International journal of heat and fluid flow, 2010. 31(4): p. 659-666.
60. Kennaird, D., et al., *In-cylinder penetration and break-up of diesel sprays using a common-rail injection system*. SAE Technical Paper, 08/2002; DOI: 10.4271/2002-01-1626.
61. Siebers, D.L., *Liquid-phase fuel penetration in diesel sprays*. SAE technical paper, 980809, 1998, doi:10.4271/980809.
62. Aleiferis, P., et al., *Effect of fuel temperature on in-nozzle cavitation and spray formation of liquid hydrocarbons and alcohols from a real-size optical injector for direct-injection spark-ignition engines.* International Journal of Heat and Mass Transfer, 2010. 53(21): p. 4588-4606.
63. Tabata, M., et al., *Mean drop diameter of a diesel spray in a vaporizing process.* JSME International Journal, Series II, Vol. 34, No.3, pp 369-378,1991.
64. Aleiferis, P., et al., *Mechanisms of spray formation and combustion from a multi-hole injector with E85 and gasoline.* Combustion and Flame, 2010. 157(4): p. 735-756.
65. Allen, J., G. et al, *In-nozzle and spray diagnostic techniques for real sized pressure swirl and plain orifice gasoline direct injectors*. SAE Technical Paper, 2003-01-3151, 2003, doi:10.4271/2003-01-3151.
66. Chen, S.K. et al, *Spray cone angles of effervescent atomizers.* Atomization and Sprays, 1994. 4(3).
67. Chang, C. et al, *A study on the effects of fuel viscosity and nozzle geometry on high injection pressure diesel spray characteristics*. SAE Technical Paper, 970353, 1997, doi: 10.4271 / 970353.
68. Grimaldi, C. et al., *Experimental comparison between conventional and bio-derived fuels sprays from a common rail injection system*. SAE Technical Paper, 2000-01-1252, 2000, doi:10.4271/2000-01-1252.
69. Mazumdar, A., *Principles and Techniques of Schlieren Imaging Systems.* 2013, Columbia University Computer Science Technical Reports.
70. Berckmüller, M., et al. *In-cylinder crank-angle-resolved imaging of fuel concentration in a firing spark-ignition engine using planar laser-induced fluorescence*. in *Symposium (International) on Combustion*. 1994. Elsevier.
71. Seitzman, J. et al., *Two-line planar fluorescence for temporally resolved temperature imaging in a reacting supersonic flow over a body.* Applied Physics B, 1993. **57**(6): p. 385-391.
72. http://faculty.sdmiramar.edu/fgarces/LabMatters/Instruments/UV_Vis/Cary50.htm#Theory.

73. Suntz, R., et al., *Two-dimensional visualization of the flame front in an internal combustion engine by laser-induced fluorescence of OH radicals.* Applied Physics B, 1988. 47(4): p. 287-293.
74. Arnold, A., et al., *Flame front imaging in an internal-combustion engine simulator by laser-induced fluorescence of acetaldehyde.* Optics letters, 1990. 15(15): p. 831-833.
75. Lawrenz, W., et al., *Quantitative 2D LIF measurements of air/fuel ratios during the intake stroke in a transparent SI engine*. SAE Technical Paper, 922320, 1992, doi:10.4271/922320.
76. Réveillé, T., *Study of fuel injection and mixture formation for a gasoline direct injection engine.* PhD thesis, Cranfield University 2005.
77. Le Gal, P., et al., *Laser sheet dropsizing of dense sprays.* Optics & Laser Technology, 1999. 31(1): p. 75-83.
78. Dantec-Dynamics, *BSA Flow Software Version 4.10 Installation & User's Guide.* 10th ed, 2006.
79. Marčič, M., *A new method for measuring fuel-injection rate.* Flow Measurement and Instrumentation, 1999. 10(3): p. 159-165.
80. Marčič, M., *Measuring method for diesel multihole injection nozzles.* Sensors and Actuators A: Physical, 2003. 107(2): p. 152-158.
81. Bower, G.R. et al., *A Comparison of the Bosch and Zuech rate of injection meters*. 1991, SAE Technical Paper, 910724.
82. Phan, A., *Development of a rate of injection bench and constant volume combustion chamber for diesel spray diagnostics. Anthony Phan,* Graduate Theses and Dissertations. 10691. 2009.
83. Bosch, W., *The fuel rate indicator: a new measuring instrument for display of the characteristics of individual injection*. SAE Technical Paper, 660749, 1966, doi: 10.4271/ 660749.
84. Shen, T.R., *Fuel Injection Rate Measurement Device.* Final year thesis,University of Birmingham, 2012.
85. Li, Y., *Experimental study on spray and combustion characteristics of diesel-like fuels.* PhD thesis, The University of Birmingham, 2012.
86. Dernotte, J., et al., *Influence of physical fuel properties on the injection rate in a Diesel injector*. Fuel, 2012. 96: p. 153-160.
87. Payri, R., et al., *An experimental study of gasoline effects on injection rate, momentum flux and spray characteristics using a common rail diesel injection system.* Fuel, 2012. 97(0): p. 390-399.
88. Seykens, X., et al., *Modeling of common rail fuel injection system and influence of fluid properties on injection process.* Proceedings of VAFSEP, 2004: p. 6-9.
89. Park, S.H., et al., *Effect of cavitating flow on the flow and fuel atomization characteristics of biodiesel and diesel fuels.* Energy & Fuels, 2007. 22(1): p. 605-613.
90. Park, S.H., et al., *A study on the fuel injection and atomization characteristics of soybean oil methyl ester (SME).* International Journal of Heat and Fluid Flow, 2009. 30(1): p. 108-116.
91. Payri, R., et al., *Flow regime effects over non-cavitating diesel injection nozzles.* Proceedings of the Institution of Mechanical Engineers, Part D: Journal of Automobile Engineering, 2011, 226: 133.

92. Jiménez-Espadafor, F.J., et al., *Experimental analysis of low temperature combustion mode with diesel and biodiesel fuels: a method for reducing NOx and soot emissions.* Fuel Processing Technology, 2012. 103: p. 57-63.
93. Vergnes, C., et al., *Discharge coefficients for a diesel injector during cold starting conditions.* Atomization and sprays, 2009. 19(7).
94. Payri, R., et al., *Effect of fuel properties on diesel spray development in extreme cold conditions.* Proceedings of the Institution of Mechanical Engineers, Part D: Journal of Automobile Engineering, 2008. 222(9): p. 1743-1753.
95. Kazancev, K., et al., *Cold flow properties of fuel mixtures containing biodiesel derived from animal fatty waste.* European Journal of Lipid Science and Technology, 2006. 108(9): p. 753-758.
96. Joshi, R.M. et al., *Flow properties of biodiesel fuel blends at low temperatures.* Fuel, 2007. 86(1): p. 143-151.
97. Winston-Galant, M., et al., *Temperature Effect on Performance of a Commercial Fuel Filter for Biodiesel Blends with ULSD*. SAE Technical Paper, 2010-01-0473, 2010, doi: 10.4271/ 2010-01-0473.
98. Soteriou. C, et al., *The flow characteristics of high efficiency diesel nozzles with enhanced geometry holes.* THIESEL Conference, 2006.
99. Payri, R., et al., *Influence of injector technology on injection and combustion development–Part 1: Hydraulic characterization.* Applied Energy, 2011. 88(4): p. 1068-1074.
100. Zhao, F., et al., *Automotive spark-ignited direct-injection gasoline engines.* Progress in energy and combustion science, 1999. 25(5): p. 437-562.
101. Sherrit, S. et al., *Characterization of piezoelectric materials for transducers.* Arxiv, http://arxiv. org/ftp/arxiv/papers/0711/0711.2657. pdf, 2007.
102. Ma, X., et al., *High speed imaging study on the spray characteristics of dieseline at elevated temperatures and back pressures*. SAE Technical Paper, 7(1):159-166, 2014, doi: 10.4271/ 2014-01-1415.
103. Desantes, J.M., et al., *Experimental study of biodiesel blends' effects on diesel injection processes.* Energy & Fuels, 2009. 23(6): p. 3227-3235.
104. Fox, T. and J. Stark, *Discharge coefficients for miniature fuel injectors.* Journal of Aerospace Engineering, 1989. 203: p. 75-78.
105. Payri, R., et al., *Study of cavitation phenomena based on a technique for visualizing bubbles in a liquid pressurized chamber.* International Journal of Heat and Fluid Flow, 2009. 30(4): p. 768-777.
106. Salvador, J., *Influencia de la cavitación sobre el desarrollo del chorro Diesel*. 2007: Reverté, ISBN-13: 978-8429147100.
107. Badock, C., et al., *Investigation of cavitation in real size diesel injection nozzles.* International journal of heat and fluid flow, 1999. 20(5): p. 538-544.
108. Schlichting, H., et al, *Boundary-layer theory*. 2000: Springer Science & Business Media.
109. Wu, P.K., et al., *Primary breakup in gas/liquid mixing layers for turbulent liquids.* Atomization and Sprays, 1992. 2(3).

110. Fujimoto, H., et al., *Visualization of micro structure in a diesel spray by use of photography with high spatial resolution*. SAE Technical Paper, 2008-01-2465, 2008, doi:10.4271/ 2008-01-2465.
111. Patterson, M.A. et al., *Modeling the effects of fuel spray characteristics on diesel engine combustion and emission*. SAE Technical Paper, 980131, 1998, doi:10.4271/980131.
112. Manin, J., et al., *Microscopic investigation of the atomization and mixing processes of diesel sprays injected into high pressure and temperature environments.* Fuel, 2014. 134(0): p. 531-543.
113. Shoba, T., et al., *Optical characterisation of diesel, RME and kerosene sprays by microscopic imaging.* ILASS -Europe 2011, 24th European Conference on Liquid Atomization and Spray Systems, Estoril, Portugal, 2011.
114. Hattori, H., et al., *Analysis of initial breakup mechanism of diesel spray injected into high-pressure ambience*., SAE Technical Paper, 2004-01-0528, 2004, doi: 10.4271 /2004 -01 -0528.
115. Crua, C., et al., *High-speed microscopic imaging of the initial stage of diesel spray formation and primary breakup*. SAE Technical Paper, 2010-01-2247, 2010, doi:10.4271/2010-01-2247.
116. Sou, A., et al., *Effects of cavitation in a nozzle on liquid jet atomization.* International journal of heat and mass transfer, 2007. 50(17): p. 3575-3582.
117. Ganippa, L.C., et al., *The structure of cavitation and its effect on the spray pattern in a single-hole diesel nozzle*. SAE Technical Paper, 2001-01-2008, 2001, doi:10.4271/2001-01-2008.
118. Dan, T., et al., *Effect of nozzle configurations for characteristics of non-reacting diesel fuel spray*. SAE Technical Paper, 970355, 1997, doi:10.4271/970355.
119. Leick, P., et al. *X-ray measurements of the mass distribution in the dense primary break-up region of the spray from a standard multi-hole common-rail diesel injection system*. in *21st Annual ILASS-Europe Conference, Mugla, Turkey*. 2007.
120. Zigan, L., et al. *Effect of fuel properties on primary breakup and spray formation studied at a gasoline 3-hole nozzle*. in *23rd Annual Conference on Liquid Atomaation and Spray Systems. Czech Republic: ILASS-Europe*. 2010.
121. Reitz, R. et al., *Mechanism of atomization of a liquid jet.* Physics of Fluids (1958-1988), 1982. 25(10): p. 1730-1742.
122. Smallwood, G.et al., *Views on the structure of transient diesel sprays.* Atomization and Sprays, 2000. 10: p. 355-386.
123. El-Amin, M., et al., *Boundary layer theory approach to the concentration layer adjacent to a ceiling wall of a hydrogen leakage: far region.* international journal of hydrogen energy, 2008. 33(24): p. 7642-7647.
124. Roisman, I., et al., *Effect of ambient pressure on penetration of a diesel spray.* International journal of multiphase flow, 2007. 33(8): p. 904-920.
125. Christian, S., et al., *Experimental Investigation of the Primary Breakup Zone of High Pressure Diesel Sprays from Multi-Orifice Nozzles.* Lehrstuhl für Wärmeübertragung und Klimatechnik, 2003.

126. Mayer, W. et al, *Atomization characteristics on the surface of a round liquid jet.* Experiments in fluids, 2004. 36(4): p. 528-539.
127. Ohnesorge, W.V., *Die bildung von tropfen an düsen und die auflösung flüssiger strahlen.* ZAMM - Journal of Applied Mathematics and Mechanics/Zeitschrift für Angewandte Mathematik und Mechanik, 1936. 16(6): p. 355-358.
128. Czerwonatis, N. et al., *Disintegration of liquid jets and drop drag coefficients in pressurized nitrogen and carbon dioxide.* Chemical engineering & technology, 2001. 24(6): p. 619-624.
129. Su, T., et al., *Experimental and numerical studies of high pressure multiple injection sprays*. SAE Technical Paper, 960861, 1996, doi:10.4271/960861.
130. Arai, M. et al., *Dynamic behavior of multi-stage injection diesel spray*. SAE Technical Paper, 970044,1997, doi:10.4271/970044.
131. Desantes, J., et al., *Study of the influence of geometrical and injection parameters on diesel sprays characteristics in isothermal conditions*. SAE Technical Paper, 2005-01-0913, 2005, doi:10.4271/2005-01-0913.
132. Naber, J. et al., *Effects of gas density and vaporization on penetration and dispersion of diesel sprays*. SAE technical paper. 960034, 1996, doi:10.4271/960034.
133. Kostas, J., et al., *Time resolved measurements of the initial stages of fuel spray penetration.* Fuel, 2009. 88(11): p. 2225-2237.
134. Hillamo, H., et al., *Diesel spray penetration and velocity measurements*. SAE Technical Paper, 2008-01-2478.
135. Zhang, Z., et al., *Characteristics of the Multiple Injection Diesel Spray Employed Common Rail System.* Journal of Thermal Science and Technology, 2013. 8(1): p. 106-119.
136. Hiroyasu, H., et al., *Empirical equations for the Sauter mean diameter of a Diesel spray*. SAE Technical Paper, 890464, 1989, doi:10.4271/890464.
137. Martinez-Martinez, S., et al., *Liquid penetration length in direct diesel fuel injection.* Applied Thermal Engineering, 2008. 28(14): p. 1756-1762.
138. Payri, F., et al., *Characterization of DI Diesel sprays in high density conditions*. SAE Technical Paper, 970054, 1996.
139. Lacoste, J., et al., *Pda characterisation of dense diesel sprays using a common-rail injection system*. SAE Technical Paper, 2003-01-3085, 2003, doi:10.4271/2003-01-3085.
140. Ficarella, A., et al., *Experimental investigation of the sprays of an axi-symmetric nozzle of a common-rail high pressure electro-injector*. SAE Technical Paper, 970054, 1997, doi:10.4271/970054.
141. Doudou, A., *Turbulent flow study of an isothermal diesel spray injected by a common rail system.* Fuel, 2005. 84(2): p. 287-298.
142. Elkotb, M., *Fuel atomization for spray modelling.* Progress in Energy and Combustion Science, 1982. 8(1): p. 61-91.